UiT The Arctic University of Norway

Faculty of Science and Technology

Department of Automation and Process, IAP

The Impact of Ambient Temperature on Low Carbon Energy Supply

Modelling and optimization studies on the supply of hydrogen energy from northern Norway

Steve Jackson

A dissertation for the degree of Philosophy Doctor, September 2021

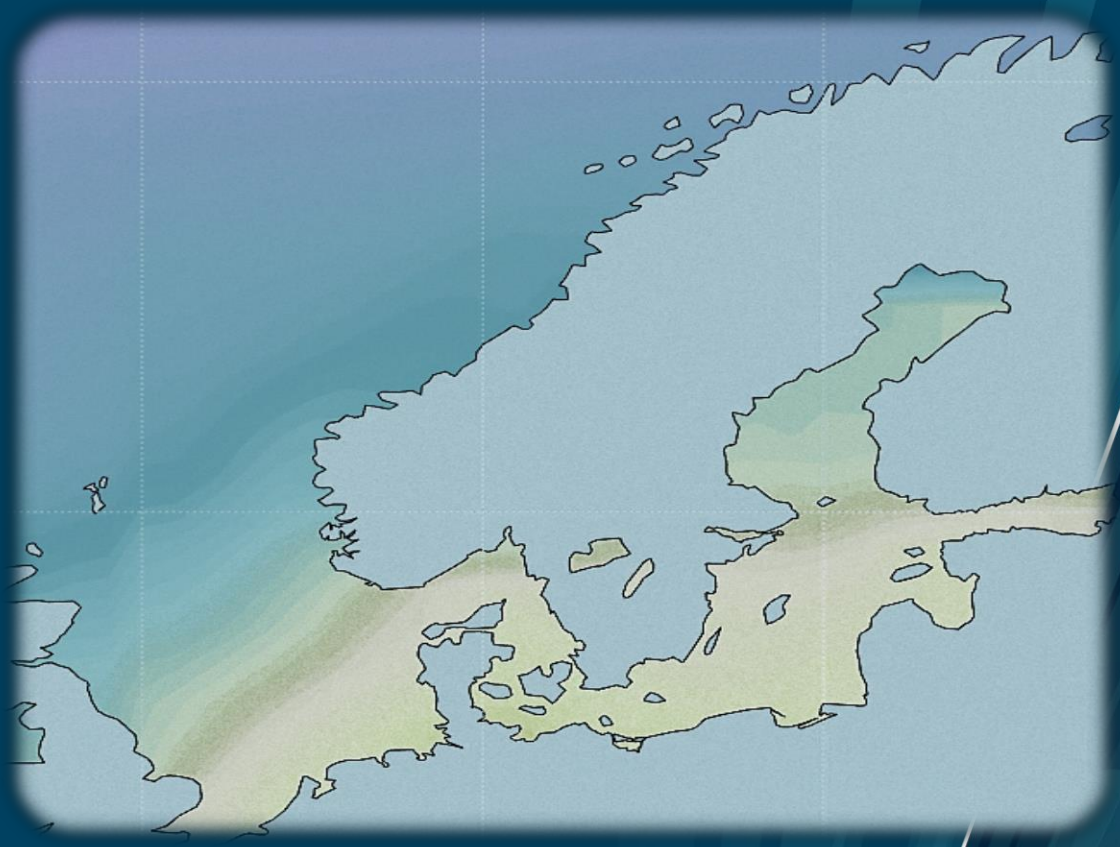

Foreword

I feel very fortunate to have had the opportunity to both write a PhD thesis *and* work on a topic that I believe is relevant to the important global challenge of reducing greenhouse gas emissions. My good luck in each respect is a direct result of the support and encouragement of my colleges at the Institute of Automation and Process (IAP), IVT faculty, UiT. In particular, I have benefited from the patient support and guidance of my main supervisor Eivind Brodal and supporting supervisors Hassan Khawaja and Lars Erik Øi. Special thanks must also go to my wife, Marie, who—whilst lacking a fully developed interest in process modelling—always listens patiently and supportively to my chuntering and grumbling.

The majority of the articles supporting this thesis have been published in open access journals, thereby maximising the availability of the work for other researchers. This was done to support UiT's goal of making all academic publications available in open access journals or repositories and with the support of the university publishing fund.

Although I am happy to be finally completing this work and hope that the results are of some use to others, I write these final words feeling more certain than ever that the production of fossil fuels must now come to an end quickly. A growing number of studies looking at the impact of fugitive emissions associated with natural gas and, by extension, blue hydrogen production, have made uncomfortable reading towards the end to my work on this PhD project. As a result, I end this work with an undecided feeling about the role blue hydrogen should play in emission reduction strategies. Although it is certainly true that the natural gas industry in Norway has a much stronger focus on emissions than in most other countries, whether this sufficiently alters the balance of benefits offered by blue hydrogen I cannot say as of now. I only hope that my work, like that of others in this field, helps to build a reasonable consensus of opinion and, thereby, make a positive contribution emissions reduction efforts.

Table of Contents

List of Tables

List of Figures

Abbreviations

ATR	Auto Thermal Reforming
CCGT	Combined Cycle Gas Turbine
CCS	Carbon Capture and Storage
CCSU	Carbon Capture Storage or Utilization
COP	Coefficient Of Performance
EOS	Equation of State
ETI	Energy Technologies Institute
GCCSI	Global CCS Institute
GEBCO	General Bathymetric Chart of the Oceans
HVDC	High Voltage Direct Current
LHL	Large-scale Hydrogen Liquefaction
MFC	Mixed Fluid Cascade
MR	Mixed Refrigerant
NGCT	Next Generation Capture Technology
PR	Peng Robinson
SEC	Specific Energy Consumption
SMR	Steam Methane Reforming
SOA	State-of-the-art
SQP	Sequential Quadratic Programming
SRK	Soave Redich Kwong
SST	Sea Surface Temperature
UiT	Norges Arktiske Universitet

Nomenclature

$\mathrm{COP_I}$	COP for an ideal process
COP_R	COP for a real process
DPt	Dew point pressure
e	Pipeline roughness
E_{el}	Electrical power (work) energy flow
E_{Ht}	Heat energy flow
Ex_i	Exergy flow stream *i*
Ex_{D}	Exergy flow destruction
$Ex_{j,\mathrm{in}}$	Exergy flow unit '*j*' in
$Ex_{j,\mathrm{out}}$	Exergy flow unit '*j*' out
$f_{\mathrm{CO_2,NW}}$	CO_2 compression energy consumption factor, NW case ($\mathrm{kJ/kg_{CO2}}$)
$f_{\mathrm{CO_2,UK}}$	CO_2 compression energy consumption factor, UK case ($\mathrm{kJ/kg_{CO2}}$)
f_{HL}	Hydrogen liquefaction energy consumption factor ($\mathrm{kWh/kg_{H2}}$)
f_{LNG}	LNG process energy consumption factor ($\mathrm{kWh/tonne_{feed}}$)
f_{SMR}	SMR power generation factor ($\mathrm{kW_{el}/kW_{feed}}$)
P_{max}	CO_2 pipeline maximum pressure
P_{min}	CO_2 pipeline minimum pressure
Pr_i	Pressure ratio stage *i*
Q_C	Heat duty of a refrigeration process
Q_H	Heat supplied to a thermal power cycle
$\dot{Q}_{\mathrm{H2\rightarrow el}}$	Energy delivered from hydrogen fuel as electrical power
$\dot{Q}_{\mathrm{H2\rightarrow ht}}$	Energy delivered from hydrogen fuel as heat
$\mathrm{SST_{mean}}$	Average sea surface temperature
T_{Amb}	Ambient temperature
T_C	Process Cooling Temperature
T_H	Hot reservoir temperature
T_L	Cold reservoir temperature
T_S	Heat sink temperature
T_{SST}	Sea Surface Temperature
U	CO_2 pipeline heat transfer coefficient (overall)
$\dot{W}_i$	Work flowrate of stream *i*
η_{SMR}	SMR efficiency ($\mathrm{kW_{H2}/kW_{feed}}$)
η_{Ex}	Exergy efficiency
η_{I}	Efficiency of an idea cycle
η_{R}	Efficiency of a real cycle

Summary of Main Articles

A list of the main articles supporting this thesis is presented below. The individual articles are also attached in the Appendix to this document.

Table 1 – Summary of the Main Articles Supporting the Thesis

1	**Jackson, Steven; Eiksund, Oddmar; Brodal, Eivind.** Impact of Ambient Temperature on LNG Liquefaction Process Performance: Energy Efficiency and CO_2 Emissions in Cold Climates. Industrial & Engineering Chemistry Research 2017; Volume 56 (12). ISSN 0888-5885.s 3388 - 3398.s doi: 10.1021/acs.iecr.7b00333.	2017
2	**Jackson, Steven; Brodal, Eivind.** Optimization of the Energy Consumption of a Carbon Capture and Sequestration Related Carbon Dioxide Compression Processes. Energies 2019; Volum 12 (9). ISSN 1996-1073.s 1 - 13.s doi: 10.3390/en12091603.	2019
3	**Jackson, Steven; Brodal, Eivind.** Optimization of a Mixed Refrigerant Based H_2 Liquefaction Pre-Cooling Process & Estimate of Liquefaction Performance with Varying Ambient Temperature. *Energies* 2021, *14*(19), 6090 doi: 10.3390/en14196090	2021
4	**Jackson, Steven.** Development of a Model for the Estimation of the Energy Consumption Associated with the Transportation of CO_2 in Pipelines. Energies 2020; Volume 13 (10). ISSN 1996-1073.s doi: 10.3390/en13102427.	2020
5	**Jackson, Steven.** Sensitivity Analysis and Case Studies for CO_2 Transportation Energy Consumption. Linköping Electronic Conference Proceedings 2020. ISSN 1650-3686.s doi: 10.3384/ecp20176257.	2020
6	**Jackson, Steven; Brodal, Eivind.** Case Studies into Low-Carbon derived Hydrogen Energy Supply to the UK from Norway, Steve Jackson and Eivind Brodal.	*

* Draft ready for submission.

Summary of Other Relevant Publications

Table 2 presents a summary of publications that are relevant to the subject matter of the thesis but do not directly support the research questions formulated under Heading 1. A full list of my publication can be found at my UiT website[1].

Table 2 – Summary of Other Related Research Work

1	**Brodal, Eivind; Jackson, Steven; Eiksund, Oddmar.** Performance and Design Study of Optimized LNG Mixed Fluid Cascade Processes. Energy 2019; Volum 189. ISSN 0360-5442.s doi: 10.1016/j.energy.2019.116207.	2019
2	**Jackson, Steven; Brodal, Eivind.** Optimization of the CO2 Liquefaction Process-Performance Study with Varying Ambient Temperature. Applied Sciences 2019; Volum 9 (20). ISSN 2076-3417.s doi: 10.3390/app9204467.	2019
3	**Eiksund, Oddmar; Brodal, Eivind; Jackson, Steven.** Optimization of Pure-Component LNG Cascade Processes with Heat Integration. Energies 2018; Volum 11 (1). ISSN 1996-1073.s doi: 10.3390/en11010202.	2018
4	**Jackson, Steven; Brodal, Eivind.** A comparison of the energy consumption for CO_2 compression process alternatives. IOP Conference Series: Earth and Environmental Science (EES) 2018; Volume 167. ISSN 1755-1307.s 1 - 14.s doi: 10.1088/1755-1315/167/1/012031.	2018
5	**Jackson, Steven; Brodal, Eivind.** An assessment of the Energy Saving Potential of Unconventional CO_2 Compression Approaches, TCCS-9, 2017-06-12 to 2017-06-14.	2017
6	**Brodal, Eivind; Jackson, Steven; Eiksund, Oddmar.** Energy saving potential of CO2 transportation processes in cold climate locations. Industrial & Engineering Chemistry Research 2016; Volume 55 (44). ISSN 0888-5885.s 11597-11605.s doi: 10.1021/acs.iecr.6b03037.	2016
7	**Font Palma, Carolina; Errey, Olivia; Corden, Caroline; Chalmers, Hannah; Lucquiaud, Mathieu; Saez, Maria Sanchez del Rio; Jackson, Steven; Medcalf, D; Livesey, B; Gibbins, Jon; Pourkashanian, M.** Integrated Oxyfuel Power Plant with Improved CO2 Separation and Compression Technology for EOR application. Process Safety and Environmental Protection 2016. ISSN 0957-5820.s doi: 10.1016/j.psep.2016.06.024.	2016

[1] https://uit.no/ansatte/steve.jackson

Abstract

To avoid the worst impacts of climate change a rapid green energy transition is required where traditional fossil fuels are replaced by low-carbon alternatives. One promising candidate is blue hydrogen, which has lower CO_2 emissions that traditional hydrogen production. Although the lifecycle emissions of greenhouse gasses associated with blue hydrogen production is debated, its usage forms an important part of both UK and European hydrogen strategies. For natural gas exporters, such as Norway, blue hydrogen also represents an attractive approach to emissions reduction, but determining how this is best realized requires the evaluation of several hydrogen supply chain alternatives.

One option for blue hydrogen supply from Norway, which is referred to in this work as *conventional*, is the continued export of natural gas with hydrogen generated at the end user. An *alternative* approach is to generate hydrogen in Norway and export it as a liquid using tanker ships or as a gas using re-purposed gas pipelines. The use of tanker ships can allow hydrogen to be transported over large distances, facilitating the exploitation of remote resources, but introduces a very energy intensive liquefaction step.

Seawater temperature is northern Norway is often 10 °C cooler than EU counties bordering the North Sea, which offers a benefit to many industrial processes. This is well illustrated by the performance achieved by the Snøhvit LNG plant, which is the most efficient of its type. Several of the links in blue hydrogen supply chains could also benefit from access to low temperature cooling. The aim of this work is, therefore, to study how this impacts on the relative energy efficiency of *conventional* and *alternative* alternatives for blue hydrogen supply based on natural gas produced in northern Norway.

The method used in the research work presented in this thesis is to conduct detailed process modelling for each of the process links in the blue hydrogen supply chain where ambient temperature is expected to significantly affect performance. Each of the studies are based on the optimization of process operating parameters at different cooling temperature cases. Common system design parameters are carried throughout each of the different parts of the modelling work to ensure a consistency in approach. Ultimately, the results of each optimization study are combined into a system model for the supply of blue hydrogen and sensitivity studies are conducted where there exists significant uncertainty in the modelling parameters used to better understand the results.

The results from the individual optimization studies serve to highlight the important role that ambient temperature can play in determining process performance. For example, when ambient temperature is reduced from 30 °C to 20°C the energy consumption of an LNG process is found to improve by around 10%, that of CO_2 compression by around 8% and for hydrogen liquefaction around 5%. The results of the modelling of the CO_2 transportation process show that the impact of ambient temperature can also be important more significant that other design parameters such as pipeline and reservoir characteristics. The results from the modelling of blue hydrogen supply chains shows that that the efficiency of the Norway based production scenario is always higher than the *conventional* scenario based on LNG export if more than 75% of the product is required in the liquid form. Sensitivity studies show that the trade-off fraction for liquids supply could be as low as 30% and that ambient temperature plays a significant role in the performance of the Norway based production scenario.

The main conclusion of this study is that the advantage offered by low ambient temperature in northern Norway is sufficient to make the supply of blue hydrogen from norther Norway more efficient that a *conventional* LNG based supply scenario over a range of realistic operating cases. The implication of this is that the basis for projects based on a conventional approach should be considered in more detail to ensure that they are based on a sound footing.

1 Introduction

This thesis presents a summary of the research work contained in six main articles that form the basis of my PhD project. These six articles are summarized in Table 1 and reproduced in full at the end of this document. A short list of other, related, publications is also presented in Table 2. The structure, content and aims of each part of the report is summarised below.

1. **Introduction** is divided into four sub-headings: *Background*, *Motivation*, *Problem Statement* & *Research Questions. Background* is where the wider context of the research work is presented. *Motivation* provides a brief description of both the basis for my own interest in this research field. *Problem Statement* sets out the central concept addresses in this project. *Research Questions* breaks the problem statement down into three specific elements that form the basis for the structure of the rest of the document.
2. **Literature Review** is arranged under three main headings that reflect the three research questions. The aim is to present a brief review of literature relevant to the thesis that sets the research work discussed under subsequent headings in the context of the wider research work in this field.
3. **Method** is arranged under three main headings that reflect the three research questions with sub-headings for each of the six main articles. This aim is to present a summary of the main aspects of the method involved in the approach to answering the *Research Questions* with a particular focus on common aspects of the work that link the articles together.
4. **Results** is arranged in the same way as the *Method* heading. The aim is to present a summary of the main results from the six articles that form the basis of this thesis with a focus on those results that link the articles together and support the *Research Objectives.*
5. **Discussion** is arranged without sub-headings. The main aim of this section is to present how the results from the individual articles build together to generate the main results from the work as whole. Also discussed are the strengths, weaknesses and implications of the work as a whole along with suggestions for further study work.
6. **Conclusions** provides a brief summary of the main implications for other research in the field.
7. **References**
8. **Appendix** presents the six main articles summarised in Table 1.

1.1 Background

1.1.1 A Rapid Transition to Green Energy

The recent publication of the IPCC's sixth assessment report[2], along with a summer of heat waves, wildfires, and flooding, have provided a new impetus for discussions relating to climate change. In the context of the work described in this thesis, the most important conclusion from recent debate is that to avoid the worst impacts of global warming a *rapid* reduction in CO_2 emissions is now required. The scale of the challenge is illustrated in Figure 1, which shows how the reduction rate depends on when peak emissions occur. The steepest curve—which is quite close to vertical—represents the rate of reduction required if the temperature rise is to be limited to 2 °C and emissions to peak in 2028; to keep warming at 1.5°C, the IPCC's sixth assessment report states that global emissions must peak by 2025.

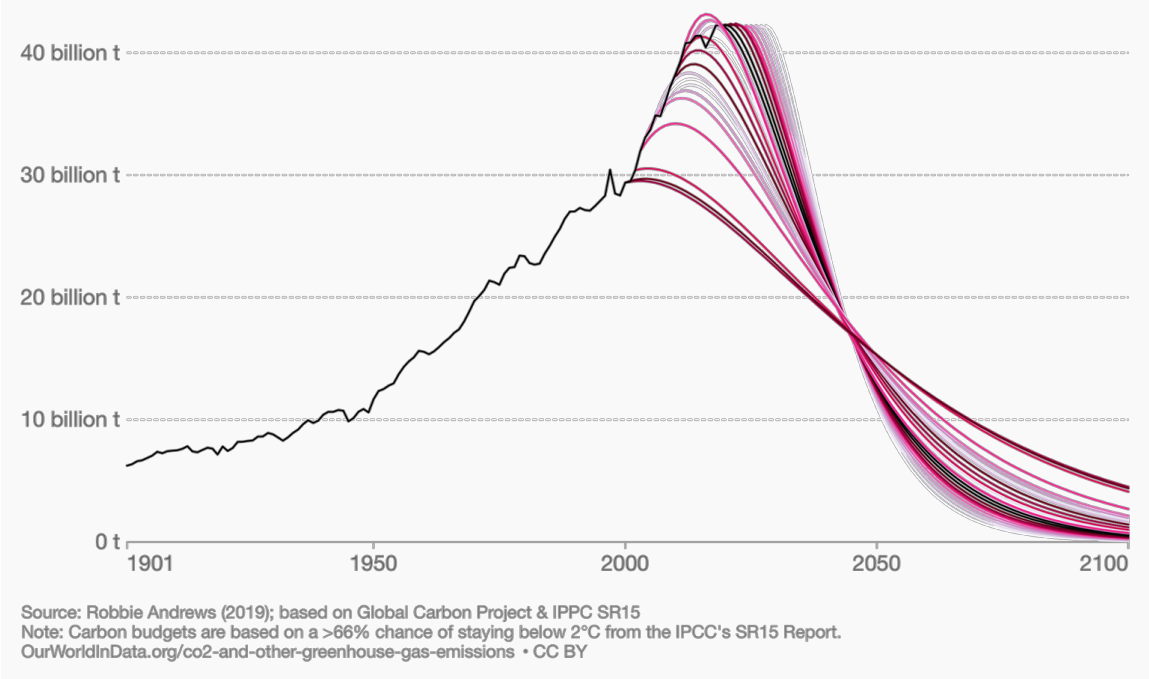

Figure 1 – Rate of CO_2 Emissions Reduction Required for Different Emissions Peak Year [3]

It is, however, still possible to identify a variety of future energy supply technologies that could allow this rapid reduction rate to be achieved; the main challenge now seems to be the speed at which the transition to these new technologies must happen. The IEA report *Net Zero by 2050*[4] states that achieving the required transition will require "a complete transformation of the global energy system".

1.1.2 The Role of Hydrogen in a Green Energy Transition

Hydrogen can used to displace traditional hydrocarbon fuels in the supply of heat and electrical power generation. It can also be used as an alternative to hydrocarbon feedstocks in several important industrial processes, including the manufacture of ammonia and steelmaking. Because of this, it is seen as an important enabler in the green energy transition. The recent EU *Hydrogen Energy Roadmap*[5] estimates

[2] https://www.ipcc.ch/assessment-report/ar6/
[3] https://ourworldindata.org/grapher/co2-mitigation-2c?country
[4] https://www.iea.org/reports/net-zero-by-2050
[5] https://www.fch.europa.eu/news/hydrogen-roadmap-europe

that this could lead to a seven-fold increase in the hydrogen demand in Europe by 2050, whereas in the earlier mentioned IEA report, *Net Zero by 2050*, the need for global hydrogen production is described as "expand[ing] from less than 90 Mt in 2020 to more than 200 Mt in 2030" with further growth to 500 Mt by 2050 (Net Zero Emissions (NZE) model).

Although many sources agree that rapidly increasing hydrogen production will make a positive contribution to meeting climate goals, the production method that should support this is not universally agreed upon. Currently, natural gas is used as the raw material for around three quarters of worldwide hydrogen production, with most of the rest coming from coal [1]. The CO_2 emissions from conventional production are mostly released into the atmosphere and the product commonly referred to as *grey hydrogen.* Hydrogen produced from renewable sources via electrolysis is generally referred to as *green hydrogen* because of its very low CO_2 emissions. Currently, green hydrogen has a higher cost than grey hydrogen and, in the context of a rapid transition to green energy, renewable electrical power used for electrolysis will compete with other potential consumers of a growing renewable energy supply.

The CO_2 emissions from *grey hydrogen* production can be captured rather than released, the resulting product being referred to as *blue hydrogen*. Although the overall level of greenhouse gas emissions avoided by blue hydrogen production compared to other low carbon energy sources is currently the source of some debate [2], the role of blue hydrogen in meeting emissions targets is still assumed by many to be important. For example, in the earlier mentioned EU *Hydrogen Energy Roadmap* two future scenarios are identified: one described as *water electrolysis dominant* and the other *SMR/ ATR dominant*. The second of these scenarios refers to the production of blue hydrogen from natural gas and the first to production of green hydrogen. What is notable is that across both of these two future scenarios, the proportion of blue hydrogen varies from around 20% to around 80%, i.e., in both cases there is substantial blue hydrogen production. The recently released UK hydrogen strategy[6] is based on a similar understanding of the potential for rapid growth in green hydrogen production and is also based around a 'twin-track' approach utilizing both blue and green hydrogen.

1.1.3 Hydrogen Transport

Although the production of hydrogen is normally the first topic of interest in the discussion around future hydrogen economies, increases in the current capacity for the transportation of hydrogen will also be required. It is possible to transport hydrogen in trucks, either as a compressed gas or a liquid at low temperature, in pipelines as a gas, or in ships as a liquid at low temperature. In a close parallel to the transportation of natural gas as LNG, the optimum transportation strategy is considered to depend on both capacity and distance to market [3]. When the transportation distance is significant and the required capacity is large, it is reasonable to expect that shipping of liquefied hydrogen will be favoured. This assumption has already been put into the early stages of commercial practice with the world's first liquid hydrogen carrier ship launched in Japan in 2019 [4].

A significant disadvantage associated with shipping liquid hydrogen is, however, the need for a liquefaction process, which is very energy intensive. The specific energy consumption (SEC) of the most efficient currently operating large-scale hydrogen liquefaction (LHL) plants lies in the range 13–15 kWh_{el}/kg_{H2} [5], which is much higher, for example, than the most efficient LNG processes, which have a SEC around 0.24 kWh_{el}/kg_{LNG}. The consequence of this energy demand is reduced efficiency in both liquefied blue and green hydrogen energy supply chains, which in-turn provides a significant

[6] https://www.gov.uk/government/publications/uk-hydrogen-strategy

disincentive to the large-scale transportation of hydrogen over long distances. Where hydrogen supply is based on the conversion of existing natural gas supplies, the energy intensive hydrogen liquefaction step can potentially be avoided through the production of blue hydrogen at the end-user. The disadvantage to this approach is that the captured CO_2 emissions must also be dealt with at the end-user.

1.1.4 Carbon Capture and Emissions Targets

A key enabling technology associated with the development of blue hydrogen supply is Carbon Capture and Storage (CCS), which refers to a broad mixture of technologies aimed at mitigating CO_2 emissions. *Carbon Capture* is a term often associated with the recovery of CO_2 from the flue gasses of fossil-fuel based power generation, but CO_2 can also be captured from a range of industrial processes including the production of hydrogen, fertilizers, cement and natural gas. The focus for the storage of CO_2 on the scale envisioned for most CCS projects is the use of depleted petroleum reservoirs and saline aquifers. At present the most common form of storage is the practice of enhanced oil recovery (EOR), which involves the injection of CO_2 into an oil reservoir to increase recovery. EOR is an established industry in the US where the CO_2 required is recovered from a variety of industrial and natural sources, transported in pipelines over significant distance and injected into oil reservoirs.

The role that CCS could play in limiting the level of global warming has been studied over many years and is often a source of controversy since investment in CCS projects competes with investment in renewable energy projects. When CCS is considered in the context of decarbonising natural gas supplies, controversy also exists around the impact of supply chain methane emissions, which can represent an additional, and partially hidden, environmental impact. Despite this, CCS is a technology that could be implemented rapidly and many studies show that CCS could form an important part of meeting CO_2 emissions targets. For example, the earlier mentioned IEA report *Net Zero by 2050* finds that "A failure to develop CCS for fossil fuels would substantially increase the risk of stranded assets and would require around USD 15 trillion of additional investment in wind, solar and electrolyser capacity to achieve the same level of emissions reductions."

1.1.5 Norway's Role in the Development of CCS

Norway has played a leading role in the development of CCS technologies and has the only active CO_2 storage projects in Europe. Since 1996, the CO_2 resulting from natural gas production on the Sleipner platform has been captured and reinjected into subsea formations [6]. In terms of the available CO_2 storage capacity available, Norway along with UK, is better placed to store emissions CCS projects than any other country in Europe. Norway also hosts one of the largest test centres used in the development of new carbon capture technologies at the Mongstad oil refinery [7] and is now committed to the development of Europe's first full-chain industrial CCS demonstration project, the Langskip project[7].

At the same time as Norway's ambition is to be a world leader in CCS technology is clear, it is also true that the vast majority of the CO_2 emissions associated with Norway's petroleum exports are released at the point where the gas (or oil) is used. The Northern Lights project[8] (part of the Langskip project) provides part of an answer to this problem through its aim to develop a hub for the storage of CO_2 from

[7] https://langskip.regjeringen.no/longship/
[8] https://northernlightsccs.com/

other CCS projects across Europe, but other approaches to the decarbonization of hydrocarbon based energy exported from Norway also exist that avoid the export of CO_2 emissions.

1.1.6 Norway's Potential as a Green Energy Exporter

Norway is one of Europe's most important energy suppliers. Currently, most of this energy is exported in the form of natural gas and oil, but in the context of a rapid green energy transition this cannot continue indefinitely. In place of these existing energy exports, Norway has significant potential to generate more renewable energy than it consumes. "With abundant unexploited wind resources, e.g., along the coast of Central Norway and in Finnmark, Norway has the potential to export renewable based hydrogen to Europe." [8]. Although some portion of the energy generated from further development of Norway's wind energy resources could be transported to markets in Europe using high voltage direct current (HVDC) electrical interconnectors, extending that infrastructure to the cost of Finnmark in northern Norway may present some challenges that could be solved by storing this energy as hydrogen.

Electrolysis of hydrogen also provides an opportunity to optimize production of electrical power from intermittent renewable energy sources, but hydrogen produced in this way will still lie a long distance from the main future markets for green hydrogen. In this context, the development of storage and transportation infrastructure in Norway for the supply of hydrogen produced by remote wind resources becomes important. Production of blue hydrogen produced in Norway would also require this type of transport infrastructure and could, therefore, support the development of early green hydrogen production.

1.1.7 Norway's Role in Hydrogen Supply

As a major exporter of natural gas, it is logical that climate mitigation measures focused on the development of blue hydrogen production attract support. Equinor's home page for hydrogen[9] currently lists five large natural gas to hydrogen projects under development in which Equinor plays a role (accessed August 2021). The first of these projects, the H21 project[10], is focussed on the conversion of the UK natural gas grid to hydrogen. The second is another UK project, the H2H Saltend project[11], which is similar in its aims to the H21 project. Also listed are three European projects. Each of these projects follows the energy supply chain model referred to in this thesis as *conventional* because they are based on current model of gas export from Norway with production of hydrogen at the end user. This approach places none of the hydrogen transportation chain infrastructure in Norway.

Another feature of the *conventional* type of hydrogen supply projects mentioned above is that they are normally developed based on an assumed phased transition to green hydrogen as the technology and infrastructure required becomes cost effective. Although the rate of this transition is difficult to guess, it is likely that it must happen quickly to meet emissions targets and that in optimistic cases the transition should occur within a decade. This is a much shorter timeframe that the normal design life assumed for most large-scale energy projects. A recent presentation by NEL highlighted that green hydrogen based supply chains are already benefiting from the rapidly decreasing costs for wind and solar power generation[12], but a rapid transition to green hydrogen for projects based on the *conventional* model will

[9] https://www.equinor.com/no/what-we-do/hydrogen.html
[10] https://h21.green/
[11] https://www.zerocarbonhumber.co.uk/
[12] Norway-Singapore webinar series 2020: Decarbonization, May 18 -29, 2020.

be dis-incentivized by established blue hydrocarbon investments. An alternative to the *conventional* type of blue hydrogen supply project is to produce hydrogen close to the origin of the hydrocarbon feedstock and then transport the hydrogen to market using infrastructure that could serve both green and blue hydrogen sources.

One way to supply hydrogen produced in Norway would be to re-purpose the natural gas pipeline network connecting southern Norway to the UK and Europe, which is the main scenario envisaged in the recently published Hydrogen4EU report [13]. The results of the modelling presented in the Hydrogen4EU report suggest both that "Norway becomes the main producer of hydrogen in Europe" and that "Norway mostly produces low-carbon hydrogen via reformers equipped with CCS and exports hydrogen via pipeline to the continent". However, although the re-purposing of existing natural gas pipelines for hydrogen supply from southern Norway is a good fit with large-scale blue hydrogen production in southern Norway, it may not be a good fit with future wind-based production of green hydrogen in the north. In addition, not all of the natural gas production infrastructure is connected to the pipeline network: in northern Norway, the gas produced from the Snøhvit gas field is produced as LNG from the Melkøya LNG plant.

Another approach to the large-scale supply of hydrogen from Norway would be to liquefy it and transport it in tanker ships. As discussed earlier, this approach has an impact on energy efficiency, but in some cases the economics may still be favourable. One recent study into the supply of liquefied hydrogen from Norway to Japan finds that the economics are "close to meeting the 2030 hydrogen cost target of Japan" [9]. In other parts of the world where the economics are already more favourable projects based on this type of supply chain are already in the early stages of development. The HySTRA project[14] is an example of this which is based on the supply of blue hydrogen generated from fossil-fuel in Australia to Japan.

Although recent publications such as the earlier mentioned Hydrogen4EU study are keen to promote findings that support the need for both blue and green hydrogen to reach zero emissions, the longer-term expectation must ultimately be that the production of blue hydrogen will eventually be displaced by green hydrogen production as the economics and capacity of renewable power generation improve. On the basis of this, it is logical to assume that there is an advantage in investment in blue hydrogen supply chains that include hydrogen transport infrastructure which could also support development of green hydrogen supply.

1.1.8 The Advantage of a Cold Climate

Under the headings set out above, several general aspects of the potential contribution that Norway could make to the green energy transition are discussed. The resources available to Norway that could form the foundation of this contribution can be summarised as follows: access to petroleum-based energy, a well-developed gas transport infrastructure, a well-developed process industry suitable to supporting CCS projects, political support for CCS, good access to CO_2 storage sites, and access to an abundance of renewable wind energy. In addition to all of these, the average ambient temperature in Norway, particularly in northern Norway, offers an additional advantage to the performance of many important industrial processes, including some of the processes that form part of blue hydrogen supply.

[13] https://www.hydrogen4eu.com/
[14] http://www.hystra.or.jp/en/

The efficiency of industrial process that convert work into heat and vice versa is affected by the temperature at which heat can be rejected to the environment. The maximum theoretical efficiency of a process converting heat into work (e.g., a conventional steam power plant) is described by a Carnot cycle. The efficiency of this ideal cycle, η_{I}, can be calculated from only the temperature of the available heat reservoir, T_H (e.g., the maximum temperature at which steam is generated in a steam power plant) and the temperature available cold sink, T_S (e.g., the steam cycle condenser temperature) using the Carnot efficiency formula:

$$\eta_{\mathrm{I}} = \frac{W}{Q_H} = \frac{T_H - T_S}{T_H} \tag{1}$$

where W is the work generated, Q_H is the heat energy input from a hot reservoir. In a real cycle, the cold sink temperature, T_S, is often limited by some approach the ambient temperature, T_{Amb}, in the location where the process operates. So, for a fixed T_H the maximum efficiency achievable depends only on T_{Amb}.

For process operating below ambient temperature (e.g., a standard vapour compression refrigeration process) the performance of an ideal process can be defined as a Coefficient of Performance ($\mathrm{COP_I}$), which is also defined in terms of two temperature levels:

$$\mathrm{COP_I} = \frac{Qc}{W} = \frac{T_L}{T_S - T_L} \tag{2}$$

where Q_C is the refrigeration duty supplied by the process and T_L is the temperature at which Q_C is supplied—the refrigeration temperature. T_S, as before, is the temperature at which heat is rejected from the refrigeration process to the cold-sink—usually the temperature of the local environment.

The ratio of the efficiency achieved by a real process, η_{R}, to the efficiency of an ideal process can be referred to as the second law efficiency, η_{2nd}. The value of η_{2nd} for a real process gives us a measure of how well its design is optimized for the conditions that it operates with and how efficient the individual equipment items are that are used in the process. If the design of two similar processes is equally well optimised and they use the same type of equipment items, we can assume that η_{2nd} is the same for both processes and, subsequently, that the ratio $\eta_{\mathrm{I}}/\eta_{\mathrm{R}}$ and $\mathrm{COP_I}/\mathrm{COP_R}$ will also be constant.

Figure 2 illustrates how η_{I} and $\mathrm{COP_I}$ vary for two ideal processes operating at with two different heat sink temperatures. Also plotted is the relative performance of these two cases. This illustrates the performance advantage offered by a lower heat sink temperature to thermal cycles operating both below and above ambient temperature, assuming η_{2nd} is constant.

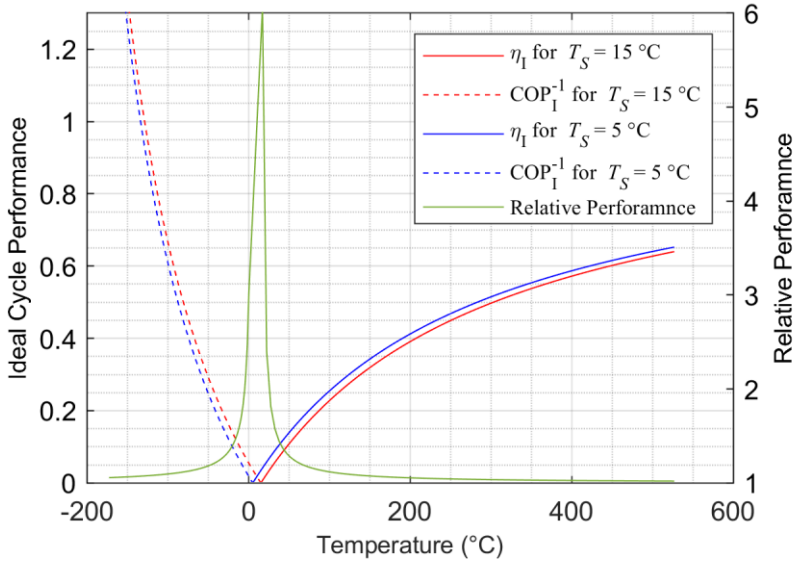

Figure 2 – The Impact of Cold Sink Temperature on the Relative Performance of two Ideal Cycles

What is notable in Figure 2 is the efficiency advantage gained by a lower temperature heat-sink increases rapidly for processes operating close to ambient temperature. For example, an idealized refrigeration process operating at -5 °C and rejecting heat to the environment at 5 °C is around 50% more efficient that the same process rejecting heat at 15 °C. The effect becomes less pronounced as the temperature difference across which the process operates widens, but for process working around ambient the difference can be significant.

In northern Norway, the average sea surface temperature, SST, is between 5 and 10 °C lower that experience in northern Europe. In the context of what is described above, this offers a significant opportunity to some types of industrial processes. A good example of this is the LNG plant located at Melkøya, which is claimed to be the most efficient LNG plant in the world [10]. A hydrogen liquefaction process located in norther Norway would also benefit from this inherent advantage and could also be reasonably expected, if built, to be the most efficient of its type in the world.

1.1.9 Summary

It is clear that a rapid transition from fossil energy is now needed to limit global. In the transition period blue hydrogen production is seen by many as a promising way reduce emissions. It can also be seen as a way of kick-starting the production of green hydrogen, but there are a number of drawbacks. Converting natural gas to hydrogen consumes a significant proportion of the energy content of the fuel, capturing CO_2 and transporting it to a storage reservoir consumes a significant amount of energy, and liquefying hydrogen for long distance transport consumes a large amount of energy. There are two main options can be envisaged for how Norwegian natural gas production can support demand for blue hydrogen in Europe: hydrogen could be produced in Norway and supplied using either re-purposed natural gas pipelines or liquefied and transported in ships; or *conventional* natural gas supplies from Norway could be used to produce hydrogen at the end user location. In the second option, the energy associated with hydrogen liquefaction for shipping is avoided, but in the first option the infrastructure required for hydrogen supply is developed in Norway, better supporting future green hydrogen production. Low ambient temperature in Norway, particularly in the north, may also offers a unique advantage to some of the process units required in the first option, such as the hydrogen liquefaction step.

1.2 Motivation

Prior to my current position at UiT I worked in the UK gas processing industry. From 2000 to 2013 I was employed as a process engineer with Costain Energy and Process (Manchester, UK). From around 2008 I was given the opportunity to act as a focal point for Costain's efforts to develop technologies related to CCS. In particular, I was responsible for the technical part of the UK government funded OXYPROP project [11] and responsible for the development of the technology that formed the basis for the Energy Technologies Institute (ETI) funded NGCT project [12, 13]. While working on these projects I also took on a more general responsibility for developing, promoting and disseminating Costain's work on CCS and through this developed a keen interest in this potentially important set of technologies. As a result, I was eager to continue my research work in CCS when I joined UiT.

Working at UiT, before the official start of my PhD project, I was involved with several pieces of research work looking at the impact of ambient temperature in northern Norway on process performance [14, 15]. Linking this research to my own background in CCS I started to consider how the inherent advantage offered by low temperatures in northern Norway might help improve the efficiency of CCS related technologies, which eventually led to the work described here. My hope is that the results from this work might provide some useful input to the debate surrounding the role CCS and hydrocarbon based energy should play during the transition to more sustainable energy sources.

1.3 Problem Statement

Under Heading 1.1, some issues surrounding the role of blue-hydrogen in a green energy transition and what contribution Norway might make to this have been discussed under heading 1.1.9 a summary is made of the main issues relevant to this thesis that forms the basis for the problem addressed in this thesis, which can be stated as follows:

> *The approach proposed in several early projects to the supply of blue hydrogen derived from Norwegian natural gas is production at the point of demand. An alternative approach, where blue hydrogen is produced in Norway would potentially provide a better stepping-stone for future green hydrogen exports but requires the large-scale liquefaction of the hydrogen product for shipping, which is very energy intensive. A realistic comparison of these two scenarios for blue hydrogen supply should include the advantage offered by low ambient temperature at the supply end of the chain, which in-turn requires the development of a modelling basis that can account for this impact.*

A deliberate choice is made in setting the research question that no economic evaluations are include in the scope of the work. The basis for this is not that I consider them unimportant, rather that that development of economic analysis falls both outside my core skill set and my research interest area.

1.4 Research Questions & Objectives

In response to the problem statement made above, three Research Questions can be formulated:

- RQ1 - How does ambient temperature effect the performance of industrial processes relevant to the supply of blue hydrogen?
- RQ2 - How is the energy consumption associated with CO_2 transportation affected by ambient temperature and the location of the source/ storage reservoir?
- RQ3 - Under what conditions is the energy efficiency of blue hydrogen based energy supply chain originating in northern Norway better than an equivalent *conventional* blue hydrogen supply chain based on the export of natural gas from northern Norway?

These questions are answered by the research work summarised in the six main articles that form the basis for the subsequent parts of this thesis. The relationships between these six main articles and the research questions is illustrated below in Figure 3. How these research questions are translated into a set of research objectives is summarized in Table 1.

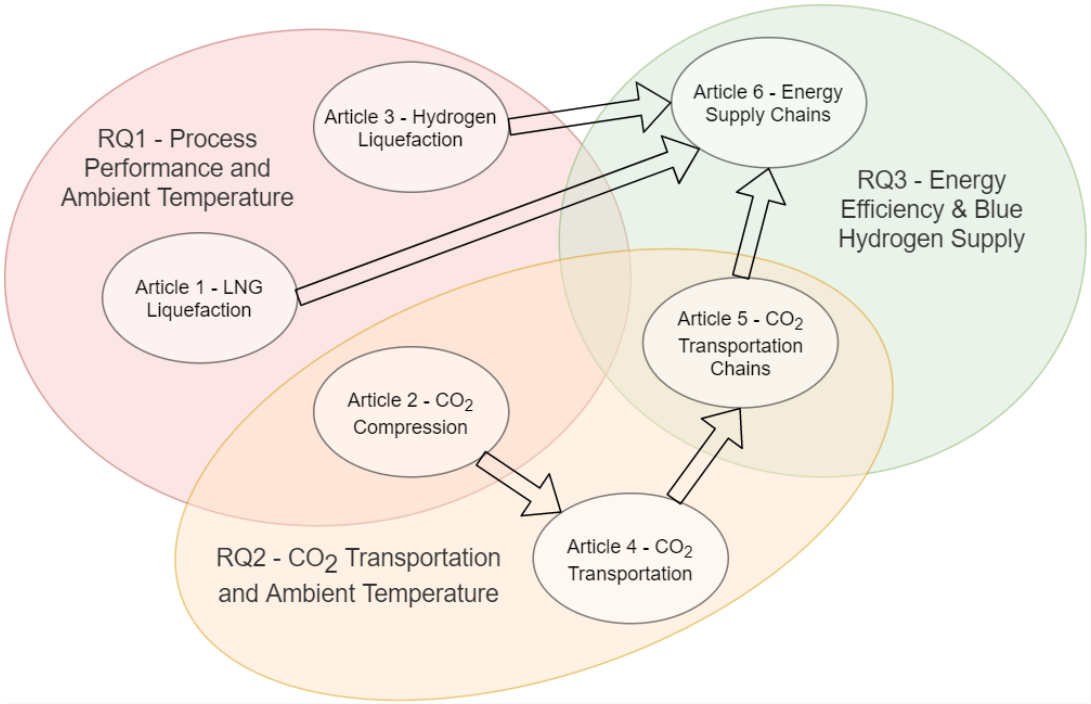

Figure 3 – Relationship between the Six Main Articles and the Research Questions

Table 3 – Summary of Research Questions and Objectives

Question	**Objective**	**Articles**
RQ1	Develop a set of data that quantifies the variation in energy consumption with ambient temperature for key process units in blue hydrogen energy supply chains	1, 2 & 3
RQ2	Provide basis data for how energy consumption of different CO_2 transport chains varies with location and ambient temperature	4 & 5
RQ3	Develop a model that can compare the energy efficiency of two different concepts for blue hydrogen supply from northern Norway	6

2 Literature Review

A brief literature review is presented below that has the aim of setting the research work discussed under later headings in the wider context of the work in this field. The description presented here is based, in the main, on works cited in the main articles associated with this thesis. It does not aim to be exhaustive in the strict sense of a literature review, although some updates and additions to earlier literature search work are made where it is considered beneficial for this document. Parts of the literature search work from my own earlier published works are re-used when appropriate.

2.1 RQ1- Process Performance & Ambient Temperature

Research relevant to the supply of blue hydrogen can potentially include a wide range of topics: the design and performance of hydrogen production processes, the performance of the supply chain for the feedstock, CCS related elements, hydrogen storage distribution and shipping are all topics of interest. However, in the specific context of the impact of ambient temperature (i.e., the theme of this thesis), the search can be narrowed to process units that operate below and immediately around ambient temperature.

Based on a qualitative review of the role heat-sink temperature plays in limiting efficiency (refer to Figure 2) a short-list of the processes that are likely to be the most impacted by ambient temperature can be produced: LNG liquefaction, hydrogen liquefaction and CO_2 liquefaction. In addition, it can be expected that a small efficiency gain could be made to the CO_2 compression process and the combined cycle gas turbine (CCGT) power generation processes.

Although the impact of ambient temperature on CCGT has been widely studied, this has primarily been from the perspective of off-design operating conditions, i.e., how does a process with a design optimized for one heat-sink temperature perform with a different heat sink temperature. This is not, however, the aim of the present work. The aim of this work is to compare the performance of a process optimised for operation with one particular heat sink temperature compares to the same type of process optimized to operate with a different heat sink temperature, i.e., both processes operating at their optimum efficiency.

Although studies into the off-design performance of CCGT units have shown ambient temperature to have a small impact on efficiency, for example the work of Gonzalez-Díaz, et al. shows efficiency varying by 3% over the range 15 °C to 45 °C [16], studies looking at the performance of an optimized CCGT design find the impact to be lower. The study of Arrieta and Lora, for example, found that a 3% variation in heat rate corresponded to ambient varying between 0 to 35 °C [17]. In addition, and illustrated by the results shown in Figure 2, the impact of ambient temperature can be expected to decrease for this type of thermodynamic cycle where the upper temperature level is well above ambient temperature. Because of this, the scope of RQ1 and the literature review described below is limited to the liquefaction and compression processes mentioned earlier.

2.1.1 LNG Process Modelling

Khan, et al. identify the first example of an optimization study for an LNG process to be that of Ait-Ali, et al. in 1979 [18]. In the work of Ait-Ali, et al. a two-dimensional numerical search was used to find the key trade-offs for a MR LNG process [19]. Over the subsequent decades many more modelling and optimization studies have been made: a comprehensive literature review looking at the use of optimization in LNG process design and operation made in 2014 by Austbø, et al. [20] identified 186

published works. In the subsequent years the total number will surely have increased. On this evidence, it is reasonable to assume that the modelling and optimization of LNG processes has, in general, been well researched with few obvious research topics omitted.

Several themes relevant to the present work are identifiable in the review made by Austbø, et al. One such theme is that a variety of modelling environments have been used, ranging from industry standard software packages like Aspen HYSYS to more generic environments such as MATLAB. Another is that the Peng-Robinson (PR) and Soave–Redlich–Kwong (SRK) equations of state (EOS) are those most commonly used to model properties. Another is that a range of optimization techniques both deterministic, stochastic and hybrid type optimization approaches have been applied. And still another is that the objective function is usually minimum power, although exergy efficiency and economic assessments have also been made. However, it is also identifiable that studies looking at the impact of ambient temperature on performance are not well represented.

The study of Xu, et al. [21], which considers the correlation between mixed refrigerant composition and ambient conditions in the PRICO LNG process is one example identified by Austbø, et al. In this work, the influence of ambient temperature on the optimal refrigerant composition is studied for a single mixed refrigerant (MR). The findings are that "When increasing the cold-box inlet temperature from 263.15 K to 313.15 K, the shaft work requirement increases by approximately 60%." Also identified by Austbø, et al. is the study of Rian and Ertsevåg looking at the significance of ambient temperature on the Snøhvit LNG plant [22]. In this work the findings are that "Reducing the ambient temperature from 36 to 4 °C implied a reduction in exergy consumption by 19.9%, while a reduction from 20 to 4 °C gave a reduction of 10.9%.

Literature searches conducted as part of the work described in this thesis also identify the study of Castillo, et al. [23], which compared the performance of different designs of an LNG precooling process in a warm climate to a cold climate. However, this study does not identify a structured approach to optimization and did not produce a set of data points for performance evaluation. Also identified in the present work is the study of Park, et al. [24], which looked at the performance of a SMR type LNG process for a range of ambient temperatures and optimization cases. This study finds that specific power increases by between 16% and 42% over the temperature range 10−25 °C and used a Particle Swarm type optimization approach.

In contrast to the references identified above, the aim of LNG modelling work conducted as part of this thesis is to study only the performance of the most efficient LNG process, the Mixed Fluid Cascade (MFC) process, and only to study how energy consumption varies over the range of ambient temperatures that are typical for northern Europe and northern Norway. In addition, the aim of the current work is to assess this performance data using a consistent set of basis parameters that can be carried over the other modelling work involved.

2.1.2 H_2 Liquefaction Process Modelling

At the same time as political interest in the potential of hydrogen as a future energy source has risen, so has research associated with hydrogen energy [25]. Popular research topics include the development of novel production approaches, new applications (e.g., steelmaking) and transport. Included in the latter group are several studies looking at the improvement of large-scale hydrogen liquefaction, LHL, which is a key element in the supply of hydrogen over large distances.

Recent research relating to improved LHL processes includes a variety of topics. Novel process designs such as ones integrating renewable energy sources in the cooling process (for example, solar energy [26] and geothermal energy [27]) have been studied along with more conventional types of design improvements such as the use of mixed refrigerants (MR) for pre-cooling [28-30]. Other research has focused on the impact of the catalytic conversion of ortho-hydrogen to para-hydrogen in the liquefaction process [31, 32] and the relative performance of different exchanger types [29, 32, 33]. The suggested efficiency of these proposed concepts for LHL lie in the range 5-8 kWh/kg [5], which represents a substantial improvement over the performance of existing plants, which lies in the range 13-15 kWh/kg [5]. This provides a significant motivation for the implementation of these technologies in the next generation of LHL plants.

Although there exists a broad base of research into the performance of LHL processes no references were found to articles that specifically study the impact of ambient temperature on the performance of the liquefaction process. The explanation for this is probably that the impact of cooling utility temperature on the optimum design of liquefaction process design is assumed to be relatively small since the bulk of the process operates well below ambient temperature. However, the results from similar studies into LNG process performance have shown that ambient temperature can have a significant impact on process performance [34]. The logical extension of the findings related to LNG plants is that the impact of ambient temperature on LHL is also likely to be significant. Additionally, given that LHL represents one of the most important process steps in a liquid based blue hydrogen supply chain, the impact of ambient temperature is also likely to be significant for whole energy supply chain.

2.1.3 CO_2 Compression Modelling

CCS has been a research topic that has received a lot of attention over the last decade. The study of Wang et al. [35], for example, recorded more than 200 articles published in Canada in the year 2018 and more than 1600 published in China in the same year. The earlier study of Li, et al., [36] found more than 4000 total CCS related publications in 2017. However, of the varied research topics identified in these reviews, the capture elements of CCS are found to be more often studied that the transportation of CO_2. In their assessment of 'The co-occurrence network of CCS keywords', Li, et al. found 78 examples of 'Capture' within 'CCS' but only 15 examples of 'Transport'.

The focus on capture of CO_2 rather than the transport of CO_2 derives, in some part, from the fact that the capture element of a CCS chain is responsible for the main part of the energy consumption. The study of Lucquiaud, et al. [37] report that for an "nth of a kind CCS plant with current state-of-the-art solvent technology" the energy need by the capture plant will be 250-300 kWh of electrical energy per tonne CO_2 captured ($kWh_{el}/tonne_{CO2}$); whereas common estimates of the energy consumption for the compression of CO_2 for transport should lie in the range 90-120 $kWh_{el}/tonne_{CO2}$ [38]. However, the contribution of transportation is still significant and, as more advanced capture technologies are developed, may also grow in significance.

Transportation of CO_2 within CCS projects normally consists of CO_2 compression to above its critical pressure followed by transmission in pipelines. An alternative, discussed separately, is to liquefy the CO_2 at lower pressure and then transport it in tankers. CO_2 compression is generally viewed as a mature technology and *conventional* multi-stage centrifugal CO_2 compressor designs have been widely used in the fertilizer and petroleum industries for decades. It has been proposed by some authors that alternative approaches to compression, such the liquefaction of CO_2 at some intermediate pressure followed by pumping to pipeline pressure [39] or shockwave compression [40] will be more efficient than a

conventional compression process, but earlier associated research work has found that this is unlikely to provide a significant reduction in overall energy consumption [41].

Although research work has been published that studies the optimum design of CO_2 compression, for example looking at the optimum number of compression stages [42], or the recovery of heat from after-coolers [43], little has been done that analyses the particular impact that ambient temperature has on the optimization of the compressor design and the associated energy consumption. This research work is the subject of Article 2.

2.1.4 Modelling of CO_2 Liquefaction

The CO_2 liquefaction process is a good example of a process whose optimum design and performance could be expected to be impacted significantly by the temperature of the available heat sink.

Although the liquefaction and shipping of CO_2 is an established industry [44, 45], the scale and costs of planned CCS projects has placed a new focus on the energy efficiency of the CO_2 liquefaction process and several studies have looked at how the design can be improved. Over a decade ago, the study of Hegerland, et al. found that there we two main design alternatives: when low temperature cooling water is available, CO_2 should be used directly as a cooling medium; above some trade-off temperature, an in-direct ammonia refrigeration process is the best option [45]. Although many of the subsequent research publications have focused on the optimization of either the open-cycle CO_2 processes or closed-cycle ammonia refrigeration processes, others have also studied more novel approaches such as the use of absorption refrigeration [46], cascade refrigeration [39], and the application of turbo expanders [47]. The study of Alabdulkarem et al. compares a broad range of different schemes [39].

The chosen CO_2 transport pressure is an important design parameter for the liquefaction process. Hegerland [45] stated that "to reduce investment costs of storage and ship tanks, it is required to operate as close to the triple point of 5.17 bara and −56.6 °C as practically feasible." However, Aspelund et al. [48] and Lee et al. [49] studied 6.5 bara transportation pressure, and Decarre et al., [50] compared liquefaction at 7 bara and 15 bara, finding that transportation at 15 bara offers both lowest cost and lowest energy consumption. Seo et al., over the course of two papers, [51] and [52], also found that the overall cost was lowest for 15 bara cases. More generally, both Seo et al. [51], Alabdulkarem et al. [39], and Jackson et al. [41] found the optimum liquefaction pressure for the transportation of CO_2 by pipeline to be around 50 bara, which is above the practical limits for ship-based transport.

Hegerland et al. [45] and Lee et al. [53] also investigated the relationship between cooling temperature and liquefaction process performance. However, both studies only consider liquefaction at low pressure and Lee, et al. limit their study to the performance of open cycle CO_2 processes. Although not presented here as a main article, the performance of the CO_2 liquefaction process has been studied in two related publications [54, 55]. The approach adopted in these works was to study the impact of cold-sink temperature using a range of liquefaction flow-schemes using a range of potential liquefaction pressures.

2.2 RQ2 - CO_2 Transportation & Ambient Temperature

While the transportation of CO_2 both in high-pressure pipelines, and in low-temperature tankers is already practiced at industrial scale (as discussed earlier) the potential size and costs of planned CCS projects has motivated significant new research work related to the design and operation of CO_2 transportation systems. Notable focal points for research are the economics of different transportation

chain options, the selection of optimum operating conditions, risk management, and the accurate determination of CO_2 mixture properties—particularly phase equilibrium—at transportation conditions.

Although it is well documented that cubic equations of state (EOS) such as Peng Robinson and SRK generally form a suitable basis for modelling in many gas processing applications (for example, LNG liquefaction), greater uncertainty surrounds the modelling of CO_2 mixtures that are likely in CCS applications. The accurate modelling of the behaviour of CO_2 mixtures has been a research focus for several years now because of the potential impact on the cost and performance of CCS systems [56]. A particular focus is the phase behaviour of high-pressure mixtures of CO_2 with the contaminants expected in CCS projects [57-59]. For example, one of the important outputs of the EU funded IMPACTS project [60] was the publication a new high-accuracy EOS for the modelling of CO_2 rich mixtures, EOS-GC [59], which is made publicly available via the TREND software package [61].

Other aspects of CO_2 pipeline design that have been studied include heat transfer [62-64], transient flow behaviour [65] and economic optimization [66-68]. In the context of the economic basis for specific CCS projects the selection of the optimum transportation alternative is normally studied, for example by Jakobsen, et al. [69]. Also, to support the economic assessment of CCS projects in general, tools for modelling full CCS chains have been developed that allow comparison of different transportation cases, for example Jakobsen, et al. [70]. Studies have also been conducted into the identification of a more general economic trade-off distance between shipping and pipelines, for example Mallon, et al. [71].

Less research work has focused specifically on ship-based transportation, but there are still a large number of studies looking at both technical and economic aspects of CO_2 shipping [48, 72, 73] and, as discussed previously, particular attention has been given to the energy consumption associated with the compression and liquefaction processes [38, 39, 47, 52, 55, 74].

The research work described in this thesis is confined to the study of optimum pipeline system operating conditions and how the associated energy consumption is impacted by ambient temperature, which is not represented in the work described above. The present work does, however, build on the previous studies relating to the optimum design of CO_2 pipelines and in particular the modelling of CO_2 mixture properties through its use of the TREND properties package for the modelling of CO_2 mixture properties.

2.3 RQ3 – Energy Efficiency & Blue Hydrogen Supply

The comparison of different CCS based energy supply chains is a more specialized task that the study of either the individual elements that might constitute a particular supply chain or a group of elements that might work together to form, for example, a CO_2 transportation process. In the specific context of blue hydrogen production derived from Norwegian natural gas, the number of relevant studies is, therefore, quite limited.

Although the modelling of country, regional or world scale energy supply is conducted by a number of organizations, the fine details associated with specific energy supply chain alternatives is normally not specifically studied. For example, the recent study published by the Hydrogen for Europe research project[15] claims to address “the potential of hydrogen in decarbonizing the European energy system in

[15] https://www.hydrogen4eu.com/

a holistic and detailed manner" but does not study any single example of a hydrogen supply chain in detail. In addition, the basis for this study is proprietary and therefore cannot be interrogated to understand the details of the method.

A limited number of academic studies such as that of Stiller, et al., published in 2008 [75] have looked at different low-carbon energy supply chains linking Norway and Germany. Included in the study of Stiller, et al. supply chains based on LNG export from Northern Norway with SMR in Germany (Case 3a) were compared with liquid hydrogen export from Northern Norway (Cain 3b). And, alhough the focus of the analysis was an economic comparison of the pathways studied, the relative energy consumption was also considered. While the ecomomics of the two options (3a and 3b) were found to be similar in terms of a hydrogen product cost, the energy efficiency of the liquid hydrogen export route was found to be higher than that of the LNG export option. This resulted from the assumption that end product in both cases was only liquefied hydrogen. In this study a propriatory tool was also used to calculated costs and energy cosumtpions[16]. Another, more recent academic work, the study of Ishimoto, et al. [9], looked at the economics of two different liquefied energy supply chains based on the production of hydrogen and ammonia in Norway which was to be exported to Japan. In this work the main finding was that "close to meeting the 2030 hydrogen cost target of Japan", but no comparison was made against the export of LNG with hydrogen production in Japan.

Tools have also been developed aimed at the study of different CCS value chains, for example the iCCS tool developed by the BIGCCS centre [70], but no examples have been found that support an analysis where the specific benefit of low ambient temperature is of interest. The work described in this thesis is therefore unique in its aims and subsequently limited in the scope of its conclusions compared to the more general studies described above.

[16] http://www.e3database.com/

3 Research Method

The following section sets out some of the common themes related to the research method employed in each of the main articles. Some of the details presented here are reproduced from the individual main articles attached with this thesis, but at the same time, only a sample of the most important aspects of the method are presented here. The descriptions are split out under separate headings reflecting the relationship of each article to the three research questions.

3.1 RQ1 - Process Performance and Ambient Temperature

Two general aspects of the method underpinning the research work supporting RQ1 are briefly described under the first two headings; the method used in the modelling work for each of the three main articles supporting this part of the thesis is then described separately under three more headings.

3.1.1 Setting the Scope for Detailed Modelling

The method used in setting the scope of the work is accurately described as an evolutionary process, meaning that the scope was not fixed until several of the initial research activities had been completed. The scope of these initial works was generally based on experience gained in other, related research work, which is described above under Heading 1.2, Motivation. Some of the early work on CO_2 compression was also published as a poster at TCCS9 [54]. The knowledge and experience gained from the write-up and presentation of this early work helped to point the way for later activities and the scope for the detailed modelling work. Table 4 presents a retrospective summary of the process used to set the scope of work, including an illustration of the qualitative assessments used in the process.

Table 4 – Summary of the Approach Used for Process Modelling.

System Element	Energy Consumption	Temperature Dependency	Article	Modelling Approach
Natural gas processing	Low	L	Article 6	Factors from literature
NG pipelines	L	L	-	Not modelled
LNG Liquefaction	High	H	Article 1	Detailed modelling
LNG shipping	L	L	-	Not modelled
CO_2 Compression	Medium	M	Article 2	Detailed modelling
CO_2 Pipelines	M*	M*	Article 4 Article 5	Detailed modelling
CO_2 Liquefaction	M	H	**	***
CO_2 Shipping	L	L	-	Not modelled
Hydrogen liquefaction	H	H	Article 3	Detailed modelling
Hydrogen reforming	H	L	Article 6	Factors from literature
Hydrogen shipping	L	L	-	Not modelled
CCGT with CCS	H	L	Article 6	Factors from literature

* Impact from link to compression, ** Optimization of the CO_2 Liquefaction Process-Performance Study with Varying Ambient Temperature [55]. *** Not part of this work

3.1.2 Setting a Common Modelling Basis

One key objective for all the work presented here is to develop process performance data on a common basis that facilitates the combination of performance data for different units in a model of larger energy supply chains. The aim of this is to allow a realistic comparison of the performance of the different energy supply chains consisting of a mixture of different process units with different geographic locations. One example of how this was implemented is that the efficiency of all large centrifugal compressors is considered to be 85% isentropic across all of the studies presented in this thesis.

Another important general aspect of setting the modelling basis was to follow a common philosophy to the selection of the technology employed in each of the process units studied in detailed modelling. Although the approach varied in detail from article to article, the philosophy in all cases was to identify the most likely near future state-of-the-art (SOA) for each process considered.

The same principle was applied to the basis used in all cases for fluid properties modelling. To benefit from SOA properties predictions methods (as described above under Heading 2, Literature Review) the TREND software was used in this work when modelling of CO_2 rich systems is required. When modelling hydrocarbon mixtures, the SRK EOS has generally been used to facilitate validation exercises against reference studies.

Finally, the range of cold-sink temperatures used as the basis for all modelling and optimization work was set based on the open access data for global SST available from the Japan Meteorological Association [76]. Additionally, in all cases the cold-sink temperature, T_S, is assumed to be an ambient temperate, T_{Amb}, which is in turn considered to be equal to SST, T_{SST}. In all cases the temperature of all process streams that are cooled against the cold sink, T_c, are then assumed to have a temperature approach of 5 °C to T_{SST}:

$$T_C = T_{SST} + 5\ °\mathrm{C}. \tag{3}$$

Further details of how this common basis was applied in each of the detailed modelling and optimization studies that support RQ1 is set out below under separate headings for each article.

3.1.3 Article 1 – Modelling & Optimization of LNG Liquefaction

The research work presented in Article 1 includes the modelling and optimization of several different LNG liquefaction processes. For the purpose of this thesis, the LNG process that is considered most consistent with defining process performance in the context of near future SOA, is the MFC process used at the Melkøya LNG plant. Consequently, the summary of the method provided below focusses only on the modelling and optimization work conducted for the MFC process in Article 1.

When modelling processes such as LNG liquefaction, the standard approach in industry is to use a flowsheet type modelling package such as Aspen HYSYS[17]. This type of modelling package offers a user-friendly modelling environment with a range of EOS, pre-defined equipment templates and optimization routines, along with many other industry-focused features. However, the optimization of processes where the process configuration itself is a variable is not facilitated by this type of modelling environment. For this reason, in Article 1, a split approach to modelling and optimization was adopted

[17] https://www.aspentech.com/en/products/engineering/aspen-hysys

with Matlab used for pure component cascade type processes and HYSYS used for the MFC process. Consistency between the two approaches was demonstrated by comparing several sets of results.

In Article 1, the basis for modelling the MFC process was taken from the study of Jensen et al [77]. Initially, a replica of the case optimized by Jensen, et al. for a cooling temperature of 11 °C was compared to the model developed in the new study using HYSYS for the purpose of validation. Following this, an optimization study was conducted that looked at how design parameters and performance were affected by the temperature used for the cold sink. The scope of the optimization study was simplified by setting the outlet temperature for the pre-cooling process as a constant, which thereby fixed operating parameters in the second and third MR stages. The optimization parameters were then limited to the composition and flowrate of the mixed refrigerant used in the pre-cooling stage, MR1.

The optimization process itself was carried out using the HYSYS 'original' optimizer method using the 'mixed' method, which is based on a combination of the in-build BOX and SQP algorithms. The objective function was defined as the compression power and two constraints were used to ensure a minimum temperature approach in each part of the pre-cooling exchanger was maintained. Bound constraints were also applied to the MR1 composition to help reduce calculation time spent exploring infeasible solutions. The process was optimized across a range of cold-sink temperatures consistent with operation in Northern Norway based on SST data from JMA as described earlier.

3.1.4 Article 2 – Optimization of the CO_2 Compression Process

The aim of the optimization study conducted in Article 2 was, again, to find the variation in energy consumption with ambient temperature. Based on earlier work that had compared the performance of several options for unconventional compression approaches [41], the near future SOA for compression technology was set as a conventional multi-stage centrifugal design. Also based on earlier work, the approach selected for optimization was to search for minimum energy consumption allowing the number and pressure-ratio of the compressor stages to vary. Three CO_2 mixture compositions were considered to represent pre, post and oxyfuel CO_2 capture. The basis for the mixture compositions used was selected from the literature.

The model developed to support the optimization approach was constructed in MATLAB to allow CO_2 mixture properties to be easily called from the TREND properties package [61]. Building custom process models in MATLAB also facilitated a high of flexibility in model construction and access to the large number of build-into optimization algorithms. In the case of the CO_2 compression study a mixed approach to optimization was used with both the deterministic type Fmincon and Fminsearch algorithms used in combination with the stochastic type 'genetic' algorithm, GA. Initial runs were made with the deterministic algorithms followed by runs using the GA. In this way, reasonable initial guesses could be quickly found that formed the basis for the slower, but more accurate stochastic algorithm.

The optimization variables used were the compressor stage pressure ratios, Pr_i, of which $n-1$ could be optimized, the final stage pressure ratio, Pr_n, being determined from the other stages and the compressor discharge pressure. Two cases were studies: one where there was no upper bound on Pr_i and one where $Pr_i < 2$. In both cases, a lower bound, $1.2 < Pr_i$, was used to avoid unrealistic solutions. To avoid two-phase conditions at the inlet to any compressor stage, a constraint was used in the form of a penalty function that had the aim of maintaining a minimum approach to the dew-point pressure at each stage inlet.

3.1.5 Article 3 – Optimization of Hydrogen Liquefaction

The likely near-future SOA for hydrogen liquefaction was determined by a review of the studies identified in the earlier literature search. The study of Skaugen et al. [29], which is based on the design of a MR pre-cooled Claude cycle type liquefaction process, was taken as the basis for the optimization study presented in Article 3. As with the earlier study work looking at LNG liquefaction, the break-point temperature for the pre-cooling process was not used as a variable, which allowed the optimization of the MP pre-cooling process to be studied in isolation from that of the Claude cycle. However, the impact of ambient temperature on the low-temperature part of the hydrogen liquefaction process was taken into account in terms of the impact that reduced aftercooler temperature has on the Claude cycle refrigerant compressor.

The model used in Article 3 was again built in MATLAB to allow access to the wides range of deterministic and stochastic optimization algorithms available. MR properties were calculated using the SRK EOS as implemented in the TREND properties package to facilitate model validation, which was done against results from the study of Skaugen et al. [29].

Based on an initial phase of testing, the *fmincon* algorithm with sequential quadratic programming, (SQP) options was found to provide a fast and accurate solution. To help avoid local minima, the final results for the study were determined by testing the solution against a range of initial starting points generated using the *MultiStart* and *GlobalSearch* algorithms. Since the process was optimized across a range of cold-sink temperatures, the consistency of each optimization problem solution could also be compared against the value obtained for neighbouring temperature levels.

The objective function in all cases was the MR compressor shaft power. The optimization variables were the MR composition and the MR compressor discharge pressure. A constraint was used to meet a minimum temperature approach target in the main exchanger and a set of bound constraints were used to limit the search area to likely feasible solutions.

3.2 RQ 2 - CO_2 Transportation and Ambient Temperature

The approach used to answer this research question is divided into two parts: the development of a general model for CO_2 transportation in pipelines, which builds directly upon the performance data resulting from Article 2; and the application of the CO_2 transportation model to generate performance data for the specific transportation chains of interest to RQ3. The first part of this work is described in Article 4, the second in Article 5. A summary of the method used in each article is set out below under separate headings.

3.2.1 Article 4 – Developing a Model for CO_2 Pipeline Transport

Article 4 describes the development of a model for the pipeline transport of CO_2 from an assumed costal source to a sub-sea reservoir. The aim of the model is to provide a basis for estimating the energy consumption associated with the transportation process. The way the model does this is to calculate a pipeline pressure profile based on the depth and location of the storage reservoir and convert this into a required compression duty based on the performance maps developed in Article 2.

The method used to develop the pressure profile is to break the pipeline down into a large number of small segments across which the density of the flowing CO_2 stream is assumed constant. The frictional pressure drop is then calculated based on the length of each segment and any static pressure loss (or

gain) determined by the elevation profile. The pipeline elevation profile is generated automatically based on bathymetry data from GEBCO using functions from MATLAB's Mapping Toolbox[18]. The method used to calculate the elevation profile is validated against a reference case. The pressure drop calculations are verified against an identically specified model that was developed in HYSYS.

As illustrated by Figure 4, the minimum acceptable pipeline operating pressure is set 10 bar above bubble point of the mixture and the pipeline inlet pressure calculated as the minimum pressure that meets this constraint while also meeting the required pipeline outlet pressure. The required pipeline outlet pressure is defined by a set of reservoir over-pressure cases that are intended to represent the conditions that are likely to exist over the lifetime of the reservoir.

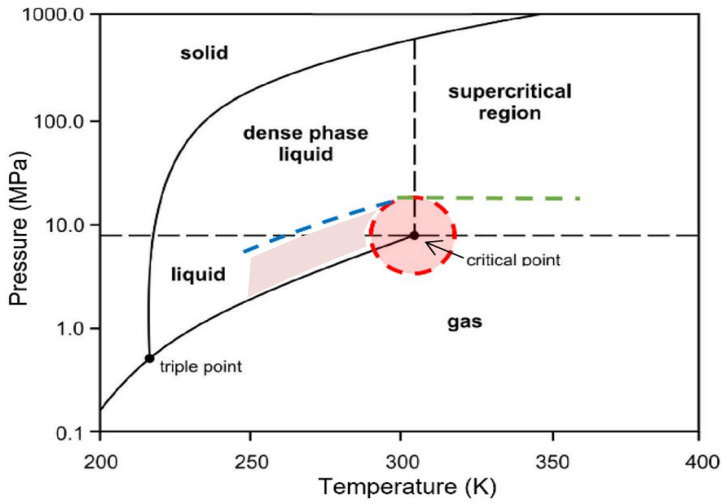

Figure 4 – Illustration of The CO_2 Pipeline Operating Pressure Limits Used in Article 4.

The pipeline diameter used in the model is calculated from the given flowrate and an upper constraint on the pipeline operating pressure of 180 barg. Results for three pipeline diameters that meet this constraint are provided as results by the model.

Since the particular focus of this work is to study the impact of ambient temperature on process performance, the model also takes into account the operating temperature within the pipeline based on SST data made available by the Japan Meteorological Association [76]. The data from JMA is used in a way that ensures that the seawater temperature used in design calculations, T_{SST}, is represents maximum normal temperature for 95% of the mean SST across the year:

$$T_{\mathrm{SST}} = \mathrm{SST}_{\mathrm{mean}} + 2\sigma \tag{4}$$

where $\mathrm{SST}_{\mathrm{mean}}$ is calculated from monthly data over the period 2009-19. A summary of the main parameters used in the model is presented in Table 5.

[18] https://www.mathworks.com/products/mapping.html

Table 5 – Summary of the Main Parameters Used in the CO_2 Pipeline Model in Article 4.

Parameter	Value	Basis
Seawater temperature, T_{SST}	$\text{SST}_{\text{mean}} + 2\sigma$	Monthly average 2009-19 [76]
CO_2 pipeline elevation profile	Case specific	GEBCO's gridded bathymetric data set
CO_2 pipeline min. pressure, P_{min}	DPt + 10 bar	Assumed margin
CO_2 pipeline heat transfer, U	4 W/m^2-K	Sensitivity study conducted
CO_2 pipeline roughness, e	15 µm	Sensitivity study conducted
CO_2 pipeline Max. pressure, P_{max}	180 barg	Pipe specification break

3.2.2 Article 5 – Case Studies for CO_2 Pipeline Transport

The Global CCS Institute (GCCSI) maintains a database of CCS projects worldwide and produces an annual report on the status of CCS[19]. In the 2020 report the GCCSI identify "65 commercial CCS facilities in various stages of development globally". Many of these projects are in the early development phase, but they often publish studies supporting their plans. To allow the modelling work that is the aim of this project, the data needed includes planned CO_2 pipeline routes and storage location characteristics such as reservoir depth. This data was found to be available for three projects that were therefore identified as the basis for Article 5: Case 1, the Langskip CCS project[20]; Case 2, the proposed H21 project[21]; and Case 3, the operational Melkøya CCS project. A summary of the data used in Article 5 as the base description for these projects is presented below in Table 6.

Table 6 – Cases Identified for CO_2 Transportation Chain Modelling (Article 5, Table 2).

Parameter	Case 1	Case 2	Case 3
Source location	9.69 E, 59.06 N	0.12 E, 53.65 N	23.59 E, 70.69 N
Liquefaction location	9.69 E, 59.06 N	-	-
Compression location	-	0.12 E, 53.65 N	23.59 E, 70.69 N
Pipeline location	4.89 E, 60.56 N	0.12 E, 53.65 N	23.59 E, 70.69 N
Pipeline length (km)	107	129	151
Reservoir location	3.42 E, 60.45 N	2.00 E, 54.00 N	4.89 E, 60.56 N
Wellhead depth (m)	300	76	318
Reservoir Depth (m)	2000	1300	2500
Sea Temperature, T_{SST} (°C)*	15.3	18.0	10.9

*$T_{SST} = SST_{mean} + 2\sigma$ based on monthly average 2009-19 [76].

The aim of Article 5 was to study the sensitivity of the transportation model developed in Article 4 to a variety of design parameters including ambient temperature. The method used to study ambient temperature was to apply a modification to the standard value calculated by the model based on JMA SST data as described earlier. The results were summarized for the default pipeline size selection: the first pipeline size that results in a pipeline pressure under 180 barg. Subsequently, the results generated in Article 5 were used as part of the basis for Article 6.

[19] https://www.globalccsinstitute.com/resources/global-status-report

[20] Langskip CCS: For at Norge og EU kan nå sine klimamål (ccsnorway.com)

[21] H21 (https://h21.green/)

3.3 RQ3 – Energy Efficiency & Blue Hydrogen Supply

RQ3 is answered by the research work summarised in Article 6. The method used can be broken down into four main parts: defining the study cases, the development of the modelling approach, the development of the performance comparisons and the development of several sensitivity studies.

3.3.1 Article 6 – Defining the Study Cases

The objective of RQ3 is to study the performance of hydrogen energy supply from Norway to the UK. Taking the CO_2 transportations studied in Article 5 as the basis, the source of the natural gas used in Article 6 was set as the Snøhvit LNG plant located at Melkøya in northern Norway and the supply point for the hydrogen product set as Teesside in the northeast of the UK. Two supply chain configurations were then defined: Scenario 1 with LNG export from Norway and hydrogen production in the UK, also referred to as the *conventional* case; and Scenario 2, with hydrogen production at Melkøya and liquid hydrogen shipped to the UK. The process units making up these two supply chains are summarised below in Figure 5 and Figure 6, which are reproduced from Article 5.

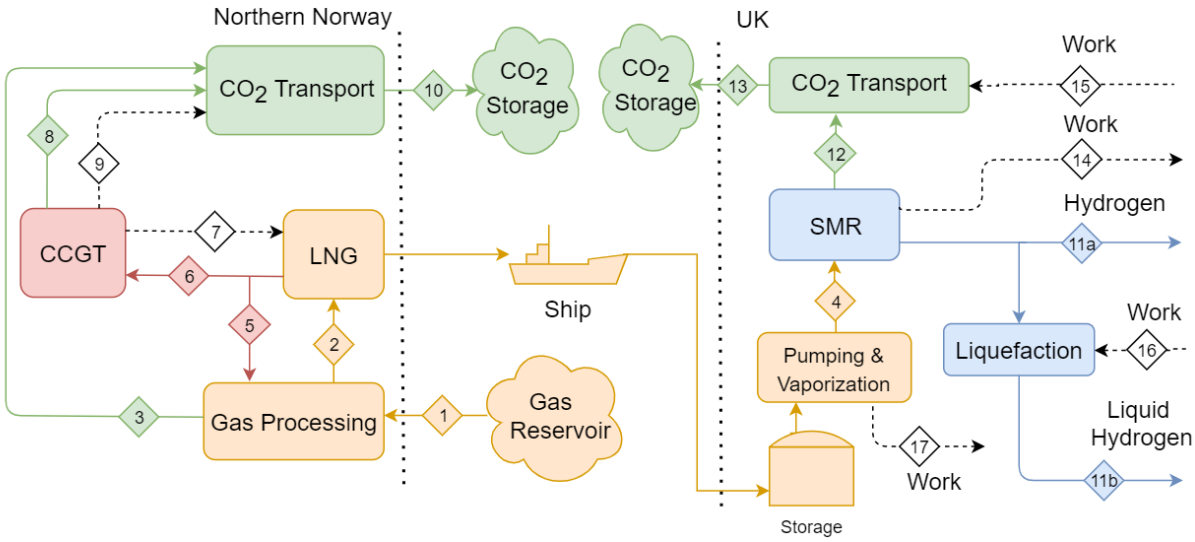

Figure 5 – Main Process Units, Material and Energy Flow for Scenario 1 (Article 6, Figure 1).

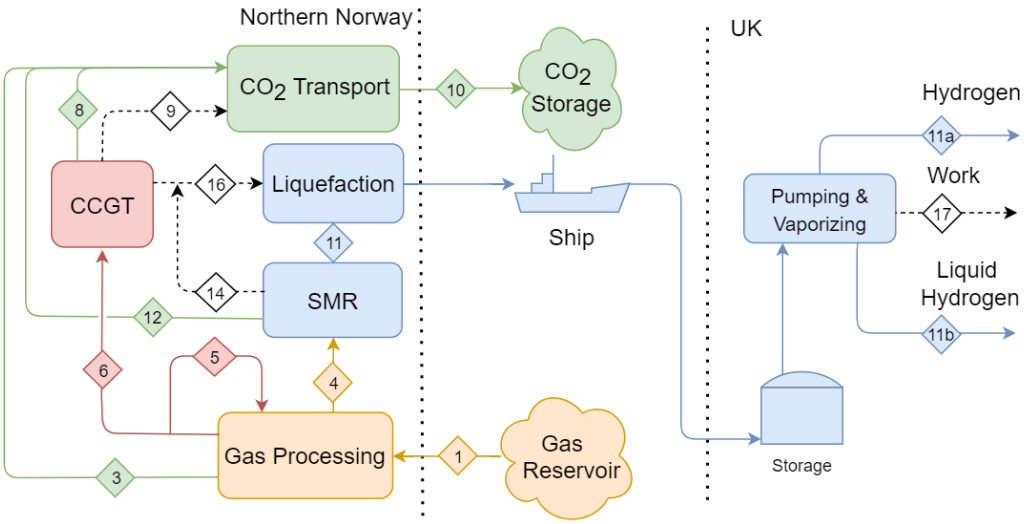

Figure 6 – Main Process Units, Material and Energy Flow for Scenario 2 (Article 6, Figure 2).

3.3.2 Article 6 – Model Development

The model that was developed to estimate the performance of the two hydrogen supply chains described above was constructed in MATLAB. The model consisted of a set of material and energy balances that were defined using performance factors for each of the process units identified. The feed gas composition was based on the DECARBit project [78] and the CO_2 and Hydrogen products were assumed to be pure component streams. The flowrate of utility streams, such as cooling water, were not calculated.

The performance factors used in the model were, as far as possible, taken from earlier work. Where elements in the chain had not been modelled earlier in detail, the method employed was to identify a suitable modelling approach based on performance data from the literature. A particular focus of the performance factors used from earlier work was that they were incorporated into the model as temperature dependant parameters, which would allow the sensitivity of the results to ambient temperature to be studied. Table 4 provides a summary of the temperature dependant performance parameters used in the model, which were extracted directly from the results of Article 1, Article 3 and Article 5.

Table 7 – Temperature Dependant Performance Parameters (Article 6, Table 4)

Ambient Temperature, T_{SST} (°C)	LNG Energy Consumption, f_{LNG} ($\mathrm{kWh/tonne_{feed}}$)	LHL Energy Consumption, f_{HL} ($\mathrm{kWh/kg_{H2}}$)	CO_2 Transport, Norway basis, $f_{\mathrm{CO_2,NW}}$ ($\mathrm{kJ/kg_{CO2}}$)	CO_2 Transport, UK basis, $f_{\mathrm{CO_2,UK}}$ ($\mathrm{kJ/kg_{CO2}}$)
5.0	187	5.92	296	-
10	196	6.05	310	308
15	207	6.19	324	322
20	217	6.33	339	336
25	230	6.48	-	354

3.3.3 Article 6 – Performance Comparisons

In setting the scope of the modelling work, it was decided to consider only the process units that are necessary in the energy supply chain. This approach resulted in a combination of electrical power and hydrogen fuel supplied to the interface with the end user in the UK. Process performance was therefore calculated in terms of the total energy supplied to the end user on two basis: total heat supplied, E_{ht}, which assumes fuel is burnt in a conventional boiler and electrical power converted to heat using a heat pump; and total electrical energy supplied, E_{el}, with fuel converted to electrical energy in a fuel cell. An exergy efficiency, η_{Ex}, of the overall process and exergy losses associated with each unit were also calculated to provide a more complete view of how the performance of each unit contributed to the performance of the overall energy supply chain.

$$E_{\mathrm{el}} = \sum \dot{W}_i + \dot{Q}_{\mathrm{H2\rightarrow el}} \tag{5}$$

$$E_{\mathrm{ht}} = \mathrm{COP} \sum \dot{W}_i + \dot{Q}_{\mathrm{H2\rightarrow ht}} \tag{6}$$

$$\eta_{Ex} = \frac{\sum \dot{W}_i + \sum Ex_{\mathrm{prod}}}{Ex_{\mathrm{feed}}} \cdot 100\% \tag{7}$$

where $\dot{W}_i$ are the work flowrate streams interfacing with the end user, $\dot{Q}_{\mathrm{H2\rightarrow el}}$ is the electrical power equivalent of the energy supplied in the hydrogen product, COP is the coefficient of performance of a

heat pump, $Q_{\mathrm{H2\rightarrow ht}}$ is the heat equivalent of hydrogen supply, Ex_{prod} is the exergy of product stream and Ex_{feed} is the exergy of the feed stream.

The physical exergy associated with material streams was calculated based on enthalpy and entropy data provided by the TREND properties package. Chemical exergy was based on the standard values given in Ertesvåg, at al. [79] and the stream composition from the material balance. The exergy destruction for each unit, Ex_{D}, was defined simply by a balance of the inlet and outlet streams:

$$Ex_{\mathrm{D}} = \sum Ex_{j,\mathrm{in}} - \sum Ex_{j,\mathrm{out}} \tag{8}$$

where $Ex_{j,\mathrm{in}}$ is the exergy of an inlet stream to unit j and $Ex_{j,\mathrm{out}}$ is the exergy of an outlet stream from unit j. Following the same approach taken for material and energy balances, the exergy associated with cooling utilities, the inlet air flow to the CCGT and its flue gas (post CCS) were omitted from the assessment.

In Scenario 2 the liquefaction of hydrogen is an integral part of the supply chain, but in Scenario 1 gaseous hydrogen is the main product. The relative performance of these two scenarios therefore depends strongly on the delivery conditions of the hydrogen product: comparing on a liquid hydrogen basis will always favour Scenario 2 and on a gaseous product basis it would be natural to assume that Scenario 1 is generally more efficient. The approach taken to study the relative performance of these two scenarios was to extend them into a range of sub-scenarios. Scenario 1a was defined as a version of Scenario 1 where hydrogen is supplied to the end user in the gas phase (i.e., typical of a scenario for UK gas-grid conversion to hydrogen). Scenario 1b is a version of Scenario 1 where hydrogen is supplied as a liquid (e.g., for use as transport fuel). Likewise, Scenario 2a is a version of Scenario 2 parallel to 1a, where the gaseous hydrogen is the product, and Scenario 2b is a parallel to 1b.

3.3.4 Article 6 – Sensitivity Studies

To provide a better understanding of the results generated for the base-case in Article 6, several sensitivity studies were made to investigate the performance of the model where significant uncertainty existed regarding process performance parameters. One of these looked at the performance of the SMR process. Two alternative cases were studied: A1 based on ‘Case 3’ from the study of Collodi, et al. [80] and A2 based on the ‘SMR HTLT MDEA 90’ case from the study of Antonini, et al. [81]. The parameters used in the sensitivity cases are presented in Table 8.

Table 8 – Sensitivity Study Parameters for SMR Performance (Article 6, Table 3).

Parameter	Base	A1	A2	Units
SMR efficiency, η_{SMR}	0.620	0.691	0.778	$\mathrm{kW_{H2}/kW_{feed}}$
SMR power generation, f_{SMR}	0.081	0.015	0.010	$\mathrm{kW_{el}/kW_{feed}}$

Another sensitivity study looked at how ambient temperature affected the relative performance of the two supply chain scenarios. The method used in this study was to apply a temperature modification to the base–case cooling temperature used in the model for the Norwegian end of the supply chain. The aim of this was to provide some insight into the impact on performance if the supply end of the same energy supply chain was located in a warmer climate, e.g., southern Norway or Northern Europe. The results of this work are presented in the following section of this report.

4 Results

4.1 RQ1 - Process Performance and Ambient Temperature

4.1.1 Article 1 – LNG Process Performance

Article 1 studies the impact of ambient temperature on the energy consumption associated with LNG liquefaction. The main aim of this article, in the context of this thesis, is to supply temperature dependant performance data that can be used in the modelling of energy supply chains where LNG liquefaction forms one of the links. In Article 1, several different LNG processes are studied. In this thesis, only the performance data associated with the MFC process is relevant to later work because it represents the near-future SOA for LNG process technology. Consequently, the results from MFC modelling work form the focus of the discussion presented below.

In Article 1, the specific energy consumption of the same LNG process located in three different parts of the world are compared. Figure 7 provides an illustration of this comparison for the MFC process. The main findings associated with this comparison is that "… the energy consumption of any optimized gas liquefaction process will be 20−26% higher in the Middle East or Northern Australia than in an Arctic climate such as that found in Northern Norway" (Article 1, Abstract).

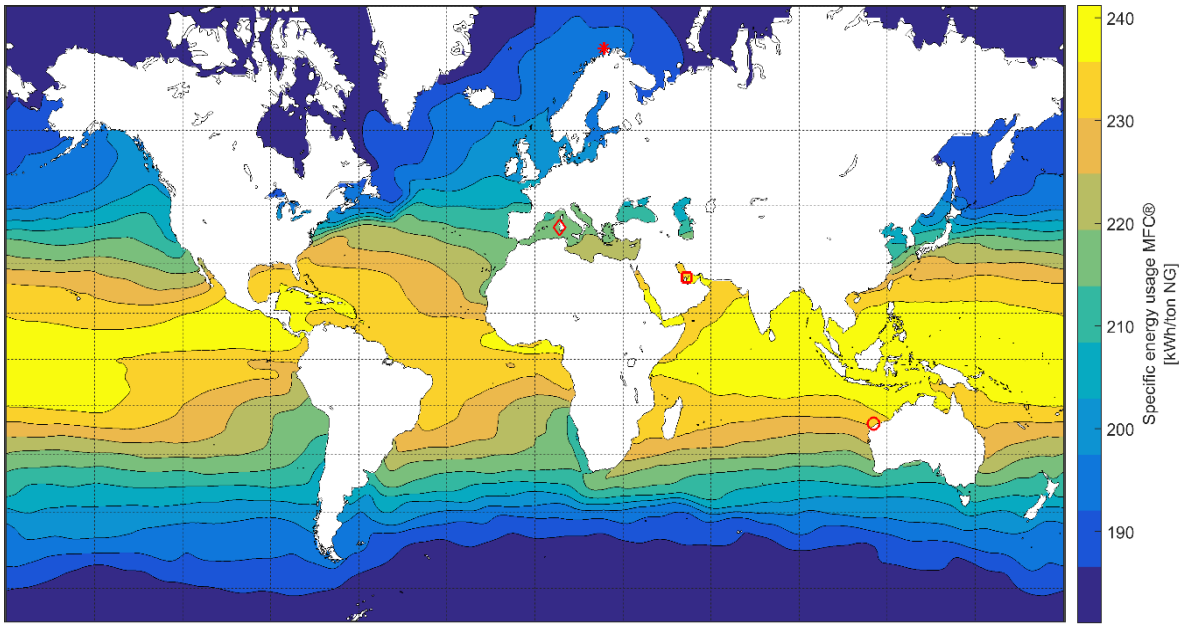

Figure 7 – Average Energy Consumption for the MFC® Process. Melkøya (Norway) Is Marked "", Oristano (Italy) is Marked "◊", Ras Laffan (Qatar) is Marked "□" and Barrow Island (Australia) is Marked "○" (Article 1, Figure 3)*

The importance of this result is two-fold: firstly, an LNG plant in a cold climate consumes less energy and, therefore produces lower CO_2 emissions if its own energy supply come from natural gas; secondly, if CO_2 emissions are lower, then the energy consumption associated with capturing the emissions from this process are likewise reduced. If the energy consumption of the CO_2 transportation also benefits from low ambient temperature, the percentage marginal improvements are multiplied together, and the advantage will grow. This forms the motivation for later work.

The results from Article 1 that are used directly in Article 6 are presented below in Figure 8. These results were used as the basis for the data presented in Table 7. Figure 8 shows how the energy consumption of various LNG liquefaction processes varies with ambient temperature for three different

LNG process designs. In Article 6 only the results for the MFC process are used since this is taken to represent the near future SOA for LNG liquefaction processes. For this process, the results presented in Figure 7 show that the energy consumption of the process falls by around 10% as the average temperature of the medium used for cooling the process falls from 30 to 20 °C.

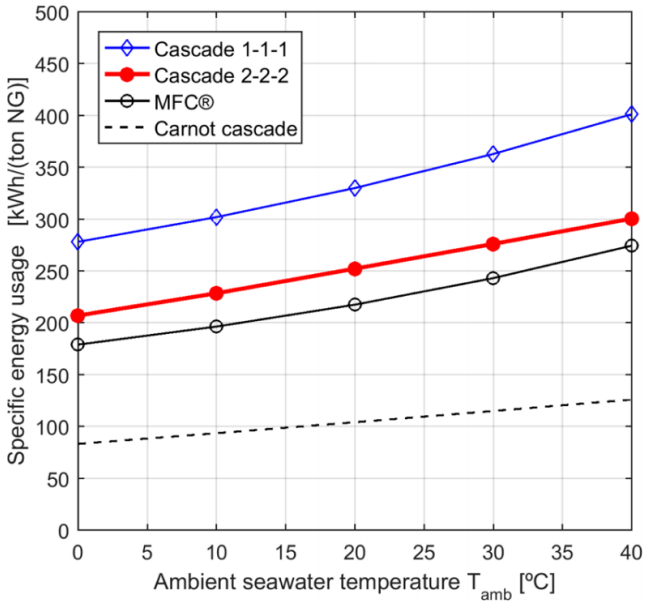

Figure 8 – Specific Energy Usage for Different T_{amb} (Article 1, Figure 8).

4.1.2 Article 2 – CO_2 Compression Process Performance

In the study work associated with Article 2, three CO_2 mixture compositions were considered: post, pre and oxyfuel combustion. In Articles 4 and 5 a range of CO_2 mixture compositions were also studied, but in Article 6, only the post combustion capture is relevant to the scenarios considered and therefore, only the results for that case, which support RQ3 are discussed in detail here.

The main results from Article 2 constitute performance data showing how the energy consumption associated with an optimized CO_2 compression process varies with both ambient temperature and the discharge pressure from the compressor. A sample of the main results from this work is presented below in Figure 9.

In Figure 9 we can see that the impact of the cooling temperature on energy consumption is generally larger than the impact of the discharge pressure. Although this appears counter-intuitive, it is explained by the fact that final stage of the compression process occurs from above the critical pressure and, therefore, that the waste energy generated (exergy destroyed) in this last stage will be lower than that in the other stages because entropy varies less strongly with pressure under the dense-phase conditions present. The role of ambient temperature in determining energy efficiency for this process when it forms part of a CO_2 transportation chain is explored further in Article 5.

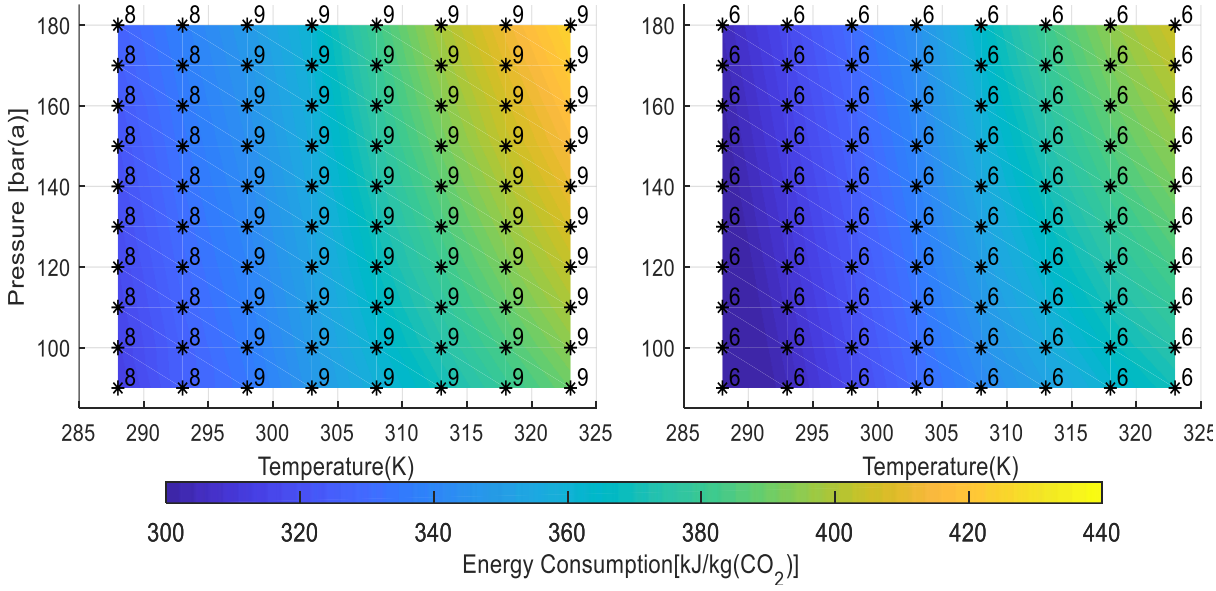

Figure 9 – Variation in Compression Energy Consumption and Optimum Number of Stages with Cooling Temperature and Discharge Pressure for (a) Constrained Cases (b) Unconstrained Cases (Article 2, Figure 7).

The importance of these results in the context of the overall thesis is that the performance maps developed—like the one presented in Figure 8—are used directly in the model described by Article 4 and subsequently as part of the basis for Articles 5 and 6. The main findings of this work were that "The results show that energy consumption is minimised through the use compressor designs with multiple impellers per stage and carefully optimized stage pressure ratios. The results form a performance map for a CO_2 compression process that is suitable for use in larger CCS system models." (Article 2, Absrtact).

4.1.3 Article 3 – Optimization of Hydrogen Liquefaction

In Article 1 the performance of an LNG liquefaction process is shown to vary significantly with the temperature of the cooling medium used as the cold sink. In Article 3, a similar study is presented for a hydrogen liquefaction process. Although the way in which the modelling work is implemented in Article 3 is different, many elements of the modelling approach are similar. The main finding of Article 3 is that "… energy consumption increases by around 20%, across the cooling temperature range 5 to 50 °C. Considering just the range 20 to 30 °C there is a 5% increase, illustrating the significant impact ambient temperature can have on energy consumption." (Article 3, Abstract).

Figure 10, shows how the energy consumption for both the MR pre-cooling process and the overall hydrogen liquefaction process are found to vary with cooling temperature. The data presented in Figure 9 is used as the basis for Article 6 is summarized in Table 7.

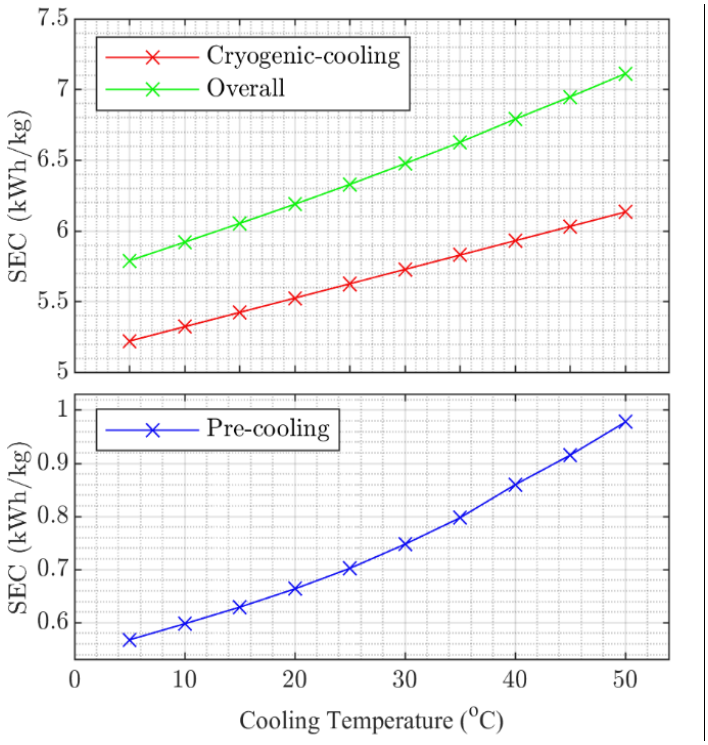

Figure 10 – Variation in Hydrogen Liquefaction SEC with Cooling Temperature (Article 3, Figure 8).

One notable feature of the results presented in Figure 10 is the contrast between the close to linear variation with temperature for energy consumption in the un-optimized cryogenic part of the cooling process with the non-linear variation visible in the results for the pre-cooling process. The linear behaviour in the cryogenic cycle reflects the fact that, although the duty of this part of the cooling process does not vary—since the pre-cooling temperature is fixed—its efficiency is affected to a small extent by cooling temperature. In the pre-cooling process by contrast, the non-linear behaviour reflects two things: firstly, that the both the cooling duty and the efficiency of the process are affected by the cooling temperature; and secondly, that the process is less well optimized at cooling temperatures above 25 °C.

Results presented in Article 3 show that above a cooling temperature of 25 °C, a better approach to optimum efficiency would be possible if additional, heavier, components were added to the MR blend. Further efficiency gains for the overall process may also be possible by adjusting parameters in the Claud cycle if the impact of varying ambient temperature was allowed to better cascade down into the lower temperature part of the process by allowing the break-point temperature between the MR and the Claude cycle to vary.

Another notable feature of the results presented in Figure 10 is that the percentage overall efficiency variation in Article 3 is smaller than the variation in efficiency for the LNG processes studied in Article 1. For example, in Article 1 increasing the ambient temperature from 20 to 30 °C results in around a 10 % variation in specific energy consumption (see Figure 7), whereas in the results presented in Figure 10 the same variation in cooling temperature only results to approximately 5 % variation in the SEC of the overall process. This is explained in part by behaviour of ideal cycles presented in Figure 2, which shows that the relative efficiency gain achievable reduces steadily as we move further away from ambient temperature. An additional factor here is that the proportion of the overall process

duty that is optimized in Article 1 is greater than in Article 3 thereby limiting the impact ambient temperature has on the overall process performance.

4.2 RQ2 - CO_2 Transportation & Ambient Temperature

4.2.1 Article 4 – Developing a Model for CO_2 Pipeline Transport

The aim of the work presented in Article 4 was the development of a model that could be used to estimate the energy consumption associated with CO_2 transport, including factors like pipeline route, reservoir characteristics and local ambient temperature. The model was developed using compressor performance data from Article 2, which was combined with SST data from JMA and bathymetry data from GEBCO to make a model of a full CO_2 transportation chain.

The main findings were not a set a performance data that could be used directly in later work, but the validation of the modelling approach. Figure 11 presents results from Article 4 that illustrate how the modelled pipeline elevation profile was validated against a reference profile and Figure 12 presents results illustrating how the pressure drop calculations were validated.

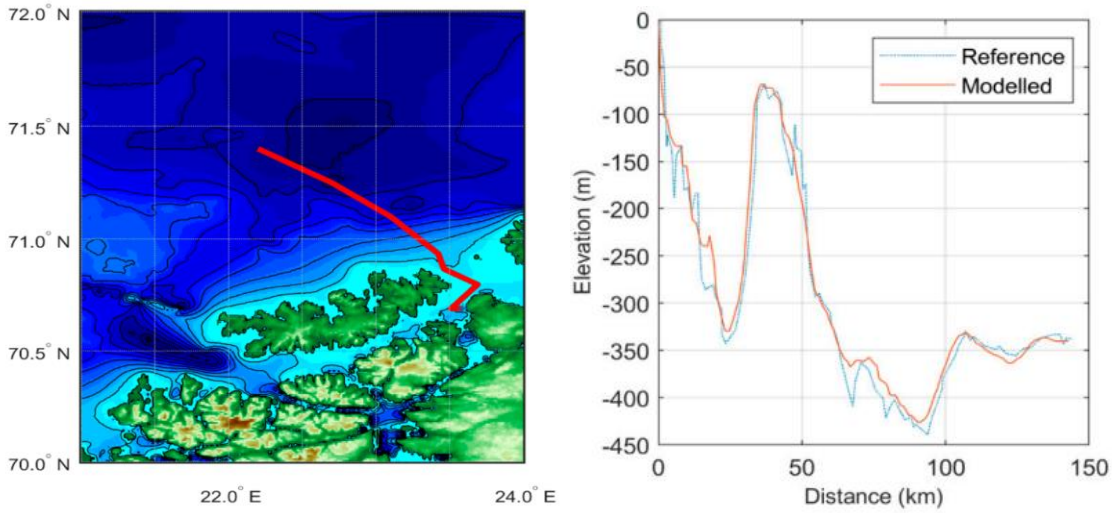

Figure 11 –Validation of a Model-Generated Pipeline Profile (Article 4, Figure 7 and 2b).

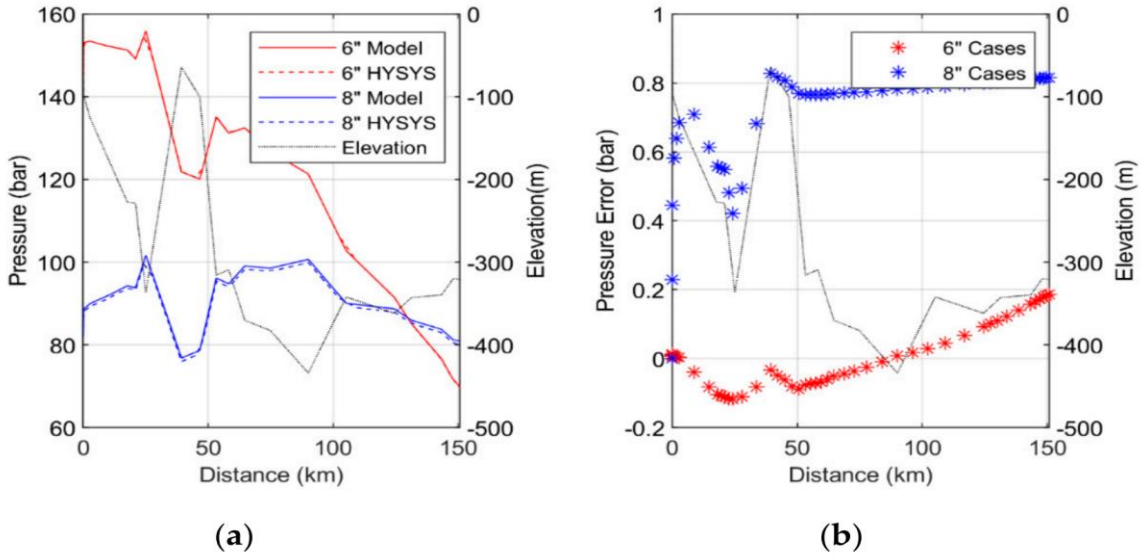

Figure 12 –Pipeline Pressure Drop Calculation Validation vs. HYSYS (Article 4, Figure 6).

The results presented in figures 10 and 11 illustrate very good agreement between the reference model and the data generated by the new model. As described in the Method section, the basis for the performance predications made by the transportation model is a minimum pressure condition limited by a 10 bar approach to the mixture dew-point temperature. Since the maximum pressure error illustrated in Figure 12(b) is a little under 1 bar, we can say with confidence that the design margin is sufficient from the perspective of pressure drop calculations. From the perspective of uncertainty in the dew-point calculation we can see in the work of Gernert, et al. [59] that the inaccuracy of phase equilibrium predictions made using EOS-GC (available via the TREND properties package) should be no higher than 2% [59], equating to less than 2 bar across the range of conditions of interest, which also falls within the range of acceptable accuracy from the point of view of model calculations. The validation of the model developed in Article 4 forms the basis for the work done in Article 5.

4.2.2 Article 5 – Case Studies for CO_2 Pipeline Transport

The aim of the work described in Article 5 was to provide performance data that could support the modelling work conducted in Article 6. Specifically, the energy consumption of two CO_2 transportation alternatives were selected for study: one located in northern Norway at Melkøya and the second located in the UK, which was based on the H21 CCS project. In Article 5 these two alternatives were compared to the performance of the planned Northern Lights CO_2 transportation project. The work consisted of several sensitivity studies, the most important of which being—in the context of this thesis—the comparison of the impact of ambient temperature on the three alternatives.

The results presented in Figure 13 show that the impact of ambient temperature on energy consumption is similar for all the cases considered. An exception to this is the behaviour of the Melkøya cases below -6 °C temperature modification, which results from a limit imposed in the model on the approach to the freezing point of water.

The results also show that ambient temperature appears to be the most important factor in determining energy consumption. For example, based on the data presented in Table 6 the different in the baseline cooling temperature, T_{SST}, between Case 3 (Melkøya) and Case 2 (Norther Lights, NL) is 4.4 °C and between Case 3 and Case 1 (H21) is 7.1 °C. If all cases are considered at the same T_{SST} as Melkøya, the data presented in Figure 13 (looking only at the data presented for pipeline transport) shows that the energy consumption for Melkøya is 311 kJ/kg, NL would lie between 309 and 312 kJ/kg (depending on the pipeline sizing basis) and H21 is 310 kJ/kg. By contrast, energy consumption for NL at the baseline value for T_{SST} lies between 319 and 323 kJ/kg, and for H21 it is 330 kJ/kg—i.e., 6% higher that the Melkøya case.

Looking also at the cases presented for shipping liquefied CO_2, Figure 13 shows that transporting CO_2 by ship is less energy efficient than using pipelines regardless of the ambient temperature available for cooling. Interestingly the shipping of liquid CO_2 from Melkøya is also more efficient than any of the other pipeline transport cases—apart from the Melkøya pipeline case. This, again, highlights the benefit that ambient temperature offers. The data presented in Figure 13 is used directly in Article 6 as the basis for modelling work is summarized in Table 7.

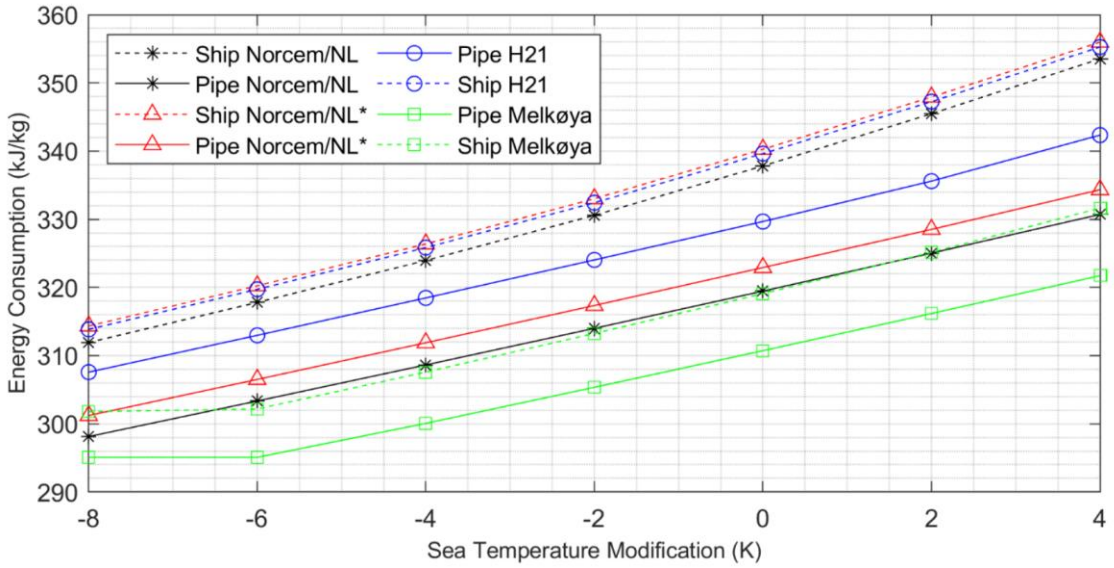

Figure 13 – Variation in Energy Consumption with Sea Temp. Modification. (Article 5, Figure 10).

4.3 RQ3 – Energy Efficiency & Blue Hydrogen Supply

4.3.1 Article 6 – Comparing Scenarios for Blue Hydrogen Supply

The main results of Article 6 are illustrate in Figure 14, which shows the total energy supplied to the end user on the three different basis described in the Method section: energy supplied considered as heat (E_{ht}), energy supplied considered as electrical power (E_{el}), and energy supplied considered on an exergy efficiency basis (Ex). Scenarios 1a and 2a are represented by the points where the fraction of liquid hydrogen supplied is equal to zero and scenarios 1b and 2b given by the points where the fraction liquid hydrogen supplied is equal to one. The most important feature illustrated by Figure 14 is that a trade-off point between Scenario 1 and Scenario 2 exists at some fraction of liquid hydrogen supplied for all measures of performance.

In more detail, the data presented in Figure 14 shows that if some un-defined mixture of both heat and power is the end product in both scenarios, the trade-off point between scenarios 1 and 2 can be said to lie between 65 and 75% fraction liquid hydrogen supplied. In the context of the two energy supply chains considered this trade-off point can be thought of generally as the trade-off between the energy required by the LNG process and the energy required by the hydrogen liquefaction process.

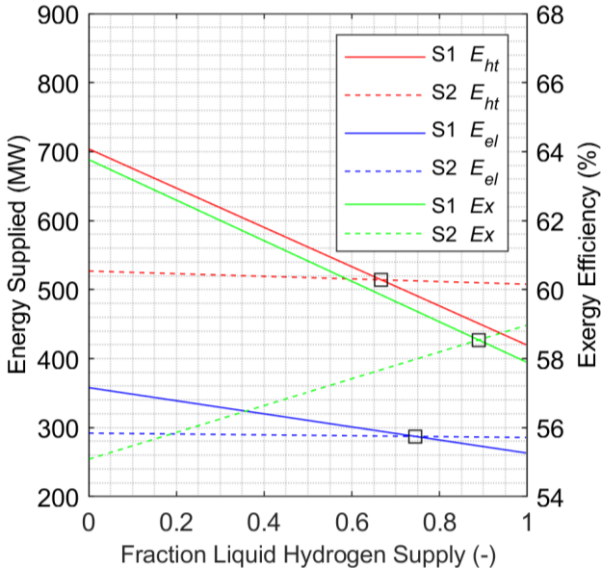

Figure 14 – Variation of Power, Heat and Exergy Efficiency. S1 = Scenario 1, S2 = Scenario 2 (Article 6, Figure 4)

The results presented in Figure 15 help to show how this trade-off point originates by illustrating where energy is wasted in each element of the supply chain. In all cases the exergy destruction associated with the performance of the SMR process is the largest contributor to the overall chain performance and thus important to gaining a good understanding of the results. The next highest level of exergy destruction is seen to be associated with the hydrogen liquefaction process and the CCGT, which in Scenario 2-a (S2-a) and Scenario 2-b (S2-b) is principally generating power for the liquefaction process.

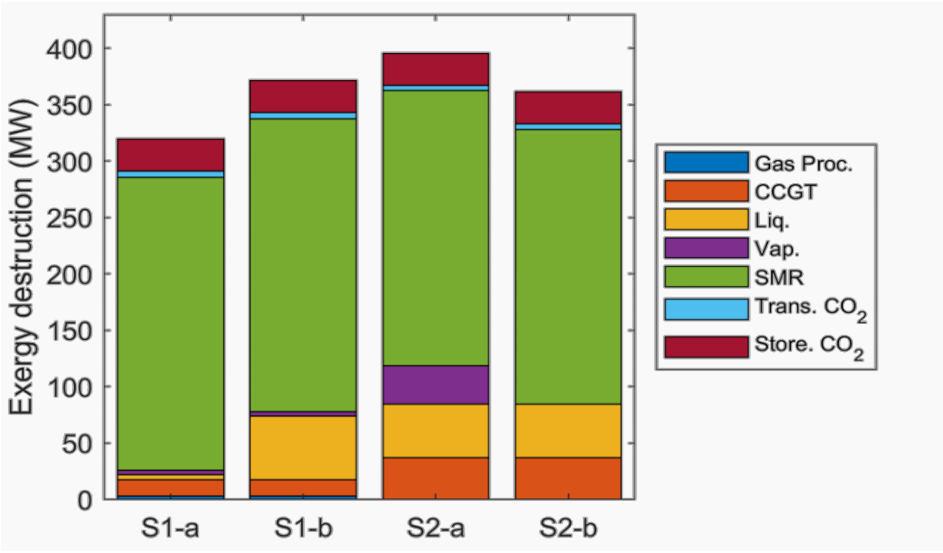

Figure 15 – Summary of Exergy Destruction by Process Unit (Article 6, Figure 3)

To gain a more robust understanding of the results, the sensitivity of the model predictions to the parameters used to describe the performance of the SMR process was tested using two alternative sets of performance parameters. Figure 16 presents the results from this sensitivity, which show a significant impact on the overall results in terms of the trade-off point between scenarios 1 and 2. It is notable that in both cases the trade–off point is lower.

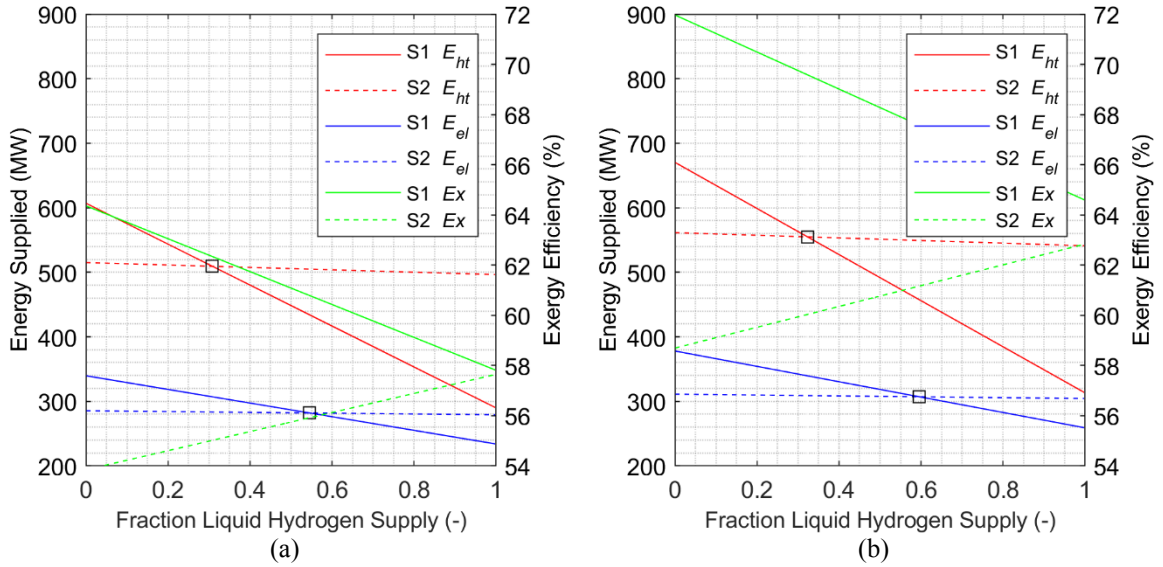

Figure 16 – Variation of Power (MW), Heat (MW) and Exergy Efficiency (%) with Fraction Liquid Supply for SMR (a) Case A1 (b) Case A2 (Article 6, Figures 5 & 6).

Assuming some mixture of heat and power being the end product of the energy supplied, Figure 16 shows that the trade–off point for these cases lies between 30 and 60% liquids supplied, much lower than the range of 65 to 75% found in the base case for SMR modelling. Also noticeable is that neither of these new cases deliver as much energy as Scenario 1a measured on a heat basis (E_{ht}), but the results in Figure 16 (b) do show increased energy delivered on a power basis (E_{el}) and exergy basis (E_{ex}). Indeed, relative to Scenario 1a, the results presented in Figure 16 (a) can be taken to indicate an overall reduction in supply chain efficiency, whereas Figure 16 (b) could be a generally more efficient supply chain. The fact that the trade–off point is lower than in Figure 15 reflects the important role played by of the balance between electrical power and hydrogen product delivered by the SMR process.

Because the performance of each process unit modelled reflects the ambient temperature at the geographic location in which it is placed, the impact of ambient temperature is built into in the results presented in Figure 14, Figure 15 and Figure 16. However, because the model is built using cooling temperature dependant performance parameters, the impact of variation in the temperature of the available cooling medium can also be studied.

Figure 17 illustrates how the trade-off point for liquids supply and the relative efficiency varies with cooling temperature. In Figure 17 the relative efficiency at the trade-off point is calculated using the efficiency of Scenario 1a, which in all cases represents the highest efficiency point. In this sensitivity study the modification to ambient temperature is only applied at the Norwegian end of the energy supply chain. The premise of this sensitivity study could be considered to be the illustration of the impact of less conservative approach to heat exchanger design (i.e., a reduction in the design value for the temperature approach used, $\Delta T = T_C - T_{\mathrm{Amb}}$), or indicative of the performance of a different (warmer) hydrogen production location (i.e., value of T_{Amb}), e.g., southern Norway, or northern Europe.

The results presented in Figure 17 show that even a small change in the cooling temperature can have an impact on the performance of the overall supply chain and the trade-off point between Scenario 1 and Scenario 2. It is notable in the results presented in Figure 17 show that a reduction in cooling

temperature both reduces the trade-off point for the fraction of liquids supplied and raises the efficiency at the trade-off point relative to the best performing scenario.

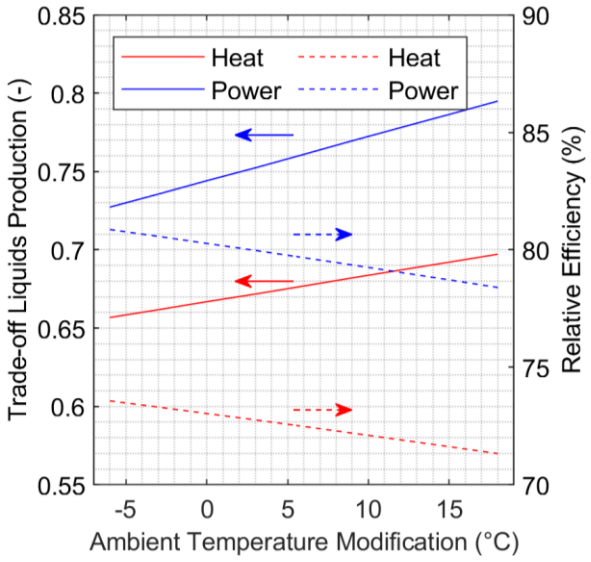

Figure 17 – Variation in Trade-off Liquid Product Fraction (left y-axis, solid lines) and Relative Efficiency (right y-axis, dashed lines) with Ambient Temperature (Article 6, Figure 7).

5 Discussion

Relationship between the articles

As illustrated by Figure 3 the six main articles that form the basis for this thesis build together to answer the three research questions posed in the introduction. The first three articles, supporting RQ1, are concerned with the performance of three important links in the supply of blue hydrogen based energy. The main objective of these articles is to generate performance data that can be used as the basis of later modelling work. Articles 4 and 5, supporting RQ2, use data generated from Article 2 to enable the study of the impact of geographic location and ambient temperature on the performance of three different CO_2 transportation chains. The data generated by articles 4 and 5 along with that supplied from articles 1 and 3 then form the basis of Article 6. The work presented in Article 6 combines results from earlier work in the study of two specific blue hydrogen based energy supply scenarios and provides an answer to question posed in RQ3.

Results

The results that support RQ1 are presented in Articles 1 to 3. The main findings of this work are that the impact of ambient temperature on the processes studied is significant. Taking the cooling temperature range 20 to 30°C, as an example, the impact on LNG process performance found in Article 1 is a specific energy consumption variation of approximately 10%. In Article 2 over same temperature range the variation in CO_2 compression energy consumption is around 8% (post combustion case) and in Article 3 the variation for the hydrogen liquefaction process is close to 5%. By way of comparison, the variation in heat rate for optimized CCGT designs over the much larger ambient temperature range 0 to 35 °C is found to be only 3% in the study of Arrieta and Lora [17].

The results supporting RQ2 are presented in Articles 4 and 5. The main findings here are that the performance of the CO_2 transportation chain is also significantly affected by ambient temperature and due to this, that the CO_2 transportation case based on Melkøya offers lowest overall energy consumption. Figure 13 shows that over a 10 °C range of cooling temperature variation the energy consumption of the Melkøya pipeline case varies by around 8%. In addition, the impact of ambient temperature is found to be more significant the other factors affecting performance such as pipeline and reservoir characteristics: Figure 13 shows that considered at the same ambient temperature, the energy consumption of all three cases considered lies within a 1% range.

The results from Article 6 illustrate the relative performance of two blue hydrogen energy supply chain scenarios under different modelling basis assumptions, which supports RQ3. The main finding of Article 6 is that an energy supply chain based on the production and liquefaction of hydrogen in northern Norway is more efficient than one based on hydrogen production in the UK when the proportion of liquid hydrogen product delivered is more than 75%. Subsequent sensitivity studies highlight the important impact that SMR performance can have on this result and show the small but significant role the temperature of the available cold sink plays in the relative efficiency of the two scenarios. The results from these two sensitivity studies show that the trade-off point between the two scenarios could be as low 30% liquid product.

Strengths of the work

One important strength of the work lies in the development and application of a consistent and robust approach to modelling. This approach allows the results from several separate pieces of study work to be combined in a reliable and transparent way. For example, a consistent approach was used in modelling the variation in the temperature of the available cold sink throughout the work, where

$T_{amb} = T_{SST}$, and a common approach was used to defining the temperature that a process rejects heat to ambient, where $T_C = T_{SST} + 5$ °C.

Another strength of the work is the use of advanced modelling tools and approaches. Examples of this include the application of a range of deterministic and stochastic algorithms in the optimization work and the use of advanced properties modelling packages for CO_2 rich systems. Although, the best method for modelling and optimization was considered on an article-by-article basis, consistency in approach was also maintained where possible. For example, the TREND properties package was used in all cases to model the properties of CO_2 rich systems. In addition, across all the work done a focus was placed on the validation of modelling results against suitable reference cases to provide firm foundations for the modelling work conducted.

Weaknesses of the work

An unavoidable weakness in the modelling and optimization studies conducted is the constraint of the optimization problems considered to a limited number of variables. For example, in the study of the hydrogen liquefaction pre-cooling process, the break point temperature between the pre-cooling step and the cryogenic cooling process could also have been considered as an optimization variable. A similar weakness in the modelling work associated with Article 6 could be identified as the omission of heat integration between the different gas process units. For example, a commonly studied enhancement for the design of CO_2 compression processes is the integration of compressor after-coolers with heat recovery as part of power generation. Another example is that in modern LNG plants, waste heat from power generation is often used as a heat source in the acid gas regeneration unit. Details such as these are omitted from the scope of Article 6 but could have a small impact on the results and may be worthy of further research work.

Limitations of the work

A number of limitations also apply to the work presented. For example, the work does not generally consider the impact of process equipment performance characteristics such as compressor performance maps. Similarly, it does not consider the interplay of process performance, design and economics, such as the trade-off between heat exchanger cost, size and temperature pinch. However, this approach is deliberate, both from the point of view of minimising the complexity of the process modelling conducted and from the perspective of focusing on the specific objectives of the work. In other words, in all of the optimization work conducted, the aim is not to study off-design performance, but to identify the best set of design parameters for a particular set of conditions and study how the performance of an optimized design is affected when the operating conditions (specifically ambient temperature) are varied. In this context, the use of simple, generic, performance parameters is more consistent with the objectives. However, an example where this level of simplification may be considered a weakness is in the modelling of aftercooler pressure drop in Article 2. In Article 2 the pressure-drop was set to a fixed value for all compressor stages, something that may unduly incentivise higher initial stage pressure-ratios in the optimization process. Further study of the CO_2 compression process with a multi-parameter approach where cost is also considered could address this weakness and other similar weaknesses in the work presented.

A separate limitation of the work is its focus purely on supply chain efficiency. In none of the work is a study of the economics of the different processes and supply chains made. Likewise, the greenhouse gas emissions associated with each scenario are considered only from a limited perspective, with no allowance made for fugitive supply-chain and life cycle emissions of methane, such as those associated with exploration, development and operation. As discussed in the introduction, the topic of fugitive

emissions associated with the consumption of natural gas has been the focus of significant recent debate, which has highlighted that this could represent a significant disincentive to the development of blue hydrogen projects. While Norway's natural gas production industry has lower emissions than many other countries, the impact of fugitive emissions may still be important to blue hydrogen production. It is therefore undoubtable that this aspect of supply chain performance is a limitation of the present work.

Another limitation of this study is its single focus on natural gas supplied in the form of LNG. Scenarios where natural gas is exported using existing pipeline connections between Norway and the UK or Europe as the basis are not considered in this work. In this work it is considered improbable that large-scale natural gas pipeline infrastructure is extended further north than its current limit at the Aasta Hansteen platform and in this context the results of the work remain unaffected. However, the efficiency of blue hydrogen production based on the export of pipeline gas from southern Norway will be significantly higher than that based on LNG gas exports from northern Norway and, therefore, no comparison can be draw between the scenarios considered here and pipeline gas based scenarios.

Implications of the work

The findings of Articles 1 to 3 show that ambient temperature can have an important impact on the performance of several industrial process that are likely to be important in future energy supply chains, something that is relevant to any development of industry in the norther part of Norway. In addition, the results presented in Article 4 show that for a CO_2 transportation process, the ambient temperature in the location where the CO_2 originates has more impact on energy consumption that the location of the eventual storage location. These results have implications for the study of any CCS project by highlighting the important fact that some industrial processes have significantly higher efficiency when they have access to low temperature cooling.

The findings of Article 6 show that, in addition to the operating cases where the efficiency of the alternative energy supply chain configuration is better than *conventional* approach, that there exists a range of other operating cases where the performance is very similar for both scenarios. The implication of this finding for the wider assessment of potential future energy supply is that the *conventional* approach, which forms the basis of most planned projects at present, should be challenged for cases where natural gas is supplied as LNG.

Contribution to the Research Field

The literature review presented under Heading 2.3 lists a small number of studies that have actively considered different options for blue hydrogen supply from Norway. Although the research work presented in these studies has themes common with the work presented here in Article 6, none of them specifically address the important role ambient temperature can play in assessing relative performance. It is hoped, therefore, that the work presented in this thesis will help to provide a better basis for further studies looking at this type of future energy supply chain.

Further Research

Two main topics for further research can be identified that build on the work presented here that would make a significant contribution to the comparison of the relative merits of blue hydrogen export and natural gas export from the Norwegian perspective. Firstly, the combination of the present work with economic modelling would undoubtedly improve the usefulness of the results presented here; secondly, the incorporation into the modelling work of all supply chain and life-cycle emissions to better assess the relative environmental impact of these two options for blue hydrogen supply.

6 Conclusions

The scope of the work presented in this thesis is defined by the three research questions that are described in the Introduction. How the conclusions that can be drawn from the six main articles supporting this thesis provide an answer to these research questions is set out below.

- *RQ1 - How does ambient temperature effect the performance of industrial processes relevant to the supply of blue hydrogen?*

  The conclusion that can be drawn from the work presented in articles 1, 2 and 3 is that access to a low temperature cooling medium provides a significant performance advantage to several of the industrial processes relevant to blue hydrogen supply. The specific processes studied in this work are natural gas liquefaction, hydrogen liquefaction and CO_2 compression. Over a 10 °C variation in ambient temperature, the performance of these three potential links in blue hydrogen supply varies by 10 %, 5% and 8% respectively. The implication of this level of performance variation is that not only the impact on individual process links is important but also that the cumulative performance impact is important to the full energy supply chain.

- *RQ2 - How is the energy consumption associated with CO_2 transportation affected by ambient temperature and the location of the source/ storage reservoir?*

  The conclusion that can be drawn from Articles 4 and 5 is that the temperature of the available cooling medium—and therefore ambient temperature—has a significant impact on the performance of CO_2 transportation. In particular, the role of the available heat sink temperature in the location where the CO_2 emissions originate is found to be more significant that other design parameters such as the length of the pipeline or the depth of the reservoir.

- *RQ3 - Under what conditions is the energy efficiency of a blue hydrogen based energy supply chain originating in northern Norway better than an equivalent conventional blue hydrogen supply chain based on the export of natural gas from northern Norway?*

  The study of the efficiency of two different blue hydrogen supply chain alternatives in this thesis shows that a *conventional* approach to blue hydrogen supply based on LNG exports from northern Norway does not necessarily provide the highest energy efficiency when compared to the direct export of blue hydrogen as a liquid in tanker ships. Specifically, the results show that when the proportion of hydrogen product supplied to the end user as a liquid is above 75%, the production and shipping of hydrogen as a liquid from northern Norway will be more efficient that the *conventional* case. The implication for this finding is that the *conventional* approach to blue hydrogen supply, which forms the basis of several planned projects, should be investigated and challenged to ensure it best supports both current and future hydrogen supply.

More generally, I hope that the results presented here and the conclusions that can be drawn from them will provide some a basis and some motivation for further study of unconventional blue hydrogen supply scenarios.

7 References

1. IEA. 2019 [cited 2019 24.10.2019]; Available from: https://www.iea.org/topics/hydrogen/production/.
2. Howarth, R.W. and M.Z. Jacobson, *How green is blue hydrogen?* Energy Science & Engineering, 2021. **n/a**(n/a).
3. Yang, C. and J. Ogden, *Determining the lowest-cost hydrogen delivery mode.* International Journal of Hydrogen Energy, 2007. **32**(2): p. 268-286.
4. Hoshi, M. *World's first liquid hydrogen carrier ship launches in Japan*. 2019 [cited 2021 15.04.2021]; Available from: https://asia.nikkei.com/Business/Energy/World-s-first-liquid-hydrogen-carrier-ship-launches-in-Japan.
5. Aasadnia, M. and M. Mehrpooya, *Large-scale liquid hydrogen production methods and approaches: A review.* Applied Energy, 2018. **212**: p. 57-83.
6. Norske Petroleum. 2019 [cited 2019 24.10.2019]; Available from: https://www.norskpetroleum.no/en/environment-and-technology/carbon-capture-and-storage/.
7. Gassnova. 2019 [cited 2019 24.10.2019]; Available from: http://www.gassnova.no/no/teknologisenteret.
8. Skjervold, V.T., et al., *Framework conditions, policies and projections for clean energy export from Norway*. 2020, SINTEF Energy Research.
9. Ishimoto, Y., et al., *Large-scale production and transport of hydrogen from Norway to Europe and Japan: Value chain analysis and comparison of liquid hydrogen and ammonia as energy carriers.* International Journal of Hydrogen Energy, 2020. **45**(58): p. 32865-32883.
10. Bauer, H.C. *Mixed fluid cascade, experience and outlook*. in *Paper 25a, 12th Topical Conference on Gas Utilization, AIChE 2012 Spring Meeting, Houston, Texas*. 2012.
11. Font-Palma, C., et al., *Integrated oxyfuel power plant with improved CO_2 separation and compression technology for EOR application.* Process Safety and Environmental Protection, 2016. **103**: p. 455-465.
12. Jackson, S., C. Corden, and P.W. Howells, *PROCESS AND APPARATUS FOR THE SEPARATION OF CARBON DIOXIDE AND HYDROGEN*, WIPO, Editor. 2012: UK.
13. Jackson, S., *Improving Carbon Capture for IGCC Power Plants*, in *IChemE Gasification 11*. 2012, IChemE: Cagliari, Sardinia, Italy.
14. Brodal, E., S. Jackson, and O. Eiksund, *Energy saving potential of CO_2 transportation processes in cold climate locations.* Ind. Eng. Chem. Res., 2016. **55**(DOI: 10.1021/acs.iecr.6b03037): p. 11597 - 11605.
15. Khawaja, H.A., E. Brodal, and S. Jackson, *Study of Refrigerants for Cold Climate Heat Pump Operations*, in *The International Conference of Multiphysics*. 2014: Sofia.
16. González-Díaz, A., et al., *Effect of the ambient conditions on gas turbine combined cycle power plants with post-combustion CO2 capture.* Energy, 2017. **134**: p. 221-233.
17. Arrieta, F.R.P. and E.E.S. Lora, *Influence of ambient temperature on combined-cycle power-plant performance.* Applied energy, 2005. **80**(3): p. 261-272.
18. Ait-Ali, M.A., *Optimal Mixed Refrigerant Liquefaction of Natural Gas.* 1979.
19. Khan, M.S., I.A. Karimi, and D.A. Wood, *Retrospective and future perspective of natural gas liquefaction and optimization technologies contributing to efficient LNG supply: A review.* Journal of Natural Gas Science and Engineering, 2017. **45**: p. 165-188.
20. Austbø, B., S.W. Løvseth, and T. Gundersen, *Annotated bibliography—Use of optimization in LNG process design and operation.* Computers & Chemical Engineering, 2014. **71**: p. 391-414.
21. Xu, X., et al., *The correlation between mixed refrigerant composition and ambient conditions in the PRICO LNG process.* Applied Energy, 2013. **102**: p. 1127-1136.
22. Rian, A. and I. Ertesvåg, *Exergy Evaluation of the Arctic Snøhvit Liquefied Natural Gas Processing Plant in Northern Norway - Significance of Ambient Temperature.* Energy Fuels, 2012. **26**: p. 1259-1267.
23. Castillo, L., et al., *Conceptual analysis of the precooling stage for LNG processes.* Energy Conversion and Management, 2013. **66**: p. 41-47.

24. Park, K., W. Won, and D. Shin, *Effects of varying the ambient temperature on the performance of a single mixed refrigerant liquefaction process.* Journal of Natural Gas Science and Engineering, 2016. **34**: p. 958-968.
25. Kang, J.-N., et al., *Energy systems for climate change mitigation: A systematic review.* Applied Energy, 2020. **263**: p. 114602.
26. Ghorbani, B., et al., *Hydrogen liquefaction process using solar energy and organic Rankine cycle power system.* Journal of Cleaner Production, 2019.
27. Yilmaz, C., *Optimum energy evaluation and life cycle cost assessment of a hydrogen liquefaction system assisted by geothermal energy.* International Journal of Hydrogen Energy, 2019.
28. Ansarinasab, H., M. Mehrpooya, and A. Mohammadi, *Advanced exergy and exergoeconomic analyses of a hydrogen liquefaction plant equipped with mixed refrigerant system.* Journal of Cleaner Production, 2017. **144**: p. 248-259.
29. Skaugen, G., D. Berstad, and Ø. Wilhelmsen, *Comparing exergy losses and evaluating the potential of catalyst-filled plate-fin and spiral-wound heat exchangers in a large-scale Claude hydrogen liquefaction process.* International Journal of Hydrogen Energy, 2020. **45**(11): p. 6663-6679.
30. Cardella, U., et al., *Process optimization for large-scale hydrogen liquefaction.* International Journal of Hydrogen Energy, 2017. **42**(17): p. 12339-12354.
31. Donaubauer, P.J., et al., *Kinetics and Heat Exchanger Design for Catalytic Ortho-Para Hydrogen Conversion during Liquefaction.* Chemical Engineering & Technology, 2019. **42**(3): p. 669-679.
32. Wilhelmsen, O., et al., *Reducing the exergy destruction in the cryogenic heat exchangers of hydrogen liquefaction processes.* International Journal of Hydrogen Energy, 2018. **43**(10): p. 5033-5047.
33. Skaugen, G. and O. Wilhelmsen, *Comparing the Performance of Plate-Fin and Spiral Wound Heat Exchangers in the Cryogenic Part of the Hydrogen Liquefaction Process*, in *15th Cryogenics 2019 Iir International Conference*, V. Chrz, et al., Editors. 2019, Int Inst Refrigeration: Paris. p. 318-324.
34. Jackson, S., O. Eiksund, and E. Brodal, *Impact of Ambient Temperature on LNG Liquefaction Process Performance: Energy Efficiency and CO 2 Emissions in Cold Climates.* Industrial & Engineering Chemistry Research, 2017. **56**(12): p. 3388-3398.
35. Wang, J.-W., et al., *Research trends in carbon capture and storage: A comparison of China with Canada.* International Journal of Greenhouse Gas Control, 2020. **97**: p. 103018.
36. Li, H., et al., *An analysis of research hotspots and modeling techniques on carbon capture and storage.* Science of The Total Environment, 2019. **687**: p. 687-701.
37. Lucquiaud, M., et al., *Addressing technology uncertainties in power plants with post-combustion capture.* Energy Procedia, 2013. **37**: p. 2359 – 2368.
38. Jordal, K. and A. Aspelund, *Gas conditioning—The interface between CO_2 capture and transport.* International Journal of Greenhouse Gas Control, 2007. **1**(3): p. 343–354.
39. Alabdulkarem, A., Y.H. Hwang, and R. Radermacher, *Development of CO_2 liquefaction cycles for CO_2 sequestration.* Applied Thermal Engineering, 2012. **33-34**: p. 144-156.
40. Harkina, T., A. Hoadley, and B. Hooper, *A comparison of the Process Integration of Shockwave CO_2 compression with conventional turbo machinery into PCC power station design.* Science Direct, 2011. **Energy Procedia**(4): p. 1339–1346.
41. Jackson, S. and E. Brodal. *A comparison of the energy consumption for CO_2 compression process alternatives*. in *Earth and Environmental Science*. 2018. Barcelona: IOP COnference Series.
42. Calado, M., *Modeling and design synthesis of a CCS compression train system via MINLP optimization*. 2012, Instituto Superior Técnico, Universidade de Lisboa. p. 77.
43. Pei, P., et al., *Waste heat recovery in CO_2 compression.* International Journal of Greenhouse Gas Control, 2014. **30**: p. 86–96.
44. Metz, B., et al., *Carbon Dioxide Capture and Storage ; IPCC, 2005: IPCC Special Report on Carbon Dioxide Capture and Storage*. 2005: Cambridge University Press.

45. Hegerland, G., T. Jørgensen, and J.O. Pande, *Liquefaction and handling of large amounts of CO_2 for EOR*, in *Proceedings of the 7th International Conference on Greenhouse Gas Control Technologies*. 2005, Elsevier Science Ltd. p. 2541-2544.
46. Duan, L., X. Chen, and Y. Yang, *Study on a novel process for CO_2 compression and liquefaction integrated with the refrigeration process.* International Journal of Energy Research, 2013. **37**(12): p. 1453-1464.
47. Øi, L.E., et al., *Simulation and Cost Comparison of CO_2 Liquefaction.* 2016.
48. Aspelund, A., M.J. Mølnvik, and G. De Koeijer, *Ship Transport of CO_2: Technical Solutions and Analysis of Costs, Energy Utilization, Exergy Efficiency and CO_2 Emissions.* Chemical Engineering Research and Design, 2006. **84**(9): p. 847-855.
49. Lee, U., et al., *Carbon Dioxide Liquefaction Process for Ship Transportation.* Ind. Eng. Chem. Res., 2012. **51**(46): p. 15122-15131.
50. Decarre, S., et al., *CO_2 maritime transportation.* International Journal of Greenhouse Gas Control, 2010. **4**(5): p. 857-864.
51. Seo, Y., et al., *Evaluation of CO_2 liquefaction processes for ship-based carbon capture and storage (CCS) in terms of life cycle cost (LCC) considering availability*. 2015. p. 1-12.
52. Seo, Y., et al., *Comparison of CO_2 liquefaction pressures for ship-based carbon capture and storage (CCS) chain.* International Journal of Greenhouse Gas Control, 2016. **52**: p. 1-12.
53. Lee, S.G., G.B. Choi, and J.M. Lee, *Optimal Design and Operating Conditions of the CO2 Liquefaction Process, Considering Variations in Cooling Water Temperature.* Industrial & Engineering Chemistry Research, 2015. **54**(51): p. 12855-12866.
54. Jackson, S. and E. Brodal, *An assessment of the Energy Saving Potential of Unconventional CO2 Compression Approaches*, in *9TH TRONDHEIM CONFERENCE ON CO2 CAPTURE, TRANSPORT AND STORAGE, TCCS-9*. 2017: Trondheim.
55. Jackson, S. and E. Brodal, *Optimization of the CO_2 Liquefaction Process-Performance Study with Varying Ambient Temperature.* Applied Sciences, 2019. **9**.
56. Eickhoff, C., A. Brown, and F. Neele, *Techno-economic Issues and Trade-offs for CO_2 Purity in CCS Chains.* Energy Procedia, 2017. **114**: p. 6698-6707.
57. Wilhelmsena, Ø., et al., *Evaluation of SPUNG# and other Equations of State for use in Carbon Capture and Storage modelling.* Energy Procedia 23, 2012: p. 236-245.
58. Mazzoccoli, M., et al., *Comparison of equations-of-state with P-p-T experimental data of binary mixtures rich in CO2 under the conditions of pipeline transport.* The journal of supercritical fluids, 2014: p. 474-490.
59. Gernert, J. and R. Span, *EOS–CG: A Helmholtz energy mixture model for humid gases and CCS mixtures.* The Journal of Chemical Thermodynamics, 2016. **93**: p. 274-293.
60. Brunsvold, A., et al., *Key findings and recommendations from the IMPACTS project.* International Journal of Greenhouse Gas Control, 2016. **54**: p. 588-598.
61. Span, R.B., R.; Hielscher, S.; Jäger, A.; Mickoleit, E.; Neumann, T.; Pohl, S.; M.; Semrau, B.; Thol, M., *TREND. Thermodynamic Reference and Engineering Data 5.0*. 2020, Lehrstuhl für Thermodynamik, Ruhr-Universität Bochum.
62. Drescher, M., et al., *Heat Transfer Characteristics of a Pipeline for CO_2 Transport with Water as Surrounding Substance.* Energy Procedia, 2013. **37**: p. 3047-3056.
63. Lee, W.J. and R. Yun, *In-tube convective heat transfer characteristics of CO_2 mixtures in a pipeline.* International Journal of Heat and Mass Transfer, 2018. **125**: p. 350-356.
64. Wetenhall, B., et al., *The main factors affecting heat transfer along dense phase CO_2 pipelines.* International Journal of Greenhouse Gas Control, 2017. **63**: p. 86-94.
65. Zhang, W.B., et al., *Experimental investigations into the transient behaviours of CO_2 in a horizontal pipeline during flexible CCS operations.* International Journal of Greenhouse Gas Control, 2018. **79**: p. 193-199.
66. Mohammadi, M., et al., *Economic Optimization Design of CO_2 Pipeline Transportation with Booster Stations.* Industrial & Engineering Chemistry Research, 2019. **58**(36): p. 16730-16742.
67. McCoy, S. and E. Rubin, *An engineering-economic model of pipeline transport of CO2 with application to carbon capture and storage.* International Journal of Greenhouse Gas Control, 2008. **2**(2): p. 219-229.

68. Tian, Q., et al., *Robust and stepwise optimization design for CO2 pipeline transportation.* International Journal of Greenhouse Gas Control, 2017. **58**: p. 10-18.
69. Jakobsen, J., S. Roussanaly, and R. Anantharaman, *A techno-economic case study of CO_2 capture, transport and storage chain from a cement plant in Norway.* Journal of Cleaner Production, 2017. **144**(C): p. 523-539.
70. Jakobsen, J.P., et al., *A Tool for Integrated Multi-criteria Assessment of the CCS Value Chain.* Energy Procedia, 2014. **63**: p. 7290-7297.
71. Mallon, W., et al., *Costs of CO_2 Transportation Infrastructures.* Energy Procedia, 2013. **37**: p. 2969-2980.
72. Deng, H., S. Roussanaly, and G. Skaugen, *Techno-economic analyses of CO_2 liquefaction: Impact of product pressure and impurities.* International Journal of Refrigeration, 2019. **103**: p. 301-315.
73. Knoope, M.M.J., A. Ramírez, and A.P.C. Faaij, *Investing in CO_2 transport infrastructure under uncertainty: A comparison between ships and pipelines.* International Journal of Greenhouse Gas Control, 2015. **41**: p. 174-5836.
74. Jackson, S. and E. Brodal, *Optimization of the Energy Consumption of a Carbon Capture and Sequestration Related Carbon Dioxide Compression Processes.* 2019. **12**(9).
75. Stiller, C., et al., *Options for CO2-lean hydrogen export from Norway to Germany.* Energy, 2008. **33**(11): p. 1623-1633.
76. JMA. 2019 [cited 2019 1 11 2019]; Available from: http://ds.data.jma.go.jp/tcc/tcc/products/elnino/cobesst_doc.html.
77. Jensen, J.B. and S. Skogestad, *Optimal operation of a mixed fluid cascade LNG plant.* Computer Aided Chemical Engineering, 2006. **21**: p. 1569-1574.
78. Anantharaman R., et al., *DECARBit deliverable D 1.4.3 European Best Practice Guidelines for Assessment of CO2 capture technologies*. 2011, Sintef: Trondheim, Norway.
79. Ertesvåg, I.S., *Sensitivity of chemical exergy for atmospheric gases and gaseous fuels to variations in ambient conditions.* Energy Conversion and Management, 2007. **48**(7): p. 1983-1995.
80. Collodi, G., et al., *Techno-economic Evaluation of Deploying CCS in SMR Based Merchant H2 Production with NG as Feedstock and Fuel.* Energy Procedia, 2017. **114**: p. 2690-2712.
81. Antonini, C., et al., *Hydrogen production from natural gas and biomethane with carbon capture and storage–A techno-environmental analysis.* Sustainable Energy & Fuels, 2020. **4**(6): p. 2967-2986.

Appendix – Article 1

I&EC research
Industrial & Engineering Chemistry Research

Article

pubs.acs.org/IECR

Impact of Ambient Temperature on LNG Liquefaction Process Performance: Energy Efficiency and CO_2 Emissions in Cold Climates

Steve Jackson,* Oddmar Eiksund, and Eivind Brodal

UiT-The Arctic University of Norway, Tromsø 9037, Norway

ABSTRACT: The temperature of the available heat sink, often air or seawater, affects performance in many industrial processes. Low temperature processes, such as natural gas liquefaction, are particularly affected. Industrial development in the Arctic presents many challenges but has the benefit of access to a low temperature heat sink. Although several studies have considered the impact ambient temperature has on the performance of natural gas liquefaction, there is little agreement about the scale of the benefit. The present study focuses on the modeling and optimization of several different liquefaction processes. The results show that the energy consumption of any optimized gas liquefaction process will be 20−26% higher in the Middle East or Northern Australia than in an Arctic climate such as that found in Northern Norway, equivalent to a 0.8−1.3% reduction in CO_2 emissions for the full gas to power chain. The performance data are also combined with worldwide sea temperature to illustrate variation by geographic location.

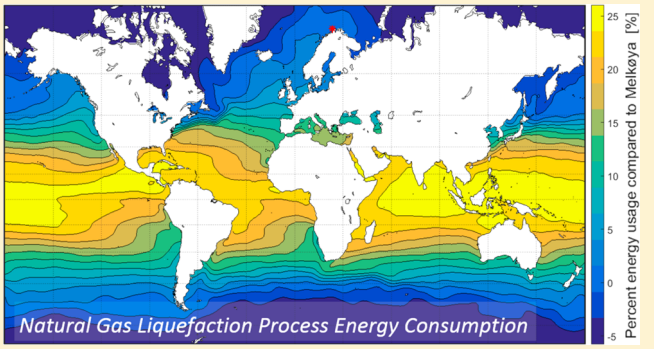

1. INTRODUCTION

Fossil fuels will remain the dominant energy sources in the near future. Power stations burning natural gas (NG) had a 30% share of fossil in 2013 and are predicted to have a 37% share in 2030, which makes NG the fastest growing fossil fuel for power generation[1,2] and an important element of global efforts to reduce CO_2 emissions.

One important route to emissions reduction is through improvements in energy efficiency. Energy efficiency measures often focus on the point at which the CO_2 is released, usually a power station, but all of the elements in the chain linking natural gas production to electrical power generation affect the total CO_2 footprint.

Gas based electrical power generation in a combined cycle gas turbine (CCGT) power plant has an environmental advantage over other fossil fuels due to high baseline thermal efficiency. Much effort has been focused on increasing the efficiency of CCGT power plants with the aim of cutting production costs and reducing CO_2 emissions. The traditional focus has been to improve process efficiencies with improved component and plant designs, but the location of the plant also has an important role to play because the temperature of the available heat sink has a fundamental effect on process efficiency.

Process efficiency and location is also important for other elements in the gas to power chain. If NG is to be transported over large distances, shipping it as liquefied natural gas (LNG) is often the preferred transport method. To liquefy natural gas around atmospheric pressure, it has to be cooled with a refrigeration process to approximately −160 °C in an energy intensive process. Liquefaction plants are also the most expensive part of the LNG supply chain, accounting for more than 40% of the total cost.[3]

There is a variety of gas liquefaction process designs and both single- and multiple-refrigeration cycles in cascade are used in industry. It is often difficult to compare directly the process efficiency of different LNG plants because there are so many possible combinations of gas composition, pressure, ambient temperature and refrigeration process designs. Process efficiency generally improves as the process complexity (the number of equipment components and cooling stages) increases, but increased process complexity also impacts the cost of the LNG plant.

The energy consumption of four different LNG processes have been modeled in this study. A liquefaction process using three stages of mixed refrigerants, commonly referred to as a mixed fluid cascade (MFC) process, is modeled to illustrate a low energy consumption case. The process is similar to the process used at Melkøya in Northern Norway, which is often claimed to be the most energy efficient baseload LNG plant in the world.[4−6] However, even though the Melkøya plant is very efficient, the gas turbines at Melkøya still release 900 000 tons of CO_2 per year and contribute nearly 2% of Norway's total CO_2 emissions.[6] The Melkøya LNG plant is also used as a base case in this study because it is the most northerly LNG plant in the world and therefore represents a good example of a location with access to low temperature seawater. Two pure component

Received: January 23, 2017
Revised: March 8, 2017
Accepted: March 8, 2017
Published: March 8, 2017

DOI: 10.1021/acs.iecr.7b00333
Ind. Eng. Chem. Res. XXXX, XXX, XXX−XXX

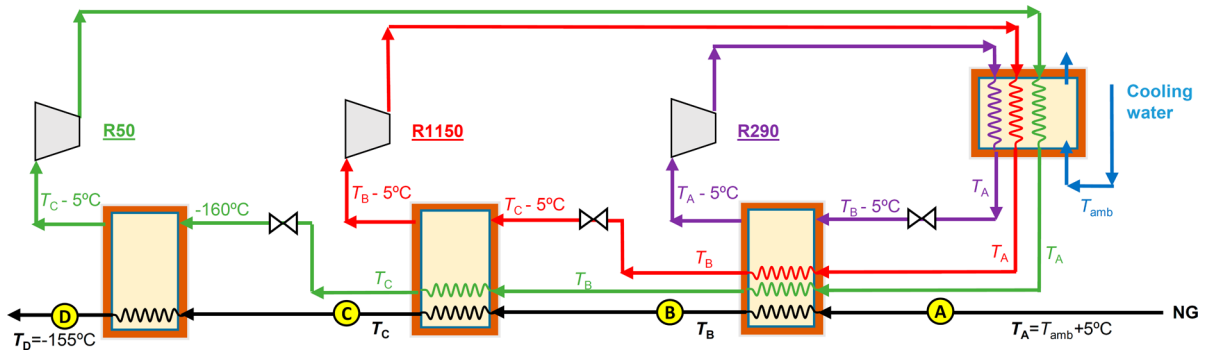

Figure 1. Flow diagram of the Cascade 1−1−1 process.

cascade processes and an idealized Carnot cycle based process are also modeled as cases for comparison.

Many studies have been conducted into the optimization of LNG process performance. Among others, Aspelund et al.[7] studied the optimal performance of a simple single mixed refrigerant (SMR) process, Hatcher et al.[2] have studied a propane precooled mixed refrigerant (MR) process, and Jensen et al.[8] have studied the MFC process. Fewer studies have looked at the link between ambient temperature and LNG process performance. Park et al.[9] and Castillo et al.[10] modeled the performance of several different types of mixed refrigerant (MR) process finding that specific power increases by between 16% and 42% over the temperature range 10−25 °C. Rian et al.[11] studied the benefit low ambient temperature gives to the LNG plant located at Melkøya using an exergy analysis and found that fuel consumption for the full plant was reduced by 19.9% over the range 36 to 4 °C. The wide range of the results suggests that the variation in performance with ambient temperature is highly dependent on the type of LNG process considered, but no study has been conducted to confirm this.

The aim of the present study is to model performance variation with ambient temperature for a range of LNG process types. To do this, it is necessary to optimize both pure component and mixed fluid type LNG processes on a consistent basis. The optimization approach selected for the pure component processes was to develop a routine in MATLAB that is capable of optimizing operating parameters and varying the number of heat exchangers used. The operating parameters of a three stage MFC were optimized using HYSYS for a fixed process flow sheet where heat is transferred in three multistream exchangers. The results are summarized in terms of specific power consumption and CO_2 emissions using global sea surface temperature (SST) data. The approach employed by Brodal et al.[12] is used to map the impact of ambient temperature globally on LNG process performance and equivalent CO_2 emissions.

2. METHODS

To accurately assess the impact of ambient temperature on CO_2 emissions and power consumption in LNG liquefaction, process models were required that could be optimized and compared for different ambient temperatures on a consistent basis. To allow this, the models developed focus on flexibility and simplicity. They also employ automated routines that were used to find optimum operating parameters for systems with the same components and process design. To investigate the impact of process complexity on efficiency, four process schemes were modeled.

1. Cascade 1−1−1 (three single-stage single component refrigerant cycles)
2. Cascade 2−2−2 (three two-stage single component refrigerant cycles)
3. MFC (mixed fluid cascade)
4. Carnot cascade (theoretical best)

To generate location specific performance data, the specific power consumption for these processes was coupled to seawater data provided by the Japan Meteorological Agency.[13]

2.1. General Modeling Basis. With the aim of creating a performance model that was simple, transparent,and easily recreated, this study used the following set of general modeling parameters:

- The feed is 60 bar and 5 °C above ambient seawater temperature (T_{amb}).
- The feed composition (in mol %) is 3.1% nitrogen, 87.7% methane, 5.4% ethane, 2.6% propane, 0.8% isobutane, and 0.4% *n*-butane.
- The liquefied NG product temperature is −155 °C.
- Streams flowing through exchangers without phase change have a 0.5 bar pressure drop.
- Refrigerants used in flooded evaporators and open intercoolers have a 0.0 bar pressure drop.
- All heat exchangers operate with a 5.0 K temperature difference.
- Pressure in the refrigeration cycles is always 1.1 bar or higher.
- All compressors have isentropic efficiency η_{is} = 0.85.

The NG composition used in this study has a lower heating value (LHV) of 47.06 MJ/kg. No heavy hydrocarbon components or NG separation steps are included in the liquefaction process. No N_2 rejection step is assumed to occur within the end flash process.

2.2. Modeling and Optimization of the Single Component Cascade Processes. The single-component cascade processes use refrigerants R290 (propane), R1150 (ethylene), and R50 (methane) and are modeled numerically in MATLAB. Property data are generated using the CoolProp fluid package.[14] In the optimization routine described below, the number and configuration of heat exchangers is a variable along with the process operating parameters. This type of flexibility is difficult to achieve in a typical flowsheet based modeling tool such as HYSYS. Using MATLAB, therefore, the optimization process includes fewer constraints resulting in a better approach to the minimum possible power.

2.2.1. Single-stage Single Component Cascade (Cascade 1−1−1) Scheme. Figure 1 illustrates the flow diagram of the

DOI: 10.1021/acs.iecr.7b00333
Ind. Eng. Chem. Res. XXXX, XXX, XXX−XXX

single-stage single component cascade process. Our objective is to minimize the total energy consumption per ton natural gas given by the function

$$w_{NG} = \frac{1}{\dot{m}_{NG}}(\Delta h_{c,R290}\dot{m}_{R290} + \Delta h_{c,R1150}\dot{m}_{R1150} + \Delta h_{c,R50}\dot{m}_{R50}) \quad (1)$$

Constraints due to minimum pressure of 1.1 bar are simplified to $T_{C,min} \leq T_C < T_B$ and $T_{B,min} \leq T_B < T_A$, where $T_{C,min}$ and $T_{B,min}$ are related to the evaporation temperatures at 1.1 bar. The mass flows are given by solving the energy balance for each heat exchanger. Looking at the R290 evaporator, this gives

$$\Delta h_{e,R290}\dot{m}_{R290} + \Delta h_{1,R1150}\dot{m}_{R1150} + \Delta h_{1,R50}\dot{m}_{R50} + \Delta h_{1,NG}\dot{m}_{NG} = 0 \quad (2)$$

where the suffix 1 in $\Delta h_{1,R1150}$ refers to the heat exchanger number. The heat exchangers are numbered from 0 to 3 according to descending temperature. This gives the easily solvable matrix equation:

$$\begin{bmatrix} \Delta h_{water} & \Delta h_{0,R290} & \Delta h_{0,R1150} & \Delta h_{0,R50} & 0 \\ 0 & \Delta h_{e,R290} & \Delta h_{1,R1150} & \Delta h_{1,R50} & \Delta h_{1,NG} \\ 0 & 0 & \Delta h_{e,R1150} & \Delta h_{2,R50} & \Delta h_{2,NG} \\ 0 & 0 & 0 & \Delta h_{e,R50} & \Delta h_{3,NG} \\ 0 & 0 & 0 & 0 & 1 \end{bmatrix} \cdot \begin{bmatrix} \dot{m}_{water} \\ \dot{m}_{R290} \\ \dot{m}_{R1150} \\ \dot{m}_{R50} \\ \dot{m}_{NG} \end{bmatrix} = \begin{bmatrix} 0 \\ 0 \\ 0 \\ 0 \\ 1 \end{bmatrix} \quad (3)$$

In this study the energy required by the seawater pump is neglected; hence, the first row of the matrix equation does not need to be solved. Specific enthalpies are computed with CoolProp. MATLAB is used to solve the mass and energy balance for the process, and to compute and optimize the total energy consumption per ton natural gas.

Four temperatures, T_A, T_B, T_C, and T_D, are specified: the final temperature T_D is fixed at −155 °C, T_A is determined by the ambient temperature, and T_B and T_C are optimized with a genetic algorithm (GA) to find the minimum energy consumption. Although this is only a two-dimensional optimization problem, which could also have been easily solved with a simpler optimization algorithm, a GA was used to maintain consistency with the other modeling work.

Figure 2 illustrates that for ambient temperatures between 0 and 40 °C, T_B and T_C are constant. These temperatures are directly related to the evaporation temperature at 1.1 bar, due to the general modeling assumption on the minimum operating pressure.

2.2.2. Two-Stage Single-Component Cascade (Cascade 2−2−2) Scheme. The Cascade 1−1−1 process can be improved in many different ways, e.g., by dividing each refrigerant stage into two stages, as discussed by Lim et al.[3] A three single refrigerant cascade with two stages in each refrigeration loop, illustrated in Figure 3, is modeled and optimized in this article. T_{D2} is fixed as in the single stage process, whereas T_A is determined by the ambient temperature. T_{B1}, T_{B2}, T_{C1}, T_{C2}, and T_{D1} are optimized to find minimum energy consumption.

Refrigerants are cooled against seawater where possible. If the refrigerants in the cascade process do not exceed ambient temperature by the minimum required 5 °C temperature difference, the heat exchanger will simply be bypassed, reducing the compressor work. The same situation can also arise for other heat exchangers. The modeling algorithm automatically adds streams to a heat exchanger wherever useful heat can be transferred between refrigerant streams without breaking the requirements in section 2.1.

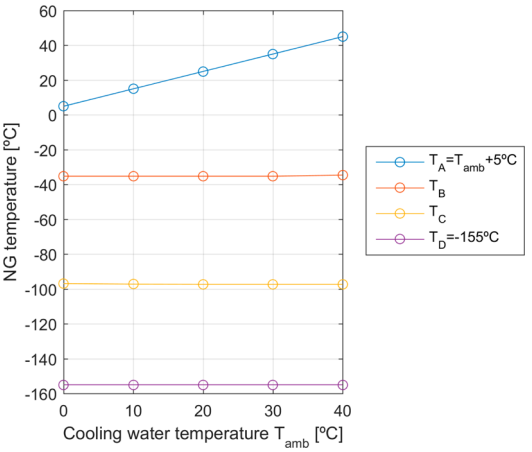

Figure 2. NG temperatures in the Cascade 1−1−1 process.

The objective function in this case is of the same form as eq 1 but requires more terms resulting in a larger matrix equation to solve. Because the process design depends on the variables to be optimized, the heat exchangers configuration varies with both the ambient temperature and all the intermediate temperatures: T_{B1}, T_{B2}, T_{C1}, T_{C2}, and T_{D1}.

The complexity of the optimization problem grows as the number of heat exchangers is increased and the possibility for multiple local optimum solutions arises. To find the optimum overall energy efficiency, a genetic algorithm (GA) included in the MATLAB library is used. The GA is one of the most common stochastic optimization routines used in process simulation[7] and is thus well suited to this optimization problem. GA is also often used in even more complex optimize problems like finding the best compositions of mixed refrigerants.[3,15]

The optimized temperatures are illustrated in Figure 4. Figure 5 shows the heat exchanger steps in the NG refrigeration process in a ph diagram.

2.2.3. Consistency between Modeling Approaches. To demonstrate that the results of the numerical modeling work described above can be compared to the later modeling work conducted in HYSYS, a selection of the optimized design configurations determined by the optimization routines in MATLAB were independently recreated in HYSYS. The results of this assessment are presented in Table 1.

The data presented in Table 1 show close agreement between the MATLAB and HYSYS models (less than 1%). These programs use different fluid packages, which can explain difference in the results.

2.3. Modeling and Optimization of the Mixed Fluid Cascade Scheme. The mixed fluid cascade (MFC) process was modeled using the HYSYS process simulation software. Refrigerant and gas properties were calculated using the SRK fluid package as implemented in HYSYS version 9.0 with standard options. Initially, a base model was developed and verified using the optimized design proposed by Jensen et al.[8] Figure 6 provides an illustration of the base model for the MFC process where MR1, 2, and 3 are mixed refrigerant 1, 2, and 3 respectively.

DOI: 10.1021/acs.iecr.7b00333
Ind. Eng. Chem. Res. XXXX, XXX, XXX−XXX

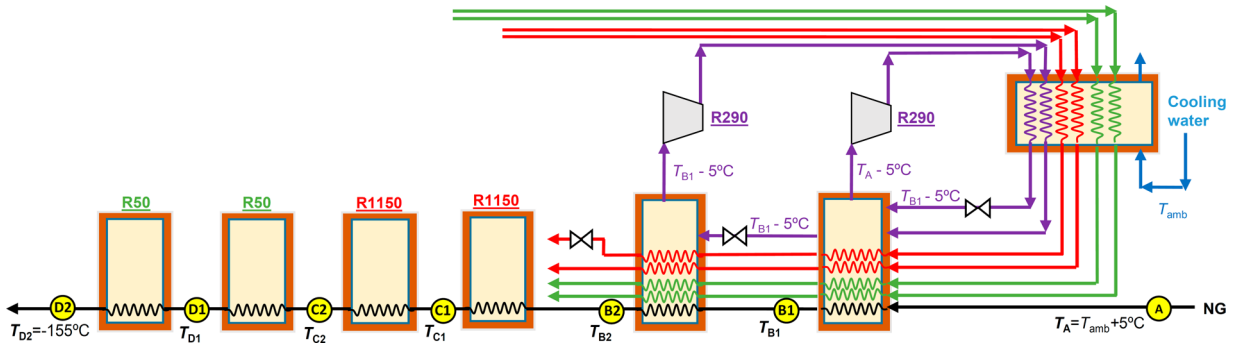

Figure 3. Flow diagram of the Cascade 2−2−2 process (only showing the propane circuit in detail).

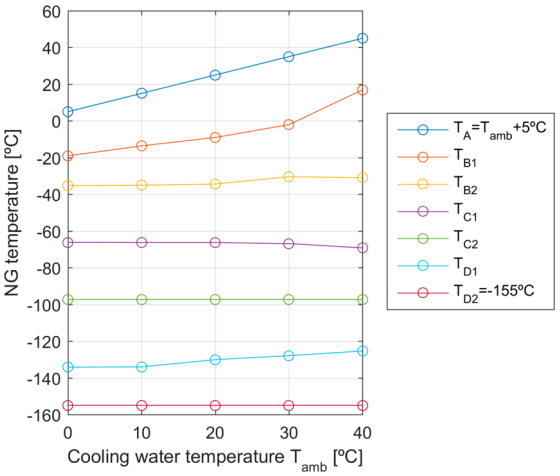

Figure 4. NG temperatures in the Cascade 2−2−2 process.

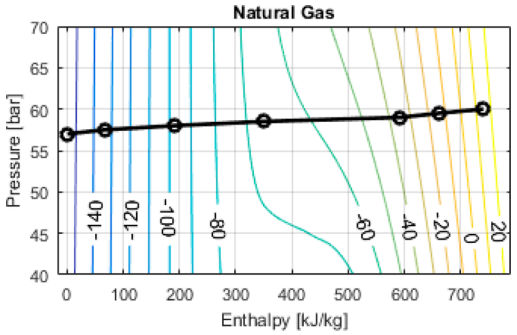

Figure 5. NG ph diagram showing the refrigeration process for the Cascade 2−2−2 process (T_{amb} = 10 °C).

Table 1. Validation Results of the Numerical CoolProp Model Based on the Cascade 2−2−2 Process

	energy consumption [kWh/(ton CO_2)]		
T_{amb} (°C)	CoolProp	HYSYS	difference (%)
0	207.1	208.7	0.8
10	228.6	231.0	1.0
20	252.3	253.9	0.6
30	276.2	278.1	0.7

The modeling basis used by Jensen et al.[8] is presented in Table 2, and the optimized process parameters found by Jensen et al.[8] are summarized in Table 3.

A comparison of the performance results from Jensen et al.[8] and the model developed for this study shows a maximum error in the flow rate of mixed refrigerant in each of the three loops of 3.0% and an overall error in specific energy consumption of 2.2%.

Once verified, the base model was updated with the general modeling basis for this study and reoptimized across the range of temperatures of interest. The optimization parameters for this liquefaction process were limited to the composition and flow rate of MR1. The optimization process was carried out using the HYSYS "original" optimizer data model.

2.4. Modeling of the Theoretical Minimum Power Consumption (Carnot Cascade). The Carnot process has the best refrigeration efficiency between two reservoirs with temperatures T_{hot} and T_{cold}. The coefficient of performance for this process is

$$\mathrm{COP}_{max} = \frac{T_{cold}}{T_{hot} - T_{cold}} \quad (4)$$

Theoretically the most efficient process to cool the NG from $T = T_{amb}$ to $T = -155$ °C, is to use an infinite number of Carnot stages with refrigeration duty $dQ_{NG} = m_{NG} \cdot dh_{NG}$. This is referred to as the "Carnot cascade" process in this article. The specific energy consumption for the Carnot cascade process (assuming ideal conditions with zero pressure drop and zero temperature difference) is

$$w_{NG}^{Carnot} = \frac{W_{Carnot}}{m_{NG}} = \int \frac{dW_{Carnot}}{m_{NG}} = \int \frac{dQ_{NG}}{\mathrm{COP}_{max} \cdot m_{NG}} = \int_{T=T_{amb}}^{T=-155\,°C} \frac{T_{amb} - T}{T}\, dh_{NG} \quad (5)$$

Because the specific enthalpy h depends on the temperature T, an approximation is computed numerically in steps for small ΔT as

$$w_{NG}^{Carnot} \approx \sum_i \frac{T_{amb} - T_i}{T_i} (h_{NG}(T_i) - h_{NG}(T_{i+1})) \quad (6)$$

where T_i = −155 °C, −155 °C + ΔT, −155 °C + 2ΔT, ..., T_{amb}. To solve eq 6, a routine was developed in MATLAB that uses NG enthalpy data generated by CoolProp at 60 bar.

2.5. Sea Surface Temperature Data. The Japan Meteorological Agency provides monthly global sea surface temperature (SST) data with a resolution of 1° latitude and 1° longitude.[16] These data can be downloaded in WMO binary code format from the Japan Meteorological Agency Web site.[13] These data have formed the basis for modeling the geographic

DOI: 10.1021/acs.iecr.7b00333
Ind. Eng. Chem. Res. XXXX, XXX, XXX−XXX

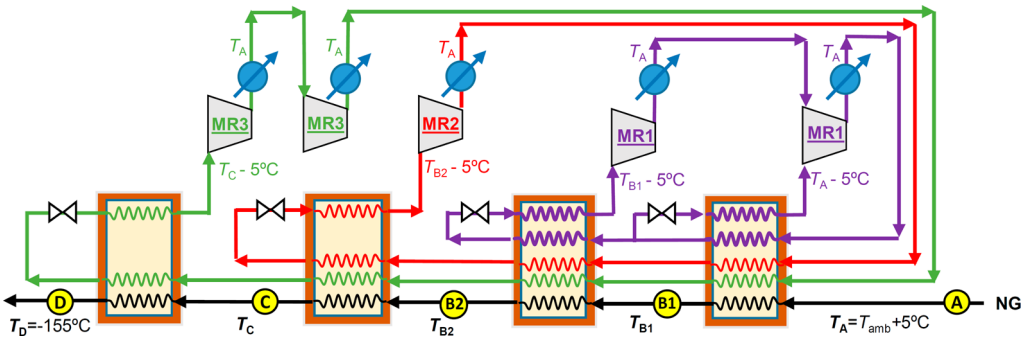

Figure 6. Flow diagram of the MFC process.

Table 2. Modelling Basis Used by Jensen et al.[8]

feed composition (mol %)	2.75 nitrogen, 88.8 methane, 5.70 ethane, and 2.75 propane
refrigerant superheating	10 °C
pressure drop, evaporators	0.20 bar
pressure drop, all other exchangers	0.50 bar
compressor efficiency	η_{is} = 0.90
properties package	SRK

Table 3. Optimized Performance Parameters from Jensen et al.[8]

parameter	units	MR1	MR2	MR3
P_l	bar	2.00	2.0	2.0
P_m	bar	6.45		28.38
P_h	bar	15.30	20.58	56.99
R50 (methane)	mol %		4.020	52.99
R170 (ethane)	mol %	37.70	82.96	42.55
R290 (propane)	mol %	62.30	13.02	
R728 (nitrogen)	mol %			4.55

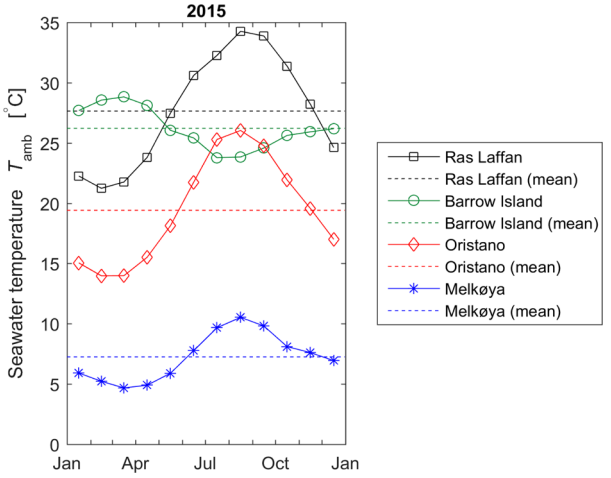

Figure 7. Variation in monthly average SST (T_{amb}) for the selected location.

variation in specific power consumption of the liquefaction processes.

In this study, four geographic locations with existing LNG industry and different climates have been selected to illustrate performance variation: Melkøya (Norway), Oristano (Italy), Ras Laffan (Qatar), and Barrow Island (Australia). These locations are shown in Figure 10 and were selected because they illustrate a wide range of ambient temperature data and have local LNG industries. Figure 7 shows the SST variation in these locations.

Figure 7 also shows that the maximum SST around Melkøya is 10 °C, and almost 30 and 35 °C in Barrow Island and Ras Laffen, respectively. Both Barrow Island and Ras Laffen have approximately a 20 °C higher average SST than Melkøya.

2.6. CO_2 Emissions and Ambient Temperature.

2.6.1. Local Emissions. The CO_2 emission from the gas turbines (GTs) powering the LNG liquefaction process is directly related to the energy consumption of the liquefaction process (w_{NG}). If the liquefaction process is powered by a gas turbine with efficiency η_{NT}, the CO_2 emissions from the gas turbine are

$$m_{CO_2,GT} = k \cdot m_{NG,GT} = k \cdot \frac{w_{NG}}{LHV \cdot \eta_{GT}} \quad (7)$$

where k is the constant describing the relationship between released CO_2 and consumed NG. The value of k depends upon the composition of the NG that is burnt, which in this assessment remains constant. Because k is a constant, it does not need to be quantified in the assessment of relative CO_2 emissions and is eliminated in the equation developed to describe overall emissions as described below.

2.6.2. Overall Emissions. LNG liquefaction is only one part of the gas to power chain. The vast majority of CO_2 emissions are generated when natural gas is consumed (burned) in the power plant (m_{LNG}), and some emissions are generated when the gas is transported. Because the electric energy (and CO_2 emissions) generated when the gas is burnt in a power plant are far greater than any energy losses (or CO_2 emissions) in the rest of the gas to power chain, the relationship between ambient temperature and the total CO_2 emissions can be modeled relatively accurately by including only the emissions from the power station and the ambient temperature dependent processes.

In this study, it is assumed that natural gas originating from the LNG process (as flash gas or boil off gas) is used to power the LNG production process (m_{NG}). The total CO_2 emission ($m_{CO_2,tot}$) relative to electric power production ($E_{el,pow}$) originating from a power plant supplied with gas from LNG, with an LHV efficiency of $\eta_{el,pow}$, is thus

$$\frac{m_{CO_2,tot}}{E_{el.pow}} = \frac{k \cdot m_{NG,tot}}{E_{el.pow}} = \frac{k \cdot (m_{LNG} + m_{NG})}{m_{LNG} \cdot LHV \cdot \eta_{el.pow}} = \left(1 + \frac{m_{NG}}{m_{LNG}}\right) \cdot \left(\frac{k}{LHV \cdot \eta_{el.pow}}\right) \quad (8)$$

DOI: 10.1021/acs.iecr.7b00333
Ind. Eng. Chem. Res. XXXX, XXX, XXX−XXX

The NG in this study has an LHV = 1.307×10^4 kWh/(ton NG). So, if a combined cycle power plant (CCPP) with efficiency $\eta_{el,pow}$ 60% is powered by this NG, it will generate 7850 kWh/(ton NG), which is around 30 times larger than the power needed to run the refrigeration cycle in the LNG plant (w_{NG}). The performance of the LNG refrigeration cycle in an LNG plant is ambient temperature dependent and it is also, by far, the largest energy consuming process in the LNG plant.[11] Because of this, the modeling of the total CO_2 emissions for an LNG plant can be further simplified by neglecting the other energy consuming processes that are present in the LNG plant ($m_{NG} \approx m_{NG,GT}$ and $w_{LNG\text{-}production} \approx w_{NG}$). That is,

$$m_{NG,GT} \cdot LHV \cdot \eta_{GT} \approx (m_{LNG} + m_{NG,GT}) \cdot w_{NG} \quad (9)$$

if the amount of flash gas is adjusted to generate the power needed by the LNG liquefaction process. Equation 9 can be rewritten as

$$\frac{m_{NG,GT}}{m_{LNG}} \approx \frac{w_{NG}}{LHV \cdot \eta_{GT} - w_{NG}} \quad (10)$$

Hence, the total CO_2 emission per kWh electricity produced by a power plant burning LNG produced from a liquefaction process with access to 10 °C ambient seawater is (ton/kWh):

$$\left[\frac{m_{CO_2,tot}}{E_{el.pow}}\right]_{@10°C} \approx \left(1 + \frac{m_{NG,GT,10°C}}{m_{LNG}}\right) \cdot \left(\frac{k}{LHV \cdot \eta_{el.pow}}\right) \approx \left(1 + \frac{w_{NG,10°C}}{LHV \cdot \eta_{GT} - w_{NG,10°C}}\right) \cdot \left(\frac{k}{LHV \cdot \eta_{el.pow}}\right) \quad (11)$$

The increase in the total CO_2 emission if replacing the LNG produced at a location with access to 10 °C ambient seawater with LNG from a location with 30 °C cooling water, is given as

$$\frac{\left[\frac{m_{CO_2,tot}}{E_{el.pow}}\right]_{@30°C} - \left[\frac{m_{CO_2,tot}}{E_{el.pow}}\right]_{@10°C}}{\left[\frac{m_{CO2,tot}}{E_{el.pow}}\right]_{@10°C}} \cdot 100\% \approx \frac{\left(1 + \frac{w_{NG,30°C}}{LHV \cdot \eta_{GT} - w_{NG,30°C}}\right) - \left(1 + \frac{w_{NG,10°C}}{LHV \cdot \eta_{GT} - w_{NG,10°C}}\right)}{\left(1 + \frac{w_{NG,10°C}}{LHV \cdot \eta_{GT} - w_{NG,10°C}}\right)} \cdot 100\% \quad (12)$$

where it is assumed that the gas turbines powering the liquefaction processes at the two locations have the same LHV efficiency.

3. RESULTS

The results of the study work are shown below in three parts. The first part presents the variation in liquefaction process performance with ambient temperature, the second presents the results from the combination of the process performance data with worldwide SST data, and the last part presents the energy savings in terms of CO_2 emissions.

3.1. Energy Consumption and Ambient Temperature.

As ambient temperature varies, so does process performance. Figure 8 shows the calculated specific energy consumption for each of the selected process schemes at different ambient temperatures. Table 4 summarizes the specific energy usage for 10 and 30 °C.

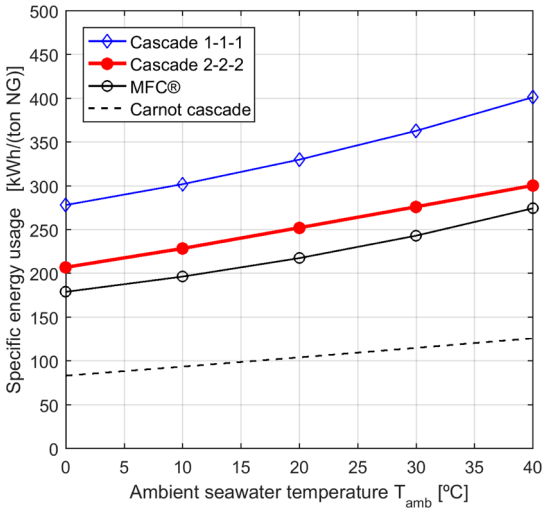

Figure 8. Specific energy consumption (w_{NG}) for different SST.

Table 4. Specific Energy Usage (Percentage Increase in Parentheses)

ambient temperature (T_{amb})	specific energy consumption (w_{NG}) [kWh/(ton NG)]			
	Cascade 1−1−1	Cascade 2−2−2	MFC	Carnot cascade
10 °C	302.1	228.6	196.5	93.6
30 °C	363.0	276.2	243.2	115.0
(increase)	(20.2%)	(20.8%)	(23.8%)	(22.9%)

3.2. Energy Consumption and Geographic Location.

The average specific energy consumption in 2015, based on the monthly SST data and the estimated process performance, is illustrated for the four selected locations in Figure 9. Figure 10 shows the specific energy consumption for the MFC process in a detailed map of the world, using MATLAB's built in map function "contourfm." Energy consumption relative to Melkøya is illustrated in Figure 11.

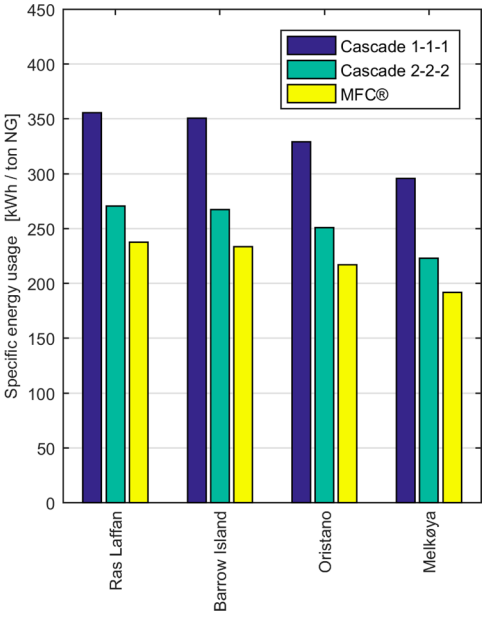

Figure 9. Energy usage at four locations (average 2015).

DOI: 10.1021/acs.iecr.7b00333
Ind. Eng. Chem. Res. XXXX, XXX, XXX−XXX

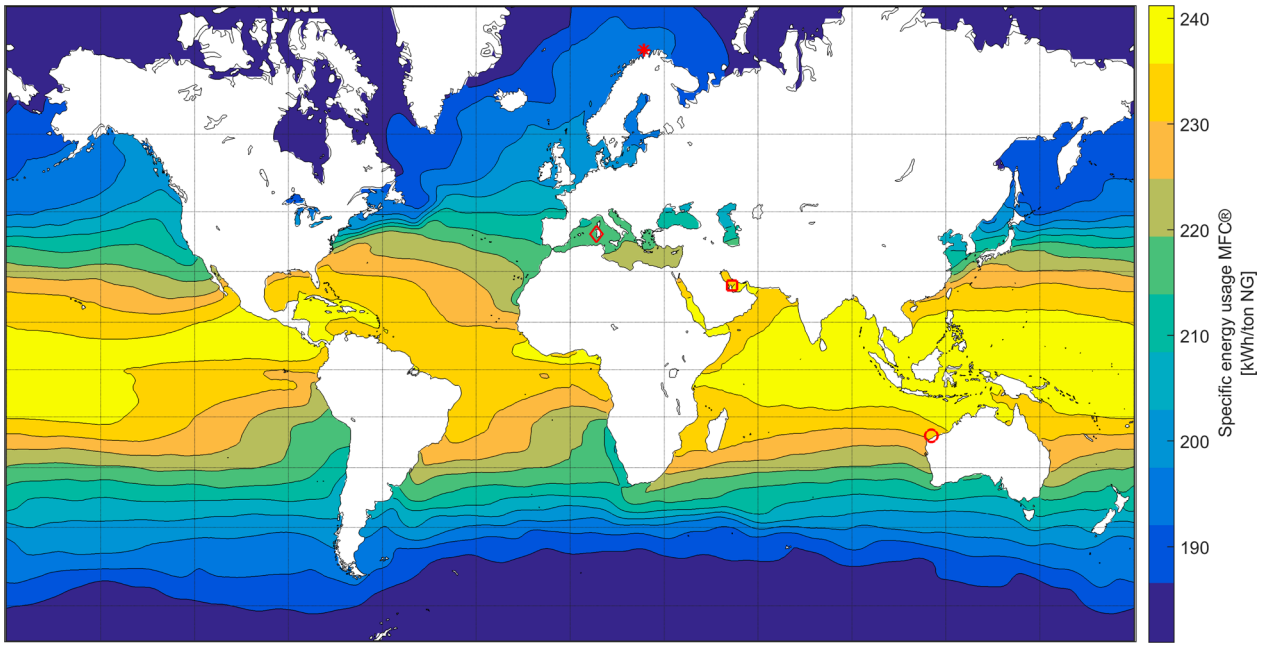

Figure 10. Average energy consumption in 2015 for the MFC process. Melkøya (Norway) is marked "*", Oristano (Italy) is marked "◊", Ras Laffan (Qatar) is marked "□" and Barrow Island (Australia) is marked "○".

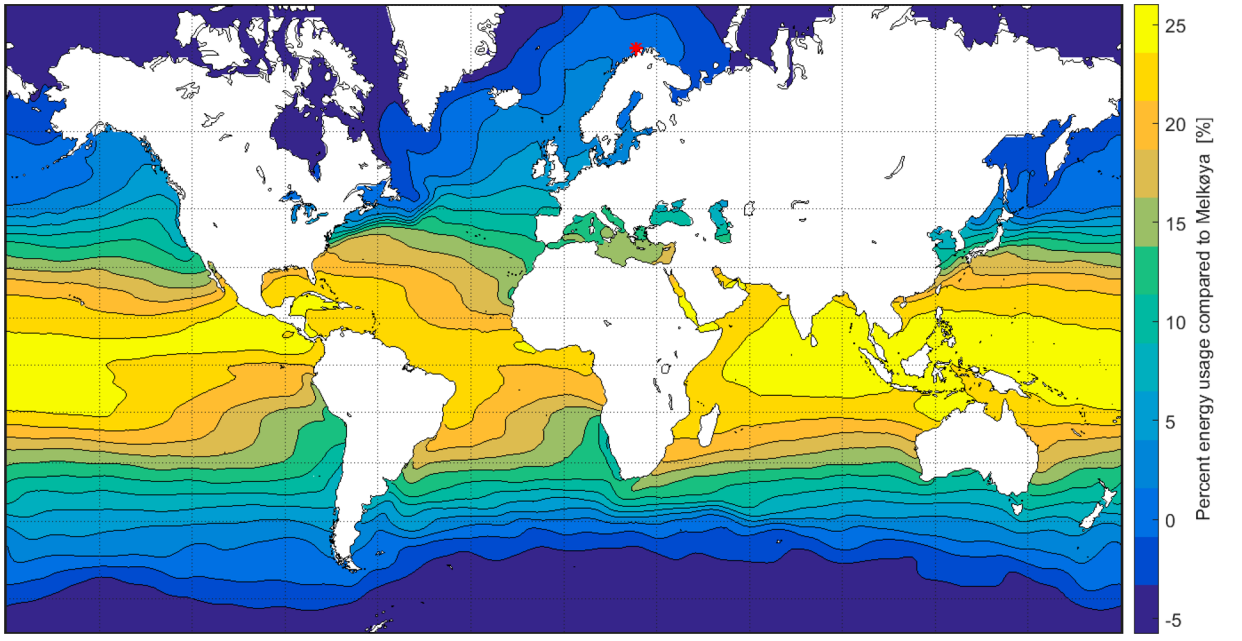

Figure 11. Energy consumption relative to Melkøya when operating the MFC process. Melkøya is marked as "*".

3.3. Impact of Ambient Temperature on CO_2 Emissions.

The power demand of LNG plants is normally supplied using gas turbines. The CO_2 emission from powering an LNG liquefaction process are proportional to the energy efficiency of the process, as described in eq 7. Hence, the variation in specific energy consumption presented in Figure 11 will be the same as the variation in specific CO_2 emission relative to Melkøya if one assumes that the GTs have the same efficiency in all locations.

Equation 12 shows that this increase in total CO_2 emission (ton CO_2/kWh) is independent of the efficiency of the power plant ($\eta_{el,pow}$). Based on eq 12 and that a typical gas turbine LHV efficiency (η_{GT}) falls in the range 30−45%,[17] Figure 12 shows how the gas turbine efficiency affects the total increase in CO_2 emissions for a gas to power chain.

The variation in total CO_2 emissions resulting from power generation using LNG produced at different locations is shown relative to Melkøya in Figure 13. The basis of Figure 13 is that a MS9001EA gas turbine, which has a 35% LHV efficiency,[17] is used for power generation in the LNG production plant.

4. DISCUSSION

A variety of different LNG liquefaction processes are used at the industrial scale. Four different liquefaction processes were used as the basis for the analysis carried out in this report with the aim of identifying common performance trends. The main

DOI: 10.1021/acs.iecr.7b00333
Ind. Eng. Chem. Res. XXXX, XXX, XXX−XXX

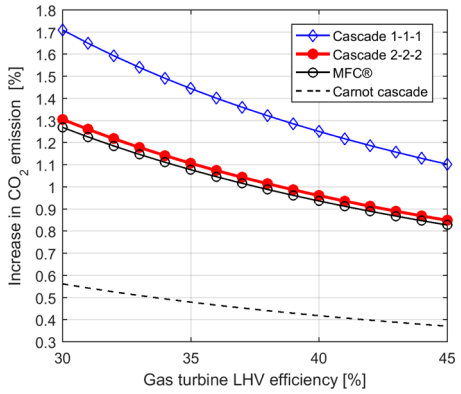

Figure 12. Increase in the total CO_2 emission when a power plant uses NG from a location with ambient temperature 10 °C instead of 30 °C, for different LNG gas turbines. (Only refrigeration is assumed to be ambient temperature dependent.)

focus of this work, however, was to analyze the potential for energy saving in cold climate locations for fixed LNG liquefaction process designs (i.e., assuming the same number and type of main equipment items).

To ensure a fair assessment of the variation in energy consumption with ambient temperature, the energy consumption of each of the processes considered was optimized with respect energy efficiency using a consistent methodology at all of the ambient temperature levels considered. The resulting performance information was then combined with global seawater temperature data from the Japan Meteorological Agency.[13]

The impact on CO_2 emissions for the LNG process was estimated by assuming that a gas turbine was used to supply power to the LNG process, and the overall CO_2 emissions were calculated assuming the LNG was used for power generation. A discussion of the methods and results from this work is presented below.

4.1. Modeling of the LNG Liquefaction Schemes. The mixed refrigerant cascade process, referred to here as MFC, is used as a base case in this study because it is one of the most efficient commercial LNG liquefaction processes available.[18]

The pure component cascade process "Cascade 2−2−2" is included to represent a simple commercial LNG process. The "Cascade 1−1−1" process, which has the lowest practical process design complexity, and the "Carnot cascade", which is the most efficient process possible, are studied to provide upper and lower bounds to the results generated.

4.2. Increase in LNG liquefaction efficiency with ambient temperature. Table 4 shows that the theoretical Carnot cascade increases in energy consumption by 22.9% as the ambient temperature is raised from 10 to 30 °C. Although the configuration of the Cascade 1−1−1, Cascade 2−2−2, and MFC processes are quite different, they also have a similar percentage increase in energy consumption as ambient temperature increases, the increase being 20.2% and 20.8% and 23.8% (respectively). Given that the impacts of temperature on efficiency are very similar for each of the processes considered, a general conclusion can be drawn that an optimized LNG liquefaction process having a fixed design (containing the same main process components) will consume 20−24% more energy in a location with 30 °C SST compared to 10 °C SST.

The results from the present study compare well with those by Park et al., who found that for a range of 5−25 °C specific power was increased by 27.6% for a fixed size of GT driving the refrigerant compressors and 25.8% if the UA value for the liquefaction exchangers was fixed.[9]

The results of Castillo et al., which show an increase of between 18% and 42% in specific power over an ambient temperature range of 6−25 °C, varying with LNG process

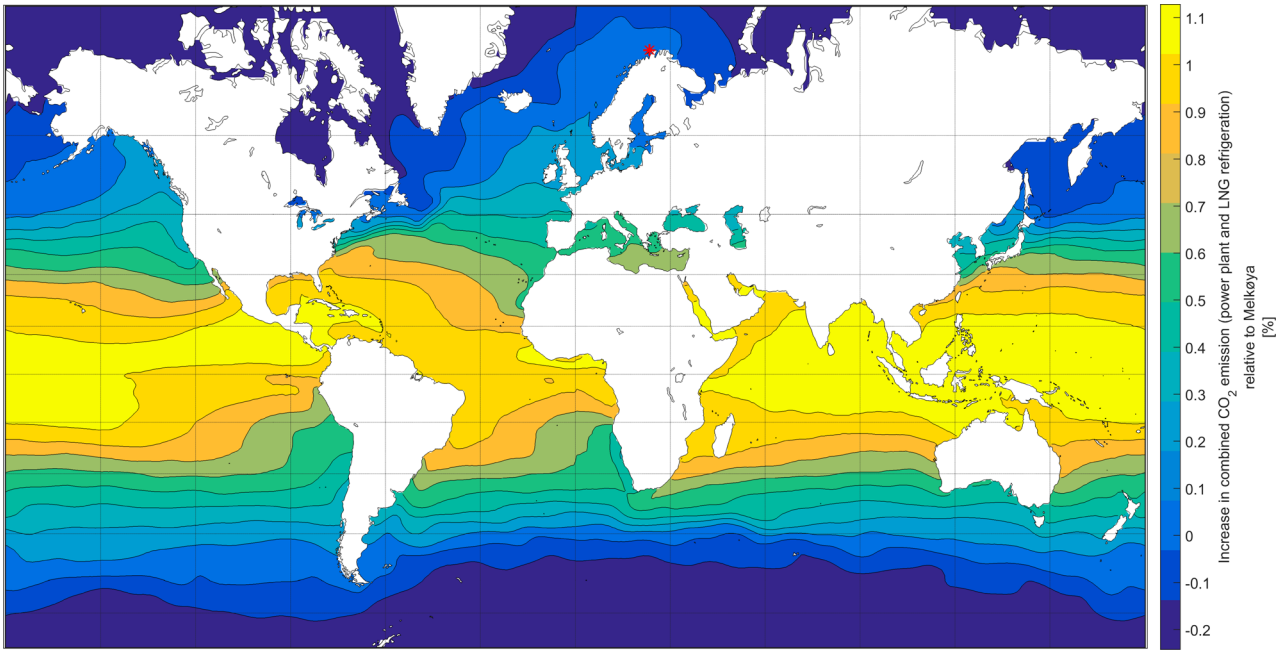

Figure 13. Increase in total CO_2 emissions from a power plant burning LNG produced using MFC at different locations relative to Melkøya. The gas turbine powering the MFC process have 35% (LHV) efficiency. Melkøya is marked as "*". (Only refrigeration is assumed to be ambient temperature dependent.)

DOI: 10.1021/acs.iecr.7b00333
Ind. Eng. Chem. Res. XXXX, XXX, XXX−XXX

design,[10] compare well with the present study. Although the modeling done by Castillo et al. was also based on the work of Jensen et al.,[8] it is thought that the lower range of results in the present study reflects the greater focus on optimization for the high ambient temperature cases.

Rian et al.[11] considered the impact of ambient temperature by using a fixed exergy efficiency for the overall gas plant process. Their findings are that an LNG processing plant with a fixed exergy efficiency would require 19.9% less fuel consumption at 4 °C compared to 36 °C, which would equate to a 25% increase in specific power for 32 °C of temperature rise, or 15.6% for a 20 °C temperature rise assuming a linear relationship, which is outside of the range found by the present study. However, because Rian et al. used an assumption of constant exergy efficiency in their LNG plant model, they do not take into account the gain in exergy efficiency that would result from lower aftercooler temperatures in the first mixed refrigerant loop of the MFC process. This simplification would therefore cause the results of Rian et al. to underestimate the impact of ambient temperature on specific power consumption.

4.3. Geographical Variations in SST and LNG Process Performance. Figure 9 shows the energy consumption of each LNG process at each of the locations studied. These results were generated by combining the SST data shown in Figure 7 and the process performance data from Figure 8. The variation in energy consumption worldwide is presented in Figure 11, which shows that a MFC based LNG plant will require 26% more energy in the warmest locations than a plant located at Melkøya. The Gulfstream warms the ocean outside Melkøya, and Figure 11 also shows that a MFC process located in the coldest regions will require 5% less energy than at Melkøya.

4.4. Impact of Other Process Elements on LNG Plant Energy Efficiency. Other process units will also influence the energy efficiency of the LNG process plant: for example, LNG storage in tanks, liquefied petroleum gas (LPG) and condensate separation, CO_2 and N_2 removal, and monoethylene glycol (MEG) treatment and regeneration. Although not considered in the present study, many of these processes could also benefit from cold climates, making the energy savings and CO_2 emission reduction even larger in cold climate.

Rian et al.[11] studied a complete LNG plant where they found that the main part of the desired energy change for an LNG plant was the cooling and liquefaction process; associated separation processes and the compression of CO_2 recovered from the feed gas contributing just 1.9% and 0.7% (respectively). Hence, the LNG liquefaction efficiency is a relatively good estimate of the efficiency of the whole LNG plant.

4.5. Impact of Ambient Temperature on Local CO_2 Emissions. The CO_2 emissions from a liquefaction process that uses gas turbine based power generation relate directly to the energy consumption of the liquefaction process and the efficiency of the gas turbine used to generate the power required. If the gas turbines have a fixed efficiency, independent of location, the percentage increase in process energy consumption becomes the same as the increase in CO_2 emissions, as illustrated in eq 7. Figure 11 shows that a MFC process operating in a warm location like Northern Australia or the Middle Eastern countries will release 20−26% more CO_2 than one located at Melkøya.

However, the CO_2 emissions associated with LNG liquefaction are far less than the emissions generated when the LNG produced is burned to generate power and for this reason, it is interesting to study the overall CO_2 emissions from the full gas to power chain.

4.6. Significance of Ambient Temperature to Overall CO_2 Emissions. In this study a simplified model is developed to estimate overall CO_2 emissions. The model considers only the impact of varying power consumption in the liquefaction process and takes no account of varying power consumption in other processes associated with LNG production that could be affected by variations in ambient temperature (e.g., feed gas treating, dehydration, NGL separation, etc.) The important assumption in this approach is that the LNG process is the dominant consumer of power, which is supported by the findings of Rian et al.[11]

The CO_2 emission from the liquefaction process depends strongly on the efficiency of the GTs used to supply power to the process, which is typically in the range 30−45% LHV efficiency.[17] Figure 12 illustrates how overall CO_2 emissions vary with gas turbine LHV efficiency and temperature. Figure 13 shows the variation in combined CO_2 emissions from LNG liquefaction and power generation with geographical location. For GTs with 35% LHV efficiency, the total CO_2 footprint of an LNG power plant is increased by 1.1% if it uses LNG produced in a Middle Eastern country instead of LNG produced at Melkøya. For GTs ranging from 30−45%, the increase is 0.8−1.3%. Although the overall emission reduction associated with LNG liquefaction location normally vary by no more than 1%, the significance of this variation is increased when compared to the potential efficiency gains that could be expected from the future development. For example, maximum efficiency for CCGT power generation has only risen less than 4% in the past decade of development.[19]

4.7. Carbon Neutral LNG Liquefaction. Making a more comprehensive reduction to the CO_2 emissions from LNG plants can only be achieved if CO_2 generated by the GTs (that power the liquefaction process) is captured and sequestered. Carbon capture and sequestration (CCS) is already employed to a limited extent at Melkøya, where CO_2 from the feed gas is captured and injected back into an offshore reservoir.

The two main energy consuming elements of a CCS process are CO_2 capture from the GT exhaust gas and CO_2 transportation (compression to pipeline/storage pressure), both of which will benefit from reduced energy consumption in the liquefaction process due to the corresponding reduction in CO_2 emissions.

In particular, earlier work has shown that CO_2 compression to normal transport pressure consumes up to 15% more energy in the Middle East than at Melkøya.[12] Therefore, a carbon neutral LNG plant equipped with CO_2 capture in the cold climate location will benefit from both improved process efficiency in the transport process and a reduction in the volume of CO_2 that must be transported. Overall, if an LNG process in warm locations like Northern Australia or a Middle Eastern country releases 20−26% more CO_2 than one located at Melkøya, the energy consumption for CO_2 capture and transport will be 20−30% higher.

4.8. Impact of Seasonal Temperature Variations. Seasonal variation in cooling temperatures is an important factor in the design for an LNG process. Process equipment (compressors, exchangers, etc.) will be sized to meet the required production capacity at a maximum design temperature, which will be related to the maximum ambient cooling temperature. If the maximum design temperature is exceeded on a few days of the year, the production capacity will be

DOI: 10.1021/acs.iecr.7b00333
Ind. Eng. Chem. Res. XXXX, XXX, XXX−XXX

affected; if the ambient temperature is below the design temperature, some reduction in power consumption and/or increase in production may be possible.

Figure 7 illustrates that Melkøya and Barrow Island exhibit a relatively low seasonal variation in SST, whereas Oristano and Ras Laffan have relatively large SST variation. A qualitative judgment can be made that locations with relatively large seasonal ambient temperature variation are likely to have higher average energy consumption, because the processes will operate further away from ambient temperature design conditions, but this is not modeled as part of this study. This study uses optimum year-round process performance, based on monthly average SST data, and does not use a detailed model of equipment performance like heat exchangers UA-value and compressor efficiency.

4.9. Limitations on SST Data. The SST data do not take into account conditions close to land, or temperature variations at different depths. For example, Alabdulkarem et al. discussed the benefit of using seawater extracted below the surface level with a temperature of 27 °C, instead of 35 °C seawater from the surface, for CO_2 liquefaction applications.[20] Obtaining the lowest accessible cooling water temperature at different locations can be identified as an area for future investigation.

4.10. Cost Impacts Due to Cold Climate. The investment and operating costs associated with LNG plants are affected by the process equipment, the size of the process trains and the arrangement of equipment items into process trains. The focus of this study is process efficiency and no attempt is made to assess the cost impact of variation in ambient temperature because of the complex mixture of factors that come into play.

One possibility is that the comparisons made here, which are based on constant process complexity, are likely to underestimate the cold climate benefits because equipment sizes and duties are generally lower in the cold climate locations, reducing costs. For example, given a fixed LNG production capacity many of the components in the refrigeration process in a warm location must be larger to compensate for chilling with ambient cooling water in cold locations. However, a location with a harsh climate such as locations in the artic, where icing and winterization become important issues which will add to the cost of the LNG plant. A detailed discussion of challenges in arctic regions are presented by Bourmistrov et al.[21]

5. CONCLUSION

This study shows that LNG plants in warm locations like North Australia and the Middle Eastern countries will require 20−26% more energy than similar processes located in cold climates such as Melkøya. Another important finding is that each of the different liquefaction processes considered has similar percentage energy savings with reduced cooling water temperature, which indicates that the energy savings is independent of process design for an optimized process.

Natural gas is generally recognized as one of the more environmentally friendly energy sources in a transition period between fossil fuel and renewable energy, making opportunities to reduce CO_2 emissions from the production of natural gas particularly important. The CO_2 emissions from gas turbines burning NG is directly related to the energy consumption. That is, the refrigeration process in warm locations release 20−26% more CO_2 than Melkøya, depending on the process used. The total CO_2 foot print of a power plant, which is fed by gas generated from LNG, will increase by 0.8−1.3% if it uses LNG produced in a Middle Eastern country instead of LNG produced at Melkøya.

Although there are many challenges associated with industrial development in the Arctic, access to a low temperature heat sink is an important benefit. The present study shows that the benefits of low temperatures include: improved energy efficiency, reduced local CO_2 emissions, and a significant reduction in overall CO_2 emissions.

AUTHOR INFORMATION

Corresponding Author

*S. Jackson. Tel.: +47 776 60365. E-mail: steve.jackson@uit.no.

ORCID

Steve Jackson: 0000-0002-2319-9783

Notes

The authors declare no competing financial interest.

NOMENCLATURE

COP coefficient of performance [−]
h specific enthalpy [kJ/kg]
k released CO_2 per kg consumed natural gas [kg CO_2/kg NG]
LHV lower heating value [MJ/kg]
$\dot{m}$ mass flow rate [kg/s]
p pressure [bar]
Q heat (kJ)
T temperature [°C]
T_{amb} ambient temperature [°C]
w_{NG} specific electrical energy consumption [kWh/ton NG]
$h_{el,pow}$ LHV efficiency of the electric power plant consuming natural gas [−]
h_{GT} isentropic efficiency (gas turbine) [−]
h_{is} isentropic efficiency of the compressors in the liquefaction process [−]

REFERENCES

(1) Pereira, C.; Lequisiga, D. Technical evaluation of C3-MR and cascade cycle on natural gas liquefaction process. *Int. J. Chem. Eng. Appl.* **2014**, *5* (6), 451−456.

(2) Hatcher, P.; Khalilpour, R.; Abbas, A. Optimisation of LNG mixed-refrigerant processes considering operation and design objectives. *Comput. Chem. Eng.* **2012**, *41*, 123−133.

(3) Lim, W.; Choi, K.; Moon, I. Current status and perspectives of liquefied natural gas (LNG) plant design. *Ind. Eng. Chem. Res.* **2013**, *52*, 3065−3088.

(4) Bauer, H. C. Mixed fluid cascade, experience and outlook. AIChE Spring Meeting and Global Congress on Process Safety, 2012.

(5) Pettersen, J.; Nilsen, Ø.; Vist, S.; Giljarhus, L. E. N.; Fredheim, A. O.; Aasekjær, K.; Neeraas, B. O. Technical and operational innovation for onshore and floating LNG. 17th International Conference & Exhibition on Liquefied Natural Gas, Houston, Texas, Houston, Texas, 2013.

(6) Statoil Konsekvensutredning Snøhvit LNG. http://www.statoil.com/no/EnvironmentSociety/Environment/impactassessments/fielddevelopments/Downloads/Sn%C3%B8hvit%20LNG%20-%20Konsekvensutredning%20-%20April%202001.pdf (accessed September 2016).

(7) Aspelund, A.; Gundersen, T.; Myklebust, J.; Nowak, M. P.; Tomasgard, A. An optimization-simulation model for a simple LNG process. *Comput. Chem. Eng.* **2010**, *34*, 1606−1617.

(8) Jensen, J. B.; Skogestad, S. Optimal operation of a mixed fluid cascade LNG plant. *Comput.-Aided Chem. Eng.* **2006**, *21*, 1569−1574.

(9) Park, K.; Won, W.; Shin, D. Effects of varying the ambient temperature on the performance of a single mixed refrigerant liquefaction process. *J. Nat. Gas Sci. Eng.* **2016**, *34*, 958−968.

DOI: 10.1021/acs.iecr.7b00333
Ind. Eng. Chem. Res. XXXX, XXX, XXX−XXX

(10) Castillo, L.; Dahouk Majzoub, M.; Di Scipio, S.; Corao, C. A. Conceptual analysis of the precooling stage for LNG processes. *Energy Convers. Manage.* **2013**, *66*, 41−47.
(11) Rian, A.; Ertesvåg, I. Exergy Evaluation of the Arctic Snøhvit Liquefied Natural Gas Processing Plant in Northern Norway - Significance of Ambient Temperature. *Energy Fuels* **2012**, *26*, 1259−1267.
(12) Brodal, E.; Jackson, S.; Eiksund, O. Energy saving potential of CO_2 transportation processes in cold climate locations. *Ind. Eng. Chem. Res.* **2016**, *55*, 11597−11605.
(13) Japan Meteorological Agency. http://ds.data.jma.go.jp/tcc/tcc/products/elnino/cobesst_doc.html (accessed May 23 2016).
(14) Bell, I. H.; Wronski, J.; Quoilin, S.; Lemort, V. Pure and pseudo-pure fluid thermophysical property evaluation and the open-source thermophysical property library CoolProp. *Ind. Eng. Chem. Res.* **2014**, *53*, 2498−2508.
(15) Moein, P.; Sarmad, M.; Ebrahimi, H.; Pakseresht, S.; Vakili, S. Z. APCI- LNG single mixed refrigerant process for natural gas liquefaction cycle: Analysis and optimization. *J. Nat. Gas Sci. Eng.* **2015**, *26*, 470−479.
(16) Japan Meteorological Agency. *Characteristics of global sea surface temperature analysis data (COBE-SST) for climate use*; 2006.
(17) GE Oil & Gas. *Liquefied natural gas - Reliable innovation for the entire LNG value chain*; IHS CERA: London, 2010.
(18) Vatani, A.; Mehrpooya, M.; Palizdar, A. Advanced exergetic analysis of five natural gas liquefaction processes. *Energy Convers. Manage.* **2014**, *78*, 720−737.
(19) Drew, R. CCGT: Breaking the 60% efficiency barrier 2010. http://www.powerengineeringint.com/articles/print/volume-18/issue-3/features/ccgt-breaking-the-60-per-cent-efficiency-barrier.html (accessed March 18th).
(20) Alabdulkarem, A.; Hwang, Y.; Radermacher, R. Development of CO_2 liquefaction cycles for CO_2 sequestration. *Appl. Therm. Eng.* **2012**, *33*, 144−156.
(21) Bourmistrov, A.; Mellemvik, F.; Bambulyak, A.; Gudmestad, O.; Overland, I.; Zolotukhin, A. *International arctic petroleum cooperation: Barents sea scenarios*. Routledge: New York, 2015.

DOI: 10.1021/acs.iecr.7b00333
Ind. Eng. Chem. Res. XXXX, XXX, XXX−XXX

Appendix – Article 2

energies

MDPI

Article

Optimization of the Energy Consumption of a Carbon Capture and Sequestration Related Carbon Dioxide Compression Processes

Steven Jackson * and Eivind Brodal

Instituttet for ingeniørvitenskap og sikkerhet IVT, UiT Norges Arktiske Universitet, 9019 Tromsø, Norway; eivind.brodal@uit.no

* Correspondence: steve.jackson@uit.no

Received: 26 March 2019; Accepted: 25 April 2019; Published: 26 April 2019

Abstract: It is likely that the future availability of energy from fossil fuels, such as natural gas, will be influenced by how efficiently the associated CO_2 emissions can be mitigated using carbon capture and sequestration (CCS). In turn, understanding how CCS affects the efficient recovery of energy from fossil fuel reserves in different parts of the world requires data on how the performance of each part of a particular CCS scheme is affected by both technology specific parameters and location specific parameters, such as ambient temperature. This paper presents a study into how the energy consumption of an important element of all CCS schemes, the CO_2 compression process, varies with compressor design, CO_2 pipeline pressure, and cooling temperature. Post-combustion, pre-combustion, and oxyfuel capture scenarios are each considered. A range of optimization algorithms are used to ensure a consistent approach to optimization. The results show that energy consumption is minimized by compressor designs with multiple impellers per stage and carefully optimized stage pressure ratios. The results also form a performance map illustrating the energy consumption for CO_2 compression processes that can be used in further study work and, in particular, CCS system models developed to study performance variation with ambient temperature.

Keywords: CO_2; Compression; Optimization; CCS

1. Introduction

Carbon capture and sequestration (CCS) is recognized as an important strategy for reducing CO_2 emissions, but its wide spread adoption is held-back by uncertainty over the energy consumption and cost impact implied by the additional infrastructure required because of this, the optimization of CCS processes to reduce their energy and cost impacts represents an important field of study.

The capture element of most CCS schemes is generally accepted to have the greatest impact on energy efficiency and cost. Lucquiaud et al. [1] report that for an "nth of a kind CCS plant with current state-of-the-art solvent technology" the energy needed by the capture plant will be 250–300 kWh of electrical energy per tonne CO_2 captured (kWh_e/tCO_2), whereas estimates of the energy consumption for CO_2 compression lie typically in the range 80–120 kWh_e/tCO_2 [2]. CO_2 compression is also a mature technology, with conventional multi-stage centrifugal CO_2 compressor designs widely used in the fertilizer and petroleum industries [3]. Suppliers of large-capacity multi-stage centrifugal CO_2 compressors include Dresser-Rand, General Electric (GE), and MAN Turbo and Diesel (MAN). Common industrial applications include enhanced oil recovery (EOR), fertilizer production, and CCS. MAN, for example, has operating references including an 8-stage compressor used for EOR with a discharge pressure of 187 bara and a capacity of 36 kg/s; a 10-stage compressor used in fertilized production with a discharge pressure of 200 bara and a capacity of 13 kg/s; and offers designs for

capacities of up to 110 kg/h [4]. Given that a 600 MW natural gas combined cycle power plant with 90% CO_2 capture requires a CO_2 compression capacity of approximately 56 kg/h [5], the scale-up of current industrial designs to CCS applications is generally considered unproblematic. As a result, fewer studies have been made into the optimization of the CO_2 compression process than have been made for the capture processes.

Some studies have studied the optimization of CO_2 compression in the context of a particular CCS capture technology. Romeo et al. [6] and Luo et al. [7] studied the optimum design for CO_2 compression in the context of heat recovery into a steam cycle. Posch et al. [8] and Font-Palma et al. [9] studied the optimization of the oxyfuel flue gas purification process where the early parts of the CO_2 compression process are integrated with the CO_2 separation process. Other studies have looked at optimization from the perspective of comparing conventional compression approaches to newer unconventional approaches. Alabdulkarem et al. [10] studied the potential benefit of liquefaction and pumping. Harkina et al. [11] and Luo et al. [7] studied the benefits of using shockwave type compression. Pei et al. [12] studied the benefits of heat recovery using ORC. A small number of studies such as Calado [13] and Jackson et al. [14] have considered the optimum number of CO_2 compression stages, but these have had a limited focus and do not apply their conclusions to the full set of operating parameters that could be expected in a range of typical CCS scenarios. Overall, most CO_2 compressor optimization studies are limited to one specific CCS scenario and focus on the capture process rather than the compression process in itself. Many do not optimize stage pressure ratios or the number of compression stages. None have been identified that consider optimization of compressor design for a wide set of operating cases.

The aim of this study is to generate a set of CO_2 compressor performance data that is based on the optimum number of compressor stages and stage pressure ratios for a wide range of operating cases. The specific intention is that this data can be used to support the development of a system model capable of comparing energy consumption of a wide variety of CCS scenarios.

2. Method

The compressor model used in this study was developed in MATLAB (2018a, The MathWorks, Natick, MA, United States) utilizing properties predictions from the TREND package (Thermodynamic Reference and Engineering Data 3.0., Lehrstuhl für Thermodynamik, Ruhr-Universität Bochum, Bochum, Germany). A literature review was conducted to identify a set of realistic CO_2 compressor design parameters; the operating parameters for the three principle CO_2 capture alternatives: Post-combustion, pre-combustion and oxyfuel; and the appropriate range of cooling temperatures and discharge pressures to be studied. Optimization of the compressor model for each set of parameters was carried out using algorithms available in MATLAB. Each of these elements of the study method are set out in Nomenclature.

2.1. Compressor Modeling

Conventional CO_2 compressor designs can either be integrally geared type, with one impeller and one gas cooler per stage; or barrel type, with multiple impellers and one gas cooler per stage [3]. In both designs the pressure ratio per impeller is limited to around 2 for CO_2 service and because of this, it is common to model CO_2 compressors with a pressure ratio per stage limit, $Pr < 2$ [6]. In this study, the cases following this convention are called the constrained cases. In a barrel type compressor design it is common to use several impellers per stage, and with an integrally geared design this is also possible, although less common. When multiple impellers are used per stage, Pr can be greater than 2, and in some studies, unconventional compressor designs with a Pr of up to 10 have been investigated [7,11], although these compressor designs are still under development. In this study, all cases where $Pr > 2$ are referred to as unconstrained cases.

Figures 1 and 2 provides an illustration of a CO_2 compressor design with n stages, where Pin_1 is the compressor feed pressure and $Pout_n$ is the compressor discharge pressure. Each stage is assigned

a sequential number, $i = \{1, \ldots, n\}$. Pin_i is the inlet pressure for stage i; Pr_i is the pressure ratio for stage i; and $Pout_i$ is the outlet pressure for stage i. The gas cooler pressure drop, ΔP, and the gas cooler outlet temperature, To, are both equal for all stages. In all cases, ΔP is fixed at 0.5 bar and To is studied over a range.

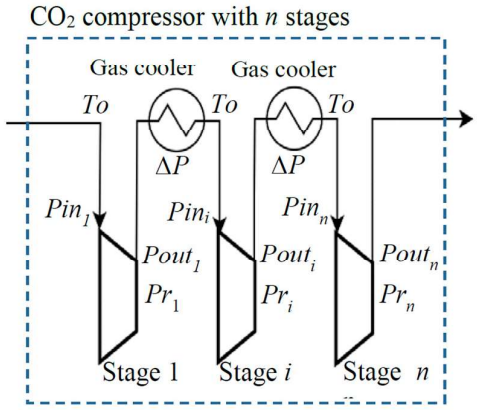

Figure 1. Illustration of a CO_2 compressor design with n stages.

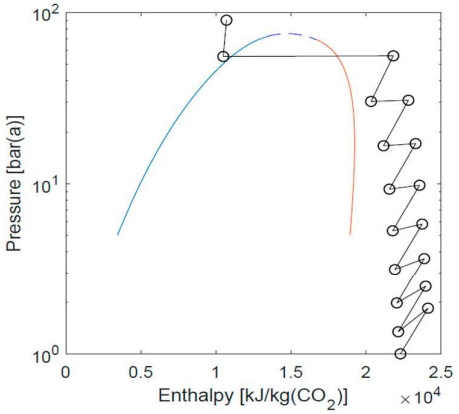

Figure 2. Illustration of a conventional nine-stage compressor in a pressure-enthalpy diagram.

The objective of the optimization study was to minimize the energy consumption required for compression, W_c, which was calculated in the model as follows:

$$W_c = \sum_{i=1}^{n} \frac{HoutS_i - Hin_i}{\eta}, \quad (1)$$

where $HoutS_i$ is the enthalpy at the outlet of an isentropic compression stage; Hin_i is the enthalpy at the compression stage inlet; and η is the compressor stage isentropic efficiency. In the literature, compressor stage isentropic efficiencies in the range 80% to 90% have been used [2,6,8,12,15,16]. In this study η is fixed at 85%.

Stage enthalpy and entropy values, $HoutS_i = f(S_i, Pout_i, x_i)$, $Hin_i = f(To, Pin_i, x_i)$, and $S_i = f(Pin_i, To)$ were calculated using the TREND properties package, where S_i is the entropy at the inlet to stage i and x_i is the composition at the inlet to stage i. In the oxyfuel study cases the CO_2 stream is dry and x_i is therefore fixed. In the other cases, the CO_2 stream is saturated with water below 30 bar(a) and, therefore, the water content and x_i varies with temperature and pressure. In these cases, $x_i = f(To, Pin_{i,})$ was also calculated using TREND.

When a liquid phase is possible at To, the final stage inlet pressure, Pin_n, is fixed 5 bar above the mixture dewpoint pressure, P_{DP}; when it is not, Pin_n is fixed 5 bar above the crycondenbar pressure for

the CO_2 mixture, P_{CR}. The final stage of the compressor represents a pump when the CO_2 stream is in the liquid phase.

A summary of the main compressor modelling parameters is provided below in Table 1.

Table 1. Summary of compressor modelling parameters.

Parameter	Constrained Cases	Unconstrained Cases
Pressure Ratio, Pr	<2	<10
Efficiency, η	85%	
Stage pressure drop, ΔP	0.5 bar	
Final stage inlet pressure, Pin_n	Minimum of P_{DP} + 5 bar and, P_{CR} + 5 bar	

2.2. Study Parameters

Three CO_2 capture scenarios were modeled: Pre-combustion capture, post-combustion capture, and oxyfuel. In all of the three scenarios the compressor discharge pressure, Pn, is studied in the range 90 bar(a) to 180 bar(a). Each compressor aftercooler has an outlet temperature, To, which is studied in the range 288 K to 323 K. The scenario specific parameters for each of the three capture cases are described below and summarized at the end of this section in Table 2.

2.2.1. Post-Combustion Capture

A typical post-combustion capture processes is represented by an amine based solvent absorption unit. This type of process produces a relatively pure stream of CO_2 at atmospheric pressure that is saturated with water. Typically, CO_2 streams that are to be transported in a pipeline are dried part-way through the compression process to take advantage of water drop-out in the early stages of compression [2]. In this study the break point for dehydration was taken as 30 bar(a): All stages below 30 bar(a) were modeled with a feed stream that was saturated with water; all above were modeled as dry. The dry stream composition used in this study, 99.99 mole% CO_2 and 0.01 mole% nitrogen, was based on an assessment of data published by DNV [17] and the TRENDS project [18].

2.2.2. Pre-Combustion Capture

There are a wide variety of competing pre-combustion capture processes [19]. Based on a review of [20,21] the basis for this study is a stream of CO_2 originating from steam-methane reformer that is captured using an MDEA solvent. As in the post combustion cases, the feed stream will be at atmospheric pressure and saturated with water below 30 bar(a). The dry composition, 99.5 mole% CO_2 and 0.5 mole% methane, was, again, based on an assessment of data published by DNV [17] and the TRENDS project [18].

2.2.3. Oxyfuel Capture

Within a normal oxyfuel flue gas purification process the operating pressure for the initial stages of the CO_2 compressor are set to optimize the performance of the purification process. This type of optimization falls outside of the scope of this study and, therefore, the feed pressure for the CO_2 compression process studied here is taken as the highest product stream pressure resulting from the oxyfuel purification process, i.e., de-coupled from the optimization of the purification process. The CO_2 stream from the purification process is dry, the main impurities being N_2, O_2, and argon [17]. The level of these impurities is not limited by technical barriers [9] and technologies for high and low purity has been investigated [8,15]. In this study, the highest pressure of the CO_2 feed stream leaving the purification unit is taken as 16.5 bar(a) and its composition 96.16 mole% CO_2, 2.45 mole% nitrogen, 0.96 mole% argon, and 0.43 mole% oxygen based on Posch et al. [8].

Table 2. Summary of compressor modeling parameters.

Parameter	Post	Pre	Oxyfuel
Cooling temperature, To	288 K to 323 K	288 K to 323 K	288 K to 323 K
Discharge pressure, Pn	90 bar(a) to 180 bar(a)	90 bar(a) to 180 bar(a)	90 bar(a) to 180 bar(a)
Inlet pressure, Pin_1	1.01 bar(a)	1.01 bar(a)	16.5 bar(a)
Dry stream composition	CO_2 99.99 mole% N_2 0.01 mole%	CO_2 99.5 mole% CH_4 0.5 mole%	CO_2 96.16 mole% N_2 2.45 mole% Ar 0.96 mole% O_2 0.43 mole%

2.3. Optimization of Compressor Energy Consumption

Optimization of the compressor stage pressure ratios, Pr_n, was carried in MATLAB using the functions GA, Fmincon, and Fminsearch. Fminsearch uses a simplex algorithm that is suitable for unconstrained, multi-variable, non-linear optimization problems. A benefit of this method is that it will usually quickly converge to a solution, a downside is that in some cases a local minimum may be obtained. Fmincon is a gradient-based method that is designed to work on problems where the objective and constraint functions are both continuous and have continuous first derivatives. GA can solve smooth or non-smooth optimization problems with or without constraints. It is a stochastic, population-based algorithm. GA is generally slower to reach a solution than Fminsearch and Fmincon, but it is more reliable in solving for the global minimum. All of these algorithms were used with MATLAB default options unless stated below.

2.3.1. Variables, Initial Guesses, and Constraints

Since the final stage inlet pressure, Pin_n, is fixed in the compressor model, the final stage pressure ratio, Pr_n, is not a variable in the optimization problem. In addition, since the penultimate stage pressure ratio, Pr_{n-1}, is calculated from the product of the other pressure ratios and Pin_n, Pr_{n-1} is not a variable in the optimisation problem either. The result is that for an n stage compressor, $n-2$ pressure ratios are variables.

The initial guesses for the stage pressure ratios were generated by assuming that all the stage pressure ratios were equal. The subsequent initial guesses used by the optimization algorithms were selected from previous optimization runs when available. The Fminsearch and Fmincon algorithms were generally used to improve initial guesses before GA was used.

In constrained cases, bound constraints are specified for all the variable pressure ratios such that $Pr_i < 2$. In both the constrained and unconstrained cases, a minimum pressure ratio bound constraint $Pr_i > 1.2$ was also used to avoid problematic optimization solutions, e.g., where $Pout_i - \Delta P < Pin_i$.

2.3.2. Objective Function

Since the pressure ratio for the next to last compression stage, Pr_{n-1}, was calculated within the compressor model and was not a variable in the optimization problem, an additional constraint was applied in the form of a penalty function, P_1, to ensure that $Pr_{n-1} > 1.2$ for all cases, and $Pr_{n-1} < 2$ in the constrained cases. The form of the penalty function was:

$$\text{if } 1.2 < Pr_{n-1} < 2,\ P_1 = 0,\ \text{else } P_1 = 100 \cdot (Pr_{n-1} - 1.5)^2. \tag{2}$$

An additional penalty function, P_2, was included to avoid two-phase conditions at any stage inlet conditions. This second penalty function had the form:

$$\text{if } To - T_{DP} > 5,\ P_2 = 0,\ \text{else } P_2 = \sum_{i=1}^{n} [0.01 + (5 - To - T_{DP})^2], \tag{3}$$

where $T_{DP} = f(P_i, x_i)$ is the dewpoint temperature of the gas mixture, x, at stage i.

The objective of the optimization problem was to minimize an objective function, X, which included contributions from the two penalty functions:

$$X = W_c + P_1 + P_2. \quad (4)$$

2.4. Identifying the Optimum Number of Compression Stages

Although the overall optimum number of compression stages is the one that corresponds with the minimum energy consumption, the percentage gain per additional compression stage is also important because of the additional costs implied. To acknowledge this, the overall optimum number of stages is defined in this study as the number of stages above which the percentage decrease in energy consumption falls below 2%. This is an arbitrary breakpoint based on a review of the optimization data.

3. Results and Discussion

The main results of the optimization work are presented below. In addition, links to the full set of data generated by this study are presented towards the end of this article under the heading Supplementary Materials.

3.1. The Benefits of Optimization

The amount of energy that is saved through the optimization of stage pressure ratios will vary from cases to case. Figure 3 illustrates that the gain could be as much as 10% of the total compression energy consumption, although in some cases it was much less.

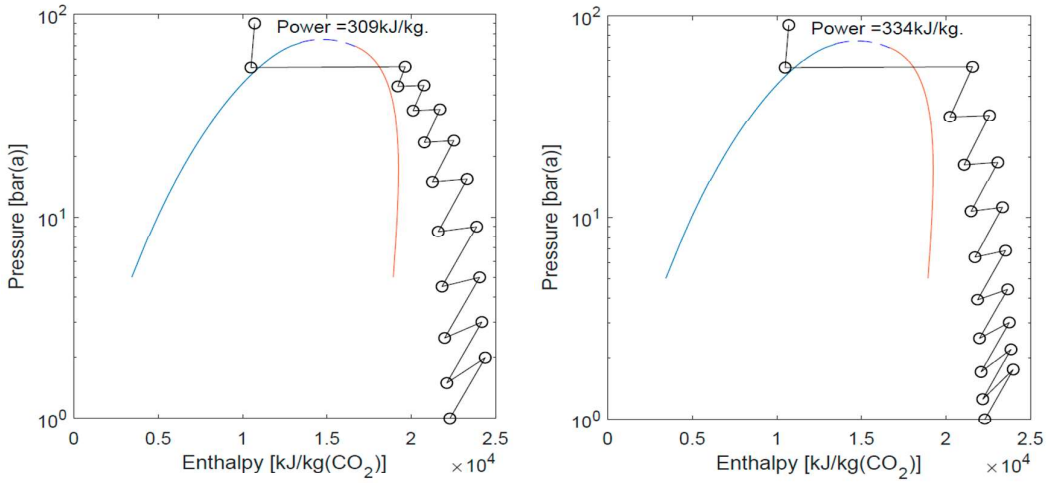

(a) **(b)**

Figure 3. Energy consumption for a 10 stage CO_2 compressor, post-combustion capture case, $P_n = 90$ bar(a) and $To = 288$ K with (**a**) constant Pr and (**b**) optimized Pr.

3.2. Consistency Checking and Optimum Stages

In Figure 4, the relative compression energy consumption vs. number of compression stages is plotted for all of the results from the post-combustion capture cases (grey crosses). Seven sets of data are highlighted to help illustrate trends. Data for the pre-combustion capture cases and the oxyfuel cases are presented in Figures 5 and 6, respectively.

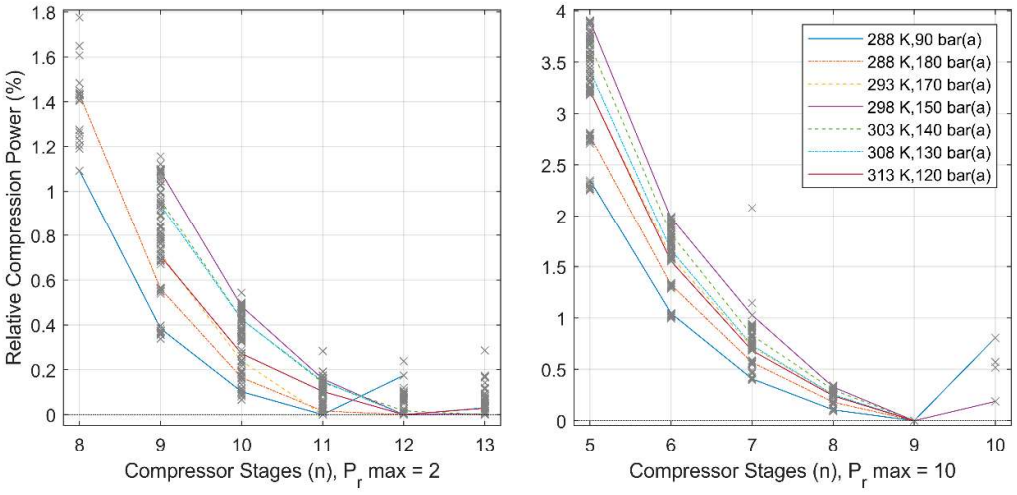

(a) **(b)**

Figure 4. Relative energy consumption vs. stages for post-combustion capture, (**a**) constrained cases and (**b**) unconstrained cases (right).

Figures 4–6 show that the energy consumption of the compression process often varied by less than 1% for compressor designs either side of the optimum number of stages, because of this, the optimization must be of high quality to accurately identify the optimum number of stages.

In many cases the fminsearch and fmincon algorithms did not give the required level of accuracy to show these trends and all the data presented here was generated by the GA algorithm, albeit, in many cases, from guesses provided by the other algorithms.

Although the trends visible in Figures 4–6 show a couple of examples of counter-intuitive behavior, overall they illustrated good consistency in the results of the study, indicating consistent and reliable level of optimization.

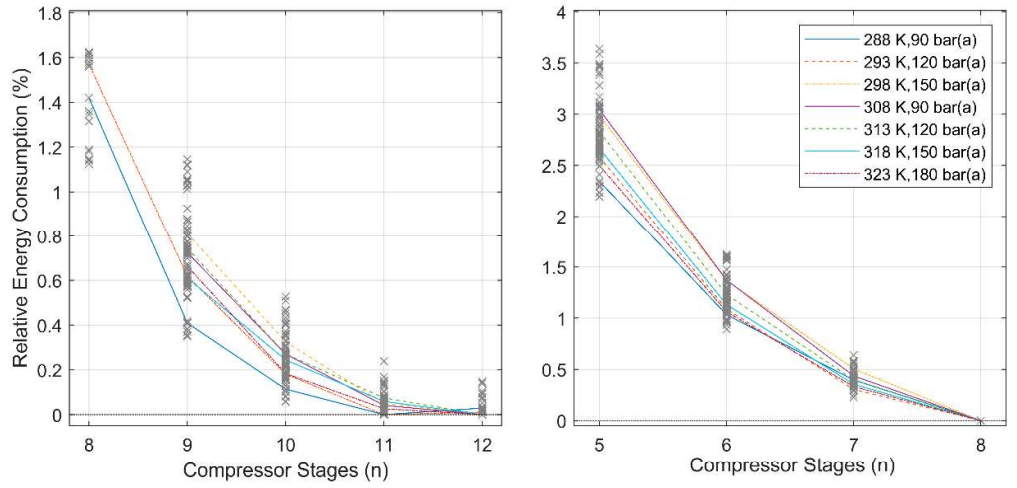

(a) **(b)**

Figure 5. Relative energy consumption vs. stages for pre-combustion capture, (**a**) constrained cases and (**b**) unconstrained cases.

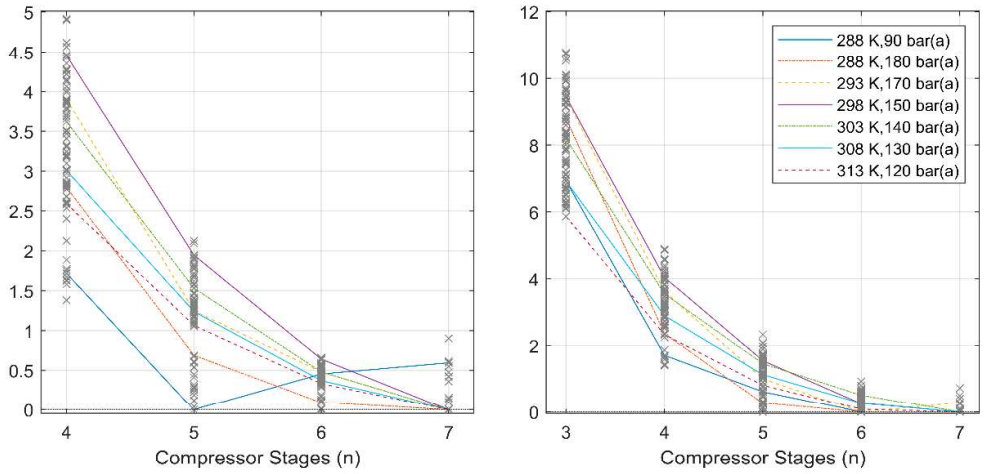

Figure 6. Relative energy consumption vs. compressor stage, oxyfuel cases, (**a**) constrained cases and (**b**) unconstrained cases.

3.3. *Variation of Energy Consumption with Cooling Temperature and Pressure*

Figures 7–9 show how compression energy consumption varied with cooling temperature and compressor discharge pressure for the three CO_2 capture scenarios. The optimum number of compression stages was overlaid.

The results show that optimum energy consumption was more strongly dependent on the cooling temperature than discharge pressure. This reflects the fact that the energy consumption for the final, pumped, stage was lower than the other compressor stages. The results also show that there was little difference between the energy consumption for the post and pre-combustion cases, which was because the composition of these two streams was very similar.

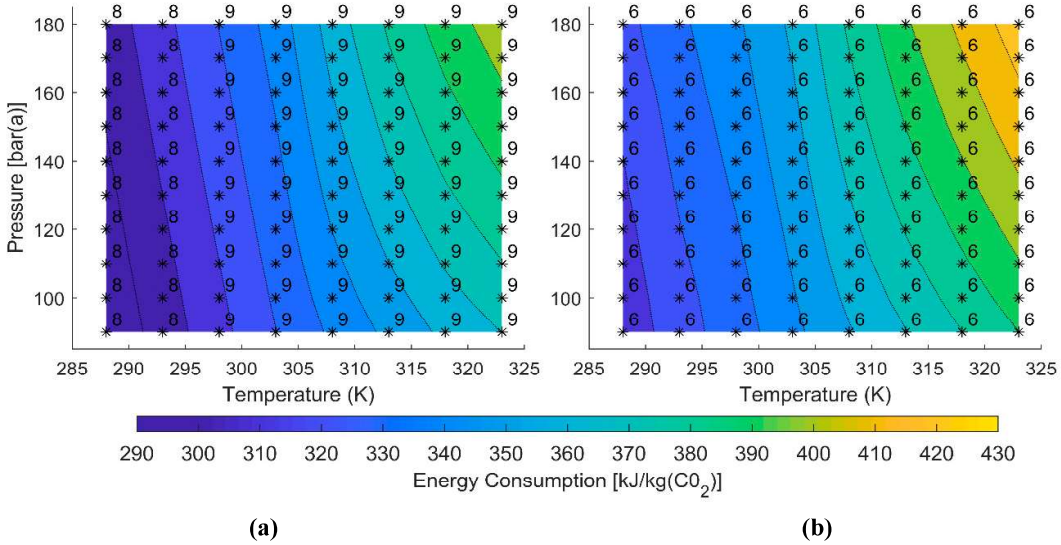

Figure 7. Post-combustion capture cases, optimized compression energy consumption and number of stages, (**a**) constrained cases and (**b**) unconstrained cases.

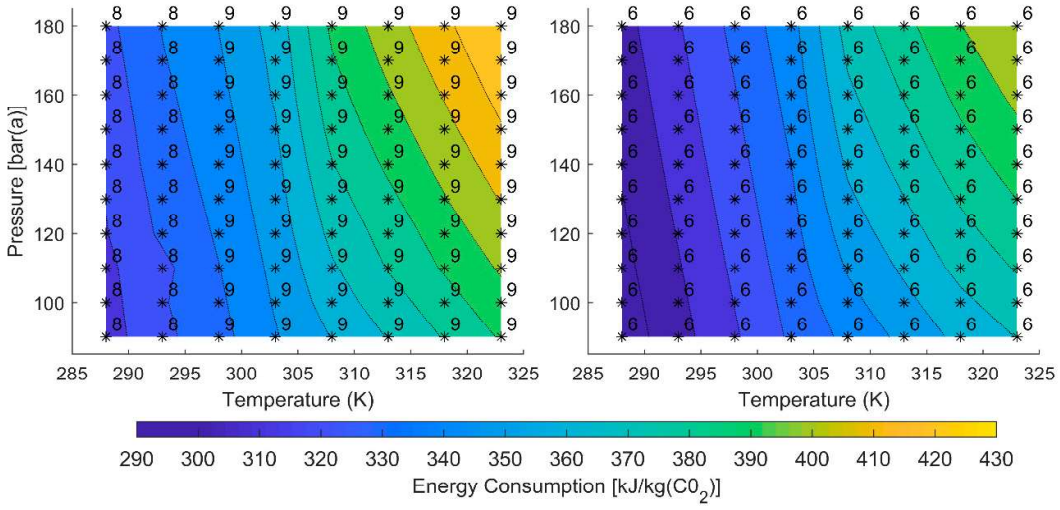

Figure 8. Pre-combustion capture cases, optimized compression energy consumption and number of stages, (**a**) constrained cases and (**b**) unconstrained cases.

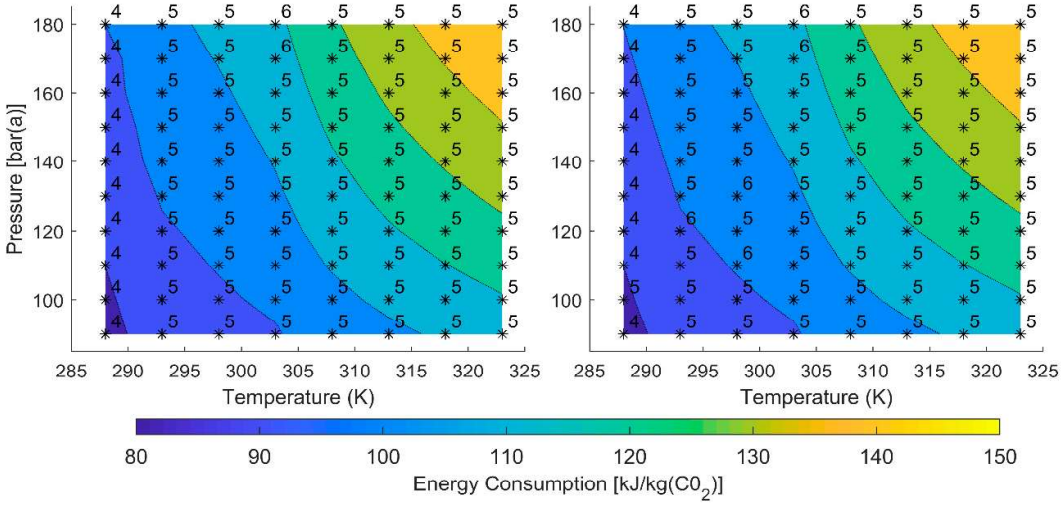

Figure 9. Oxyfuel cases, optimized compression energy consumption and number of stages, (**a**) constrained cases and (**b**) unconstrained cases.

3.4. Constrained vs. Unconstrained Cases

Figure 10 presents results for the percentage reduction in energy consumption for the unconstrained cases relative to the constrained cases, Figure 10a shows this for post-combustion cases and 10b for pre-combustion cases. The corresponding reduction in the number of compression stages required was overlaid. The oxyfuel cases were not shown here because the percentage reduction was close to zero in all cases.

The results in Figure 10 show that in all cases considered the unconstrained cases (those representing a design with multiple impellers per stage) had an optimum number of stages that was 2 to 3 fewer than the constrained cases (those assuming one impeller per stage). This represents a potentially significant saving in compressor cost. In addition, the unconstrained cases offered an average 6% saving in the energy required for compression.

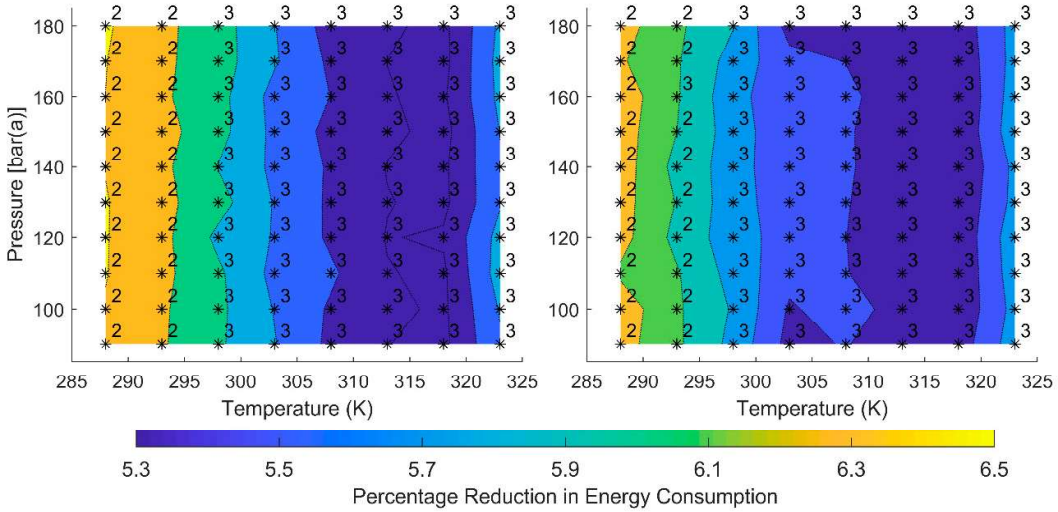

Figure 10. Reduction in energy consumption (%) for the unconstrained cases relative to the constrained cases with reduction in the number of compression stages overlaid, (**a**) post-combustion cases, (**b**) pre-combustion cases.

4. Discussion

Table 3 summarizes the results from Figures 7–9 for all constrained (const.) and unconstrained (u.const.) cases. In Table 3 we see that the energy consumption for the post combustion CO_2 compression cases varies in the range 292 kJ/kg CO_2 to 425 kJ/kg CO_2. This compares well with the range of 80–120 kWh_e/tCO_2 (equal to 288–432 $kJ/kgCO_2$) reported by Jordal et al. [2].

Table 3. Summary of the range of optimized energy consumption and number of stages.

Parameter	Post const.	Post u.con.	Pre const.	Pre u.con.	Oxy const.	Oxy u.con.
Energy, W_c [kJ/kg(CO_2)]	292 to 406	312 to 425	316 to 431	294 to 140	87 to 150	87 to 150
Stages, n (-)	8 to 9	6	8 to 9	6	4 to 5	4 to 6

Comparing some more specific cases from the literature, we see that for a post combustion case with 110 bar(a) discharge and 30 °C cooling, Amorllahi et al. [18] reported an energy consumption of 330 kJ/kg, which is practically identical to the value found in this study as presented in Figure 7a. Alhajaj et al. [22] reported the energy consumption for a 5 stage CO_2 compressor with a 14 MPa discharge pressure and 50 °C cooling (representing warm climates) to be 104.6 kWh per ton of CO_2 (= 380 kJ/kg of CO_2), which compares well with 390 kJ/kg of CO_2 found in this study, Figure 7a. Alhajaj et al. [22] also reported an energy consumption of 82.4 kWh/ton of CO_2 (= 297 kJ/kg of CO_2) for the same compressor with a 20 °C cooling temperature (representing colder climates), which also compares well with 311 kJ/kg of CO_2 found in this study from Figure 7a.

For the constrained post and pre-combustion cases the practical minimum number of stages varies between eight and nine depending on To. When $To \leq 293$ K it is possible to reach a pressure where the CO_2 stream will condense in seven stages and, hence, the overall minimum stages is eight. When $To > 293$ K, nine stages are required. Since the energy consumption for the eight and nine stage cases also falls within 2% of the overall minimum, as illustrated in Figures 4a and 5a, they also satisfy the criteria for the optimum number of compression stages used in this study. This means that the optimum number of stages presented in Figures 7a and 8a is dictated by the practical minimum number of stages for these cases.

For the unconstrained post and pre-combustion cases, Figures 4b and 5b show that the six stage cases all fall just within the 2% limit and therefore represent the optimum number of stages for this study presented in Figures 7b and 8b.

For the oxyfuel cases, the picture is less clear and Figure 6 shows that either four or five stages represent the optimum based on the definition used here. Figure 8 also shows the quality of the optimization is slightly less consistent for these cases, which is reflected in Figure 9. Figure 9 also shows that there is very little difference between the energy consumption for the constrained and unconstrained cases. This reflects the lost benefit that the use of pressure ratios greater than 2 provides to the unconstrained pre and post-combustion cases in the early stages of the compression process.

5. Conclusions

The comparison of the results from this study with other published data indicates that the energy consumptions predicted are reliable and can support the development of a system model capable of comparing energy consumption of a wide variety of CCS scenarios, which was the aim of this work.

In all cases studied here, the cooling temperature has a more substantial impact on optimum energy consumption than the compressor discharge pressure, because of this, it is concluded that the comparison of different CCS schemes and operating scenarios should consider the important role ambient temperature plays in determining the energy consumption.

This study also found that compressor designs with multiple impellers per stage have an advantage in terms of energy consumption and the optimum number of stages required compared to designs where one impeller per stage is used. Because of this, the performance maps for the unconstrained cases presented in Figure 7b, Figure 8b, and Figure 9b should be used as the basis for further study work.

Nomenclature

Hin_i	Enthalpy at the inlet to stage i
$HoutS_i$	Enthalpy at the outlet if stage i (isentropic basis)
n	Number of compressor stages
P_{CR}	Crycondenbar pressure
P_{DP}	Dew point pressure
Pin_i	Inlet pressure pressure for stage i
$Pout_i$	Outlet pressure pressure for stage i
Pr_i	Pressure ratio for stage i
ΔP	Aftercooler pressure drop
S_i	Entropy for stage i
To	Aftercooler outlet temperature
W_c	Energy used in compression
x_i	Gas composition stage i
η	Isentropic efficiency

Supplementary Materials: The following are available online at http://www.mdpi.com/1996-1073/12/9/1603/s1, Figure S1: Post-combustion capture cases, compression energy consumption with fixed (un-optimized) stage pressure ratios, (**a**) constrained cases and (**b**) unconstrained cases. Figure S2: Pre-combustion capture cases, compression energy consumption with fixed (un-optimized) stage pressure ratios, (**a**) constrained cases and (**b**) unconstrained cases. Figure S3: Oxy-combustion capture cases, compression energy consumption with fixed (un-optimized) stage pressure ratios, (**a**) constrained cases and (**b**) unconstrained cases. All data from Figures 7–9 and Figures S1–S3 in CSV .txt format.

Author Contributions: Conceptualization, S.J.; methodology, S.J.; formal analysis, S.J.; writing—original draft preparation, S.J.; writing—review and editing, E.B.; supervision, E.B.

Funding: This research received no external funding. The APC was funded by a grant from the publication fund of UiT The Arctic University of Norway.

Conflicts of Interest: The authors declare no conflict of interest.

References

1. Lucquiaud, M.; Liang, X.; Errey, O.; Chalmers, H.; Gibbins, J. Addressing technology uncertainties in power plants with post-combustion capture. *Energy Procedia* **2013**, *37*, 2359–2368. [CrossRef]
2. Jordal, K.; Aspelund, A. Gas conditioning—The interface between CO_2 capture and transport. *Int. J. Greenh. Gas Control.* **2007**, *1*, 343–354.
3. Dittmer, R.; Strube, R. Integrally-geared compressors as state-of-the-art technology. *Carbon Capture J.* **2015**, *47*, 15–18.
4. Habel, R.; Wacker, C. Innovative and proven CO_2 compression technology for CCS and EOR. *Carbon Capture J.* **2009**, *11*, 15–18.
5. Irlam, L. *Global Costs of Carbon Capture and Storage, 2017 Update*; Global CCS Institute: Docklands, Australia, 2017.
6. Romeo, L.M.; Bolea, I.; Lara, Y.; Escosa, J.M. Optimization of intercooling compression in CO_2 capture systems. *Appl. Therm. Eng.* **2009**, *29*, 1744–1751. [CrossRef]
7. Luo, X.; Wang, M.; Chen, J. Heat integration of natural gas combined cycle power plant integrated with post-combustion CO_2 capture and compression. *Fuel* **2015**, *151*, 110–117. [CrossRef]
8. Posch, S.; Haider, M. Optimization of CO_2 compression and purification units (CO_2CPU) for CCS power plants. *Fuel* **2012**, *101*, 254–263. [CrossRef]
9. Font-Palma, C.; Errey, O.; Corden, C.; Chalmers, H.; Lucquiaud, M.; Sanchez Del Rio, M.; Jackson, S.; Medcalf, D.; Livesey, B.; Gibbins, J.; et al. Integrated oxyfuel power plant with improved CO_2 separation and compression technology for EOR application. *Process. Saf. Environ. Prot.* **2016**, *103*, 455–465. [CrossRef]
10. Alabdulkarem, A.; Hwang, Y.; Radermacher, R. Development of CO_2 liquefaction cycles for CO_2 sequestration. *Appl. Therm. Eng.* **2012**, *33*, 144–156. [CrossRef]
11. Harkina, T.; Hoadley, A.; Hooper, B. A comparison of the Process Integration of Shockwave CO_2 compression with conventional turbo machinery into PCC power station design. *Energy Procedia* **2011**, *4*, 1339–1346. [CrossRef]
12. Pei, P.; Barse, K.; Gil, A.J.; Nasah, J. Waste heat recovery in CO_2 compression. *Int. J. Greenh. Gas Control.* **2014**, *30*, 86–96. [CrossRef]
13. Calado, M. Modeling and design synthesis of a CCS compression train system via MINLP optimization. Instituto Superior Técnico, Universidade de Lisboa. 2012. Available online: https://fenix.tecnico.ulisboa.pt/downloadFile/395144614662/ExtendedAbstract_MarioCalado_12Outubro2012.pdf (accessed on 26 April 2019).
14. Jackson, S.; Brodal, E. A comparison of the energy consumption for CO_2 compression process alternatives. Available online: https://iopscience.iop.org/article/10.1088/1755-1315/167/1/012031/pdf (accessed on 26 April 2019).
15. Pipitone, G.; Bolland, O. Power generation with CO_2 capture: Technology for CO_2 purification. *Int. J. Greenh. Gas Control.* **2009**, *3*, 528–534. [CrossRef]
16. Amrollahi, Z.; Ystad, P.A.M.; Ertesvåg, I.S.; Bolland, O. Optimized process configurations of post-combustion CO_2 capture for natural-gas-fired power plant—Power plant efficiency analysis. *Int. J. Greenh. Gas Control.* **2012**, *8*, 1–11. [CrossRef]
17. D.N.V. Recommended Practice, DNV-RP-J202, Design and Operation of CO_2 Pipelines. DNV, 2010. Available online: https://rules.dnvgl.com/docs/pdf/DNV/codes/docs/2010-04/RP-J202.pdf (accessed on 26 April 2019).
18. Eickhoff, C.; Neele, F.; Hammer, M.; DiBiagio, M.; Hofstee, C.; Koenen, M.; Fischer, S.; Isaenko, A.; Brown, A.; Kovacs, T. IMPACTS: Economic Trade-offs for CO_2 Impurity Specification. *Energy Procedia* **2014**, *63*, 7379–7388. [CrossRef]
19. Damen, K.; Troost, M.v.; Faaij, A.; Turkenburg, W. A comparison of electricity and hydrogen production systems with CO_2 capture and storage. Part A: Review and selection of promising conversion and capture technologies. *Prog. Energy Combust. Sci.* **2006**, *32*, 215–246. [CrossRef]
20. IEA Greenhouse Gas R&D Programme. Techno-Economic Evaluation of SMR Based Standalone (Merchant) Hydrogen Plant with CCS. 2017. Available online: https://ieaghg.org/exco_docs/2017-02.pdf (accessed on 26 April 2019).

21. Tanaka, Y.; Sawada, Y.; Tanase, D.; Tanaka, J.; Shiomi, S.; Kasukawa, T. Tomakomai CCS Demonstration Project of Japan, CO_2 Injection in Process. *Energy Procedia* **2017**, *114*, 5836–5846. [CrossRef]
22. Alhajaj, A.; Mac Dowell, N.; Shah, N. A techno-economic analysis of post-combustion CO_2 capture and compression applied to a combined cycle gas turbine: Part I. A parametric study of the key technical performance indicators. *Int. J. Greenh. Gas Control.* **2016**, *44*, 26–41. [CrossRef]

Appendix – Article 3

energies

MDPI

Article

Optimization of a Mixed Refrigerant Based H_2 Liquefaction Pre-Cooling Process and Estimate of Liquefaction Performance with Varying Ambient Temperature

Steven Jackson * and Eivind Brodal

IAP, UiT-Norges Arktiske Universitetet, Tromsø, Norway; eivind.brodal@uit.no
* Correspondence: steve.jackson@uit.no

Abstract: Hydrogen used as an energy carrier can provide an important route to the decarbonization of energy supplies, but realizing this opportunity will require both significantly increased production and transportation capacity. One route to increased transportation capacity is the shipping of liquid hydrogen, but this requires an energy-intensive liquefaction step. Recent study work has shown that the energy required in this process can be reduced through the implementation of new and improved process designs, but since all low-temperature processes are affected by the available heat-sink temperature, local ambient conditions will also have an impact. The objective of this work is to identify how the energy consumption associated with hydrogen liquefaction varies with heat-sink temperature through the optimization of design parameters for a next-generation mixed refrigerant based hydrogen liquefaction process. The results show that energy consumption increases by around 20% across the cooling temperature range 5 to 50°C. Considering just the range 20 to 30°C, there is a 5% increase, illustrating the significant impact ambient temperature can have on energy consumption. The implications of this work are that the modelling of different liquified hydrogen based energy supply chains should take the impact of ambient temperature into account.

Keywords: hydrogen; liquefaction; optimization; ambient temperature; mixed refrigerant

Citation: Jackson, S.; Brodal, E. Optimization of a Mixed Refrigerant Based H_2 Liquefaction Pre-Cooling Process and Estimate of Liquefaction Performance with Varying Ambient Temperature. *Energies* **2021**, *14*, x. https://doi.org/10.3390/xxxxx

Academic Editor: Bahman Shabani

Received: 2 September 2021
Accepted: 21 September 2021
Published: date

1. Introduction

Hydrogen used as a fuel, as an energy source for industrial processes or for generating electrical power can provide an important route to the decarbonization of energy supplies and the integration of renewable energy systems. The study of Acar and Dincer [1], for example, identifies that hydrogen can play "eight significant roles" in the green energy transition. Recent studies have also made the case that achieving a transition to carbon-free energy in the EU is impossible without a large increase in hydrogen production [2], and energy system modeling has found that "hydrogen and synfuels add up to between 20% and 50% of [EU] energy demand in transport in 2050" [3]. This positive view of the role that hydrogen could play in future low-carbon development is also reflected in political intent via the EU hydrogen strategy [4].

Reflecting this political support, research related to hydrogen energy has increased over recent years [5]. Important research topics include energy demand and supply modelling [2,3], the novel integration of renewable energy sources such as solar power [6], the development of enhanced electrolysis based production methods [7], the development of new applications such as use a reductant in steel manufacturing [8] and the assessment of alternative sources such as methanol [9].

In all envisaged future hydrogen-based economies, a significant increase in the transportation capacity for hydrogen is required. It is possible to transport hydrogen as a com-

pressed gas or as a liquid at low temperature, in pipelines as a gas. The optimum transportation strategy will depending on both transportation capacity and the distance [10]. When the distance is significant it is reasonable to expect that shipping of hydrogen will be favored, and while researchers such as Ishimoto et al. [11] have studied the economics of shipping liquefied hydrogen, some commercial steps have also been made, with the world's first liquid hydrogen carrier ship launched in Japan in 2019 [12].

If hydrogen is transported at large-scale as a liquid, a key part of the supply chain will be the liquefaction process, which is very energy intensive. The specific energy consumption (SEC) of the most efficient currently operating large-scale hydrogen liquefaction (LHL) plants lies in the range 13 to 15 kWh/kg [13], which is much higher that even the most efficient LNG processes, which have a SEC of around 240 kWh/tonne. Because of this, there is significant interest in the development of new and improved LHL technologies that can help reduced SEC.

Research topics relating to improved LHL technologies include the integration of renewable energy sources, such as solar energy [14] and geothermal energy [15]; the use of mixed refrigerants (MR) for pre-cooling [16–18]; and the use of helium in the cryogenic cooling and liquefaction part of the process [19,20]. Other research has focused on the impact of the conversion of ortho-hydrogen to para-hydrogen on the liquefaction process [21,22] and the relative performance of different heat exchanger types [17,22,23]. The suggested efficiency of the proposed concepts for LHL studied lie in the range 5 to 8 kWh/kg [13], which represents a substantial motivation for the implementation of these technologies in the next generation of LHL plants.

The proposed use of a MR in the pre-cooling part of LHL processes represents a close parallel to the use of MR in the design of some of the largest and most efficient natural gas liquefaction processes and because of this, represents one of the most promising near-future improvements to LHL design. LNG plants based on the use of MRs include the Snøhvit plant located at Melkøya in northern Norway, which uses a cascade of three MR loops and is claimed to be the most efficient LNG plant in the world [24]. While the efficiency achieved by the Snøhvit LNG plant is due, in part, to its advanced design, the plant also benefits from its cold-climate location and subsequent access to a lower temperature heat sink than most other LNG plants.

The study of Rian and Ertesvåg [25] looked at the impact of ambient temperature on the Snøhvit LNG plant, finding that a reduction in the available heat sink temperature from 20 to 4°C gives a reduction in exergy destruction of 10.9%. A small number of other studies have also considered the impact of ambient temperature on the performance of other types of LNG process [26–29] providing similar results. The study of Park et al., for example, finds that specific power consumption of single MR process increases by between 16% and 42% over the temperature range 10 to 25°C, varying with the approach used in process optimization. This significance of this variation in energy consumption with ambient temperature is not only relevant to the design of LNG plant itself, it is large enough to affect the whole energy supply chain. For example, the study of Jackson et al., [29] finds that the CO_2 emissions for a power plant supplied by gas from an LNG plant located in northern Norway will be between 0.8 and 1.3% lower than if it were supplied by the same design of LNG plant located in the Middle East. It is therefore logical to expect that the performance of LHL plants using MR pre-cooling and the performance of energy supply chains based on LHL will be significantly affected by the ambient temperature at the liquefaction plant location.

Given the close parallel between MR based LNG processes and MR pre-cooled LHL processes and given the demonstrated impact of ambient temperature the performance of LNG processes, ambient temperature can be expected to have a significant impact on the performance of the type of LHL processes likely to be used in the near future. Although several studies have been made into the performance of MR pre-cooled type LHL process and studies have looked at the impact of ambient temperature on LNG process performance, no studies quantifying this impact of ambient temperature on LHL processes are

currently found in the literature. The aim of this study is, therefore, to generate a set of data illustrating the impact of ambient temperature on the performance of MR pre-cooled type LHL process.

2. Materials and Methods

2.1. Selection of the Modeling Basis

Although only a handful different types of liquefaction process are used in current operating LHL plants, a wide range of improved processes have been proposed. In the present study a comprehensive review of the various improved liquefaction technologies is outside the scope of work. Instead, a single, representative, improved process was selected to be used as the basis for the present study. The details of the selection process are described below.

Because the results from this study are intended to support further research in future low-carbon energy supply and, specifically, how different supply chain configurations affect efficiency, the improved concepts of most relevance are those technologies likely to be used in the near future. Taking the techno-economic analysis of Cardella et al. [30] as a basis, the improved technology that fits best with the aim of the study is the use of a mixed refrigerant (MR) for pre-cooling of the hydrogen feed stream.

Most current, and much improved, hydrogen liquefaction processes are based on the division of the overall process into two parts: a pre-cooling step and a cryogenic-cooling step. In conventional LHL plant designs, the pre-cooling stage often uses liquid nitrogen (LIN) as a refrigerant, whereas the cryogenic-cooling step uses either helium in a Brayton cycle, or hydrogen in a Claude cycle [18]. In the cryogenic step, the hydrogen feed is generally cooled from below around −90°C to the final liquefaction temperature. Although the break-point temperature between the pre-cooling and the cryogenic step, T_{p}, is potentially an optimization variable, the present study assumes that the impact of ambient temperature on operating parameters in the cryogenic step is small and, therefore, that T_{p} can be fixed.

Typical of the concepts for improved energy consumption using MRs is the process studied in the work of Skaugen et al. [17], which is based on a Claude cycle in cryogenic-cooling step and a MR in the pre-cooling step. In this process the pre-cooling step and the portion of the cryogenic step that operates above T_{p} are not integrated. This allows the present study to consider the optimization of the pre-cooling process independently from the operation of the cryogenic-cooling process. In addition, because the details of the composition and operating conditions for the proposed MR cycle are clearly set-out in the work of Skaugen et al. [17], the present study uses the work of Skaugen as the basis for model development and validation.

Although the operating parameters in the cryogenic-cooling step are assumed fixed in the present study (i.e., they are not affected by ambient temperature), the energy consumption of the cryogenic-cooling cycle compressor is still affected by the exit temperature that the inter and after-coolers, T_{c}, are designed to operate with, which would normally be set relative to the ambient temperature of the seawater, or air, used as the heat-sink. Because of this, modelling of the performance of the cryogenic cycle compressor as it varies with T_{c} does form part of the present study.

Another important factor in the design and optimization of hydrogen liquefaction processes is the conversion of ortho to para hydrogen. This process releases a significant quantity of heat, affecting both the process design and the selection of optimum operating parameters. The conversion of the ortho isomer during liquefaction is typically promoted using a catalyst. The effectiveness of the catalyst and the residence time in the heat exchangers affects the approach to the equilibrium concentration and, subsequently, the temperature profile in the heat exchangers. However, across the range of temperatures experienced in the pre-cooling process, the equilibrium concentration of para hydrogen varies by less than 5% [21]. Moreover, as in the study of Skaugen et al. [17]—which is a

reference case for this study—catalytic conversion is assumed after the pre-cooling process. This will result in a low approach to the equilibrium conversion in the pre-cooling process and, therefore, in this study the modelling of the conversion of ortho to para hydrogen is set outside the scope of work.

2.2. Process Model Development

As described above, the process model used in this study consists of two separate parts: a model of the MR pre-cooling step, and a model of the cryogenic-cooling step cycle compressor. The development of these two models is described below. A block diagram showing the relationship between the cryogenic-cooling step and the pre-cooling step is also presented in Appendix A.

Figure 1 illustrates the process flow scheme used for the MR pre-cooling process, which is based on the flow scheme used in the reference study of Skaugen et al. [17]. The main equipment items shown in Figure 1 are a compressor (comprising RC-1 and RC-2), two process coolers (PC-1 and PC-2), a MR separator (VV-1), a pump (PP-1), and the main heat exchanger (HX-1). The MR compressor comprises two stages (RC-1 and 2), both with after-cooling (PC-1 and 2) to T_c. Any liquids condensed liquids after the first stage are separated in VV-1. Liquids separated in this way are pumped (PP-1) to the compressor discharge pressure—bypassing the second stage of compression (RC-2)—and mixed with the vapor stream entering the main heat exchanger (HX-1). The main heat exchanger is modelled as a multi-stream type heat exchanger with two hot streams: H_2 and high-pressure MR, and one cold stream: low-pressure MR. The low-pressure MR stream exiting the main heat exchanger returns to the MR compressor. Hydrogen leaving HX-1 is cooled to T_p.

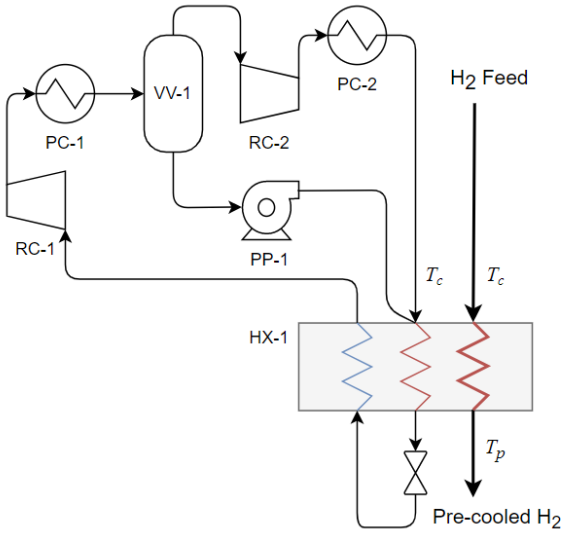

Figure 1. Flow diagram for the MR H_2 pre-cooling process.

To allow the calculation of process energy consumption a simplified model of the process presented in Figure 1 was developed in MATLAB [31] with the TREND software package [32] used to calculate thermo-physical properties. Table 1 presents the set of fixed modelling parameters, MP, used in the model of the MR pre-cooling process. In general, the parameters in Table 1 were selected to reflect those used in the reference study [17].

Table 1. Summary of MR process fixed modelling parameters.

Parameter	Value	Units
Hydrogen Feed Pressure	20	bara
H_2 pre-cooling temperature, T_p	−159	°C
Compressor/ pump efficiency	85	% *
HX-1 pressure-loss (hot streams)	0.5	bar
HX-1 pressure-loss (cold streams)	0.1	bar
PC-1 and 2 pressure-loss	0.5	bar

* Isentropic efficiency.

For simplicity, the pressure-loss in the main heat exchanger was scaled linearly with temperature and the two MR streams were assumed to be mixed before entering the heat exchanger and the combined MR stream enters the main heat exchanger at the H_2 feed temperature.

The temperature profiles for the combined hot streams and the cold stream in HX-1—the hot and cold composite curves—were estimated by splitting the heat exchanger into n equally sized temperature intervals, each sized $(T_{\text{in}} - T_{\text{out}})/n$ and stream enthalpies calculated for each temperature point ($n + 1$, total). Then the heat exchanger duty was also split into n equally sized intervals ($Q_{\text{HX}-1}/n$), and the hot and cold composite temperatures, T_{HC} and T_{CC}, interpolated at each point ($n + 1$, total) using linear interpolation of the temperature-enthalpy data. Finally, the temperature approach was calculated for each point, $\Delta T = T_{\text{HC}} - T_{\text{CC}}$. In both cases, n was set to 50 to give a high degree of accuracy to the calculations.

Figure 2 provides a sketch of the cycle compressor (comprising H2-1 to 4) for the cryogenic-cooling step which forms the basis of the present study. The stream LP H_2 represents the low-pressure hydrogen stream returning from the liquefaction process. This stream is compressed in two compressor stages (H2-1 and H2-2) before blending with medium-pressure hydrogen. The combined stream is then compressed in two further compressor stages (H2-3 and H2-4) before being passed-back to a multi-stream heat exchanger (HX-2), which cools the HP stream down to T_{p}. The compressor inter-stage pressures are calculated assuming equal stage pressure ratios.

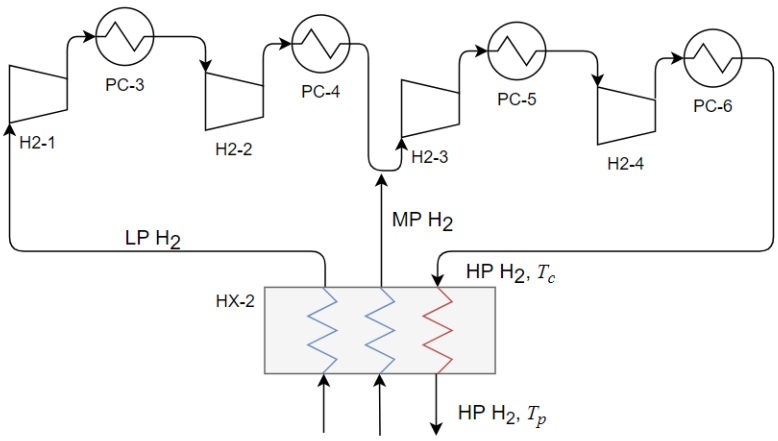

Figure 2. Flow diagram of the cryogenic-cooling step H_2 cycle compressor.

The model of the cryogen-cooling step compressor shown in Figure 2 was also developed in MATLAB using the same basis as the MR process model. Table 2 presents the fixed modelling parameters used in the study performance of this compressor, which are based on the reference model [17]. The outlet temperature of the four after-coolers (PC-3

to 6) were assumed equal to T_c and the inlet temperature of the LP and MP streams to the compressor was assumed to have a 2°C approach to T_c in all cases.

Table 2. Summary of fixed modelling parameters for the cryogenic-cooling cycle compressor.

Parameter	Value	Units
LP H2 Feed Pressure	1.1	bara
LP H2 flowrate	51.5	tpd
MP H2 feed pressure	8.0	bara
MP H2 flowrate	1121.5	tpd
HP H2 return pressure	29.8	bara
PC-3 to 6 pressure-loss	0.5	bar

* Isentropic efficiency.

In addition to the cycle compressor, the reference study describes several turbo-expanders within the cryogenic cooling step. These produce 2.8 MW of shaft power, which is assumed in the reference study to be recovered as electrical energy with as efficiency of 80% [17]. Assuming, as before, that the parameters in the cryogenic process remain constant with varying T_c, this recovered energy equates to a specific energy production for the expanders, SEC_{Ex}, of approximately 0.43 kWh/kg, which is a constant value for all cases studied in this work.

Where operating parameters were not available in the reference study, they have been inferred from the data that is presented there. Because of this, it cannot be claimed that there is any direct equivalence between the results presented here and the reference model.

2.3. MR Pre-Cooling Model Validation

An important aspect of successful optimization is the minimization of temperature differences in HX-1, and since the targeted minimum approach temperature is only 1 K, the accuracy of the property predications used in the process model is very important. In the TREND software package, several properties methods are available; to select the basis that is most appropriate for the present work, three of these were compared against results from the reference study: Peng Robinson (PR), Soave-Redlich-Kwong (SRK) and the TREND Helmholtz free energy model. Tables 3 and 4 present the parameters used in the validation work. The results of the validation work were used to select the properties method used in the later optimization work.

Table 3. Validation case MR composition.

Component	Mole Fraction
Nitrogen	0.101
Methane	0.324
Ethane	0.274
Propane	0.031
n-Butane	0.270

Table 4. Validation case MR modelling parameters.

Parameter	Value	Units
Hydrogen Feed Flow	125	tpd
MR feed temperature	12	°C
MR return temperature	−1.0	°C
MR feed pressure	35	bara
MR return pressure	4.25	bara

2.4. Optimization Problem Defenition

The objective of the optimization study was to minimize the energy consumption of the MR pre-cooling process whilst satisfying a minimum temperature approach constraint. The objective function was formulated as described in Equation 1:

$$\min\{\mathrm{SEC_{MR}}\}, \text{ such that } \begin{cases} \mathrm{lb}_i < \mathrm{OP}_i < \mathrm{lb}_i \\ \Delta T_{\min} - \Delta T_{\mathrm{acc}} > 0. \\ \dot{m}_{\mathrm{MR}} > 0 \end{cases} \quad (1)$$

In Equation (1), $\mathrm{SEC_{MR}}$ is the specific energy consumption of the MR process, OP_i are the set of i optimization parameters (see Table 5), lb_i and ub_i are a set of lower and upper bounds for each parameter, $\Delta T_{\min}$ is the minimum approach temperature in HX-1 ($\Delta T_{\min} = \min\{\Delta T_n\}$), ΔT_{acc} is the minimum acceptable approach temperature in HX-1 and $\dot{m}_{\mathrm{MR}}$ is the mass flowrate of the MR. $\mathrm{SEC_{MR}}$ was calculated from the sum the compression stage energy consumptions, W_{MR}, which are, in turn, a function of OP_i, MP_i (see Table 1) and T_{c} is described by Equation (2):

$$\mathrm{SEC_{MR}} = \sum W_{\mathrm{MR}}\left(\mathrm{OP}_i, \mathrm{MP}_i, T_{\mathrm{c}}\right) / \dot{m}_{\mathrm{H2}}. \quad (2)$$

In Equation (2), $\dot{m}_{\mathrm{H2}}$ is the mass flowrate of hydrogen in the pre-cooling process.

The set of optimization parameters, OP_i, used in the study are summarized in Table 5 along with the initial values used ($\mathrm{OP}_{i,0}$) and initial values of the boundary constraints (lb_i and ub_i).

Table 5. Summary of Optimization Parameters with Initial ($\mathrm{OP}_{i,0}$) and Constraint Values.

Parameter	Description	$\mathbf{lb}_i < \mathbf{OP}_{i,0} < \mathbf{ub}_i$
OP_1	MR mole fraction N2	0.05 < 0.11 < 0.25
OP_2	Mole fraction CH4	0.20 < 0.32 < 0.50
OP_3	MR mole fraction C2	0.15 < 0.27 < 0.50
OP_4	MR mole fraction C3	0.00 < 0.03 < 0.10
OP_5	RC-1, Pin (bara)	2.00 < 4.25 < 6.00

Although the ultimate purpose of the boundary constraints shown in Table 5 was to limit the optimization process to physically meaningful solutions—e.g., component mole fractions greater than zero—the initial boundary constraints were also used to limit the search area around the likely optimum values. This was done to reduce optimization time. The initial values of lb and ub shown in Table 5 were set based on results from the reference case, but where the optimization solution was found close to the initial limits, the bounds were extended to ensure that the overall optimum solution was not missed.

In addition to the optimization parameters listed in Table 5, the MR compressor inter-stage pressure, MR compressor discharge pressure and HX-1 warm-end approach temperature could be considered as optimization parameters. However, in this work these have been excluded to limit complexity. The MR compressor discharge pressure is, therefore, fixed at the value used in the reference study, the MR inter-stage pressure set in each case to maintain equal stage pressure ratios, and the HX-1 warm-end approach set to 5°C. The MR mole fraction for butane is also not identified as an optimization parameter because it is calculated from the sum of the other components.

2.5. Optimization Algorithm

In a phase of initial testing the *Fmincon* (FMC) algorithm with the SQP option was found to provide fast and generally accurate optimization results, although in some cases local minima were found. In all subsequent cases, FMC was used with the solution tolerance set to 0.001 kWh/kg and all other options left as default.

To help identify the global minimum solutions for each T_{c}, the boundary constraints shown in Table 5 were evaluated in a manual, stepwise, process: after the initial results

had been gathered, new initial guesses were specified when the original initial guess was found to be a long way from the solution. When a stable set of bounds enclosing the global solution had been found, the *MultiStart*, MS, and *GlobalSearch*, GS, algorithms were used to help test the quality of the results. In both cases the MS and GS runs were again based on the FMC algorithm with the parameters as before.

The quality each optimization result was assessed qualitatively using the results from other T_c cases. The basis of this assessment was the assumption that a simple, monotonic, relationship was likely between each of the optimization parameters and T_c. In addition to this assessment, the temperature profiles in HX-1 for each case were reviewed qualitatively to determine if ΔT_{acc} was consistently approached throughout the heat exchanger.

2.6. Performance Variation with Cooling Temperature

Performance variation with cooling temperature was studied for the MR pre-cooling process by finding the optimum operating parameters, OP_i, for each cooling temperature, T_c case. The fixed modelling parameters shown in Table 2 were used as the basis in all cases. The cooling temperature range studied was 5 to 50°C.

In the model developed for the cryogenic-cooling step, process parameters were not optimized: flowrates and pressure levels in the cryogenic cycle were held constant at the values shown in Table 3. The variation of the energy consumption of the cryogenic cycle compressor with T_c was modelled using the more simplistic assumption that, since the composite cooling curves in HX-2 are straight and parallel, a constant warm-end approach temperature exists across the range of cooling temperatures studied. The energy consumption of the cryogenic cycle compressor was calculated using the same basis as that of the MR pre-cooling process. A 2°C warm-end approach temperature was assumed across the cooling temperature range 5 to 50°C.

The overall SEC for the hydrogen liquefaction process was calculated as the sum of the energy consumption for the MR pre-cooling step, SEC_{MR}, and the cryogenic-cooling step, SEC_{CY}, which was—in turn—calculated as the sum of the cycle compressor stage energy consumptions minus the energy recovered in the cryogenic-cooling step expanders as described in Equations (3) and (4):

$$SEC = SEC_{MR} + SEC_{CY} \quad (3)$$

$$SEC_{CY} = \sum W_{H2}\left(MP_{H2}, T_c\right)/\dot{m}_{H2} - SEC_{Ex} \quad (4)$$

In Equation (3), W_{H2} is the energy consumption of the cycle compressors shown in Figure 2, and in Equation (4), MP_{H2} is the set of fixed modelling parameters for the cryogenic-cooling cycle compressor (see Table 2).

To provide an independent means of reviewing the trends shown in the results, the SEC for an ideal process that cooled the hydrogen from T_c to a final temperature of −259°C was also calculated. This ideal energy consumption, SEC_{ID}, was then used to calculate a second law efficiency, $\eta_{id} = SEC/SEC_{ID}$, for the overall process. The method used to calculate SEC_{ID} was to summate the ideal Carnot cycle energy consumption for a set of very small temperature steps along temperature–enthalpy data for hydrogen as explained previously by Jackson et al. [29].

3. Results and Discussion

3.1. Process Modelling and Validation

Table 6 shows the results from the model validation work. In addition to the results from the reference study, three sets of results are presented in Table 6: Case A uses the TREND implementation of the Peng Robinson (PR) equation of state; Case B the TREND/SRK equation of state; and Case C the TREND/ Helmholtz free energy properties method.

Table 6 Summary of modelling parameters for the model validation work.

	Reference	Case A	Case B	Case C	
Properties method	-	PR	SRK	Hel.	
MP supply pressure	35.0	35.0	35.0	35.0	bara
MR return pressure	4.25	3.0 **	4.25	4.25	°bara
MR return temp.	112	112.8	112.3	109.6	C
MR mass flowrate	1600 *	1395	1703	1709	tpd
HX-1 min. approach	1.00	1.05	0.49	0.51	°C
HX-1 duty	12.6	11.2	13.2	12.9	kW

* Given only as an approximate value in the reference case. ** Adjusted to give a positive value for min. approach.

Of the three cases compared in Table 6, Case C—using the TREND/ Helmholtz free energy properties method—is considered to represent the closest match to the reference case, but since Case B also offers good agreement and significantly reduced calculation time, SRK is selected as the basis for further work.

Figure 3 presents the composite temperature profile data for Case B and C in Table 6. The results show that, although the shape of the curves differs between the two cases, the results from both cases show a very good fit between the warm and cold curves throughout the heat exchanger. These results, therefore, add confidence to the validation work and the selection of Case B as the modelling basis.

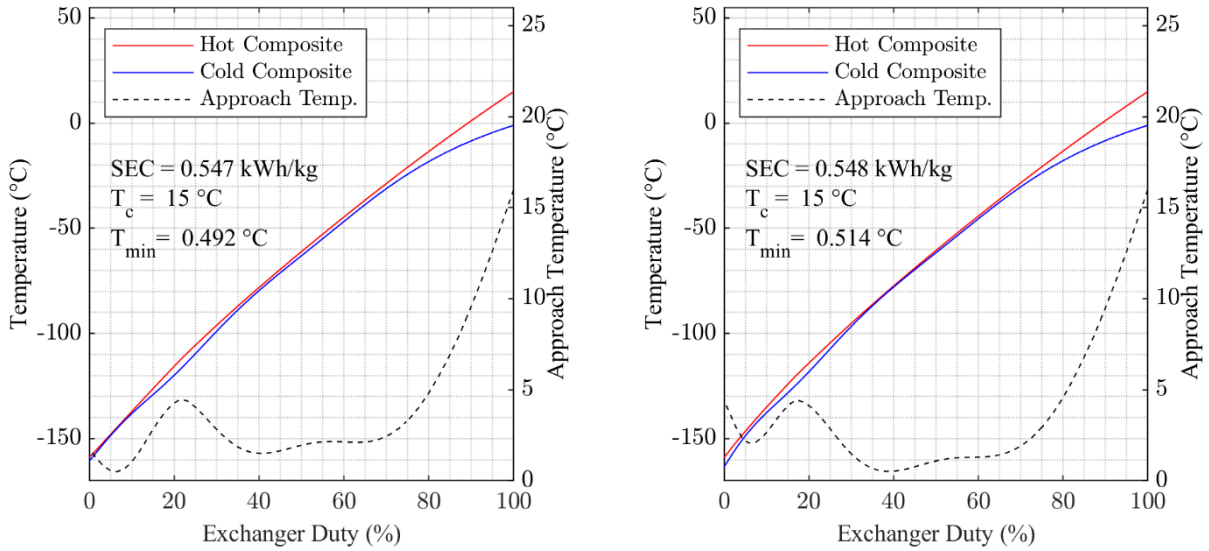

Figure 3. Composite Curves and Key Performance Parameters for HX-1, MR Pre-cooling Process: (**a**) Case B; (**b**) Case C.

While Table 6 and Figure 3 show that the selection of a good modelling basis is important to the determination of the optimum operating parameters for this process, no claim is made here that the modelling basis selected is the one that is most accurate for the modelling of this process, just that it provided a good match with the reference case in the validation work presented.

A limitation of the present study is that the heat generated during ortho-para hydrogen conversion is omitted form the model. This is a simplification that limits the extent to which this modelling work reflects the performance of a hydrogen liquefaction process operating in the real world. The main claim made here regarding the modelling basis is that it provides provide a consistent basis to study performance across the operating cases

considered. The implication of this for further work is that the study of the variation in energy consumption with cooling temperature made here is valid and can provide some insight into how the performance real hydrogen liquefaction processes can be expected to vary when designed for utility cooling at different temperatures.

3.2. Performance Variation with Cooling Temperature

Figures 4 and 5 show how the five optimization parameters vary with T_c, and Figures 6 and 7 provide two examples of the optimized cooling curves resulting from these runs. In Figures 4 and 5 all of the data collected over the final set of optimization runs (two using GS and two using MS) are presented as points and the overall optimum datasets are connected by dotted lines.

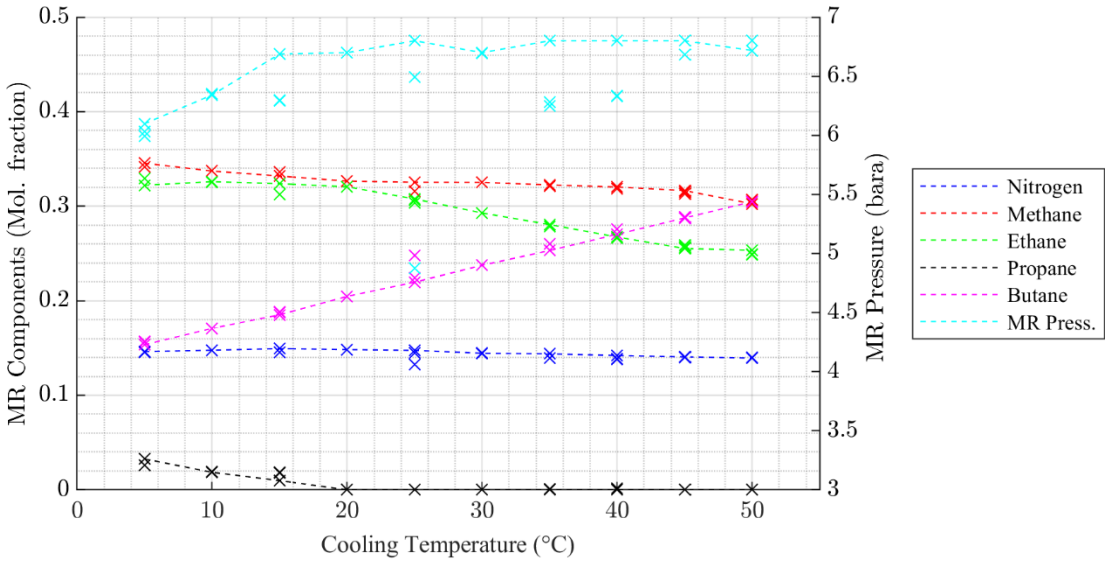

Figure 4. Variation in OP for the MR pre-cooling step with cooling temperature.

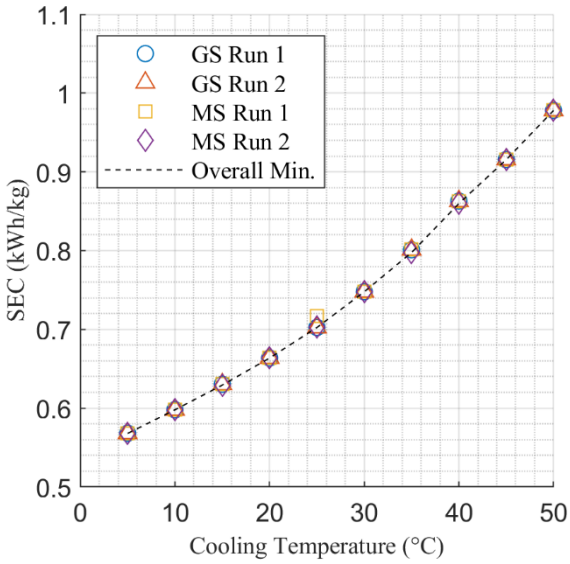

Figure 5. Variation in SEC for the MR pre-cooling step with cooling temperature.

The results presented in Figure 4 for MR composition show quite clear trends with the component mole fraction of each component a monotonic function of cooling temperature in the majority of cases. The impact on butane is largest, which is due to the steadily increasing heat duty at the warm end of HX-1 as the cooling temperature increases. The impact on the optimum nitrogen content in the MR is affected least by cooling temperature, reflecting the relatively static conditions at the cold end of HX-1.

The data presented in Figure 4 that represents optimum MR pressure solutions is less consistent with a slight upward trend visible across the range of cooling temperatures considered. This indicates that the optimum combination of MR composition and MR operating pressure is more difficult to determine and that the overall minimum may not have been found in all cases. However, Figure 5 shows a very consistent trend in how the SEC for the MR pre-cooling process varies with T_c, which provides confidence that a solution close to the overall minimum was found in all cases.

Figures 6 and 7 present the hot and cold composite cooling curves for the overall minimum SEC solutions found for T_c = 5°C and T_c = 50°C. Generally, the results in Figures 6 and 7 show that the optimization algorithm has found a good fit for the cooling curves, with the 2°C pinch temperature approached in multiple locations within HX-1 in both cases. The cooling curves for each of the temperature points studied between T_c = 5 °C and T_c = 50°C are presented in Figures A2–A9, which are contained in the Appendix A.

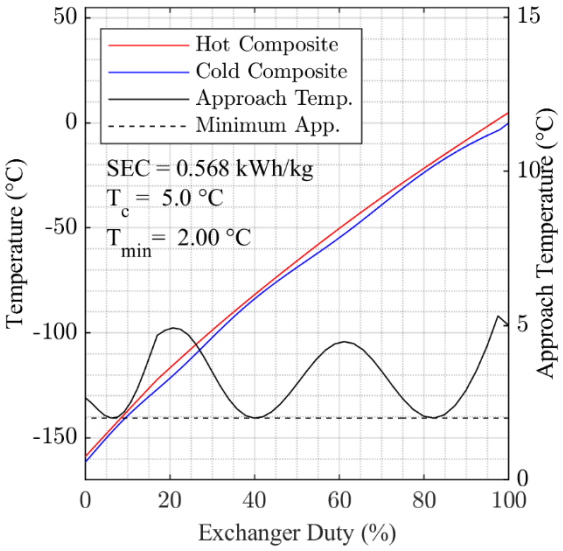

Figure 6. Composite curves in HX-1 and key performance parameters, 5°C cooling temperature case.

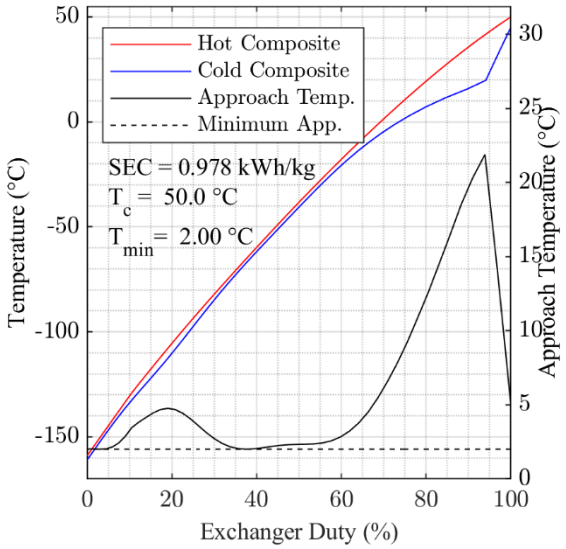

Figure 7. Composite curves in HX-1 and key performance parameters, 50°C cooling temperature case.

Comparing the variation in minimum approach temperature data presented in Figure 6 for T_c = 5°C with that presented in Figure 7 for T_c = 50°C, it can also be observed that the optimization process has found a set of parameters that better minimize the temperature approach in HX-1 for the T_c = 5°C case. Looking at the T_c = 50°C case, we see that it becomes more difficult to maintain a close approach at the warm end of the heat exchanger suggesting that SEC could be reduced further through the addition of heavier components to the MR.

Figure 8 presents the SEC for the pre-cooling step, the cryogenic-cooling step, and the overall process. Figure 9 presents the same data in terms of the % change relative to the 25°C case. Moreover, presented in Figure 9 are the corresponding second law efficiencies expressed as a percentage.

Figure 8 shows that the contribution of the pre-cooling process to overall SEC across the range of cooling temperatures investigated is approximately 10%. In addition, Figure 8 shows non-linear variation in SEC with cooling temperature for the pre-cooling part of the overall process that contrasts with the linear relationship between SEC and cooling temperature for the cryogenic process. This non-linear relationship for the pre-cooling process reflects the fact that lower cooling temperatures both reduced cooling duty and increase efficiency, whereas the close to linear impact on the cryogenic process is a result of only reduced increased efficiency. Further insight into this is provided by the results presented in Figure 9.

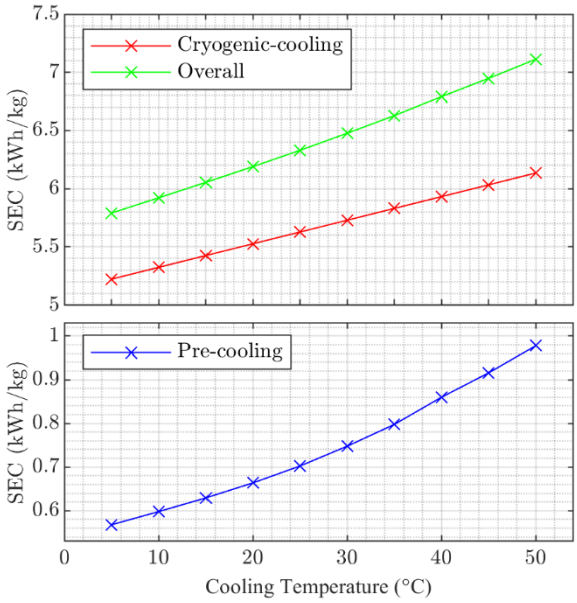

Figure 8. Variation in SEC with cooling temperature for the pre-cooling, cryogenic-cooling and overall cooling processes.

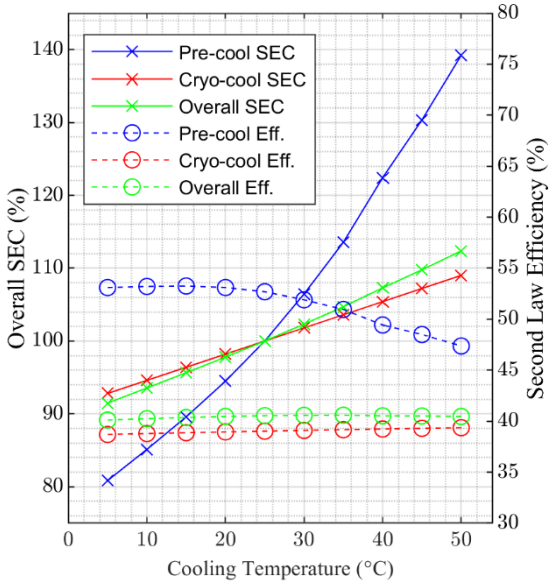

Figure 9. Percentage variation in overall SEC and second law efficiency for the pre-cooling, cryogenic-cooling and overall cooling processes.

The results presented in Figure 9 show that energy consumption for the overall liquefaction process increases by around 20% across the cooling temperature range 5 to 50°C and 5% over the range 20 to 30°C. For the pre-cooling process the increase is close to 80 % over the full temperature range. Figure 9 also shows that while the second law efficiency of the cryogenic-cooling process increases slightly across the range of temperatures considered, the efficiency of the pre-cooling process drops above 25°C. The cause of this drop in efficiency as the cooling temperature increases can be seen in Figure 6 and Figure 7, which show that the mean temperature approach for the higher temperature cases is higher than that of the lower temperature cases. It is this reduced level of optimization as cooling temperature increases above 25°C that accentuates the non-linear behavior notable in Figure 8.

The implication of the results presented in Figure 9 is the same as discussed earlier: that design changes in the MR process could help to improve performance for the cases where the cooling temperature is higher than 25°C. Both the addition of heavier components to the MR mixture could provide a more optimized design or the division of the MR loop into additional pressure levels. Both of these design alternatives could form the basis of further study work.

4. Conclusions

A model for a hydrogen liquefaction process has been developed and validated against results from an independent study. Although the validation process highlighted the significant impact that different properties models can have on model predictions, the validation results also indicate that the present model is suitable for the study of the impact of ambient temperature on process performance.

A set of optimization parameters were selected, and an optimization method developed that was shown to be suitable for the study of process performance across a range of process cooling temperatures through the consistency of the results obtained. The MR studied is limited to a mixture of five components. It is indicated in the results presented that the addition of heavier components could be used to improve efficiency for cooling temperatures above 25°C, although the available gains would be small.

The results of the optimization work show that the specific energy consumption, SEC, of the MR pre-cooling process increases by around 80%, from approximately 0.57 to 1.0 kWh/kg, across the cooling temperature range 5 to 50°C. These results, combined with the calculated process performance for the cryogenic-cooling step (not optimized here), show that total energy consumption for the hydrogen liquefaction process increases by around 20%, from 5.8 to 7.1 kWh/kg, across the same temperature range. Considering just the range 20 to 30°C, there is a 5% increase, which illustrates the significant impact ambient temperature can have on energy consumption.

The variation in energy consumption with cooling temperature implies a significant benefit for liquefaction processes operating in low ambient temperature locations, especially given that the hydrogen liquefaction process represents a very energy intensive step in the supply of liquid hydrogen. The aim of further work is to combine these results into a larger system model that considers the impact of ambient temperature on the supply of low-carbon energy from natural gas.

Author Contributions: Conceptualization, S.J.; methodology, S.J. and E.B.; validation, S.J.; formal analysis, S.J.; investigation, S.J.; data curation, S.J.; writing—original draft preparation, S.J.; writing—review and editing, S.J. and E.B.; supervision, E.B. All authors have read and agreed to the published version of the manuscript.

Funding: This research received no external funding.

Institutional Review Board Statement:

Informed Consent Statement:

Data Availability Statement:

Conflicts of Interest: The authors declare no conflicts of interest.

Appendix A

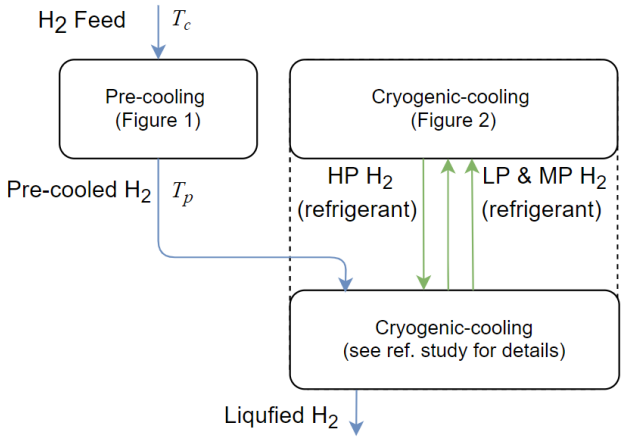

Figure A1. Block flow diagram of the overall liquefaction process.

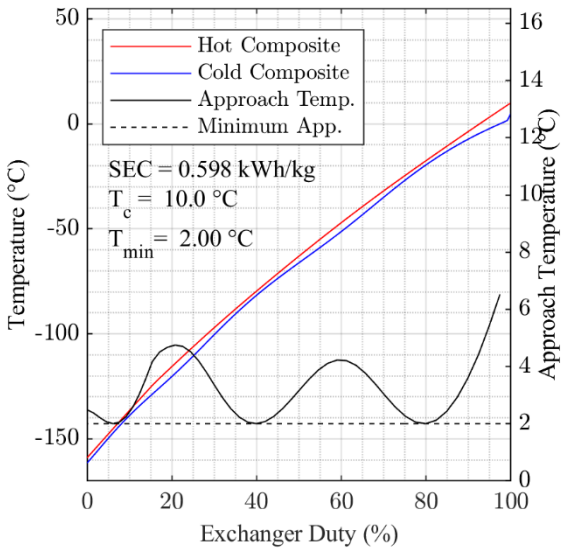

Figure A2. Optimized composite cooling curves for 10°C cooling temperature.

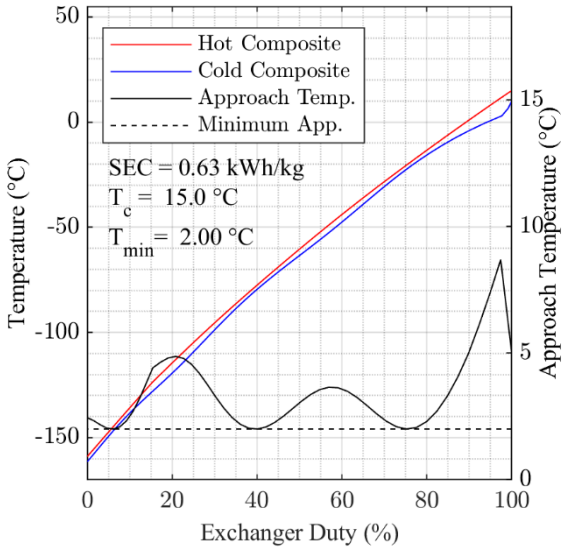

Figure A3. Optimized composite cooling curves for 15°C cooling temperature.

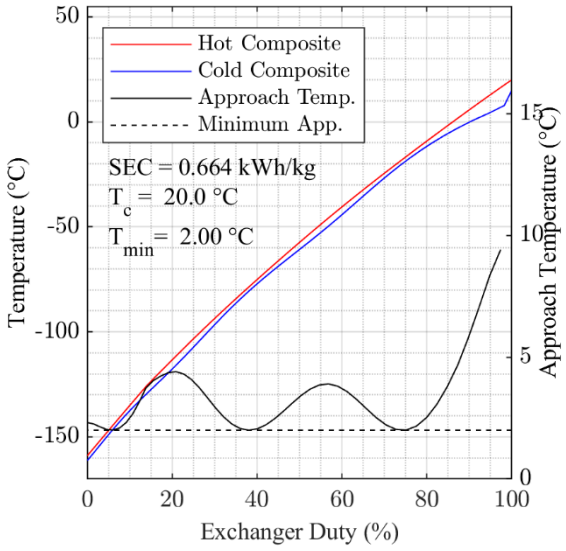

Figure A4. Optimized composite cooling curves for 20°C cooling temperature.

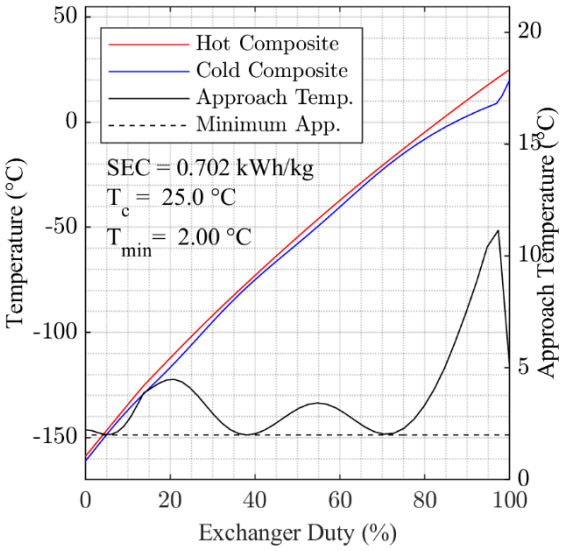

Figure A5. Optimized composite cooling curves for 25°C cooling temperature.

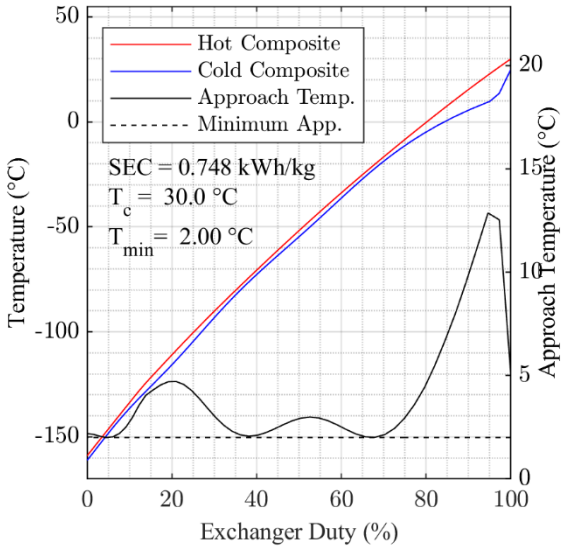

Figure A6. Optimized composite cooling curves for 30°C cooling temperature.

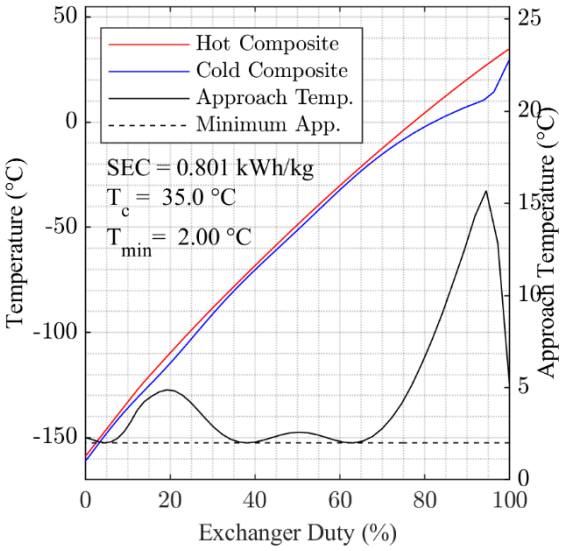

Figure A7. Optimized composite cooling curves for 35°C cooling temperature.

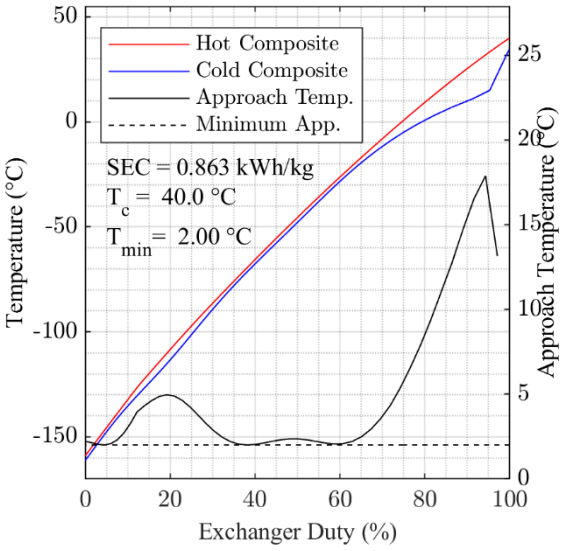

Figure A8. Optimized composite cooling curves for 40°C cooling temperature.

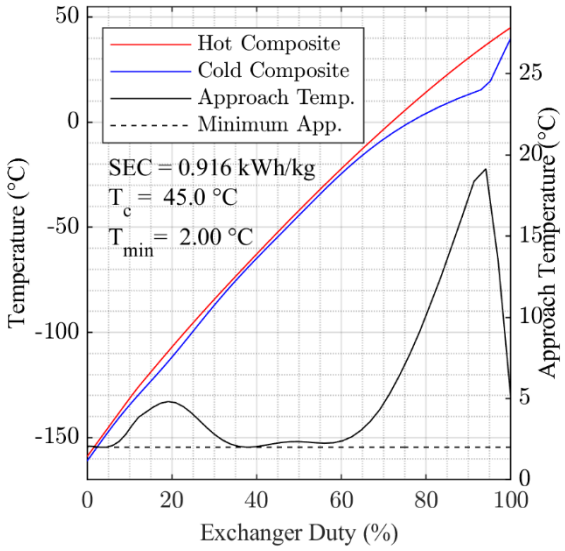

Figure A9. Optimized composite cooling curves for 45°C cooling temperature.

References

1. Acar, C.; Dincer, I. Review and evaluation of hydrogen production options for better environment. *J. Clean. Prod.* **2019**, *218*, 835–849, https://doi.org/10.1016/j.jclepro.2019.02.046.
2. Hydrogen Roadmap Europe-A Sustainable Pathway for the European Energy Transition. *Fuel Cells Hydrog. Jt. Undert.* **2019**, doi:10.2843/341510.
3. Moya, J.; Ioannis; Dalius; Wouter. *Hydrogen Use in EU Decarbonisation Scenarios*; Available online: https://ec.europa.eu/jrc/sites/default/files/final_insights_into_hydrogen_use_public_version.pdf (accessed on 01 09 2021).
4. The European Comission. *A Hydrogen Strategy for a Climate-Neutral Europe*; The European Comission: Brussels, Belgium, 2020.
5. Kang, J.-N.; Wei, Y.-M.; Liu, L.-C.; Han, R.; Yu, B.-Y.; Wang, J.-W. Energy systems for climate change mitigation: A systematic review. *Appl. Energy* **2020**, *263*, 114602, doi:10.1016/j.apenergy.2020.114602.
6. Yuksel, Y.E.; Ozturk, M.; Dincer, I. Energetic and exergetic assessments of a novel solar power tower based multigeneration system with hydrogen production and liquefaction. *Int. J. Hydrogen Energy* **2019**, *44*, 13071–13084, doi:10.1016/j.ijhydene.2019.03.263.
7. Sher, F.; Al-Shara, N.K.; Iqbal, S.Z.; Jahan, Z.; Chen, G.Z. Enhancing hydrogen production from steam electrolysis in molten hydroxides via selection of non-precious metal electrodes. *Int. J. Hydrogen Energy* **2020**, *45*, 28260–28271, doi:10.1016/j.ijhydene.2020.07.183.
8. Karakaya, E.; Nuur, C.; Assbring, L. Potential transitions in the iron and steel industry in Sweden: Towards a hydrogen-based future? *J. Clean. Prod.* **2018**, *195*, 651–663, doi:10.1016/j.jclepro.2018.05.142.
9. Pethaiah, S.S.; Sadasivuni, K.K.; Jayakumar, A.; Ponnamma, D.; Tiwary, C.S.; Sasikumar, G. Methanol Electrolysis for Hydrogen Production Using Polymer Electrolyte Membrane: A Mini-Review. *Energies* **2020**, *13*, 5879.
10. Yang, C.; Ogden, J. Determining the lowest-cost hydrogen delivery mode. *Int. J. Hydrogen Energy* **2007**, *32*, 268–286, doi:10.1016/j.ijhydene.2006.05.009.
11. Ishimoto, Y.; Voldsund, M.; Nekså, P.; Roussanaly, S.; Berstad, D.; Gardarsdottir, S.O. Large-scale production and transport of hydrogen from Norway to Europe and Japan: Value chain analysis and comparison of liquid hydrogen and ammonia as energy carriers. *Int. J. Hydrogen Energy* **2020**, *45*, 32865–32883, doi:10.1016/j.ijhydene.2020.09.017.
12. Hoshi, M. World's First Liquid Hydrogen Carrier Ship Launches in Japan. Available online: https://asia.nikkei.com/Business/Energy/World-s-first-liquid-hydrogen-carrier-ship-launches-in-Japan (accessed on 15 April 2021).
13. Aasadnia, M.; Mehrpooya, M. Large-scale liquid hydrogen production methods and approaches: A review. *Appl. Energy* **2018**, *212*, 57–83, doi:10.1016/j.apenergy.2017.12.033.
14. Ghorbani, B.; Mehrpooya, M.; Aasadnia, M.; Niasar, M.S. Hydrogen liquefaction process using solar energy and organic Rankine cycle power system. *J. Clean. Prod.* **2019**, *235*, 1465–1482.
15. Yilmaz, C. Optimum energy evaluation and life cycle cost assessment of a hydrogen liquefaction system assisted by geothermal energy. *Int. J. Hydrogen Energy* **2019**, *45*, 3558–3568.
16. Ansarinasab, H.; Mehrpooya, M.; Mohammadi, A. Advanced exergy and exergoeconomic analyses of a hydrogen liquefaction plant equipped with mixed refrigerant system. *J. Clean. Prod.* **2017**, *144*, 248–259, doi:10.1016/j.jclepro.2017.01.014.

17. Skaugen, G.; Berstad, D.; Wilhelmsen, Ø. Comparing exergy losses and evaluating the potential of catalyst-filled plate-fin and spiral-wound heat exchangers in a large-scale Claude hydrogen liquefaction process. *Int. J. Hydrogen Energy* **2020**, *45*, 6663–6679, doi:10.1016/j.ijhydene.2019.12.076.
18. Cardella, U.; Decker, L.; Sundberg, J.; Klein, H. Process optimization for large-scale hydrogen liquefaction. *Int. J. Hydrogen Energy* **2017**, *42*, 12339–12354, doi:10.1016/j.ijhydene.2017.03.167.
19. Yuksel, Y.E.; Ozturk, M.; Dincer, I. Analysis and assessment of a novel hydrogen liquefaction process. *Int. J. Hydrogen Energy* **2017**, *42*, 11429–11438.
20. Chang, H.M.; Ryu, K.N.; Baik, J.H. Thermodynamic design of hydrogen liquefaction systems with helium or neon Brayton refrigerator. *Cryogenics* **2018**, *91*, 68–76, doi:10.1016/j.cryogenics.2018.02.007.
21. Donaubauer, P.J.; Cardella, U.; Decker, L.; Klein, H. Kinetics and Heat Exchanger Design for Catalytic Ortho-Para Hydrogen Conversion during Liquefaction. *Chem. Eng. Technol.* **2019**, *42*, 669–679, doi:10.1002/ceat.201800345.
22. Wilhelmsen, O.; Berstad, D.; Aasen, A.; Neksa, P.; Skaugen, G. Reducing the exergy destruction in the cryogenic heat exchangers of hydrogen liquefaction processes. *Int. J. Hydrogen Energy* **2018**, *43*, 5033–5047, doi:10.1016/j.ijhydene.2018.01.094.
23. Skaugen, G.; Wilhelmsen, O. Comparing the Performance of Plate-Fin and Spiral Wound Heat Exchangers in the Cryogenic Part of the Hydrogen Liquefaction Process. In Proceedings of the 15th Cryogenics 2019 Iir International Conference, Prague, Czech Republic, 8–11 April 2019; Chrz, V., Haberstroh, C., Herzog, R., Kaiser, Z., Klier, J., Kralik, T., Lansky, M., Mericka, P., Schustr, P., Srnka, A., et al., Eds.; Refrigeration Science and Technology; International Institute of Refrigeration: Paris, France, 2019; pp. 318–324.
24. Bauer, H.C. Mixed fluid cascade, experience and outlook. In Proceedings of the AIChE Spring Meeting and Global Congress on Process Safety, Houston, TX, USA, 1–4 April 2012.
25. Rian, A.B.; Ertesvåg, I.S. Exergy Evaluation of the Arctic Snøhvit Liquefied Natural Gas Processing Plant in Northern Norway—Significance of Ambient Temperature. *Energy Fuels* **2012**, *26*, 1259–1267, doi:10.1021/ef201734r.
26. Xu, X.; Liu, J.; Jiang, C.; Cao, L. The correlation between mixed refrigerant composition and ambient conditions in the PRICO LNG process. *Appl. Energy* **2013**, *102*, 1127–1136, doi:10.1016/j.apenergy.2012.06.031.
27. Castillo, L.; Dahouk Majzoub, M.; Di Scipio, S.; C.A., D. Conceptual analysis of the precooling stage for LNG processes. *Energy Convers. Manag.* **2013**, *66*, 41–47.
28. Park, K.; Won, W.; Shin, D. Effects of varying the ambient temperature on the performance of a single mixed refrigerant liquefaction process. *J. Nat. Gas Sci. Eng.* **2016**, *34*, 958–968.
29. Jackson, S.; Eiksund, O.; Brodal, E. Impact of Ambient Temperature on LNG Liquefaction Process Performance: Energy Efficiency and CO 2 Emissions in Cold Climates. *Ind. Eng. Chem. Res.* **2017**, *56*, 3388–3398, doi:10.1021/acs.iecr.7b00333.
30. Cardella, U.; Decker, L.; Klein, H. Roadmap to economically viable hydrogen liquefaction. *Int. J. Hydrogen Energy* **2017**, *42*, 13329–13338, doi:10.1016/j.ijhydene.2017.01.068.
31. The MathWorks, Inc. *MATLAB*; The MathWorks, Inc.: Natick, MA, USA, 2018.
32. Span, R.B., R.; Hielscher, S.; Jäger, A.; Mickoleit, E.; Neumann, T.; Pohl, S.; M.; Semrau, B.; Thol, M. *TREND. Thermodynamic Reference and Engineering Data 5.0*; Lehrstuhl für Thermodynamik, Ruhr-Universität Bochum, Bochum, Germany, 2020.

Appendix – Article 4

energies

MDPI

Article

Development of a Model for the Estimation of the Energy Consumption Associated with the Transportation of CO_2 in Pipelines

Steven Jackson

UiT—The Arctic University of Norway, 9019 Tromsø, Norway; steve.jackson@uit.no

Received: 31 March 2020; Accepted: 29 April 2020; Published: 12 May 2020

Abstract: All Carbon Capture and Storage (CCS) projects require the transportation of CO_2 from a source to a storage location. Although, a compressor and a large diameter pipeline is the normal method used to achieve this, liquefaction, shipping and pumping is sometimes attractive. Identifying the economic optimum is important for all CCS projects, minimizing energy consumption is also important because it corresponds to a resource efficiency in fossil-fuel based projects. This article describes the development and validation of a model that estimates the energy consumption associate with CO_2 transportation using the geographic location of the source and the reservoir to incorporate ambient temperature and bathymetry data. The results of the validation work show an average absolute temperature and pressure error less than 1 °C and 1 bar compared to a reference model. The model has been developed using openly accessible data and is made available in a repository for open research data.

Keywords: pipelines; liquefaction; shipping; CO_2; transport; CCS; energy

1. Introduction

There are currently 19 large-scale Carbon Capture and Storage (CCS) projects in operation worldwide [1], but to achieve the level of CO_2 emissions in the International Energy Agency's Sustainable Development Goals (SDGs) the number of industrial scale facilities will need to increase to more than 2000 by 2040 [2]. Each of these projects requires the transportation of CO_2 from a point of origin to a storage location and, since the transportation distance is often significant, over 200,000 km of CO_2 pipelines will be required by 2050 by CCS projects [3]. Although the majority of CO_2 is likely to be transported using pipelines, the success of many future CCS projects will depend on transportation using ships. For example, the Northern Lights Project, which will be one of the first full-chain projects in Europe [4], is based on ship transportation of CO_2 from a source to a hub where a sub-sea pipeline will then connect to the storage location in the Norwegian Sea.

Research supporting the design of CO_2 transportation processes has been widely published. A particular focus has been CO_2 mixture properties in high-pressure pipelines [5–9], but many other aspects of CO_2 pipeline design have been studied, including heat transfer [10–12], transient flow behavior [13] and economic optimization [14–16], to name some examples. Although less research has focused specifically on ship-based transportation, there are still a large number of studies looking at both technical and economic aspects of CO_2 shipping [17–19], and a particular focus being the energy consumption associated with the compression and liquefaction processes [20–25].

Figure 1 presents an illustration of the CCS value chain. The illustration indicates that the break-point between the capture and transportation is not always clear-cut, reflecting the fact that some capture processes produce CO_2 at elevated pressure. Based on this, and because the capture process is normally the main contribution to overall energy consumption, the full chain, rather than transportation

in isolation, is often the focus of research work. However, the transport energy consumption and the capture unit energy consumption are often independent: One capture option can having multiple possible transportation possibilities with differing energy consumption.

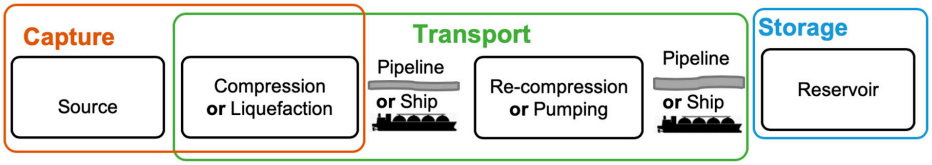

Figure 1. Simplified Illustration of a Typical CCS Value Chain.

In the context of the economic basis for specific CCS projects the selection of the optimum transportation alternative is normally studied. For example, Jakobsen, et al. studies the transportation alternatives associated with the Norcem Brevik cement plant CCS project [26]. Also, to support the economic assessment of CCS projects in general, tools for modelling full CCS chains have been developed that allow comparison of different transportation cases, for example Jakobsen, et al. [27]. Studies have also been conducted in the identification of a more general economic trade-off distance between shipping and pipelines, for example Mallon, et al. [28].

The purpose of the model presented here, in contrast to other work, is to allow the study and comparison of different CO_2 transportation chains on the basis of their energy consumption. The purpose of this article is to present details of how the model was developed and tested.

The model presented here is currently limited to pre- and post-combustion CO_2 stream composition and transportation scenarios in the North, Norwegian and Barents Seas. The inclusion of performance data for different CO_2 sources is planned for future development. The intended use of the model is not as a replacement or competitor to other modelling approaches, but as a tool that enable a perspective on CCS project alternatives focused on energy consumption. Case studies and sensitivity analysis using the mode will be developed and presented as part of future work.

2. Methods

The model described here was developed in Matlab [29] to take advantage of several useful built-in functions, particularly those available via the Mapping and Curve Fitting toolboxes, both of which are required to allow the model to run. The model is built-up from a set of 'functions' that can be called using a 'script' called *Main*. In the following description all of the files that make up the model are referred to using *italics* to highlight their significance. All of the data required for the model to run is incorporated into the model. A summary of the functions that make-up the model and the basis data which is used is provided in Table 1.

Table 1. Summary of Functions and Basis Data.

Functions	Description	Basis Data	Description
CO2TransModel	Main function taking input data from *Case*, passes data to other functions and formats the results.	*Case*	The description of the CCS transport scenario considered. User input.
PipeProf	Calculated the elevation profile based on *Case*.	*Bath* *SSTdata*	Bathymetry basis data Sea temperature basis data
PressProf *PressureDrop* *fFact* *Visc*	Calculates pressure and temperature profiles based on *PipeProf* & stream properties data. Pressure drop used in *PressProf*. Friction factor used in *PressureDrop*. Viscosity calculation.	*Post* *Pre* *Oxy* *	Stream properties data including: compositions, density data, critical constants, dew-point, bubble-point, JT coefficient, heat capacity.
TransEnergy	Calculates energy consumption for compression OR liquefaction and pumping based on *PressProf* and the *SSTdata*.	*CompPost* *CompPre* *CompOxy* * *Liq_Power*	Data relating to the energy consumption for compression, liquefaction and pumping of CO_2 at different pressure and temperature conditions.

* Data available in the model, but not implemented in the *TransEnergy* calculations.

A description of each the model input, calculation methods, basis data and outputs is presented below under several headings.

2.1. Case Defenition

An interface to the model is provided in the script *Main*, which contains guidance on defining the basis for running the model. The basis for any particular case is stored as variables in a 'structure' called *Case*. A summary of the required input data for *Case* is provided in Table 2.

Table 2. Summary of Model Input Parameters.

Name	Description
POI	Geographic reference points (decimal degrees) describing the pipeline route **
Opt	Transport type: 1 = pipeline *; 2 = ship
LiqLoc	Location of the liquefaction process (*Opt* = 2 only) in decimal degrees
WH_loc	Wellhead location: 0 = sub-sea * and 1 = surface wellheads
Res_Depth	Reservoir depth in meters **
Pipe_e	Roughness in μm, default is 15 μm
Stream	'Post' *, 'Pre' or 'Oxy' composition
T_inlet	Pipeline inlet temperature
U	Heat transfer coefficient, default value is 6 W/m^2-K
Flow	Case flowrate in Mtpa **
T_sea	Sea water temperature in °C ***
Pipe_prof	Elevation profile ***

* Default option in the model ** Default is Melkøya based on *** Optional user input: replaces default methods.

CO_2 originating from different emission sources will often have different composition. This impacts on the phase behavior of the mixture and pipeline operating conditions. To take account of this in the model and to maintain consistency with earlier work, three CO_2 mixtures can be selected in the model by specifying either 'Post', 'Pre' or 'Oxy' as the *Stream* in *Case*. These stream alternatives represent a post-combustion capture process from flue gas using a chemical solvent, a pre-combustion capture process from syngas (also using physical solvent) and an oxyfuel flue gas originating from an oxyfuel purification unit. Table 3 summarizes the composition of these streams.

Table 3. CO_2 Mixture Compositions.

Component	Post	Pre	Oxyfuel
CO_2 mole %	99.99	99.50	96.16
N_2 mole %	0.01	-	2.45
CH_4 mole %	-	0.50	-
Ar mole %	-	-	0.96
O_2 mole %	-	-	0.43

Several example cases are made available for use with the model and can be called using *Main*. Alternatively, the user can simply create their own *Case* structure using the parameters from Table 2, or they can simply run *Main* without alteration, which returns results with the default parameters specified in *Case*.

Within *Main* plotting and saving behavior can also be specified using a parameter called *Plot*, which defines the level of plot data generated: 0 = no plots, 1 = simple plots and 2 = all plots, and a parameter called *Save*, which can be set to either 1 = save results, or 0 = no save. Running *Main* calls the function *CO2TransModel*, which subsequently calls the other functions listed in Table 1.

2.2. Pipeline Elevation Profile and Sea Temperature

Pressure changes in CO_2 pipelines occur due to frictional loss, elevation change and acceleration. As the latter is very small compared to the others it is excluded from the present model. Both of the

other effects must be adequately accounted for to ensure an accurate model. Frictional pressure loss varies with pipeline length while changes in static pressure depend on pipeline elevation. Length and elevation data is used by the model in the form of the pipeline profile called *Pipe_prof*, which is generated using the *PipeProf* function and basis data from *Case*. Within *PipeProf* the profile is calculated using the *POI* defined in Case and the basis data defined in *Bath*.

The basis for the data stored in *Bath* is GEBCO's gridded bathymetric data set: GEBCO 2019 [30]. The data from the dataset was processed after downloading: the data in 'geotiff' format was converted to a georeferenced data grid using the 'geotiffread' function and then it was down sized to 20% using the built-in 'resizem' function. Data is currently only stored for the North, Norwegain and Barents Sea: latitude 47° N to 75° N and −10° E to 30° E.

Within *PipeProf* a profile is generated using the *mapprofile* function and the *POI* defined in *Case*, which must be given in decimal degrees. The profile generated reflects the contours of the seabed and not necessarily a realistic pipeline route, which would be designed to avoid abrupt changes in direction. To reflect this, the raw profile data is smoothed before it is used in the pressure drop calculations.

To ensure that the method described above gives a realistic result for the pipeline profile, published profile data from the Melkøya CO_2 pipeline [31] was used in a qualitative validation exercise, which is presented in Figure 2. The method used in the validation exercise was to define a pipeline based on the information contained in [31] and then to automatically generate a pipeline profile from the bathymetry data stored in the model. The modelled pipeline elevation profile could then be compared to the pipeline elevation profile presented in [31] to check consistency. The results of this comparison as illustrated in Figure 2.

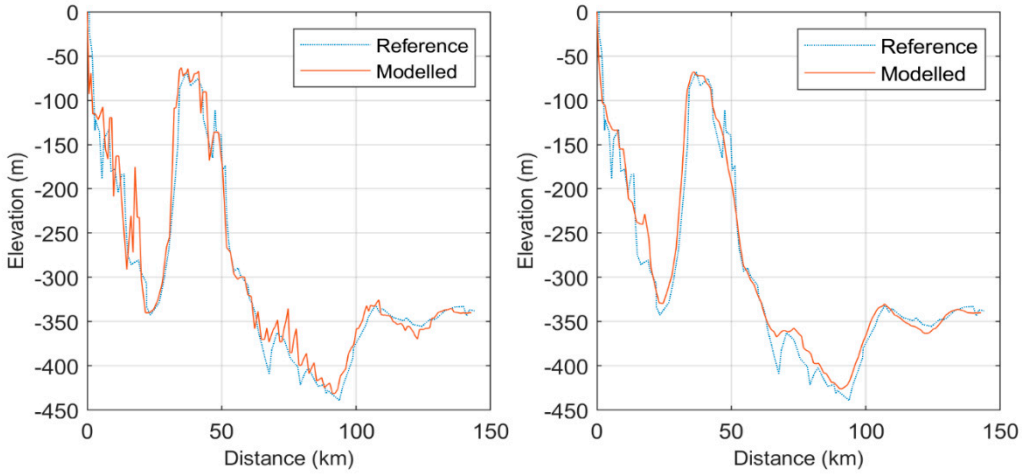

Figure 2. Elevation Profile Comparison Between Reference Data for Melkøya; [31] and (**a**) Modelled Profile with no Smoothing; (**b**) Profile with Smoothing.

To allow the comparison of pipeline operating conditions in different geographic locations the model calculates the average sea temperature for the pipeline, T_{sea}, based on Sea Surface Temperature (SST) data for the 10 year period April 2009 to April 2019. The data was obtained from Japan Meteorological Association (JMA) [32] and is stored in the model as the file *SSTdata*.

In the development of the model, raw data from JMA was converted to NetCFD format for easy use, and trimmed to cover only the area of interest. Monthly averaged data was then used to determine the mean SST value at each grid point. A value of SST equal to mean plus two standard deviations was then calculated to set a realistic maximum pipeline design operating temperature that reflects 97.5% of the monthly averaged data.

In reality, the temperature of the seawater below the surface will normally be several degrees lower than SST. This reduction in temperature below SST is difficult to generalize, and is therefore, not

used in the model. To allow flexibility, the option to manually set a value for T_{sea} is provided via the parameter T_{sea} in *Case*.

2.3. Pipeline Pressure and Temperature Profiles

Both the pipeline pressure and temperature profiles are generated by the *PressProf* function which uses the results from *PipeProf* and data for the *Stream* specified in *Case*. The procedure contained in *PressProf* is a numerical stepwise approach to the calculation of the pipeline pressure profile,

$$P_{out} = P_{in} - \sum \left(P_n^f - P_n^s \right), \tag{1}$$

where P_{out} is the pipeline outlet pressure, P_{in} is the pipeline inlet pressure, P_n^f is the frictional pressure drop for the element n in the pipeline and P_n^s is the static pressure change for elmenet n. The calculation methods associated with static and frictional pressure change are detailed under later headings.

The calculation procedure for P_{out} begins with an estimate for P_{in} and continues stepwise with the pressure in each element 'n' calculated based on the pressure in the previous element. When the pipeline pressure calculation has been completed, the calculated value of P_{out} is compared to the WHP and the minimum allowable pipeline pressure along the full length of the pipeline, P_n^{min}, and a correction is made to the estimated value of P_{in}:

$$C = \max\left(\text{WHP} - P_{out} \;\&\; P_n^{min} - P_n \right), \tag{2}$$

$$\text{and } P_{in} = P_{in} + C, \tag{3}$$

where C is a correction factor used in the calculation algorithm. The pressure drop calculation then continues iteratively until the absolute value of C is less than 1 bar. The calculation of WHP and P_n^{min} is described under the next two headings.

2.3.1. Well Head Pressure

Studies such as that of Maldal [33] and Shi et al. [34] illustrate that CO_2 reservoir pressure will normally change substantially over time, varying with reservoir conditions and operating parameters such as flowrate. This makes the selection of a representative modelling basis for WHP complicated. The approach taken in this study was, therefore, to assess the range of likely reservoir pressure conditions across the lifespan of storage reservoir from limiting cases. For example, Vishal et al. [35] state that "*Depending on the national regulatory, maximum allowed [over] pressure generally corresponds to the 50% of the initial hydrostatic pressure or the 60% of initial lithostatic pressure at the top of the storage formation*". Accordingly, the model present results for three cases where the reservoir pressure is set at 10%, 30% and 50% above initial hydrostatic pressure, which is calculated from the *Res_Depth* parameter in *Case*,

$$P_R = \rho_w \cdot h \cdot g \cdot 10^{-5}, \tag{4}$$

where P_R (bar) is the reservoir pressure, ρ_w is the density of water (kg/m^3) and h is the depth of the reservoir (m) and g is the gravitational constant (m/s^2).

Frictional pressure loss in the pipework associated with the well depends on the length of the well, its diameter and the injection rate, which in-turn depends on the number of injection wells. In this work, for simplicity, the wellhead frictional pressure drop has been based on the Norsok Standard, P-100, which calls for a pressure drop of 0.11–0.27 bar/100 m for wells operating 35–138 barg. WHP is calculated by dividing the well pipework into 100 elements and summating the static head change and frictional pressure loss in each element,

$$\text{WHP} = P_R \; R + \sum_{i=1}^{100} h_i \left(\rho_i \cdot g \cdot 10^{-5} - P_W^f \; 10^{-2} \right), \tag{5}$$

where R is the overpressure ratio (1.1, 1.3 and 1.5 being the default values in the model), h_i is the height of element i in the well pipework, ρ_n is the density of the CO_2 mixture in element (kg/m^3) and P_W^f is a constant frictional loss = 0.15 bar/100 m for the pipework associated with the well(s).

2.3.2. Minimum Pipeline Operating Pressure

CO_2 pipelines are often designed based on a minimum operating pressure that is set at a margin above the critical pressure of the CO_2 mixture present in the pipeline [3,14,36], as illustrated below by the green dashed line in Figure 3. The purpose this is to avoid a situation where a pipeline operating in the supercritical region cools to conditions close to the critical point—where density can be difficult to predict—or, worse still, where pipelines operating in the gas phase cool leading to condensation. However, sub-sea pipelines located in the North, Norwegian and Barents Sea can be expected to operate with CO_2 in the dense phase, i.e., well below the critical temperature of CO_2 (31 °C). Under these conditions, phase change can be avoided by specifying a minimum approach to the bubble point curve as illustrated by the blue dashed line in Figure 3.

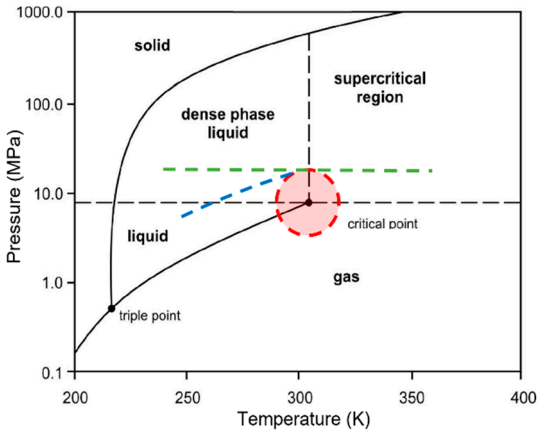

Figure 3. Illustration of Pipeline Operational Limits.

The model calculates the minimum operating pressure for each element in the pipeline as part of the pressure profile calculations in the *PressProf* function using a 10 bar margin to the bubble point pressure,

$$P_n^{\min} = P_n^{BP} + 10 \text{ bar} \quad (6)$$

where $P_n^{\min}$ is the minimum operating press in element n and P_n^{BP} is the bubble point pressure of the mixture in the pipeline at element n. Accurate prediction of the P_n^{BP} of each CO_2 mixture is important to the specification of $P_n^{\min}$ and to ensure this, bubble point data from the TREND properties package [7] is used as the basis for the model. This basis data is stored in the files *Post*, *Pre* and *Oxy* as a set of gridded interpolation data.

2.3.3. Pipeline Diameter Selection

Several studies have presented methods for determining the optimim diameter for CO_2 pipelines [14–16], which is normally based on minimising costs. Others have proposed that "the smallest diameter which ensures that pressure drops are lower than the maximum allowable pressure is the cost-optimal diameter . . . " [37], but this only transfers the determination of optimum diameter to that of the determination of the maximum allowable pressure, which has been suggested to lie between 15.3 and 20 MPa [5,15,38,39]. The approach adopted in the model is, therefore, to obviate the difficulties associated with identifying optimum diameter by presenting results for a range of suitable diameters. The range used in a particular case is defined using a minimum inside diameter, $D_{\text{ID}}^{\min}$, and the next three larger standard pipe sizes.

$D_{\mathrm{ID}}^{\mathrm{min}}$ is calculated using an erosional velocity limit, u_e, the minimum gas density in the pipeline, ρ_{min}, and the parameter *Flow* from the model input parameters,

$$D_{\mathrm{ID}}^{\mathrm{min}} = \sqrt{\frac{4 \cdot m}{\pi \cdot \rho_{\mathrm{min}} \cdot u_e}} \tag{7}$$

where m is the mass flow in the pipeline (kg/s) based on the parameter *Flow* from *Case.* The erosional velocity limit is, in turn, calculated based on the formula given in API 14C and the factor 'c' taken as 100 for continuous flow [3],

$$u_e = 0.82 \, \mathrm{c} / \sqrt{\rho_{\mathrm{min}}} \tag{8}$$

where the minimum gas density, ρ_{min}, is calculated using the worst case for all minimum operating pressure conditions along the pipeline and the minimum SST.

The three standard pipe sizes that lie above $D_{\mathrm{ID}}^{\mathrm{min}}$ are based on 2 inch intervals between the standard pipe sizes. Early testing of the model confirmed that this approach covers all of the sizes that would normally be of interest for study purposes.

The density of the CO_2 mixture is used in several of the calculations carried out by the model and, therefore, accurate prediction at different pressure and temperature conditions is important. To ensure this, density data from the TREND [7] properties package is stored for each of the streams in the files *Post*, *Pre* and *Oxy* as a set of gridded interpolation data.

2.3.4. Calculation of Frictional and Static Pressure Changes

Frictional pressure drop, P_n^f, is calculated in *Press_prof* using the Darcy–Weisbach equation:

$$P_n^f = 2 f_{\mathrm{F}} \frac{L_n}{D_{\mathrm{ID}}} \rho_n^{\mathrm{av}} u_n^2 \tag{9}$$

where f_F is the Fanning friction factor calculated using ρ_n^{av}, L_n is the length of element n, D_{ID} is the inside diameter of the pipeline (4 cases), ρ_n^{av} is the average density in element n and u_n is the average velocity in element n, which is also calculated using ρ_n^{av}.

The calculation of ρ_n^{av} is based on the assumption that, although P_n^f is generally small for short L_n, the static pressure change, P_n^s, can be significant when the elevation change is also significant. Accordingly, the average pressure and density are estimated prior to conducting the pressure drop calculation to improve accuracy using a simple linear average,

$$P_n^{\mathrm{av}} = \frac{1}{2}[P_{n-1} + (P_{n-1} + \rho_{n-1} \, g \, El_n)] \tag{10}$$

where El_n is the elevation change for the n^{th} element in the pipeline and ρ_{n-1} is the density for the preceding pipeline segment $n-1$, which is calculated as a function of pressure and temperature.

The static pressure loss in each pipeline segment is calculated using the average density:

$$P_n^s = \rho_n^{\mathrm{av}} g \, El_n. \tag{11}$$

The pressure drop calculations are made step-by-step alongside the temperature profile calculations for the full length of the pipeline. Temperature profile calculations are described under a separate heading.

2.3.5. Pipeline Roughness and Friction Factor

Pipeline roughness and friction factor have an important impact on pressure drop. In common with other studies [14,15], the model described here uses the Zirang and Sylverster equation [40] to

estimate the Fanning friction factor, f_F, which has been shown by Winning and Coole [41] to give good accuracy,

$$\frac{1}{\sqrt{f_F}} = -4\log\left\{\frac{e/D_{\mathrm{ID}}}{3.7} - \frac{5.02}{\mathrm{Re}_n}\log[\mathrm{A}]\right\} \tag{12}$$

$$\mathrm{A} = \frac{e/D_{\mathrm{ID}}}{3.7} - \frac{5.02}{\mathrm{Re}_n}\log\left[\frac{e/D_{\mathrm{ID}}}{3.7} - \frac{13}{\mathrm{Re}_n}\right] \tag{13}$$

where, e is the pipeline roughness (mm), D_{ID} is as before and, Re_n is the Reynold's number for element n:

$$\mathrm{Re}_n = D_{\mathrm{ID}}\, u_n\, \rho_n^{\mathrm{av}} / \mu_n^{\mathrm{av}}\,, \tag{14}$$

where μ_n^{av} is the average viscosity of the mixture in element n. The calculation of friction factor is carried out in the model using the *fFact* function; viscosity is calculated based on P_n^{av} and ρ_n^{av} using the function *Visc*, which is based on the Lohrenz, Bray and Clark (LBC) formula with the parameter fitting for CO_2 suggested by Nazeri [9].

The roughness, e, used in Equations (12) and (13) depends on the design of the pipeline. Large-scale gas transport pipelines are typically coated with a thin film of epoxy giving low roughness [42]. Wellong et al. [43], for example, found that for large scale natural gas pipelines "79.1% of the absolute roughness values lie in the region from 5 µm to 15 µm" while Langelandsvik [42] found average roughness of 4 µm. However, studies relating to CO_2 pipelines have often used higher values of e: Mazzoccoli [5] and McCoy [15], for example, use 45.7 µm and Chandel et al. [44] use 100 µm to reflect old pipe. The default value of e used in the model, 15 µm, reflecting that of large natural gas pipelines, but it can be adjusted to suit by the user by specifying *Pipe_e* in *Case*.

2.3.6. Pipeline Temperature Profile

The temperature of the CO_2 entering the pipeline can be expected to vary between cases and with geographic location. If the CO_2 stream entering the pipeline originates from a compressor it will normally be cooled before entering the pipeline to avoid damage to pipeline coatings: A typical limit for inlet temperature being 50 °C [38]. To reflect this, the pipeline inlet temperature is set by default to 5 °C above sea temperature T_{sea} at the pipeline entry. If the CO_2 stream entering the pipeline originates from refrigerated intermediate storage, i.e., arrives at the pipeline entry point via ship, it is then likely to be warmed before entering the pipeline and may enter the pipeline below ambient temperature. In this scenario, the model assumes that the inlet temperature is by default to 5 °C below the average sea temperature T_{sea}. If another inlet temperature is required, or a sensitivity study is to be conducted, the user can set this using *T_inlet* in *Case.*

The temperature of the CO_2 in the pipeline will change in response to both heat loss to ambient and pressure drop along the length of the pipeline. These changes are calculated in the model in parallel to the pressure profile calculations. The calculations are carried out by the *PressProf* function using a heat balance to estimate the losses to ambient and a correction to account for the Joule-Thomson (JT) effect,

$$T_n = T_{\mathrm{sea}} + \left(T_{n-1} - T_{\mathrm{SST}}^{\mathrm{av}}\right)\exp\left\{\frac{-U_o A_{\mathrm{OD}} L_n}{m.Cp_n}\right\} + \mathrm{JT}_n \tag{15}$$

$$\text{and } \mathrm{JT}_n = \alpha(P_n - P_{n-1}), \tag{16}$$

where T_n is the temperature in element n, $T_{\mathrm{SST}}^{\mathrm{av}}$ is the average seawater temperature along the pipeline route, U_o is the overall heat transfer coefficient (W/m^2-K), Cp is the specific heat capacity of the CO_2 mixture (J/kg), m is the mass flowrate (kg/s), A_{OD} is the outside area of the pipline (m^2/m), L_n is the length of pipeline element 'n' (m), JT is the JT correction factor (°C), and α is the JT coefficient (°C/bar). The basis for the JT coefficient is tabulated data for the JT coefficient that was derived from Wang et al. [6] and is stored in the model as gridded interpolation function in *Post*, *Pre* and *Oxy*.

The outside area of the pipeline, A_{OD}, is calculated from the D_{ID} and the wall thickness, t:

$$A_{OD} = \pi(D_{ID} + 2t). \quad (17)$$

The wall thickness, t, is estimated using the same method as Chandel et al. [44] and Tian et al. [16]:

$$t = \frac{P^{max} D_{ID}}{2 \cdot S \cdot F \cdot E - P_{max}}, \quad (18)$$

where P^{max} is the maximum allowable operating pressure in the pipeline (based on the pipeline pressure profile), D_{ID} is the pipeline inside diameter (i.e., represents the four selected pipeline sizes for each case), S is the minimum yield strength of the pipeline, F is a design factor and E is a longitudinal joint factor. S, F and E are set to 483 MPa, 0.71 and 1.0 based on Tian et al. [16].

The pipeline heat transfer coefficient, U_o, depends on conditions inside the pipeline, outside the pipeline and on the pipeline design itself (e.g., coating, insulation, etc.). In particular, it depends on whether the pipeline is buried or in direct contact with seawater: Drescher, et al. [10] found that the heat transfer coefficient for pipelines with water as the surrounding substance were, on average, 44.7 W/m^2-K, whereas a coefficient in the range 1 to 6 W/m^2-K have been used in the studies referenced here relating to buried onshore pipework [5,36]. In the present model, a single value of U_o can be set by the user for the full length of the pipeline using the parameter *U* in *Case*. By default, the parameter *U* is to a value of 4 W/m^2-K, but this can be altered by the user when specifying *Case*.

2.3.7. Transportation Energy Consumption

The energy consumption resulting from the transportation of CO_2 in a pipeline depends on the inlet pressure of the pipeline and the temperature of the cooling utility available to the compression or liquefaction processes. The type of transportation process used in the model is set using the parameter *Opt* in *Case*.

If the transportation type specified is 'pipe', the energy consumption is calculated based on the results of earlier modelling work [21], which is stored within the model as tabulated data for the variation in energy consumption with compressor discharge pressure and cooling temperature. The pipeline inlet pressure used to calculate the energy consumption is given by the pipeline pressure profile and the cooling temperature is set by assuming a compressor aftercooler temperature is 5 °C above the SST at the pipeline inlet location.

If the transportation type specified is 'ship', the energy consumption for transportation is the sum of the energy required for liquefaction of the CO_2 at the point of origin of the CO_2 stream and the power required to pump the CO_2 up to the pipeline inlet pressure at the point of deliver to the pipeline. The energy consumption associated with the liquefaction process is, again, based on earlier related modelling work [22], which is stored within the model as tabulated data for the variation in energy consumption with ambient temperature. The liquefaction pressure in this case is fixed at 15 bara and, therefore, energy consumption is determined using only the sea temperature in the geographic location of the liquefaction process. The energy consumption for pumping liquid CO_2 to the required pipeline inlet pressure is calculated based on a set of tabulated performance data for a pump with an adiabatic efficiency of 80% and pure CO_2 as the working fluid.

Figure 4 presents a sample of the data used as the basis for the energy consumption for transportation. The complete set of data is also freely available from previously published works [21,22].

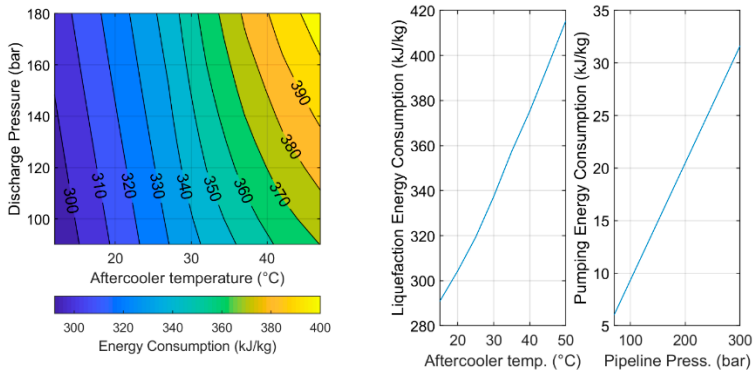

(**a**) (**b**)

Figure 4. Modeling Basis for the Energy Consumption for Compression, (**a**) Liquefaction and Pumping Power (**b**).

2.4. Model Outputs

Based on the input parameters summarized in Table 2, the model generates a set of outputs, which are summarized in Table 4. These outputs can be subsequently used to automatically generate several plots, as summarized in Table 5, by specifying the *Plot* parameter in *Main*.

Table 4. Summary of Model Outputs.

Name	Profiles
Elevation	Pipeline element length & element elevation change
Pressure	Pressure profile for 10%, 30% & 50% overpressure
Temperature	Pressure profile for 10%, 30% & 50% overpressure
Name	**Performance**
Inlet Pressure	Inlet pressure for each pipeline size & overpressure case
WHP	Well head pressure for each overpressure case
Av. Frictional DP	Simple mean of frictional pressure drop component for each case
Av. Velocity	Simple mean of gas velocity pressure drop component for each case
Energy	Summary of energy consumption for each pipeline size & overpressure case.

Table 5. Summary Plots Generated by the Model.

Name	Description
Map	Location map for the pipeline/liquefaction location
Conditions	Plot of temperature vs pressure for all pipe sizes and overpressure cases
Profiles	Pressure and temperature profiles for the smallest line size that operates under 200 bar under all conditions
Energy	Sum of pipeline and liquefaction energy consumption for all pipe sizes and overpressure cases

2.5. Model Validation

The aim of the model validation work was to verify the reliability of the pressure and temperature profile calculations carried out by the model. The method chosen was to use the Aspen HYSYS software package, in order to generate a set of reference data against which the pressure and temperature profile predictions made by the model could be compared. The HYSYS software is a process modeling package that is widely used in the gas processing industry that includes a set of built-in modelling capabilities that are suitable for calculating pipeline pressure and temperature profiles, making it well suited to the validation exercise. The approach taken to the assessment of the validation results was to calculate the absolute value of the pressure and temperature error. The limit for an acceptable validation results was

set as an average absolute error of less than 1 °C for the temperature profile and 1 bar for the pressure profile. Further details of the method used in the validation work is presented below.

As the model automatically generates a case-dependent elevation profile that often consists of more than 100 data points it was necessary to construct a simplified profile that could be manually implemented in HYSYS. The simplified profile was created by sampling 19 data points from the Melkøya profile that capture the key features and is stored in a custom case definition called *Validation* which is saved with the model and can be run using *Main*. This validation elevation profile is illustrated in Figure 2 and the data points that form the basis are presented in Table 6.

Table 6. Elevation Profile Used in the Validation.

Length (km)	Elevation (m)	Length (km)	Elevation (m)
0.0	0.0	58.7	−310
0.4	−1.2	65.1	−371
0.5	−99.1	76.1	−384
3.1	−127	91.4	−435
18.0	−228	107	−343
21.3	−230	126	−363
25.5	−338	133	−344
39.7	−65.4	145	−341
47.1	−102	149	−321
53.7	−317	152	−322

In the HYSYS model, the Peng Robinson (PR) properties package was used with default options and the mixture in the pipeline was considered to be pure CO_2. In the model, to allow a direct comparison with the HYSYS results, a set of density and heat capacity data was generated from HYSYS that formed the modelling basis for the validation work. This data is stored in the model as a stream called *Post_Val*.

The inlet pressure calculated by the model was then used to specify the inlet pressure in the HYSYS model so that the results could be directly compared. The results of this validation exercise are stored in full with the model, which is available at UiT Open Research Data [45] and presented below in the Results section.

2.6. Sample Case

As described under earlier headings, the normal basis for the density and heat capacity calculations made by the model is tabulated data from the TREND properties package. Therefore, because the results from the validation study are based on properties data generated using HYSYS, the results are not directly equivalent to the standard model output for the same input parameters. To provide a comparison against the model results for the same case, a sample set of results were generated using the case file called Melkoya, which has the same input parameters as Validation. These results are saved in full with the model available at UiT Open Research Data [45] and can also be generated by running Main with Validation selected as the example case. A summary of these results is presented in the Results.

3. Results

The results provided here are limited to the presentation of a summary of the findings of the validation exercise and the presentation of a single set of results for a Sample Case: the Melkøya CO_2 pipeline using a rough interpretation of the pipeline route from Såtendal et al. [31]. Full results for both of these cases are stored with the model at UiT Open Research Data [45].

3.1. Validation

Figure 5 provides a comparison of the temperature profile generated by the model and HYSYS for the same validation case. Figure 5b shows that the average absolute temperature difference between

the two models is less than 1 °C, which indicates that the calculations made by the model are reliable. Figure 6 provides a comparison of the pressure profile generated by the model and HYSYS for the same validation case. Again, the results from the model correspond well with the results from the HYSYS model, with a maximum pressure difference of under 1 bar across the full length of the pipeline.

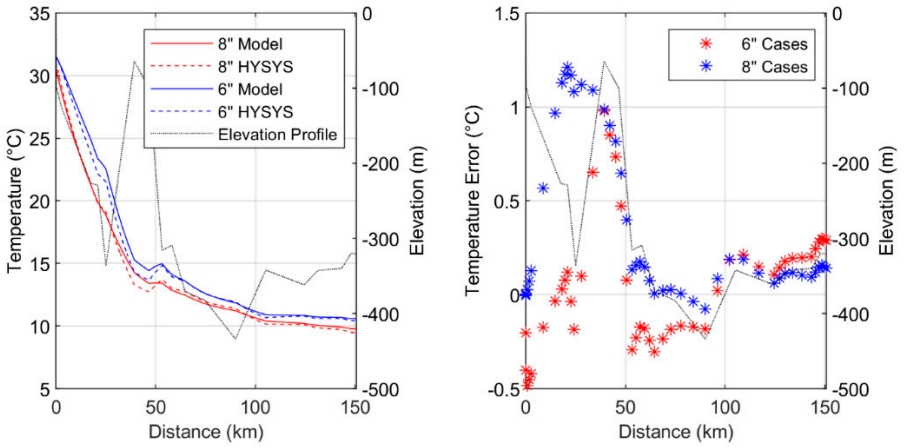

(**a**) (**b**)

Figure 5. Comparison of Model and HYSYS Results for the Validation Case, (**a**) shows a Comparison of the Temperature Profile Results for the 10% Overpressure Case; and (**b**) shows the Absolute Temperature Difference Between the Results.

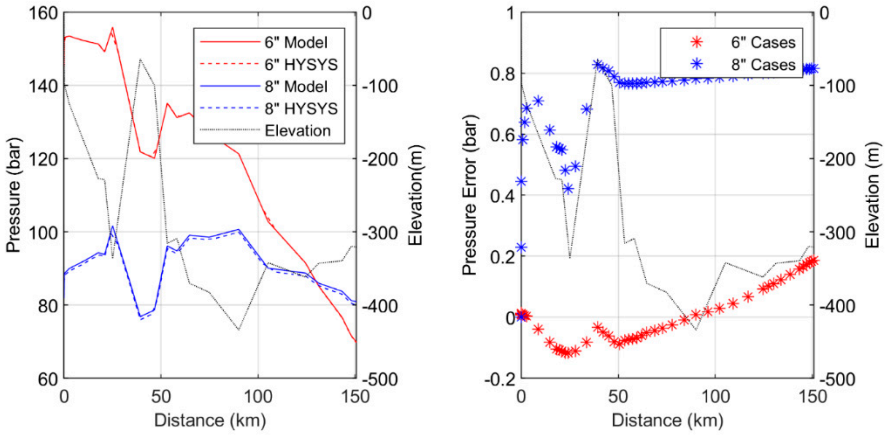

(**a**) (**b**)

Figure 6. Comparison of Model and HYSYS Results for the Validation Case: (**a**) Shows a Comparison of the Pressure Profile Results for the 10% Overpressure Case; and (**b**) Shows the Absolute Pressure Difference Between the Two Sets of Results.

3.2. *Sample Case*

Figures 7–10 present the standard set of model plots as described by Table 4. Figure 9 shows that the smallest pipeline size to ensure operating conditions under 200 bar in all operating cases is 8 inches. Figure 9 also shows that a margin is maintained against the bubble point pressure for all cases across the pipeline length. Figure 10 shows the temperature and pressure profiles for the 10% reservoir overpressure case and illustrates that the minimum pressure condition at the wellhead end only dictates the pipeline inlet pressure for the 6 inch pipeline case due to high pressure drop along the pipeline. In the other cases the minimum pipeline pressure condition (approach to the bubble point

pressure) sets the pipeline inlet pressure, which means that some pressure letdown would be required at the wellhead to reach WHP.

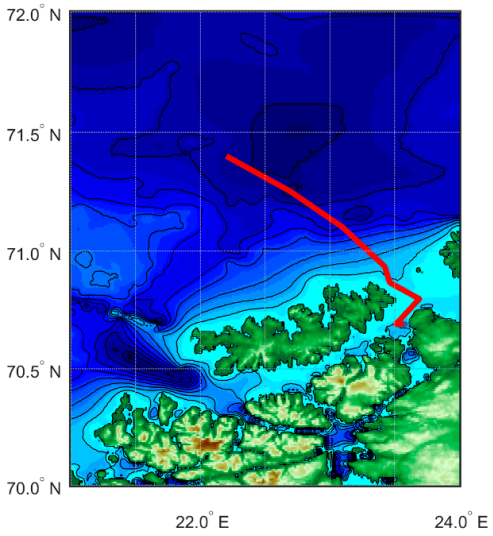

Figure 7. Approximate Melkøya CO_2 Pipeline Route.

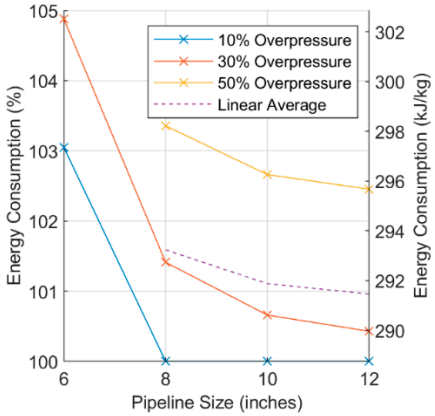

Figure 8. Summary of Energy Consumption for the Melkøya CO_2 Pipeline Example.

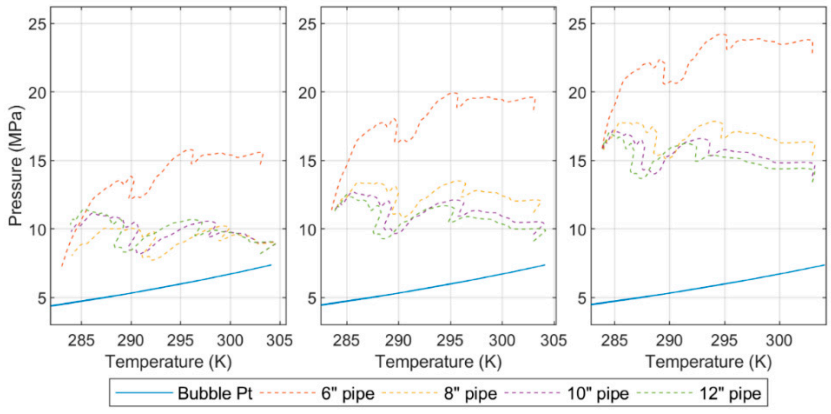

Figure 9. Summary of Pipeline Temperature and Pressure Conditions for the Melkøya CO_2 Pipeline Example. On the left is the 10% reservoir overpressure case, middle 30% and right 50% overpressure.

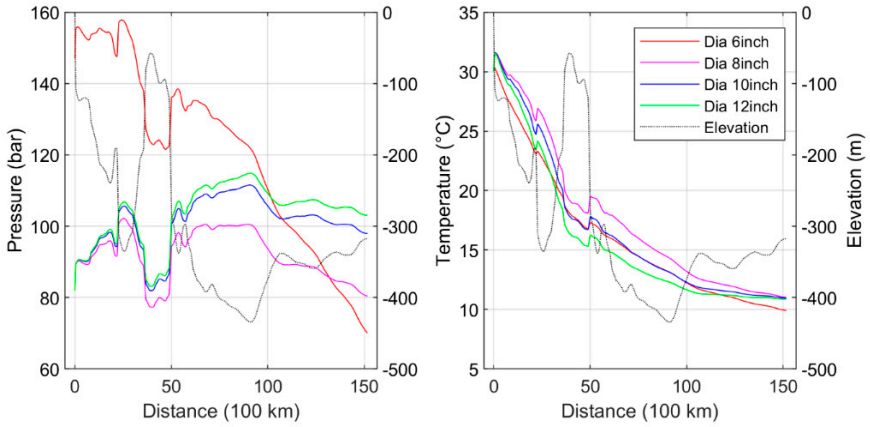

Figure 10. Summary of Pipeline Temperature and Pressure Profiles for the Melkøya CO_2 Pipeline Example for the 10% reservoir overpressure case.

The tabulated data that forms the basis for Figures 5, 6, 9 and 10 is stored with the model and available at UiT Open Research Data [45]. The raw data allows a more detailed comparison of the results obtained using the modelling basis for the validation work (illustrated in Figures 5 and 6) and the results obtained using the standard modelling basis (presented in Figures 9 and 10). For example, the data for the 6 inch line size and the 10% overpressure case shows that the inlet pressure is 144.4 bar in the validation results and 147.0 bar for the default model. A comparison of the 8 inch line outlet pressure for the 10% overpressure case shows 80.9 bar for the validation case and 80.4 bar for the default model basis. Outlet temperatures are also very similar in all cases.

4. Discussions

The scope of this article is the development and validation of a pipeline model; application of the model to compare the performance of different CO_2 pipeline alternatives will form part of future study work. In particular, the model described here is intended for use in the development of larger system models that will include the performance of the capture element of carbon free value chains.

The model presented here is presently only fully developed for the post and pre combustion CO_2 compositions. Data for the oxyfuel stream composition and transportation energy consumption can be calculated by the model, but this is not on a consistent basis with the pre- and post-combustion cases, and therefore, cannot be directly compared with these cases.

The results of the validation work show that the model can reproduce pipeline pressure profiles with good accuracy and that a representative elevation profile can be generated automatically from bathymetry data that captures the key features of a complicated pipeline route such as the one associated with the Melkøya CO_2 pipeline. A comparison of the validation results to the standard modelling basis also shows good agreement.

5. Conclusions

This article has presented the development of a model for CO_2 transportation processes. The model has been validated and tested against an example case, and can be seen to give consistent results.

The results of the validation work show that the pressure and temperature profile have an average absolute error of less than 1 bar, and 1 °C, respectively compared to the selected reference model supporting the aim of the work, which is to provide a consistent and transparent basis for the comparison of different CO_2 transportation scenarios.

The results from the sample case show how the results of the model can be used to provide useful design and performance information for CO_2 pipelines, confirming, for example, that the installed size of 8 inches [31] is the optimum size for the Melkøya pipeline.

The development of comparisons between different transport case will form the scope of future work. The code for the model presented here along with all the data needed for its use and the results presented in this article is available at UiT Open Research Data [45].

Funding: The publication charges for this article have been funded by a grant from the publication fund of UiT The Arctic University of Norway.

Acknowledgments: I would like to thank Eivind Brodal for his support and guidance.

Conflicts of Interest: The authors declare no conflict of interest.

Nomenclature

A	Area based on OD
c	Erosional velocity factor
C	Model correction factor
Cp	Heat capacity
D	Diameter
e	Absolute roughness
E	Pipeline joint factor
F	Pipeline design factor
f_F	Fanning friction factor
g	Gravitational constant
h	Reservoir depth
h	Height
JT	Joule-Thompson coefficient
L	Length
P	Pressure
P	Pressure drop
R	Reservoir overpressure factor
Re	Reynolds number
S	Min. pipeline yield strength
t	Pipe wall thickness
T	Temperature
u	Velocity
U_o	Overall heat transfer coefficient
WHP	Well head pressure
μ	Viscosity
ρ	Density
Subscripts & Superscripts	
av	Average
BP	Bubble point
e	erosion
f	Friction
i	Element 'i' in the well
ID	Based on inside diameter
in	Inlet
max	Max
min	minimum
min	Min
n	Element 'n' in the pipeline
o	Overall
OD	Based on outside diameter
out	Outlet
R	Reservoir
s	Static

sea	Average sea condition
SST	Sea surface temperature
w	Water

References

1. Global CCS Institute. *Global Status of CCS 2019*; Global CCS Institute: Melbourne, Australia, 2019.
2. IEA. *World Energy Outlook 2019*; IEA: Paris, France, 2019. [CrossRef]
3. Peletiri, S.P.; Rahmanian, N.; Mujtaba, I.M. CO_2 Pipeline design: A review. *Energies* **2018**, *11*, 2184. [CrossRef]
4. Northern Lights—A European CO2 Transport and Storage Network. Available online: https://northernlightsccs.eu/ (accessed on 5 March 2020).
5. Mazzoccoli, M.; Bosio, B.; Arato, E.; Brandani, S. Comparison of equations-of-state with P-p-T experimental data of binary mixtures rich in CO_2 under the conditions of pipeline transport. *J. Supercrit. Fluids* **2014**, *95*, 474–490. [CrossRef]
6. Wang, J.; Wang, Z.; Sun, B. Improved equation of CO_2 Joule–Thomson coefficient. *J. CO2 Util.* **2017**, *19*, 296–307. [CrossRef]
7. Span, R.E.T.; Herrig, S.; Hielscher, S.; Jäger, A.; Thol, M. TREND. In *Thermodynamic Reference and Engineering Data 3.0*; Lehrstuhl für Thermodynamik, Ruhr-Universität Bochum: Bochum, Germany, 2016.
8. Wilhelmsena, Ø.; Skaugena, G.; Jørstadb, O.; Hailong, L. Evaluation of SPUNG# and other Equations of State for use in Carbon Capture and Storage modelling. *Energy Procedia* **2012**, *23*, 236–245.
9. Nazeri, M.; Chapoy, A.; Burgass, R.; Tohidi, B. Viscosity of CO_2-rich mixtures from 243 K to 423 K at pressures up to 155 MPa: New experimental viscosity data and modelling. *J. Chem. Thermodyn.* **2018**, *118*, 100–114. [CrossRef]
10. Drescher, M.; Wilhelmsen, Ø.; Aursand, P.; Aursand, E.; de Koeijer, G.; Held, R. Heat Transfer Characteristics of a Pipeline for CO_2 Transport with Water as Surrounding Substance. *Energy Procedia* **2013**, *37*, 3047–3056. [CrossRef]
11. Lee, W.J.; Yun, R. In-tube convective heat transfer characteristics of CO_2 mixtures in a pipeline. *Int. J. Heat Mass Transf.* **2018**, *125*, 350–356. [CrossRef]
12. Wetenhall, B.; Race, J.M.; Aghajani, H.; Barnett, J. The main factors affecting heat transfer along dense phase CO_2 pipelines. *Int. J. Greenh. Gas Control* **2017**, *63*, 86–94. [CrossRef]
13. Zhang, W.B.; Shao, D.; Yan, Y.; Liu, S.; Wang, T. Experimental investigations into the transient behaviours of CO_2 in a horizontal pipeline during flexible CCS operations. *Int. J. Greenh. Gas Control* **2018**, *79*, 193–199. [CrossRef]
14. Mohammadi, M.; Hourfar, F.; Elkamel, A.; Leonenko, Y. Economic Optimization Design of CO_2 Pipeline Transportation with Booster Stations. *Ind. Eng. Chem. Res.* **2019**, *58*, 16730–16742. [CrossRef]
15. McCoy, S.; Rubin, E. An engineering-economic model of pipeline transport of CO_2 with application to carbon capture and storage. *Int. J. Greenh. Gas Control* **2008**, *2*, 219–229. [CrossRef]
16. Tian, Q.; Zhao, D.; Li, Z.; Zhu, Q. Robust and stepwise optimization design for CO_2 pipeline transportation. *Int. J. Greenh. Gas Control* **2017**, *58*, 10–18. [CrossRef]
17. Deng, H.; Roussanaly, S.; Skaugen, G. Techno-economic analyses of CO_2 liquefaction: Impact of product pressure and impurities. *Int. J. Refrig.* **2019**, *103*, 301–315. [CrossRef]
18. Aspelund, A.; Mølnvik, M.J.; De Koeijer, G. Ship Transport of CO_2: Technical Solutions and Analysis of Costs, Energy Utilization, Exergy Efficiency and CO_2 Emissions. *Chem. Eng. Res. Des.* **2006**, *84*, 847–855. [CrossRef]
19. Knoope, M.M.J.; Ramírez, A.; Faaij, A.P.C. Investing in CO_2 transport infrastructure under uncertainty: A comparison between ships and pipelines. *Int. J. Greenh. Gas Control* **2015**, *41*, 174–5836. [CrossRef]
20. Jordal, K.; Aspelund, A. Gas conditioning—The interface between CO_2 capture and transport. *International Int. J. Greenh. Gas Control* **2007**, *1*, 343–354.
21. Jackson, S.; Brodal, E. Optimization of the Energy Consumption of a Carbon Capture and Sequestration Related Carbon Dioxide Compression Processes. *Energies* **2019**, *12*, 1603. [CrossRef]
22. Jackson, S.; Brodal, E. Optimization of the CO_2 Liquefaction Process-Performance Study with Varying Ambient Temperature. *Appl. Sci.* **2019**, *9*, 4467. [CrossRef]
23. Alabdulkarem, A.; Hwang, Y.H.; Radermacher, R. Development of CO_2 liquefaction cycles for CO_2 sequestration. *Appl. Therm. Eng.* **2012**, *33*, 144–156. [CrossRef]

24. Seo, Y.; Huh, C.; Lee, S.; Chang, D. Comparison of CO_2 liquefaction pressures for ship-based carbon capture and storage (CCS) chain. *Int. J. Greenh. Gas Control* **2016**, *52*, 1–12. [CrossRef]
25. Øi, L.E.; Eldrup, N.H.; Adhikari, U.; Bentsen, M.H.; Badalge, J.C.L.; Yang, S. Simulation and Cost Comparison of CO_2 Liquefaction. *Energy Proceida* **2016**, *86*, 500–510. [CrossRef]
26. Jakobsen, J.; Roussanaly, S.; Anantharaman, R. A techno-economic case study of CO_2 capture, transport and storage chain from a cement plant in Norway. *J. Clean. Prod.* **2017**, *144*, 523–539. [CrossRef]
27. Jakobsen, J.P.; Roussanaly, S.; Brunsvold, A.; Anantharaman, R. A Tool for Integrated Multi-criteria Assessment of the CCS Value Chain. *Energy Procedia* **2014**, *63*, 7290–7297. [CrossRef]
28. Mallon, W.; Buit, L.; van Wingerden, J.; Lemmens, H.; Eldrup, N.H. Costs of CO_2 Transportation Infrastructures. *Energy Procedia* **2013**, *37*, 2969–2980. [CrossRef]
29. The MathWorks. *MATLAB*; The MathWorks: Natick, MA, USA, 2018.
30. GEBCO Compilation Group. GEBCO 2019 Grid. 2019. Available online: https://www.gebco.net/data_and_products/gridded_bathymetry_data/gebco_2019/gebco_2019_info.html (accessed on 27 January 2020).
31. Såtendal, S.H.; Laug, R.; Oaland, O. Subsea Pipeline Intervention In the Barents Sea. In Proceedings of the Seventeenth International Offshore and Polar Engineering Conference, Lisbon, Portugal, 1 January 2007; p. 7.
32. Japan Meteorological Agency. Available online: http://ds.data.jma.go.jp/tcc/tcc/products/elnino/cobesst_doc.html (accessed on 1 November 2019).
33. Maldal, T.; Tappel, I.M. CO_2 underground storage for Snøhvit gas field development. *Energy* **2004**, *29*, 1403–1411. [CrossRef]
34. Shi, J.-Q.; Imrie, C.; Sinayuc, C.; Durucan, S.; Korre, A.; Eiken, O. Snøhvit CO_2 Storage Project: Assessment of CO_2 Injection Performance Through History Matching of the Injection Well Pressure Over a 32-months Period. *Energy Procedia* **2013**, *37*, 3267–3274. [CrossRef]
35. Vishal, V.; Singh, T.N. *Geologic Carbon Sequestration: Understanding Reservoir Behavior*; Springer Nature: Cham, Switzerland, 2016. [CrossRef]
36. Zhang, Z.X.; Wang, G.X.; Massarotto, P.; Rudolph, V. Optimization of pipeline transport for CO_2 sequestration. *Energy Convers. Manag.* **2006**, *47*, 702–715. [CrossRef]
37. Roussanaly, S.; Brunsvold, A.L.; Hognes, E.S. Benchmarking of CO_2 transport technologies: Part II – Offshore pipeline and shipping to an offshore site. *Int. J. Greenh. Gas Control* **2014**, *28*, 283–299. [CrossRef]
38. Nimtz, M.; Klatt, M.; Wiese, B.; Kühn, M.; Joachim Krautz, H. Modelling of the CO_2 process- and transport chain in CCS systems—Examination of transport and storage processes. *Geochemistry* **2010**, *70*, 185–192. [CrossRef]
39. Forbes, S.M.; Verma, P.; Curry, T.E.; Friedmann, S.J.; Wade, S.M. *CCS Guidelines: Guidelines for Carbon Dioxide Capture, Transport, and Storage*; World Resources Institute: Washington, DC, USA, 2008.
40. Zigrang, D.; Sylvester, N. Explicit approximations to the solution of Colebrook's friction factor equation. *AIChE J.* **1982**, *28*, 514–515. [CrossRef]
41. Winning, H.; Coole, T. Explicit Friction Factor Accuracy and Computational Efficiency for Turbulent Flow in Pipes. *Int. J. Publ. Assoc. ERCOFTAC* **2013**, *90*, 1–27. [CrossRef]
42. Langelandsvik, L.I. *Modeling of Natural Gas Transport and Friction Factor for Large-Scale Pipelines: Laboratory Experiments and Analysis of Operational Data*; Norwegian University of Science and Technology, Faculty of Engineering Science and Technology, Department of Energy and Process Engineering: Trondheim, Norway, 2008.
43. Jia, W.; Li, C.; Wu, X. Internal Surface Absolute Roughness for Large-Diameter Natural Gas Transmission Pipelines. *Oil Gas. Eur. Mag.* **2014**, *40*, 211–213.
44. Chandel, M.K.; Pratson, L.F.; Williams, E. Potential economies of scale in CO_2 transport through use of a trunk pipeline. *Energy Convers. Manag.* **2010**, *51*, 2825–2834. [CrossRef]
45. Jackson, S. *Carbon Dioxide Transportation Energy Model*; Version 1, UiT; The Arctic University of Norway, Ed.; DataverseNO: Tromsø, Norway, 2020. [CrossRef]

Appendix – Article 5

Sensitivity Analysis and Case Studies for CO_2 Transportation Energy Consumption.

Steven Jackson

Department for Engineering & Technology (IVT), UiT – Norway's Arctic University, Norway,
steve.jackson@uit.no

Abstract

The transportation of CO_2 is important to all carbon capture and storage (CCS) projects. Both the infrastructure costs (compressors, pipelines, tanker ships, etc.) and the energy consumed in the compression or liquefaction of CO_2 are significant. Understanding how the size, capacity and energy consumption of transportation alternatives varies between projects is therefore important.

Modelling provides a useful insight into the performance of transportation alternatives, but the results are only useful when the basis for comparison is consistent and the impact of model input parameters is well understood.

This article presents the results of sensitivity studies made using a transportation model that was developed in earlier work. Several important model parameters are studied using three planned/operating CCS project cases.

The results show that while the operating pressure of the storage site is most important in determining the transportation system operating pressure, the temperature of the available cooling utility is the key parameter determining energy consumption.

Keywords: *CO_2, CCS, Transportation, Modelling*

1 Introduction

All carbon, capture and storage (CCS) projects require the transportation of CO_2 from a source to a storage location. A compressor and a large diameter pipeline is the method often used to achieve this, but as illustrated in Figure 1, the liquefaction of CO_2 to allow ship–based transportation can also form one of the links in the transportation process.

Although identifying the optimum economic case is of key importance to all CCS projects, it is also important to minimize energy consumption because the energy consumed by the process corresponds directly to the efficient consumption of non-renewable resources in fossil-fuel based CCS projects.

Most of the energy consumption associated with CO_2 transportation comprises compression and pumping energy. Compressors are often used to raise the pressure of gaseous CO_2 streams or gaseous refrigerants (in the case of liquefaction) and pumps are used to raise the pressure of liquid CO_2 streams. The pressure-level required for transportation depends on the operating parameters of the storage location, the design of the pipeline and the temperature under which the pipeline operates. Understanding how the combined effect of these parameters affects energy consumption can, therefore, provide an important insight into the relative strengths of different CCS projects.

As part of a project aimed at studying the performance of CCS project alternatives a MATLAB based model for the transportation of CO_2, *CO2TM,* has been developed and is made freely available at UiT Open Research Data (Jackson, 2020a).This model is used as the basis for the present study.

The *CO2TM* takes inputs comprising the source location, transportation type (ship or pipeline) pipeline route, storage reservoir depth and CO_2 mixture type. From these inputs, the model calculates an elevation profile for pipelines and a temperature profile using built-in bathymetry (seabed elevation profile) and sea surface temperature (SST) data. Based on elevation, temperature and CO_2 mixture data, the model estimates the reservoir and wellhead pressure (WHP) and then determines the pressure profile required to ensure

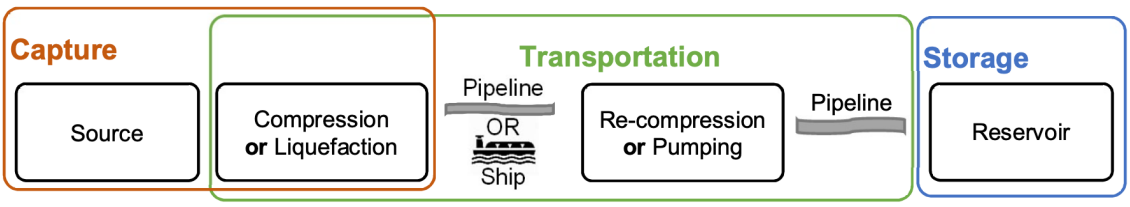

Figure 1. Illustration of the Main Associated with the Transportation of CO_2 (from Jackson, 2020).

single-phase flow in the pipeline. Finally, the energy consumption for transportation processes—comprising either compression or liquefaction—is calculated using the ambient sea temperature in location where each part of the process is situated. The development of this model is described in detail in earlier work (Jackson, 2020b).

The aim of this article is to present results from a study into the sensitivity of the *CO2TM* to various modelling parameters so that the application of this model can be better understood. The study is roughly based on three planned/ operating CCS project cases, which are used to illustrate the impact of the studied parameters on performance.

2 Method

Because the focus of earlier work—including the development of the *CO2TM*— has been the impact of ambient temperature on CO_2 transportation system performance, the main focus for this work is also the study of model sensitivity to seawater temperature. A related modelling parameter, also studied in this work, is the pipeline Heat Transfer Coefficient, HTC. In addition, this article presents results for CO_2 transportation system sensitivity to pipeline roughness, mixture composition and transportation type. The method used in the study of each of these parameters is described in more detail below under several sub-headings.

Although the development of the *CO2TM* is described in earlier work, some modifications to the original model were required to facilitate the present study. The modifications made are also described under the headings set-out below where they are relevant and will be subsequently included in an updated version of the *CO2TM*.

2.1 Sensitivity to Temperature

The *CO2TM* determines SST in the locations defined in the model input parameters using data from JMA (Japan Meteorological Agency). The resulting temperature data is then used as the basis for calculation of the energy consumption of the liquefaction and compression processes along with the temperature profile in the pipeline. For the compression and liquefaction processes, the model applies a margin of 10 °C above the seawater temperature.

Because SST varies annually, the data used in the model is based on two standard deviations above the average of yearly SST, i.e. covering around 95% of all SST measurements. This results in a conservative estimate for the energy consumption of compression and liquefaction processes and the pipeline temperature profile. It is therefore natural to study the sensitivity of the model to seawater temperature with an emphasis on reduced temperatures, which can be interpreted as either the performance during winter months or a less conservative approach to heat exchanger design. To reflect this, a range of temperatures from base -8 ºC to base +4 ºC is used in the sensitivity studies conducted here.

To allow the study of this temperature range, the original *CO2TM* required some modification. The main modification was to allow the user input of seawater temperature to apply to both the liquefaction location and the pipeline location for cases where transport is by ship. This represents an over simplification of reality where the liquefaction location may be a significant distance from the storage location, but it is one way in which sensitivity can be studied.

Another modification required was to implement limits on the minimum sea temperature used in the code to avoid extrapolation of parameters such as density and heat capacity outside of the range of the basis data included in the model. This was done by setting a minimum possible SST of 5 °C within the model.

2.2 Sensitivity to Pipeline Roughness

Pipeline roughness affects pipeline pressure-drop and can vary with both construction material and the age of the pipeline, equating to corrosion and fouling over time. In large diameter gas pipelines a coating is sometimes used to reduce pressure-loss and studies have found that absolute roughness can be as low as 4 μm (Langelandsvik, 2008). However, studies relating to CO_2 pipelines have often used higher values of roughness ranging up to 100 μm (Chandel et al., 2010). The default value of roughness used in the model is 15 μm, but this can be over-ridden using a user-specified roughness input parameter. In the present study, the roughness input parameter was varied from 2 to 100 μm to provide a range of results illustrating sensitivity.

2.3 Sensitivity to Heat Transfer

Subsea pipelines typically loose heat along their length to the surrounding seawater. The HTC, which varies with pipeline design and burial conditions, determines how quickly the pipeline contents approaches the sea temperature. In-turn, the temperature in the pipeline can impact the required operating pressure, which must be maintained at a margin above the bubble point curve of the CO_2 mixture throughout the pipeline.

The default value of the coefficient used in the model is 4 W/m^2 K, but the user can override this using a user-specified model input parameter. Studies of onshore buried pipelines have used HTC in the range 1–6 W/m^2 K (Mazzoccoli et al., 2014; Zhang et al., Massarotto et al., 2006), and for pipelines surrounded by water, up to 45 W/m^2 K (Drescher et al., 2013). The present study uses a range from 1 to 32 W/m^2 K to investigate the impact of this parameter on CO_2 pipelines.

2.4 Sensitivity to CO_2 Mixture Composition

The composition of CO_2 mixtures in transport systems depends on the source of the CO_2 and the entry

specifications set for the transportation system. The *CO2TM* has three built-in CO_2 mixture compositions with associated property data representing post, pre and oxyfuel combustion CO_2 sources.

In the previously published version of the *CO2TM,* the post combustion case is the only mixture composition made available for use. To enable the study of the sensitivity to CO_2 mixture composition in the present work, an update was required to make the oxyfuel mixture composition available for use. This work was done on the same basis as the earlier work and, although the details of the method are not described here, the composition used is provide in Table 1.

Table 1. CO_2 Mixture Compositions.

Component	*Post*	*Oxyfuel*
CO_2 mole %	99.99	96.16
N_2 mole %	0.01	2.45
Ar mole %	–	0.96
O_2 mole %	–	0.43

In addition, to provide a consistent basis for comparing energy consumption between post combustion and oxyfuel cases, an update of the *CO2TM* was required to allow the liquefaction energy consumption to be calculated for cases where the feed stream has a pressure of 15 barg— e.g. originating from a low–temperature type oxyfuel purification unit. The reduction in liquefaction energy for these cases was estimated by taking the difference between the compression energy for pipeline transport for the oxyfuel and post combustion capture cases and then deducting this from the energy consumption of the standard liquefaction process, where the feed stream is at low pressure. The updated version of the *CO2TM* will be published subsequent to the completion of the present work.

The sensitivity study conducted in the present work is based on a comparison of the performance of post and oxfuel combustion CO_2 mixture compositions. The basis of this comparison is both the transportation energy consumption and the pipeline inlet pressure. Results are summarized for the *CO2TM* default pipeline size selection: the first pipeline size that results in a pipeline pressure under 180 barg for all operating cases, and for the case where all pipelines have the same diameter.

2.5 Sensitivity to Transportation Method

The transportation cases used in this work are loosely based on three planned/operating CCS projects. Case 1 reflects the planned Norcem/Northern Lights (NL) project[1], which includes ship-based transport of CO_2 from Norcem in Brevik to the planned NL storage hub in south east Norway. Case 2 reflects the proposed H21 project, which is planned to include the conversion of natural gas to hydrogen with carbon capture in the UK with CO_2 storage in the North Sea[2]. Case 3 reflects the Melkøya CCS project, where CO_2 is removed from natural gas and returned to storage in the Barents Sea. A summary of some of the main modelling parameters associated these cases is provided below in Table 2.

Table 2. Comparison of Case Parameters.

Parameter	*Case 1*	*Case 2*	*Case 3*
Source Location	9,69 E 59,06 N	0,12 E 53,65 N	23,59 E 70,69 N
Liquefaction Loc.	9,69 E 59,06 N	-	-
Compression Loc.	-	0,12 E 53,65 N	23,59 E 70,69 N
Pipeline location	4,89 E 60,56 N	0,12 E 53,65 N	23,59 E 70,69 N
Pipeline length (km)	107	129	151
Reservoir location	3,42 E 60,45 N	2,00 E 54,00 N	4,89 E 60,56 N
Wellhead depth (m)	300	76	318
Reservoir Depth (m)	2000	1300	2500
Sea Temp. (°C)*	15,3	18,0	10,9

* Calculated by the *CO2TM*

In addition to the three cases described above, three alternative cases are also defined: Case 1A is the NL project with pipeline transport of CO_2 directly from the pipeline location; Cases 2A and 3A reflect Cases 2 and 3 with shipping to the NL pipeline as an alternative to pipeline transportation.

The model parameters used to specify the pipeline route for all cases and reservoir details are inferred from openly available data and should not be taken to accurately reflect the details of these projects. Figure 2 provides an illustration of the pipeline route used for the NL cases that was generated using the *CO2TM*.

3 Results & Discussion

The main results of the study are set out below under separate sub-headings.

3.1 Sensitivity to Pipeline Heat Loss

Figure 3 presents results that illustrate the sensitivity of pipeline inlet pressure to the heat transfer coefficient used in the model. For Cases 1A, 2 and 3 a small impact on pressure is visible, but in Case 1 there is almost no impact. This can be explained by the fact that in Case 1

[1] https://ccsnorway.com/no/

[2] https://www.h21.green/

the CO_2 mixture is very close to the seawater temperature at the point of entry to the pipeline.

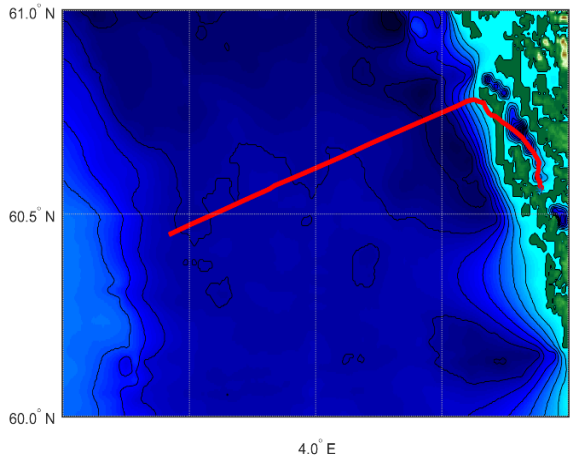

Figure 2. Illustration generated by the *CO2TM* for the Norther Lights (NL) pipeline route used in this work.

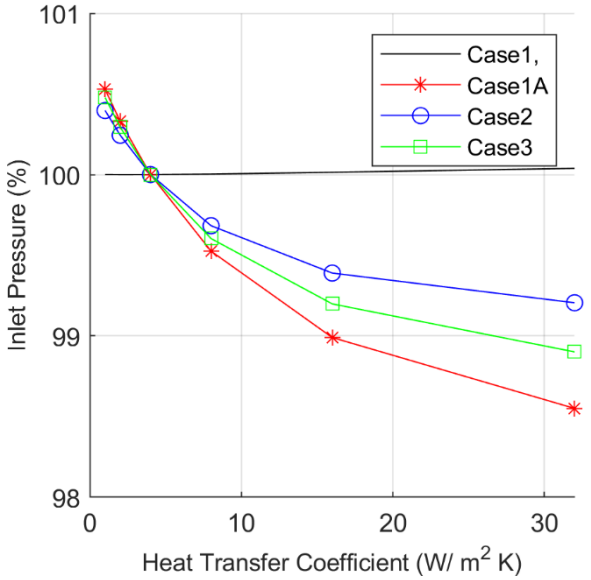

Figure 3. Variation in Pipeline Inlet Pressure with HTC where 100% is the model default basis of 4 W/m^2 K.

Figure 4 shows that the variation in pipeline inlet pressure presented in Figure 3 equates to an even smaller variation in overall energy consumption, reflecting the fact that the dominant part of the system energy consumption is associated with the earlier stages of compression, in the compression cases, and with the liquefaction process in the liquefaction cases.

3.2 Sensitivity to Pipeline Roughness

Figure 5 and Figure 6 present results for the sensitivity of pipeline inlet pressure and energy consumption to pipeline roughness. They show that roughness is a more important factor in transport system design than the HTC, although Figure 6, like Figure 4, shows that the roughness does not play a big role in determining the system energy consumption.

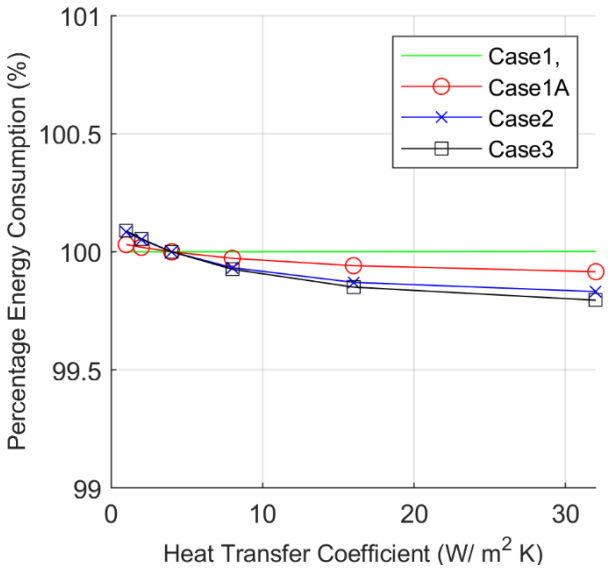

Figure 4. Variation in Energy Consumption with HTC.

However, Figure 5 does show that roughness can have a significant impact on the pipeline operating pressure, which is important to selection of the pipeline size and therefore the economics of CCS projects.

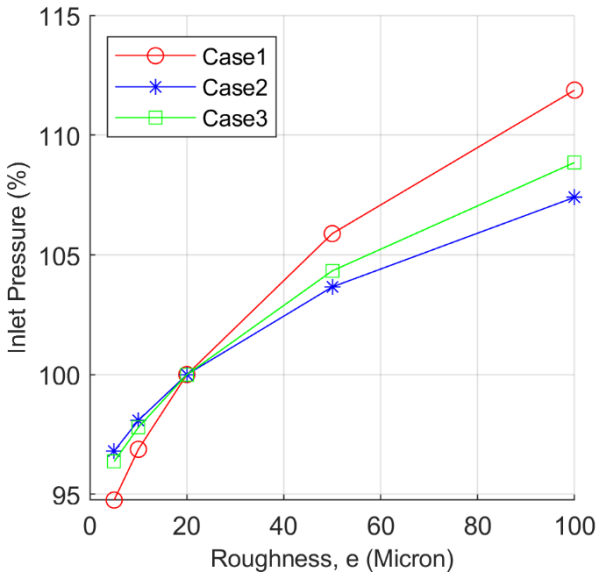

Figure 5. Variation in Percentage Pipeline Inlet Pressure with Pipeline Roughness.

3.3 Sensitivity to Temperature

Figure 7 and Figure 8 show the impact of seawater temperature on pipeline inlet pressure and energy consumption when the default seawater temperature estimated by the model is adjusted in the range – 8 °C to + 4 °C. The results are split into cases with pipeline-based transport (shown in red) and shipping based transport (shown in blue).

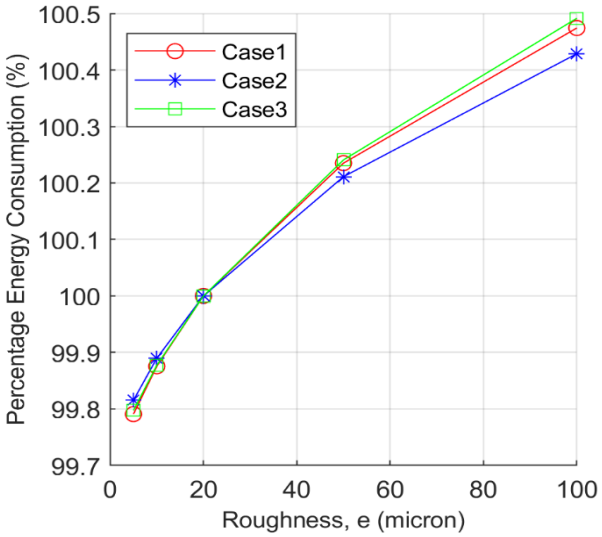

Figure 6. Variation in Percentage Energy Consumption with Pipeline Roughness.

The results show that although the impact of SST on pipeline inlet pressure is not more pronounced than that of roughness, the impact on energy consumption in all cases is much more significant. This is due to the dual impact of sea temperature, i.e. that it both affects the pipeline operating pressure and reduces the energy consumption of the associated compression and liquefaction processes.

The results presented for Case 3, Melkøya in Figure 7 and Figure 8 also show that when the seawater temperature is reduced by 8 ºC, the temperature of the pipeline falls below the lowest temperature where compressor energy consumption data is available in the model. In reality, there would be some continued reduction in energy consumption that would gradually reduce towards zero as the sea temperature is also reduced towards zero.

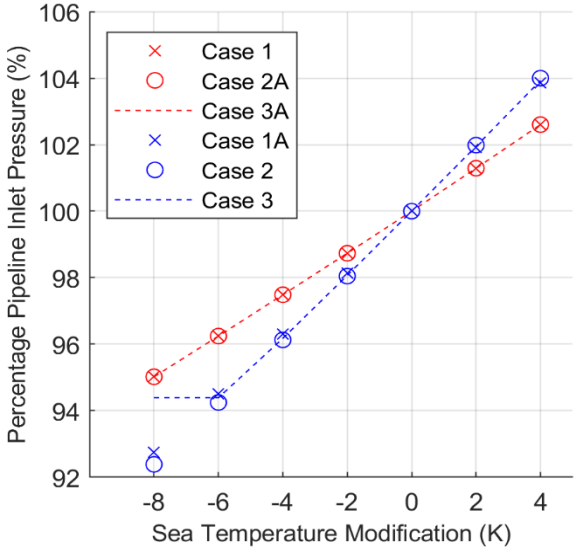

Figure 7. Variation in Energy Consumption with Seawater Temperature for Shipping Cases (in red) and Pipeline Transport (in blue).

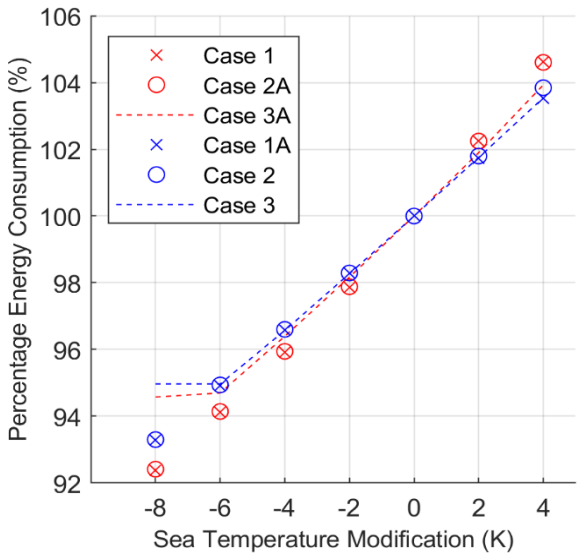

Figure 8. Variation in Energy Consumption with Sea Temperature for Shipping Cases (in red) and Pipeline Transport (in blue)

3.4 Sensitivity to CO_2 Mixture

Figure 9 shows how the pipeline pressure varies with sea temperature for two CO_2 mixture compositions representing post combustion capture and oxyfuel combustion.

All of the results indicate a small increase in operating pressure for the oxyfuel cases. This is due to an increased CO_2 mixture bubble-point pressure, which affects the minimum pipeline operating pressure: in all cases the *CO2TM* enforces a margin between bubble-point pressure and operating pressure. The sensitivity of inlet pressure to seawater temperature is similar for most cases.

Figure 9 shows results for the Norcem/NL case on two different pipeline design basis: a 14-inch pipeline sized based on the model default parameter of 180 bar maximum pipeline operating pressure (red lines), and a 16-inch pipeline sized to match the other two cases (black lines). This comparison highlights an inherent advantage of the NL pipeline that results from a combination of wellhead depth and reservoir depth (see Table 2). The results show that both of these factors have an important influence on the pressure profile calculated by the *CO2TM*.

How the variation in Inlet Pressure translates into a variation in energy consumption is presented for the post combustion cases, which are discussed under the next heading.

3.5 Sensitivity to Transportation Type

Figure 10 shows the variation in energy consumption with seawater temperature modification for a selection of pipeline and ship-based transportation cases.

The results show that in all of these cases, ship based transportation consumes more energy than sending the

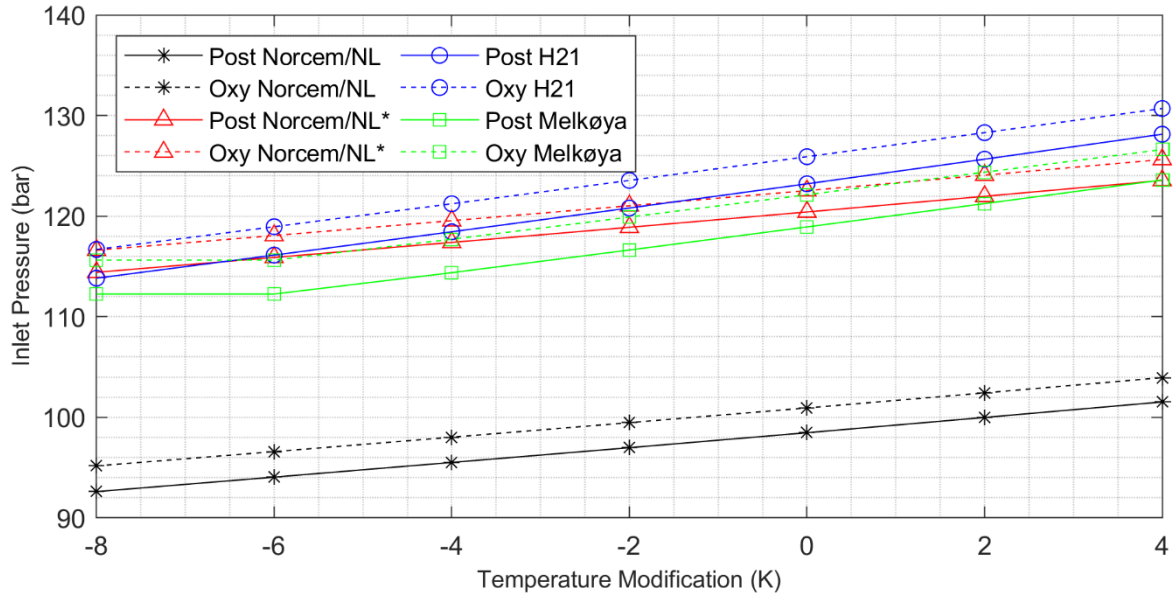

Figure 9. Impact of CO_2 Mixture Composition on Pipeline Operating Pressure.

CO_2 to a pipeline. Although the proportion of additional energy required is seen to vary between cases, the sensitivity of energy consumption to seawater temperature is similar for all cases.

Similar to Figure 9, Figure 10 presents results for both a 14-inch and a 16-inch NL pipeline diameter. However, the results presented in Figure 10 show that the impact of increasing the pipeline size on energy consumption is much smaller than the impact on pipeline operating pressure.

The results presented in Figure 10 also show that, regardless of transportation type, the energy consumption varies significantly between cases: both pipeline transport and shipping CO_2 from Melkøya results in the lowest energy consumption of all cases. This highlights the important role that ambient temperature plays in determining the energy consumption for both transportation alternatives.

4 Conclusions

When pipelines operate close to the temperature of the surrounding medium, the heat transfer coefficient has a low impact on operating pressure and energy consumption.

Pipeline roughness has a small, but potentially important impact on CO_2 pipeline operating pressure and hence the selection of the economic optimum pipeline diameter. The impact of roughness on the

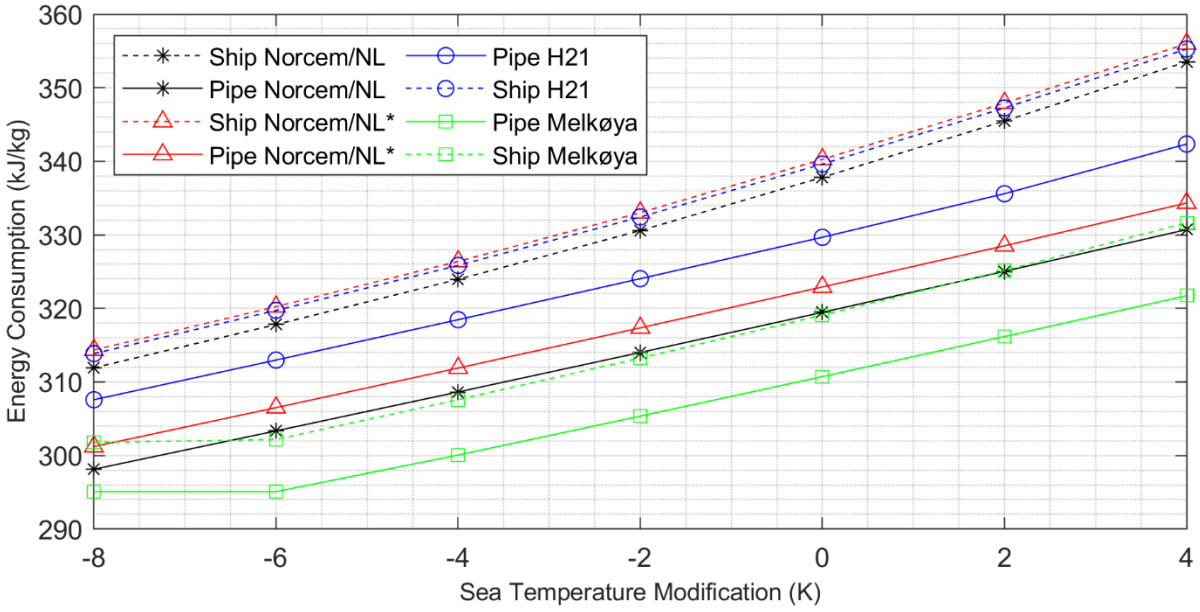

Figure 10. Impact of Transportation Type on Energy Consumption with Varying Sea Temperature

energy consumption associated with transportation of CO_2 is, however, small.

The composition of the CO_2 mixture transported in a pipeline can have an important impact on the transportation pressure.

The operating pressure of the storage reservoir and the wellhead location have the most important impact on CO_2 pipeline operating pressure and potentially the size and economics of CCS projects.

The most important factor influencing the energy consumption of both CO_2 transportation in pipelines and using ships is the temperature of the cooling utility (assumed to be seawater in this study) available in the location where the CO_2 is compressed or liquefied. The results from Figure 10 and Figure 8 show that the impact of temperature is consistent for all cases and equates to around 1 % of overall energy consumption per °C across the range of temperatures and cases studied here.

Compression or liquefaction is always needed at the source of captured CO_2 emissions in CCS projects, and therefore, CCS projects located in low ambient temperature locations can be expected to benefit from lower transportation energy consumption. Figure 10 shows that this advantage can be maximized by returning the captured CO_2 directly to a storage location using compression and pipeline transportation. Interestingly, the advantage associated with a low ambient temperature location such as Melkøya in Northern Norway is also apparent when the captured CO_2 is liquefied and shipped to a storage hub located at some distance.

Allowances for the energy consumption associated with shipping (transportation fuel, re-liquefaction energy, etc.) are not calculated by the *CO2TM* and do not form part of this study. In addition, the design parameters of the pipelines and storage locations used in this study can only be taken to be indicative of the project cases they are based upon. More detailed studies would be required to make an accurate comparison of the relative performance of these different cases. However, the results presented here can provide a guide to the sensitivity of CO_2 transportation energy consumption to some important case–specific and general design parameters.

Acknowledgements

I would like to thank my supervisor Eivind Brodal for the support and guidance he has given to my PhD project and his input to the present article.

References

M. K. Chandel, L. F. Pratson, and E. Williams. Potential economies of scale in CO_2 transport through use of a trunk pipeline. *Energy Conversion and Management, 51*, 2825-2834, 2010. doi:10.1016/j.enconman.2010.06.020

M. Drescher, Ø. Wilhelmsen, P. Aursand, E. Aursand, G. de Koeijer, and R. Held. Heat Transfer Characteristics of a Pipeline for CO_2 Transport with Water as Surrounding Substance. *Energy Procedia, 37*, 3047-3056, 2013. doi:10.1016/j.egypro.2013.06.191

S. Jackson. Carbon Dioxide Transportation Energy Model. *DataverseNO,* V1, 2020a. doi:10.18710/SAIANK

S. Jackson. Development of a Model for the Estimation of the Energy Consumption Associated with the Transportation of CO_2 in Pipelines. *Energies, 13*(10), 2427, 2020b.

L. I. Langelandsvik. Modeling of natural gas transport and friction factor for large-scale pipelines: laboratory experiments and analysis of operational data. *Norwegian University of Science and Technology, Faculty of Engineering Science and Technology, Department of Energy and Process Engineering, Trondheim* (2008:221), 2008.

M. Mazzoccoli, B. Bosio, E. Arato, and S. Brandani. Comparison of equations-of-state with P-p-T experimental data of binary mixtures rich in CO_2 under the conditions of pipeline transport. *The journal of supercritical fluids*, 474-490, 2014.

Z. X. Zhang, G. X. Wang, P. Massarotto and V. Rudolph. Optimization of pipeline transport for CO_2 sequestration. *Energy Conversion and Management, 47*(6), 702-715, 2006. doi:10.1016/j.enconman.2005.06.001.

Appendix – Article 6

Article

Case Studies into Low-Carbon derived Hydrogen Energy Supply to the UK from Norway

Steven Jackson* & Eivind Brodal

UiT-Norges Arktiske Universitetet, Postboks 6050 Langnes, 9037 Tromsø, Norway.
*Correspondence: steve.jackson@uit.no

Received: date; Accepted: date; Published: date **DRAFT**

Abstract:
This work presents a study of the efficiency of two alternative scenarios for the supply of low-carbon hydrogen from natural gas—or, 'blue' hydrogen—from northern Norway to the UK. Scenario 1 is a 'conventional' scenario where natural gas is exported from northern Norway as LNG and hydrogen produced in the UK; in Scenario 2 hydrogen is produced in Norway. The energy supply chain is modelled end-to-end on a consistent basis and its performance is compared using the total energy supplied on two basis: conversion to heat and conversion to electrical energy. The results show that Scenario 2 is more efficient than Scenario 1 when the fraction of liquid hydrogen supplied at the end-user is more than 75%. The performance of the SMR process is identified as most important to the accurate identification of the trade-off point. The performance of the hydrogen liquefaction process and the ambient temperature in the hydrogen production location are also identified as important factors affecting the relative efficiency of the two supply chain scenarios.

Keywords: H_2; CCS; CO_2; Ambient temperature; Energy

Nomenclature

Abbreviations

CCS	Carbon Capture & Storage
COP	Coefficient of performance
JT	Joule-Thompson
LH2	Liquefied hydrogen
LHL	Large-scale hydrogen liquefaction
LIN	Liquid nitrogen
LNG	Liquefied natural gas
MR	Mixed refrigerant
NW	Norwegian
SEC	Specific energy consumption
tpd	tonnes per day

Symbols

E_{el}	Electrical energy flowrate
E_{ht}	Heat energy flowrate
Ex_{D}	Exergy destruction
Ex_i	Total exergy stream *i*
$Ex_{i,\mathrm{ph}}$	Physical exergy stream *i*
$Ex_{i,\mathrm{ch}}$	Chemical exergy stream *i*
$f_{\mathrm{CO_{2,NW}}}$	CO_2 transport energy factor NW
$f_{\mathrm{CO_{2,UK}}}$	CO_2 transport energy factor UK
f_{GP}	Amine unit duty factor
f_{HL}	H_2 liquefaction energy factor

Symbols (continued)

f_{LNG}	LNG liquefaction energy factor
f_{vH2}	H_2 cold energy recovery factor
f_{vLNG}	LNG cold energy recovery factor
f_{SMR}	SMR electrical energy gen. factor
$\dot{m}_r$	LNG recycle flowrate
f_r	LNG end flash factor
H_i	Mass enthalpy stream *i*
k_i	Carbon content of component *i*
$\mathrm{LHV_i}$	Lower heating value stream *i*
$\dot{m}_i$	Mass flowrate stream *i*
MW_i	Molecular weight stream *i*
$\dot{Q}_{\mathrm{H2\rightarrow el}}$	Electrical energy eq. of H_2 product
$\dot{Q}_{\mathrm{H2\rightarrow ht}}$	Heat energy eq. of H_2 product
s_{p}	Amine unit CO_2 specification
S_i	Mass entropy stream *i*
T_{amb}	Ambient temperature
$\dot{W}_i$	Work flowrate in stream *i*
$x_{i,j}$	Mole fraction component *i* stream *j*
β	Flue gas capture rate
η_{Ex}	Exergy efficiency
η_{Fc}	Fuel cell efficiency
η_{GP}	Amine reboiler efficiency
η_{GT}	CCGT efficiency
η_{SMR}	SMR efficiency

1. Introduction

For several decades Norway has been an important supplier of energy in the form of natural gas to Europe. Over the next three decades, however, both the EU and the UK have stated the objective of achieving net zero greenhouse gas emissions. Meeting these targets will require a rapid transition away from traditional energy supplies, include a rapid reduction in the use of energy in the form of natural gas. The replacement of fossil-based electrical power generation with renewables will form part of the transition, another likely part will be the replacement of fossil-based energy with hydrogen in transport, energy intensive industries and possibly domestic heat. The recent EU *Hydrogen Energy Roadmap* (Cells and Undertaking 2019) estimates that this could lead to a seven-fold increase in the hydrogen demand in 2050.

Norway has the potential to play a leading role in the required transition, both via the export of surplus renewable energy and the decarbonization of its existing fossil-fuel resources through the application of Carbon Capture and Storage (CCS) technologies. One way in which the latter might support EU and UK emissions objectives is through the conversion of natural gas to hydrogen with CCS. This type of hydrogen supply is commonly referred to as *blue hydrogen*, as opposed to *green hydrogen*, which is hydrogen produced from renewable energy.

With the aim of increasing UK and European hydrogen production, several projects have been initiated including the H21 project[1], the H2H Saltend project[2], and the H-Vision project[3]. All of these are supported by Equinor, the Norwegian state-owned energy multinational, and all are based on an energy supply chain configuration where blue hydrogen is produced at the end-user. An alternative supply chain configuration that has received less attention is the production of blue hydrogen in the supplier location, which requires the hydrogen product to be transported to the end user as a compressed gas or as a liquid.

The optimum transportation strategy for hydrogen, depends on the both the capacity and transportation distance (Yang and Ogden 2007). Over long distances, liquefied hydrogen (LH2) transport is often the optimum, but the liquefaction of hydrogen for transport is a very energy intensive process. The specific energy consumption (SEC) of the most efficient currently operating large-scale hydrogen liquefaction (LH2) plants lies in the range 13-15 kWh/kg$_{H2}$ (Aasadnia and Mehrpooya 2018), which, for example, is far higher than the SEC of the most efficient currently operating LNG liquefaction plant, which lies around 240 kWh/tonne$_{LNG}$ (Bauer 2012).

Although the liquefaction of hydrogen inevitably has a large impact on the efficiency of the overall supply chain, it can be minimised through a combination of the application of an efficient liquefaction process in a low ambient temperature location. A direct parallel to this is the Melkøya LNG plant located in Northern Norway, which is claimed to be the most efficient LNG plant in the world (Bauer 2012). Earlier related study work has shown that the energy consumption for hydrogen liquefaction increases by around 20% across the cooling temperature range 5 to 50 °C, which illustrates the significant impact ambient temperature can have on energy consumption (Jackson and Brodal, submitted Aug 2021).

The economics of energy supply chains based on hydrogen production in Norway has been studied, with one recent study finding that the economics are "close to meeting the 2030 hydrogen cost target of Japan" (Ishimoto, Voldsund et al. 2020). In other parts of the world, blue hydrogen supply projects based on the shipping of liquefied hydrogen are already in development, for example, the HySTRA project[4].

The aim of this work is to compare the performance of two alternative blue hydrogen based energy supply chains linking Northern Norway and the UK from the perspective of energy efficiency. The base-case or *conventional* scenario studies will be the supply of natural gas as LNG with hydrogen

[1] https://h21.green/projects/h21-north-of-england/

[2] https://www.equinor.com/en/what-we-do/h2hsaltend.html

[3] https://www.h-vision.nl/en

[4] http://www.hystra.or.jp/en/

production in the end-user location; an alternative scenario will be the production of blue hydrogen in Northern Norway.

2. Materials and Methods

Two scenarios form the basis for this study. In both scenarios the origin of the natural gas is northern Norway with an end-user location in north-east England; a conventional Steam Methane Reforming (SMR) process is used for hydrogen generation; and Carbon Capture and Storage, CCS for all of the main CO_2 emission points—both in Norway and the UK as appropriate. Scenario 1 represents the 'conventional' case for hydrogen energy supply, where natural gas (in the form of LNG) is imported and converted into hydrogen at the point of import; Scenario 2 represents an alternative where hydrogen is generated in Norway and supplied as a liquid.

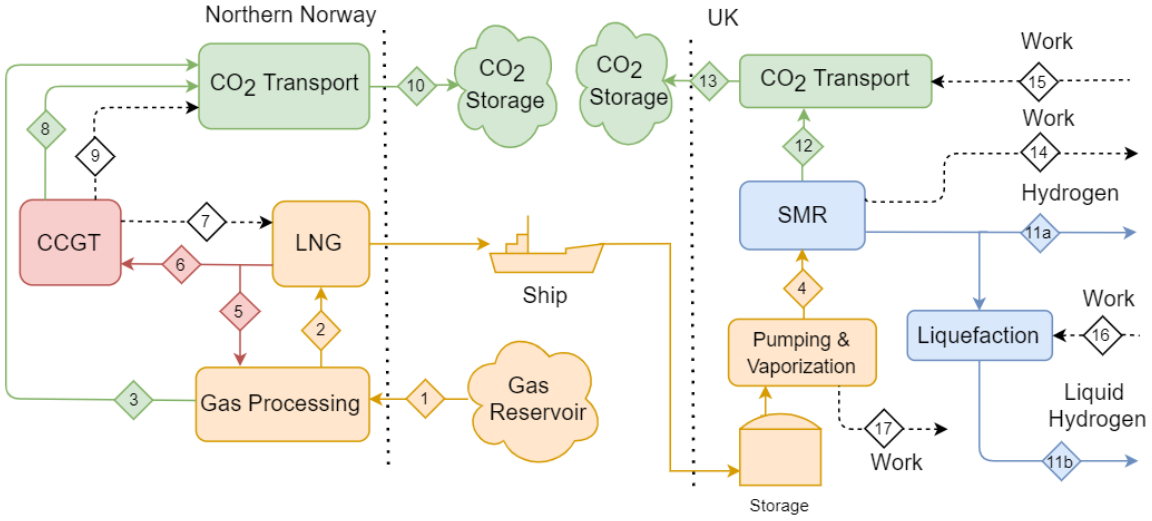

Figure 1 – Scenario 1, Summary of Main Process Units, Material and Energy Flow for Scenario 1.

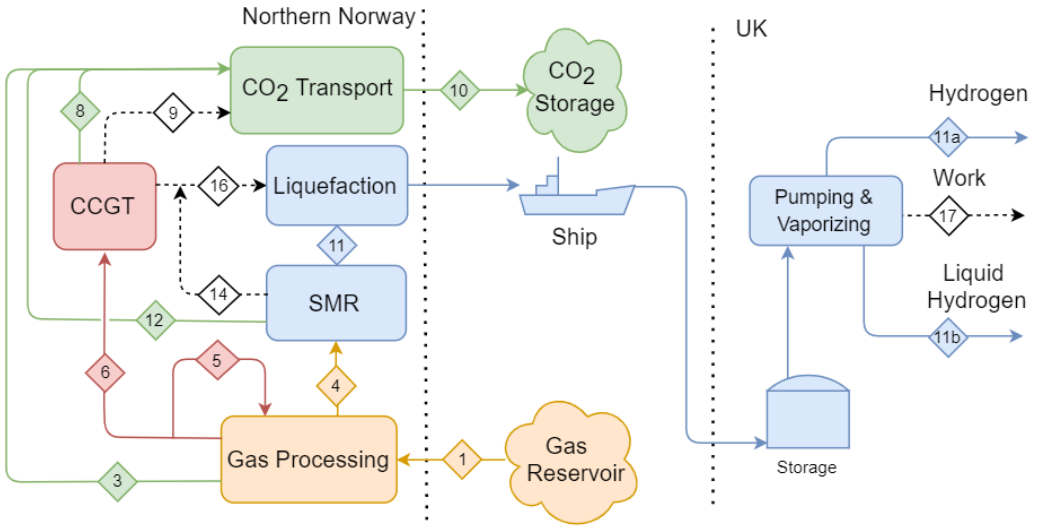

Figure 2 – Summary of Main Process Units, Material and Energy Flow for Scenario 2.

To allow a performance comparison of these scenarios a mathematical model was constructed in MATLAB (The MathWorks). The model of the of the end-to-end processes illustrated in Figures 1 and 2 is built up from process unit models that are used to calculate the mass and energy balance of the overall process. The basis upon which each process unit is modelled is set out below under separate headings. Table 1 provides a summary of the feed gas composition based on the DECARBit project (Anantharaman R., Bolland O. et al. 2011).

Table 1. Feed Gas Basis.

Component	mol%
Methane	89.00
Ethane	7.000
Propane	1.000
iButane	0.050
nButane	0.050
iPentane	0.005
nPentane	0.004
Carbon dioxide	2.000
Nitrogen	0.890

2.1. Gas Processing

The removal of free liquids (hydrocarbons and water), CO_2, sulphur compounds, and sometimes nitrogen from natural gas can be required to meet sales gas specifications. When feeding an LNG plant, removal specifications are generally tightened: CO_2 and water removal targets are lowered to avoid freezing and additional the heavy hydrocarbon and nitrogen removal may be required.

Dehydration and CO_2 removal processes typically require heat for regeneration. In this work the heat required for dehydration is omitted, being small compared to that required for CO_2 removal. The CO_2 removal level is defined by a parameter, s_{p} which is set at 0 in Scenario 1, and 0.02 in Scenario 2. The mass flow of CO_2 product from gas processing can then be calculated from the feed gas CO_2 content, $x_{\mathrm{CO_2},1}$, as follows:

$$\dot{m}_3 = \dot{m}_1 \cdot \max\{0, x_{\mathrm{CO_2},1} - s_{\mathrm{p}}\} \cdot \frac{\mathrm{MW_{co_2}}}{\mathrm{MW_1}}, \tag{1}$$

where $\mathrm{MW_{co_2}}$ is the molecular mass of CO_2 and $\mathrm{MW_1}$ is the molecular mass of Stream 1. Although it is often possible in the design of LNG plants to utilize waste heat from power generation to supply the heat energy required for regeneration of the CO_2 removal process, in this work, the heat required is assumed to be provided directly from the combustion of a portion fuel gas:

$$\dot{m}_5 = \frac{\dot{m}_3 \cdot f_{\mathrm{GP}}}{\eta_{\mathrm{GP}} \cdot \mathrm{LHV_5}}, \tag{2}$$

where f_{GP} is a factor describing the energy required for regeneration of the removal unit ($\mathrm{kJ/kg_{CO2}}$), $\mathrm{LHV_5}$ is the lower heating value of the fuel gas stream (kJ/kg) and η_{GP} is the thermal efficiency of the regeneration process heater.

Natural Gas Liquefaction, LNG

The design of the LNG process in Scenario 1 is based on the Melkøya LNG plant with performance modelling based on earlier study work (Jackson, Eiksund et al. 2017). Fuel gas for power generation, CCGT, is taken from the LNG process flash gas. The flow of fuel gas required by LNG process, $\dot{m}_{6,\mathrm{LIQ}}$, depends on throughput, the efficiency of the LNG process, the efficiency of CCGT, and the heating value of the fuel gas:

$$\dot{m}_{6,\mathrm{LIQ}} = \frac{\dot{W}_7}{\eta_{\mathrm{GT}} \cdot \mathrm{LHV_2}} = \frac{(\dot{m}_2 + \dot{m}_r) \cdot f_{\mathrm{LNG}}}{\eta_{\mathrm{GT}} \cdot \mathrm{LHV_2}}, \tag{3}$$

where $\dot{W}_7$ is the work flowrate in stream 7, η_{GT} is the LHV efficiency of CCGT, $\mathrm{LHV_2}$ is the lower heating value for Stream 2, f_{LNG} is the specific energy consumption of the LNG process on a feed gas basis and $\dot{m}_r$ represents a recycle flow of flash gas. The recycle flow depends on both the fraction of flash gas, f_r, and the flow of fuel gas to the GGCT ($\dot{m}_6$) and gas processing ($\dot{m}_5$):

$$\dot{m}_r = (1 + f_r)\dot{m}_2 - \dot{m}_5 - \dot{m}_6. \tag{4}$$

Hydrogen Production

Although a range of advanced hydrogen production technologies are under development, Steam Methane Reforming, SMR, with Pressure-swing Adsorption, PSA, based purification is currently most common. The most mature process considered for CO_2 capture is solvent based absorption (Voldsund, Jordal et al. 2016). Therefore, to best provide an assessment of near-future hydrogen supply alternatives, the modelling done in this study is based on SMR technology.

Recent studies looking at the performance of SMR with solvent-based CCS have been conducted by several authors (Collodi, Azzaro et al. 2017, Antonini, Treyer et al. 2020, Roussanaly, Anantharaman et al. 2020). The results of these studies shown some variation in the process performance with LHV efficiencies in the range 68 to 77%. There is also significant variation in the balance between electrical energy exported and hydrogen produced.

In the present study, the flow of hydrogen from the SMR process, $\dot{m}_{11}$, and the electrical energy produced, $\dot{W}_{14}$, are calculated from the SMR feed rate, $\dot{m}_4$, using performance factors based on the study of Roussanaly, et al:

$$\dot{m}_{11} = \dot{m}_4 \cdot \frac{\mathrm{LHV}_4}{\mathrm{LHV}_{11}} \cdot \eta_{\mathrm{SMR}}, \tag{5}$$

$$\dot{W}_{14} = \dot{m}_4 \cdot \mathrm{LHV}_4 \cdot f_{\mathrm{SMR}}, \tag{6}$$

where η_{SMR} is the LHV based thermal efficiency of the process, f_{SMR} is a factor describing the ratio of electrical energy generated. The value of f_{SMR} used in this study is extracted from the results of Roussanaly, et al. excluding CO_2 compression power, which is accounted for as part of the CO_2 transportation performance modelling. A sensitivity study looking at the range of SMR performance suggested by the studies of Collodi, et al. and Antonini, et al.

Hydrogen Liquefaction

The performance of the hydrogen liquefaction process is modelled based on the earlier study of Jackson, et al. (Jackson and Brodal, submitted Aug 2021), which looked at the variation in liquefaction energy consumption with ambient temperature. Based on the previous work a factor can be defined that relates energy consumption to product flowrate, f_{HL} ($\mathrm{kWh/kg_{H2}}$). The energy consumed by the liquefaction process and the fuel gas required by the CCGT process can therefore be calculated from the mass flowrate of Stream 11:

$$\dot{m}_{6,\mathrm{LIQ}} = \frac{\dot{W}_{16} - \dot{W}_{14}}{\eta_{\mathrm{GT}} \cdot \mathrm{LHV}_2} = \frac{\dot{m}_{11} \cdot f_{\mathrm{HL}} - \dot{W}_{14}}{\eta_{\mathrm{GT}} \cdot \mathrm{LHV}_2}. \tag{7}$$

Power Generation, CCGT

The based-line efficiency of a CCGT with CCS has been predicted to varying between 49.5- 51.9% on an LHV basis (Davison 2007, Amrollahi, Ystad et al. 2012, Lindqvist, Jordal et al. 2014, Adams and Mac Dowell 2016). The most recent studies suggest 51-52% is achievable with current CCGT technology, with CCS imposing a 6-7% efficiency penalty, inclusive of CO_2 compression. Because, in this study, the energy consumption of the CO_2 transportation process is accounted for separately, an allowance of 1.5% is made for CO_2 compression based on the results presented by Lindqvist, et al. (2014) for 20°C reboiler approach cases with 1.85 bara adsorber pressure.

The total flow of fuel gas required by the CCGT unit is the sum of the fuel gas required by the LNG or hydrogen liquefaction process, $\dot{m}_{6,\mathrm{LIQ}}$, and the flow required by the CO_2 transportation process, $\dot{m}_{6,\mathrm{CO_2}}$:

$$\dot{m}_6 = \dot{m}_{6,\mathrm{LIQ}} + \dot{m}_{6,\mathrm{CO_2}} \tag{8}$$

CO_2 Transportation

In both scenarios the flow of CO_2 captured from the SMR and CCGT units, $\dot{m}_{\mathrm{CO2}}$, is calculated based on the unit feed flowrate, $\dot{m}_{\mathrm{feed}}$, using a capture rate, β,:

$$\dot{m}_{\mathrm{CO2}} = \dot{m}_{\mathrm{feed}} \cdot \beta \cdot \frac{\mathrm{MW}_{\mathrm{co_2}}}{\mathrm{MW}_{\mathrm{feed}}} \cdot \{\sum x_{i,\mathrm{feed}} \cdot k_i\}, \quad (9)$$

where $\mathrm{MW}_{\mathrm{co_2}}$ is the molecular weight of CO_2, $\mathrm{MW}_{\mathrm{feed}}$, is the molecular weight of the feed stream, $x_{i,\mathrm{feed}}$, are the feed component mole fractions, and k_i is the carbon content of each component.

The performance of CO_2 transportation depends on several location-specific parameters and has been estimate based on earlier study work (Jackson 2020). The energy consumption associated with CO_2 originating from Norwegian end of the supply chain is based on a location close to Melkøya in northern Norway, the energy consumption at the UK end is based on the H21 project location in the Northeast of UK.

In Scenario 1, the energy consumption associate with CO_2 transport and the fuel gas flow required to supply this energy at the Norwegian end of the supply chain can be calculated using the efficiency of the CCGT process:

$$\dot{m}_{6,\mathrm{CO_2}} = \frac{\dot{W}_9}{\eta_{\mathrm{GT}} \cdot \mathrm{LHV}_2} = \frac{(\dot{m}_3 + \dot{m}_8) \cdot f_{\mathrm{CO_2,NW}}}{\eta_{\mathrm{GT}} \cdot \mathrm{LHV}_2}, \quad (10)$$

where $f_{\mathrm{CO_2,NW}}$ is the specific energy consumption for the location in northern Norway ($\mathrm{kJ/kg_{CO2}}$). The energy required at the UK end can be calculated in the same way:

$$\dot{W}_{15} = \dot{m}_{12} \cdot f_{\mathrm{CO_2,UK}}, \quad (11)$$

where $f_{\mathrm{CO_2,UK}}$ is the specific energy consumption for the CO_2 compression process located in the UK ($\mathrm{kJ/kg_{CO2}}$). In Scenario 2, the flow of CO_2 transported at the Norwegian end of the supply chain also includes that originating from the SMR:

$$\dot{m}_{6,\mathrm{CO_2}} = \frac{\dot{W}_9}{\eta_{\mathrm{GT}} \cdot \mathrm{LHV}_4} = \frac{(\dot{m}_3 + \dot{m}_8 + \dot{m}_{12}) \cdot f_{\mathrm{CO_2,NW}}}{\eta_{\mathrm{GT}} \cdot \mathrm{LHV}_4}. \quad (12)$$

Liquids Vaporization and Pumping

In both Scenario 1 and 2, liquid products (LNG and liquid H_2) are supplied to the UK that must be either partially or fully vaporized. This process is normally conducted by first pumping the liquids to the delivery pressure and then warming against a heat-sink.

Most LNG vaporization process today either reject heat to the environment (normally seawater) or burn a portion of the LNG to provide heat. To improve the efficiency of this process the cold energy from vaporization can be used in a number of ways: as a heat-sink for low-temperature industrial processes, e.g. air-separation; as a part of CCS projects, e.g., part of a liquefied—carbon free—value chain (Aspelund and Gundersen 2009); extracted directly as electrical power in an ORC; or indirectly via efficiency improvements in thermal power cycles (Romero Gómez, Ferreiro Garcia et al. 2014). The optimum utilization method is potentially a mixture of several of these approached (Atienza-Márquez, Bruno et al. 2018).

In this study, a simple approach is taken where energy recovery from LNG vaporization is modelled based on a simple vapor expansion system with a 30 bar supply pressure and heat rejection to seawater based on a factor set based on the study of Garcia (García, Carril et al. 2016):

$$\dot{W}_{17} = \dot{m}_{11} \cdot f_{\mathrm{v,LNG}}, \quad (13)$$

where $e_{\mathrm{v,LNG}}$ ($\mathrm{kJ_{el}/kg_{LNG}}$) is a factor describing the performance of the recovery process.

Fewer studies have been made into energy recovery from the vaporization of liquid hydrogen, but the study of Trevisani, et al. (Trevisani, Fabbri et al. 2007) conducts some performance modelling and is used as the basis for this study:

$$\dot{W}_{17} = \dot{m}_{11} \cdot f_{\mathrm{v,H2}}, \quad (14)$$

where $f_{\mathrm{v,H2}}$ ($\mathrm{kJ_{el}/kg_{H2}}$) is a factor describing the performance of the recovery process.

In both scenarios the hydrogen product is delivered at 20 bara and the feed to the SMR process is assumed to be 30 bara. The pumping energy required to raise the LNH and liquid hydrogen to the vaporization pressure represents a loss from the system. However, modelling with 80% isentropic efficiency shows the pumping energy required to pump LNG from 1.1 to 30 bar below 10 $\mathrm{kJ_{el}/kg_{LNG}}$, and based on this, this energy flow is omitted from the model.

2.2. Performance Summary

A direct comparison of the performance of the two scenarios is complicated by the fact that energy is supplied and consumed as a mixture of different forms. Energy is delivered as a mixture of electrical energy and liquefied or gaseous hydrogen, and energy is consumed in the form of fuel gas (in Norway) and electrical energy (in the UK). In addition, the end-use of the energy supplied can be considered on the basis of total electrical energy supplied and/ or total heat supplied. To reflect this complexity, three performance measures are used compare performance: electric energy delivery, E_{el}, heat delivery, E_{ht}, and exergy efficiency, η_{Ex}:

$$E_{\mathrm{el}} = \sum \dot{W}_i + \dot{Q}_{\mathrm{H2\rightarrow el}} = \left(\dot{W}_{14} - \dot{W}_{15} - \dot{W}_{16} + \dot{W}_{17}\right) + \dot{m}_{11} \cdot \mathrm{LHV}_{11} \cdot \eta_{\mathrm{Fc}} \tag{15}$$

$$E_{\mathrm{ht}} = \mathrm{COP} \sum \dot{W}_i + \dot{Q}_{\mathrm{H2\rightarrow ht}} = \mathrm{COP} \cdot \left(\dot{W}_{14} - \dot{W}_{15} - \dot{W}_{16} + \dot{W}_{17}\right) + \dot{m}_{11} \cdot \mathrm{LHV}_{11} \cdot \eta_{\mathrm{ht}} \tag{16}$$

$$\eta_{Ex} = \frac{\sum \dot{W}_i + \sum Ex_{11}}{Ex_1} 100\% = \frac{\dot{W}_{14} - \dot{W}_{15} - \dot{W}_{16} + \dot{W}_{17} + Ex_{11\mathrm{a}} + Ex_{11\mathrm{b}}}{Ex_1} 100\% \tag{17}$$

where $\dot{W}_i$ are the interface streams for work flowrate in the UK, $\dot{Q}_{\mathrm{H2\rightarrow el}}$ is the electrical energy equivalent of the heat supplied in the hydrogen product, η_{Fc} is the thermal efficiency of electrical energy generated using a hydrogen fuel cell, $Q_{\mathrm{H2\rightarrow ht}}$ is the heat equivalent of hydrogen supply, Ex_1 is the exergy of the feed stream, and Ex_{11} is the exergy of the product streams.

Although exergy, excluding nuclear, magnetic, electrical, and surface tension effects, can be describe as being made up of physical, Ex_{ph}, chemical, Ex_{ch}, kinetic, Ex_{ke} and potential exergy, Ex_{pe} (Dincer and Rosen 2012), in this study only Ex_{ph} and Ex_{ch} are consider in the calculations:

$$Ex_i = Ex_{i,\mathrm{ph}} + Ex_{i,\mathrm{ch}} \tag{18}$$

Physical exergy is calculated from its enthalpy and its entropy:

$$Ex_{i,\mathrm{ph}} = (H_i - H_{i,o}) - T_o(S_i - S_{i,o}) \tag{19}$$

where, H_i is the stream enthalpy of a stream at its operating conditions (T, P), $H_{i,o}$ is enthalpy at 'base conditions'; S_i is entropy at (T, P), $S_{i,o}$ is at base conditions; T_o is the base temperature (set in this study to T_{amb}).

The value of enthalpy and entropy were calculated using the Peng Robinson equation of state and mixing rules as implemented in the TREND 5.0 properties package (Span 2020). Chemical exergy was calculated from the sum of– 'component' exergy and mixture (or compositional) exergy:

$$Ex_{i,\mathrm{ch}} = \sum_n x_n Ex_{\mathrm{ch},n} + RT_o \sum_n x_n \ln\left(x_n\right) \tag{20}$$

where $Ex_{\mathrm{ch},n}$ is the chemical exergy of each component in stream *i*, and R is the gas constant. The value of $Ex_{\mathrm{ch},n}$ used in this study is based on the standard values given in Ertesvåg, at al. (2007) based on 25 °C, 1atm and 75% relative humidity.

The results of the exergy analysis are presents in terms of the overall process exergy efficiency as defined above and the exergy destruction, Ex_{D}, for each process unit:

$$Ex_{\mathrm{D}} = \sum Ex_{\mathrm{in}} - \sum Ex_{\mathrm{out}} \tag{21}$$

Some units have feed and product streams that are not shown in Figures 1 and 2. These streams include all flows of cooling water, combustion air or flue gasses. In general, these streams are at

ambient pressure and relatively low temperature and therefore have low exergy. These streams are not considered in the exergy balance. In all cases the exergy of shaft work and electrical energy flow is equal to the energy flow.

2.3 Summary of Performance Factors

Table 2 provides a summary of the performance factors defined under previous headings.

Table 2. Summary of Base Case Modelling Performance Factors.

Factor		Value	Units	Notes
Ambient temperature	T_{amb}	10.5/ 18.0	°C	Norway / UK
Amine unit CO_2 spec.	s_{p}	0 / 2	%	Scenario 1 / Scenario 2
Amine unit duty	f_{GP}	4000	$\mathrm{kJ/kg_{CO2}}$	
Amine reboiler efficiency	η_{GP}	90	% LHV	
LNG liquefaction energy	f_{LNG}	197	$\mathrm{kWh_{el}}$/tonne	Feed gas basis, NW (10.5 °C)
LNG end flash	f_r	8.0	%	End flash based on feed rate
LNG cold energy rec.	$f_{\mathrm{v,LNG}}$	235	$\mathrm{kJ_{el}/kg_{LNG}}$	
SMR efficiency	η_{SMR}	0.620	$\mathrm{kW_{H2}/kW_{feed}}$	LHV basis
SMR electrical generation	f_{SMR}	0.081	$\mathrm{kW_{el}/kW_{feed}}$	LHV basis, ex. CO_2 comp.
H_2 liquefaction energy	f_{HL}	6.6	$\mathrm{kWh/kg_{H2}}$	Based on 10.5 °C
H_2 cold energy rec.	$f_{\mathrm{v,H2}}$	1600	$\mathrm{kJ_{el}/kg_{H2}}$	
CCGT efficiency	η_{GT}	52.5	% LHV	Excludes CO_2 compression
Fuel cell efficiency	η_{Fc}	0.6	$\mathrm{kW_{el}/kW_{ht}}$	
Heat pump efficiency	COP	3.0	$\mathrm{kW_{ht}/kW_{el}}$	
Flue gas capture rate	β	90	%	SMR and CCGT units
CO_2 transport energy	$f_{\mathrm{CO_2}}$	311/ 330	$\mathrm{kJ/kg_{CO2}}$	NW, 10.5°C/ UK, 18 °C

2.4. Sensetivity Studies

Many of the factors presented in Table 2 are subject to some level uncertainty that will impact on the overall performance comparison. To enhance the performance comparison made between scenarios 1 and 2, the sensitivity of overall performance to several factors is presented in the results. The basis used for these assessments is presented below.

Sensitivity to hydrogen liquid supply fraction

In Scenario 1, liquefied hydrogen is supplied to the UK which can be vaporized or supplied as a liquid product; in Scenario 2 the opposite is true. The trade-off between the energy lost in vaporizing liquid hydrogen in Scenario 1 and liquefying hydrogen in Scenario 2 is very important in the performance comparison of the two scenarios and to investigate this, process performance is modelled over the range of liquid hydrogen supply from 0 to 100%.

Sensitivity to SMR process performance

Two alternative cases are studied: A1 based on 'Case 3' from the study of Collodi, et al. (2017) and A2 based on the 'SMR HTLT MDEA 90' case from the study of Antonini, et al. (2020). The parameters used in the sensitivity cases are presented in Table 3.

Table 3. Sensitivity Study Parameters for SMR Performance.

Parameter		**Base**	**A1**	**A2**	
SMR efficiency	η_{SMR}	0.620	0.691	0.778	$\mathrm{kW_{H2}/kW_{feed}}$
SMR electrical generation	f_{SMR}	0.081	0.015	0.010	$\mathrm{kW_{el}/kW_{feed}}$

Sensitivity to Ambient Temperature

Previous study work has shown that the performance of a number of important process units present in both Scenario 1 and 2 are sensitive to heat-sink temperature. Based on this, it is reasonable to expect that the relative performance of the two scenarios can also be expected to depend to some extent on the ambient temperature assumed in each location. In this study, the impact ambient temperature has on the performance of the LNG liquefaction process, the hydrogen liquefaction process and the CO_2 transportation process are all modelled based on earlier work (Jackson, Eiksund et al. 2017, Jackson 2020, Jackson and Brodal TBA). The data used is reproduced below in Table 4.

Table 4. Variation in LNG Process Energy Consumption with Ambient Temperature.

Ambient (°C)	$f_{\mathbf{LNG}}$ **(kWh/tonne$_{\mathbf{feed}}$)**	$f_{\mathbf{HL}}$ **(kWh/kg$_{\mathbf{H2}}$)**	$f_{\mathbf{CO_2,NW}}$ **(kJ/kg$_{\mathbf{CO2}}$)**	$f_{\mathbf{CO_2,UK}}$ **(kJ/kg$_{\mathbf{CO2}}$)**
5	187	5.92	296	-
10	196	6.05	310	308
15	207	6.19	324	322
20	217	6.33	339	336
25	230	6.48	-	354

Sensitivity to Process Efficiency

The baseline CCGT efficiency (excluding CCS) used as the basis in this study, η_{GT}, is equal to 58% LHV. There is evidence, however, that higher CCGT efficiency is possible, including currently operating examples of CCGTs with a claimed efficiency of 60% LHV (Drew 2010). Based on this, a range of CCGT efficiency equal to baseline plus 0 to + 6% is studied as a sensitivity case.

The basis used in this study the model the energy consumption of the hydrogen liquefaction process, e_{HL}, is a liquefaction process using a mixed-refrigerant pre-cooling step. This represents one of several potential next-generation technologies for large-scale hydrogen liquefaction. As such, a higher level of uncertainty is associated with this data that other parameters used in this study. To reflect this, a sensitivity study is made on this parameter looking at a +/- 20% range around the base-line efficiency.

The MFC type LNG liquefaction process used as the basis for this work is currently the most efficient LNG process available (Bauer 2012). In the view of this study there is little change of any very significant efficiency gains, so no sensitivity study made for base-line performance.

The CO_2 compression technology assumed as the basis for this work is conventional multi-stage centrifugal type compressor. Although alternative news technology options exist, the findings of earlier study work is that the impact of new technologies on overall process energy consumption is likely to be small (Jackson and Brodal 2018). Therefore, no sensitivity study made for base-line performance.

Carbon capture has a significant impact on the efficiency of both the CCGT process and the SMR processes studied here. Improved capture solvents are in development that could provide improvements to process efficiencies. More significant efficiency gains may also be available via more fundamental modification to existing technologies, such as the application of chemical looping type technologies. Because the impact of new CCS technology on the base-line efficiency of CCGT and SMR processes is a complex subject and to avoid unrealistic over-simplification, a sensitivity study looking at this aspect of process efficiency is set outside the scope of the assessments made here.

3. Results

3.1. Base Case Mass & Energy Balance Results

Table 5 presents a summary of selected model output data using the base-line performance parameters from Table 2. In scenarios 1a and 2a the hydrogen product is assumed to be delivered

entirely in the gas phase, in scenarios 1b and 2b hydrogen is supplied only as a liquid. In Figure 3 the exergy destruction associate with each case is broken down on a unit basis.

The results show that Scenario 1 is the most efficient way deliver hydrogen based energy to the UK when the end supply of hydrogen is in the gaseous phases. It is also worth noting that the shipping volume, which reflects the size and scale of the liquid transportation system needed is also significantly smaller for Scenario 1. However, when some portion of the hydrogen end-product is required in liquid form, each of the performance measures used in this study suggest that there is a trade-off point, beyond which, Scenario 2 becomes the most efficient supply chain.

Table 5. Summary Key Material and Energy Balance Results.

Unit		Scenario 1a	Scenario 1b	Scenario 2a	Scenario 2b
Feed flowrate	Mtpa	0.571	0.571	0.571	0.571
Shipping volume	Mm^3pa	1.116	1.116	1.788	1.788
Gaseous H_2	Mtpa	0.1325	0	0.1251	0
Liquid H_2	Mtpa	0	0.1325	0	0.1251
CO_2 Stored	Mtpa	1.364	1.364	1.374	1.374
CO_2 Emitted	Mtpa	0.1536	0.1536	0.1527	0.1527
Power Gen. CCGT	Mtpa	11.66	11.66	38.81	38.81
Electric Energy Export	MW	55.44	-39.45	6.349	0
Total Heat (E_{ht})	MW	597.4	597.4	564.2	564.2
Total Energy (E_{el})	MW	704.0	419.3	526.9	507.8
Exergy Efficiency (η_{Ex})	%	357.8	262.9	291.9	285.6

The distribution of exergy destruction between the process units shown in Figure 3 show that the main unit impacting on exergy destruction are the SMR, Liquefaction & CCGT. The sensitivity of overall performance to the performance of these three units along with the trade-off between liquid and gaseous hydrogen supply is studied under subsequent headings.

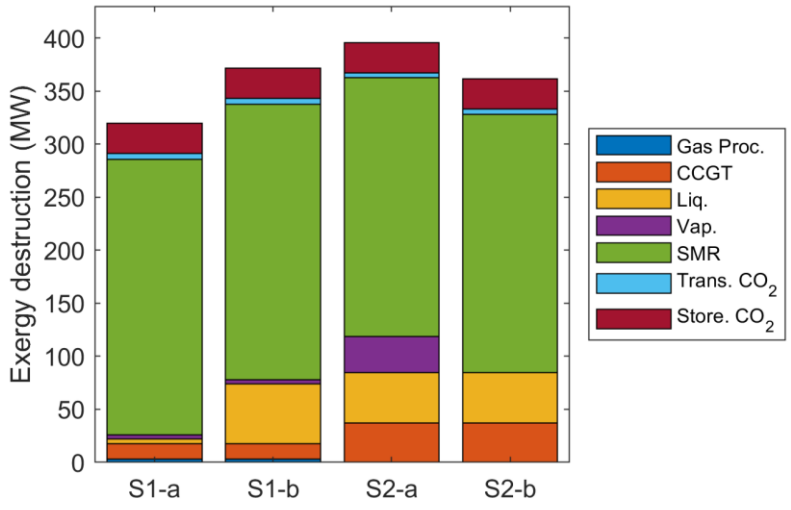

Figure 3. Summary of Exergy Destruction by Process Unit.

3.2. Sensetivity to Hydrogen Liquids Supply

Figure 4 shows how the proportion of hydrogen supplied as a liquid at the end-user interface affects the efficiency of the overall energy supply chain. The three types performance measure defined in equations 15, 16 and 17 are used to illustrate the relative performance of the two scenarios. The trade-off points are highlighted using a square box. It is notable that although a trade-off point exists for all measures, the trade-off point exergy-based measure is higher than the other two. This is due to the higher relative value given to the hydrogen product, which in both other measures is discounted by a factor relating to either fuel cell or boiler efficiency.

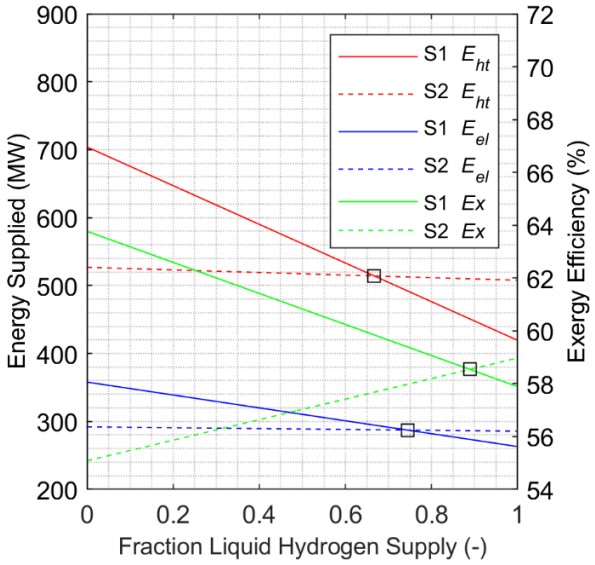

Figure 4. Variation of Electrical Energy (MW), Heat (MW) and Exergy Efficiency (%) with Fraction Liquid Hydrogen Supply for the Base Case.

3.3. Sensetivity to SMR Performance

Figures 5 and 6 show how the results presented in Figure 4 are impacted by the two different basis for SMR performance modelling presented in Table 3. In both cases the quantity of hydrogen produced per unit feed is higher, which is reflected in the results for exergy efficiency which favors Scenario 1 as discussed in the last section. The results for the other two measures of process performance, however, show a significant reduction in the trade off point, which is as low as 30% for the supply of energy as heat in case A1.

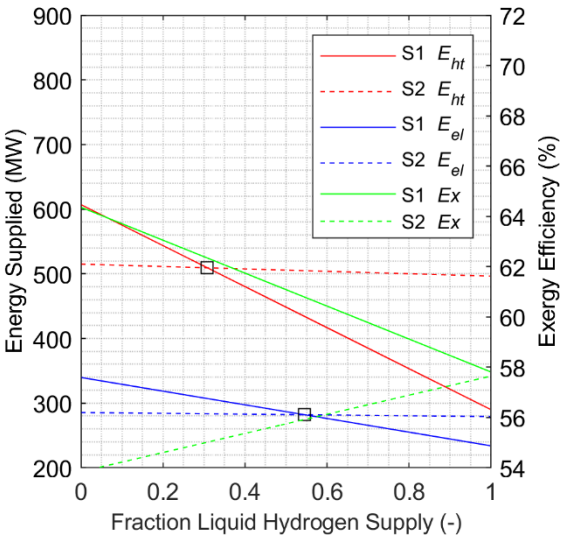

Figure 5. Variation of Electrical Energy (MW), Heat (MW) & Exergy Efficiency (%) with Fraction Liquid Supply SMR Case A1.

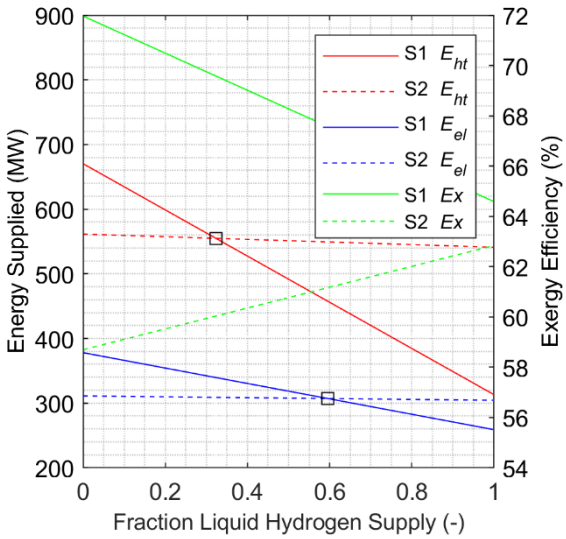

Figure 6. Variation of Electrical Energy (MW), Heat (MW) & Exergy Efficiency (%) with Fraction Liquid Supply SMR Case A2.

3.4. Sensetivity to Ambient Temperature

Figure 7 shows how the trade-off point for Scenario 1 and Scenario 2 for liquids product fraction varies with ambient temperature modification (left axis, solid lines), and how the relative process efficiency varies with ambient temperature modification (right axis, dashed lines). The relative efficiency is defined as the energy delivered at the trade-off point divided by the overall maximum energy delivered in all cases. For example, the maximum heat delivered in the base case is

approximately 700 MW (see Figure 4) so at the trade-off point with no temperature modification the heat delivered is 510 MW giving a Relative Efficiency of 73%. Ambient temperature modification is applied only to Scenario 1, i.e., the ambient temperature basis for Scenario 2 is held constant.

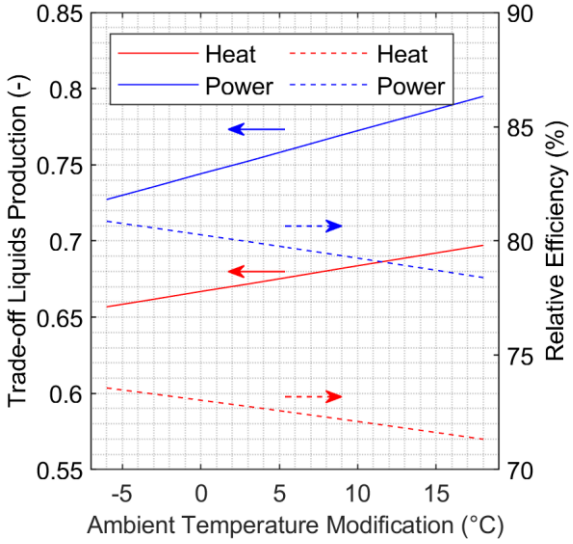

Figure 7. Variation in Trade-off Liquid Product Fraction (left axis, solid lines) and Relative Efficiency (right axis, dashed lines) with Ambient Temperature.

The trend illustrated in Figure 7 for all efficiency measures is that lower ambient temperature reduces the trade-off liquids production fraction and increases the relative efficiency at the trade-off point, both factors that favor Scenario 1. The impact, however, is low compared to the impact of SMR performance modelling. In the most extreme cases there is only a 5% impact on the trade-off point.

3.5. Sensetivity to Process Efficiency

Figure 8(a) shows how the trade-off point for liquids product fraction and relative supply chain efficiency at the trade-off point varies with the process efficiency of the CCGT. Figure 8(b) shows how the same parameters vary with hydrogen liquefaction unit efficiency. In both cases the parameters are defined as they were in the study of the sensitivity to ambient temperature, see Heading 3.2.

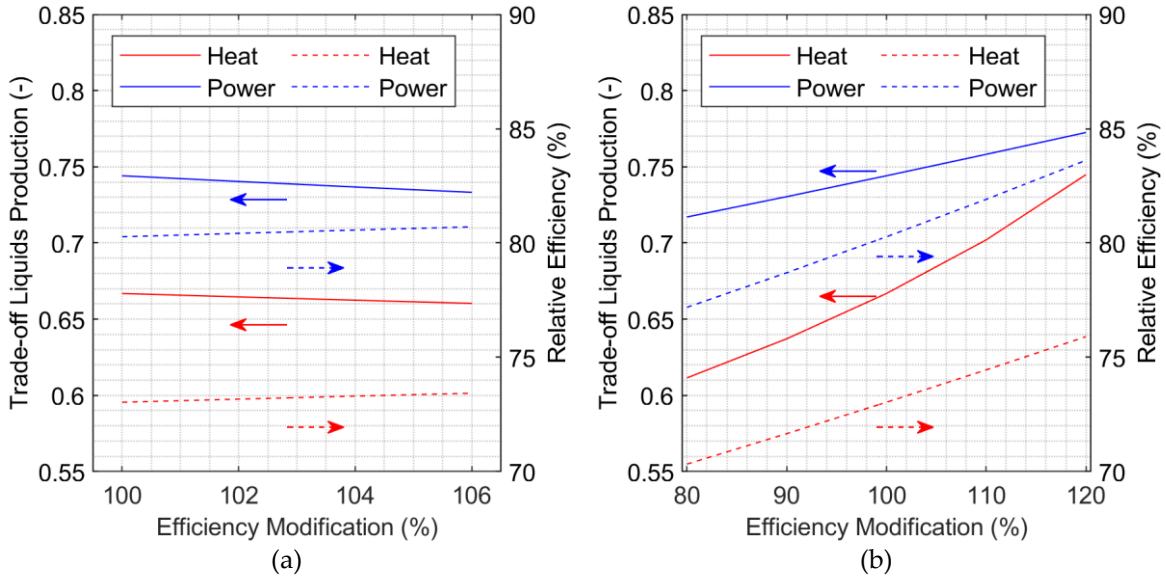

Figure 8. Variation in Trade-off Liquid Production (left axis, solid lines) and Relative Efficiency (right axis, dashed lines) **(a)** with CCGT Efficiency, **(b)** with Hydrogen Liquefaction Efficiency**.**

Figure 8(a) shows that the impact of CCGT efficiency across the range studies is small compared to the impact of either SMR performance or ambient temperature. However, Figure 8 (b) shows that impact of hydrogen liquefaction unit performance is more significant. The trends in Figure 8(b) illustrate higher efficiency in the liquefaction process (efficiency modification values greater than 100%) favor the 'conventional' energy supply chain scenario in terms of increasing the fraction of liquids production at the trade-off point, although the relative efficiency at the trade-off point is also increased.

4. Discussion

The results presented above show that in all cases there exists a trade-off point where Scenario 2 is more efficient that Scenario 1 in terms of the amount of heat, E_{ht}, or electrical energy, E_{el}, delivered by the supply chain. The results for the base-case performance parameters show that this trade-off point to lie between 65 and 75% liquids supply.

The exergy analysis presented in Figure 3 provides insight into the relative contribution made to energy efficiency by each element in the value chain. The most important elements are seen to be the performance of the SMR process, the liquefaction processes (hydrogen and LNG) and the CCGT process. Sensitivity studies are conducted on each of these elements of the supply chain that provide results that show the trade-off point for liquid hydrogen production might be substantially lower in some cases. In the most optimistic case, SMR case A1, the trade-off point lies between 30 and 55%.

In the study of alternative SMR performance cases, the balance between H_2 product and electrical energy exported from the SMR is seen to be important to the overall supply chain efficiency. The further study of SMR performance is therefore identified as the most important factor in reducing uncertainty in the comparison of these two energy supply chains.

The impact of ambient temperature is also studied and over a range of 20 °C the impact on the trade-off point was found to be up to 5%, with lower ambient temperature favoring Scenario 2. This illustrates the advantage gained by Scenario 2 due to its assumed location, Northern Norway.

5. Conclusions

The energy efficiency of the supply of blue hydrogen as a liquid from northern Norway (Scenario 2 in this work) benefits from the availability of a low temperature heat sink in the form of cold seawater. This study shows that this advantage relative to the supply of hydrogen from warmer locations is small but significant. More importantly, this study shows that under some conditions the

supply of liquid hydrogen from northern Norway could be more efficient than a more 'conventional' approach (Scenario 1) where natural gas is exported and blue hydrogen generated in the consumer location. A sensitivity study looking at the parameters used to model SMR performance finds that Scenario 2 could be more efficient that Scenario 1 for a wide range of conditions. The implications of this work are that the basis of the conventional approach to planned blue hydrogen supply projects should be more thoroughly investigated.

Author Contributions: Conceptualization, S.J.; methodology, S.J..; validation, S.J.; formal analysis, S.J.; investigation, S.J.; resources, S.J.; data curation, S.J.; writing—original draft preparation, S.J.; writing—review and editing, S.J. & E.B. supervision, E.B.

Funding: This research received no external funding.

Conflicts of Interest: The authors declare no conflict of interest.

References

Adams, T. and N. Mac Dowell (2016). "Off-design point modelling of a 420 MW CCGT power plant integrated with an amine-based post-combustion CO2 capture and compression process." Applied Energy **178**: 681-702.

Amrollahi, Z., P. A. M. Ystad, I. S. Ertesvåg and O. Bolland (2012). "Optimized process configurations of post-combustion CO2 capture for natural-gas-fired power plant – Power plant efficiency analysis." International Journal of Greenhouse Gas Control **8**: 1-11.

Anantharaman R., Bolland O., Booth N., Van Dorst E., Ekstrom C., Sanchez-Fernandes E., Franco F., E. Macchi, Manzolini G., Nikolic D., Pfeffer A., Prins M., R. S. and Robinson L. (2011). DECARBit deliverable D 1.4.3 European Best Practice Guidelines for Assessment of CO2 capture technologies. Trondheim, Norway, Sintef.

Antonini, C., K. Treyer, A. Streb, M. van der Spek, C. Bauer and M. Mazzotti (2020). "Hydrogen production from natural gas and biomethane with carbon capture and storage–A techno-environmental analysis." Sustainable Energy & Fuels **4**(6): 2967-2986.

Aspelund, A. and T. Gundersen (2009). "A liquefied energy chain for transport and utilization of natural gas for power production with CO2 capture and storage – Part 1." Applied Energy **86**(6): 781-792.

Atienza-Márquez, A., J. C. Bruno and A. Coronas (2018). "Cold recovery from LNG-regasification for polygeneration applications." Applied Thermal Engineering **132**: 463-478.

Bauer, H. C. (2012). Mixed fluid cascade, experience and outlook. Paper 25a, 12th Topical Conference on Gas Utilization, AIChE 2012 Spring Meeting, Houston, Texas.

Cells, F. and H. J. Undertaking (2019). Hydrogen Roadmap Europe-A Sustainable Pathway for the European Energy Transition, Luxemburg.

Collodi, G., G. Azzaro and N. Ferrari (2017). Techno-Economic Evaluation of SMR Based Standalone (Merchant) Hydrogen Plant with CCS, IEAGHG Technical Report, Cheltenham, UK.

Collodi, G., G. Azzaro, N. Ferrari and S. Santos (2017). "Techno-economic Evaluation of Deploying CCS in SMR Based Merchant H2 Production with NG as Feedstock and Fuel." Energy Procedia **114**: 2690-2712.

Davison, J. (2007). "Performance and costs of power plants with capture and storage of CO2." Energy **32**(7): 1163-1176.

Dincer, I. and M. A. Rosen (2012). Exergy : Energy, Environment and Sustainable Development. Oxford, UNITED KINGDOM, Elsevier Science & Technology.

Drew, R. (2010) "CCGT: Breaking the 60 per cent efficiency barrier."

Ertesvåg, I. S. (2007). "Sensitivity of chemical exergy for atmospheric gases and gaseous fuels to variations in ambient conditions." Energy Conversion and Management **48**(7): 1983-1995.

García, R. F., J. C. Carril, J. R. Gomez and M. R. Gomez (2016). "Combined cascaded Rankine and direct expander based power units using LNG (liquefied natural gas) cold as heat sink in LNG regasification." Energy **105**: 16-24.

Ishimoto, Y., M. Voldsund, P. Nekså, S. Roussanaly, D. Berstad and S. O. Gardarsdottir (2020). "Large-scale production and transport of hydrogen from Norway to Europe and Japan: Value chain analysis and comparison of liquid hydrogen and ammonia as energy carriers." International Journal of Hydrogen Energy **45**(58): 32865-32883.

Jackson, S. (2020). "Sensitivity Analysis and Case Studies for CO2 Transportation Energy Consumption." Linköping Electronic Conference Proceedings.

Jackson, S. and E. Brodal (2018). A comparison of the energy consumption for CO_2 compression process alternatives. Earth and Environmental Science, Barcelona, IOP COnference Series.

Jackson, S. and E. Brodal (TBA). "Optimization of a H2 Liquefaction Pre-Cooling Process & Estimate of Liquefaction Performance with Varying Ambient Temperature."

Jackson, S., O. Eiksund and E. Brodal (2017). "Impact of Ambient Temperature on LNG Liquefaction Process Performance: Energy Efficiency and CO 2 Emissions in Cold Climates." Industrial & Engineering Chemistry Research **56**(12): 3388-3398.

Lindqvist, K., K. Jordal, G. Haugen, K. A. Hoff and R. Anantharaman (2014). "Integration aspects of reactive absorption for post-combustion CO2 capture from NGCC (natural gas combined cycle) power plants." Energy **78**: 758-767.

Romero Gómez, M., R. Ferreiro Garcia, J. Romero Gómez and J. Carbia Carril (2014). "Review of thermal cycles exploiting the exergy of liquefied natural gas in the regasification process." Renewable and Sustainable Energy Reviews **38**: 781-795.

Roussanaly, S., R. Anantharaman and C. Fu (2020). "Low-Carbon Footprint Hydrogen Production from Natural Gas: a Techno-Economic Analysis of Carbon Capture and Storage from Steam-Methane Reforming."

Span, R. B., R.; Hielscher, S.; Jäger, A.; Mickoleit, E.; Neumann, T.; Pohl, S.; M.; Semrau, B.; Thol, M. (2020). TREND. Thermodynamic Reference and Engineering Data 5.0, Lehrstuhl für Thermodynamik, Ruhr-Universität Bochum.

The MathWorks, I. MATLAB. Natick, Massachusetts, United States.

Trevisani, L., M. Fabbri, F. Negrini and P. L. Ribani (2007). "Advanced energy recovery systems from liquid hydrogen." Energy Conversion and Management **48**(1): 146-154.

Voldsund, M., K. Jordal and R. Anantharaman (2016). "Hydrogen production with CO2 capture." International journal of hydrogen energy **41**(9): 4969-4992.

Yang, C. and J. Ogden (2007). "Determining the lowest-cost hydrogen delivery mode." International Journal of Hydrogen Energy **32**(2): 268-286.

Aasadnia, M. and M. Mehrpooya (2018). "Large-scale liquid hydrogen production methods and approaches: A review." Applied Energy **212**: 57-83.